Involvement of Scribble protein in breast cancer invasion and metastasis

Samson Adoki

A thesis submitted for the degree of Doctor of Philosophy (Ph.D)

Department of Biological Sciences

University of Essex

June 2016

Abstract

A common feature of cancer cells is the loss of cell polarity. Scribble is a cell polarity protein with an unknown mechanism for its role in tumour suppression. Changes in the phosphorylation pattern of four serine sites at the C-terminal of scribble, implicate scribble in breast cancer invasion and metastasis. This was due to CD74 overexpression in lymph node metastatic triple negative breast cancers. Investigating how changes in serine phosphorylation status at these sites affect the regulation of invasion and metastasis in breast cancer was the focus of this study. These sites were mutated by site-directed mutagenesis to generate mutant *scribble* genes grouped into A-mutants and D-mutants, based on the amino acid change to the serine sites to mimic unphosphorylated and phosphorylated scribble, respectively. Widefield and confocal bioimaging of the expression and localization of these mutants in cell line HEK293T revealed good expression but varied localization to cytoskeletal elements, intercellular contact site, microtubules, centrosome and vesicles. Wound healing, MTT and flow cytometry assays were conducted on HEK293T transfected with these mutant genes to study how their expression affected cell migration, proliferation and the cell cycle, respectively. Notable differences emerged: 1.) A-mutants migrated more than D-mutants. 2.) D-mutants proliferated more than A-mutants and 3.) There were significantly more D-mutant expressing cells in the G2 phase of the cell cycle. Protein interaction study was also conducted. The binding partners of S[1306+1309]A and S[1306+1309]D mutants of scribble were captured and analysed by Co-IP and mass spectrometry. Bioinformatics analysis identified the pathways these binding proteins were significantly involved in: S[1306+1309]A binding partners were involved in cell migration via regulation of actin cytoskeleton pathway but contribute to intercellular adhesion via the tight junction pathway. S[1306+1309]D binding partners were involved in the TSH signalling and cell cycle pathways. The results show a significant possibility that unphosphorylated and phosphorylated hScrib support cell invasion and cell proliferation, respectively, and that these processes are antagonistic.

Acknowledgements

I would like to thank my supervisor Dr. Metodi Metodiev and research fellow Dr. Gergana Metodieva for their guidance and support throughout the duration of my research. The skills and knowledge I have acquired from them were central to the fruition of my work and my development in the field of proteomics.

The first two years of my research were the hardest for me but I always found a listening ear in my uncle, Victor. During those times I wanted to quit because of the pressures in and out of my work, he helped me to see that the saddest thing a man will ever face is what might have been and that the sum of our choices do not really define who we are but our commitment to those choices. Thank you uncle!

The prayers of Pastor Chima Emenuga have been very encouraging. I thank him and other people, including A.C. Queen, who contributed financially to keep me in the course.

I am grateful to my sisters for their company and immense help during and including the difficult moments I faced during my research.

Above all my deepest appreciation goes to my mother, Mrs. Adoki. Without her immeasurable support towards aiding me financially, I would not have come this far and without your constant prayers and instilling in me self-belief, I would have become someone who fell short off the person that they wanted to be. I would say you moved heaven and earth for me.

Lastly, the words of wisdom of my late father, Mr. Adoki, have been my inspiration. If he were alive to see how much I have achieved in life so far, I believe he would smile with pride. I dedicate this thesis to him.

Contents

Contents of figures and tables

Abbreviation	Details	Abbreviation	Details
1^{o}Ab	Primary antibody	DCIS	Ductal carcinoma *in situ*
2^{o}Ab	Secondary antibody	dCTP	Deoxycytosine triphosphate
2xYT	Yeast extract (2X) tryptone media	dGTP	Deoxyguanine triphosphate
3D	3-dimensional	DLG	Discs large protein
APC	Adenomatous polyposis coli	DMEM	Dulbecco's modified eagle medium
ATM	Ataxia telangiectasia mutated	DmScribble	Scribble homolog of *Drosophila melanogaster*
ATP	Adenosine triphosphate		
ATPase	Adenosine triphosphatase	DMSO	Dimethyl sulphoxide
ATR	Ataxia telangiectasia and Rad3 related	DNA	Deoxyribonucleic acid
BRCA-1	Breast cancer type 1 susceptibility	dNTP	Deoxynucleotide triphosphate
BRCA-2	Breast cancer type 2 susceptibility	*Dpn1*	*Diplococcus pneumoniae 1*
cAMP	Cyclic adenosine monophosphate	dsDNA	Double stranded deoxyribonucleic acid
CD74	Cluster of differentiation 74	dsRNA	Double stranded ribonucleic acid
Cdc2	Cell division cycle 2	DTT	Dithiothreitol
Cdc25	Cell division cycle 25	dTTP	Deoxythymidine triphosphate
Cdk	Cyclin-dependent kinase	E2F	Transcription factor
CHK 1	Checkpoint kinase 1 protein	*E.coli*	*Escherichia coli*
CHK 2	Checkpoint kinase 2 protein	EBV	Epstein-barr virus
CO_2	Carbondioxide	ECM	Extracellular matrix
Co-IP	Co-immunoprecipitation	EDTA	Ethylenediaminetetraacetic acid
CpG	Cytosine-phosphate-guanine	EGF	Epidermal growth factor
DAPI	4',6—diamino-2-phenylindole	EGFP	Enhanced green fluorescent protein
dATP	Deoxyadenine triphosphate	EMT	Epithelial to mesenchymal transition

Abbreviation	Details	Abbreviation	Details
ERα	Oestrogen receptor alpha	kDa	Kilodalton
ERβ	Oestrogen receptor beta	LAP	LRR and PDZ
ERK	Extracellular signal-regulated kinase	LB	Luria-bertani
EtBr	Ethidium bromide	LCIS	Lobular carcinoma *in situ*
FBS	Fetal bovine serum	LC-MS/MS	Liquid chromatography tandem mass spectrometry
FCS	Fetal calf serum	LGL	Lethal giant larvae
FDR	False discovery rate	LOH	Loss of heterozygosity
FGF	Fibroblast growth factor	LRR	Leucine-rich repeat
FITC	Fluorescein isothiocyanate	LTQ	Linear trap quadrupole
G0	Quiescent or resting phase	M	Mitotic phase
G1	First growth phase	MAPK	Mitogen-activated protein kinase
G2	Second growth phase	MCS	Multiple cloning site
GFP	Green fluorescent protein	MDM2	Mouse double minute 2
H3K27	Histone 3 on Lysine 27	MET	Mesenchymal to epithelial transition
HAT	Histone acetyltransferase	MLC	Myosin light chain regulator
HDAC1	Histone deacetylase 1	MLCK	Myosin light chain kinase
HEK293T	Human embryonic kidney cell 293	MLCP	Myosin light chain phosphatise
HER-2	Human epidermal growth factor receptor 2	MQ	MilliQ water
HPLC	High performance liquid chromatography	MS	Mass spectrometry
HPV	Human papilloma virus	MTT	3-(4,5-dimethylthiazol-2-yl)-2,5-diphenyltetrazolium bromide
Hus 1	Checkpoint clamp component	Noc	Nocodazole
IBC	Invasive breast cancer	p16	Cdk4 inhibitor
IP	Immunoprecipitation	p21	Cyclin-Cdk2/4 inhibitor

Abbreviation	Details	Abbreviation	Details
p53	TP53 transcription factor	*RB1*	*Retinoblastoma 1 gene*
PAGE	Polyacrylamide gel electrophoresis	RbmAb	Rabbit monoclonal antibody
PAH	Polycyclic aromatic hydrocarbon	RO	Reverse osmosis
PAK	Protein-activating kinase	rpm	Revolution per minute
PBS	Phosphate buffered saline	S	Synthetic phase
PCR	Polymerase chain reaction	S-S	Disulphide bond
PDZ	PSD-95/Dlg/ZO-1	SDM	Site-directed mutagenesis
Pfu	*Pyrococcus furiosus*	SDS	Sodium dodecylsulphate
PI	Propidium iodide	Stdev	Standard deviation
PI3K	Phosphoinositide 3-kinase	TAE	Tris-acetate-EDTA
PR-A	Progesterone receptor A	TBS	Tris-buffered saline
PR-B	Progesterone receptor B	TBS-T	Tris-buffered saline with tween
pRb	Retinoblastoma protein	TDLU	Terminal ductal-lobular unit
PRKDC	Protein kinase, DNA-activated, catalytic polypeptide	TEMED	Tetramethylethylenediamine
PSD	Postsynaptic density	Thd	Thymidine
PTEN	Phosphatase and tensin homolog	TGF-β	Transforming growth factor beta
PTM	Post-translational modification	TNBC	Triple-negative breast cancer
PVDF	Polyvinylidene fluoride	TSG	Tumour suppressor gene
Q/m or z/m	Charge per mass ratio	TSH	Thyroid-stimulating hormone
Rad 1	Checkpoint DNA repair exonuclease	UV	Ultraviolet
Rad 9	Checkpoint clamp component A	WB	Western blot
Rad 17	Checkpoint clamp loader component for G2 arrest DNA damage	WT	Wildtype
		ZO-1	Zonula occludens-1

1. Introduction to Breast Cancer

1.1 Breast cancer- definition and classification

When the growth and division of cells in any part of the human body is unchecked by the body's cell cycle regulatory mechanisms, it leads to formation of a tumour or neoplasm (Lodish *et al.*, 2000:13.6; Chow, 2010). A tumour is an abnormal mass of tissue which could be benign or malignant (cancerous). Tumours can occur sporadically (acquired) or by hereditary (familial). An example is in cancer of the breast. Breast cancer is a disease defined by the American Cancer Society (ACS) as an abnormal growth and multiplication of cells that occurs in any part of the breast and forms tumour (or lump), with cells that can invade the surrounding tissues and other areas of the body (Cancer.org, 2016). In a broader classification of cancer types, NCI groups breast cancer as a carcinoma (National Cancer Institute, 2016). This is because it is initiated in epithelial cells that line the breasts.

1.2 Breast cancer- incidence, mortality and treatments

Out of more than 200 different types of cancer, breast cancer has become the most common cancer in the United Kingdom (UK) since 1997. Cancer research UK reported 53,696 new cases (99% in woman and 1% in men) of breast cancer in the UK in 2013 compared to 2010 (49,961 new cases). This is a 7.5% increase that contributes to the 4% increase in the incidence rate over the last 10 years, making UK the sixth highest in breast cancer incidence rate in Europe. Breast cancer deaths in the UK in 2014 were 11,433. However, comparing the last 10 years, this is a 20% decrease in mortality rate. This rise in incidence and fall in mortality rates has increased the survival rate of breast cancer in the UK to 78% i.e. 8 in 10 women would survive 10 years or more after diagnosis. It is a consequence of early detection (breast cancer screening) and improved treatments with surgery, adjuvant radiotherapy, chemotherapy and use of tamoxifen citrate in hormone sensitive breast cancer (Chew, 2001; Cancer Research UK, 2015).

1.3 Breast cancer- risk factors

The increased incidence rate is influenced by certain risk factors of which age is the most common. The probability of breast cancer occurrence increases as we age (National Cancer Institute, 2016). This increase, according to Cancer research UK, is linked with hormones, another risk factor (Cancer Research UK, 2015). Other risk factors include:

smoking, alcohol, obesity, radiation (ionizing, UV), infectious agents (viruses, bacteria, and parasites), chronic inflammation. The risk factors induce changes or events at cellular and molecular level of which this review will look into.

Understanding breast cancer relies on the knowledge of the structure and the function of the breast.

1.4 Anatomy of the human breast

All humans have a pair of breasts: on the left and right sides of the upper ventral region of the torso. The breast tissue is measured from underneath the collarbone to the level of the sixth or seventh rib, and from the sternum to the axilla. The female breast tissue comprises of external and internal features. The external feature is the central nipple (or mammilla) surrounded by a spherical disk of darkened skin called the areola. As seen in Figure 1.1, the internal features consist mainly of three tissues. (1) The milk-producing glands made up of 15 to 20 lobes. Each lobe is subdivided into smaller lobules that further branch into many tiny bulbs or alveoli where milk is produced. (2) the tubular ducts which link the lobules to the nipple and (3) the stroma, made up of fibrous connective tissues and fatty tissues that encase the lobules, ducts, blood and lymphatic vessels to provide, together with the chest muscles, a supportive framework and give the breast its distinctive shape and size (Macea and Fregnani, 2006; Ellis and Mahadevan, 2013).

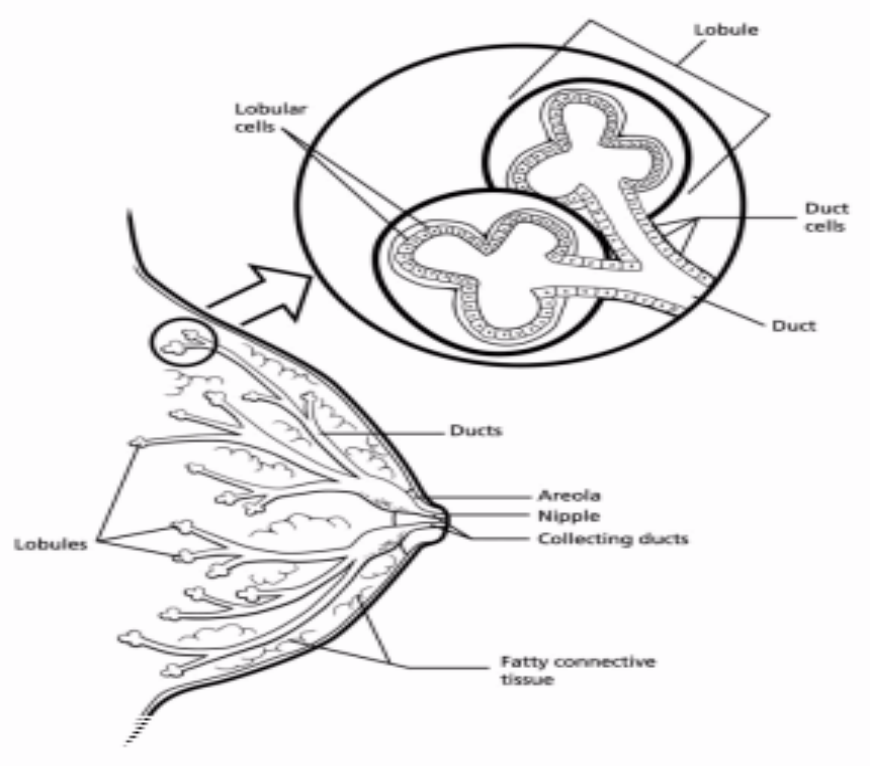

Figure 1.1 Internal anatomy of the female breast showing its distinctive shape provided by the stromal composition (connective and fatty tissues) and the organisation of epithelial cells of the ductal-lobular units that give the breast its milk-producing function. Image from Sarkar and Mandall (2011).

In addition, the breast is connected to the circulatory and lymphatic systems via blood and lymphatic vessels respectively. These connections are significant because blood delivers oxygen and nutrients to the breast tissue while removing waste material from the cells. The waste material and interstitial fluid are collected and transported via the lymphatic vessels in a clear fluid called lymph, which drains into the lymph nodes (Figure 1.2). These lymph nodes, which are significant in breast cancer diagnosis, are located in areas under the arm (axillary nodes), beside the sternum or inside the chest (internal mammary nodes) and above (supra) or below (infra) the clavicle (Suami *et al*, 2008; Ellis and Mahadevan, 2013).

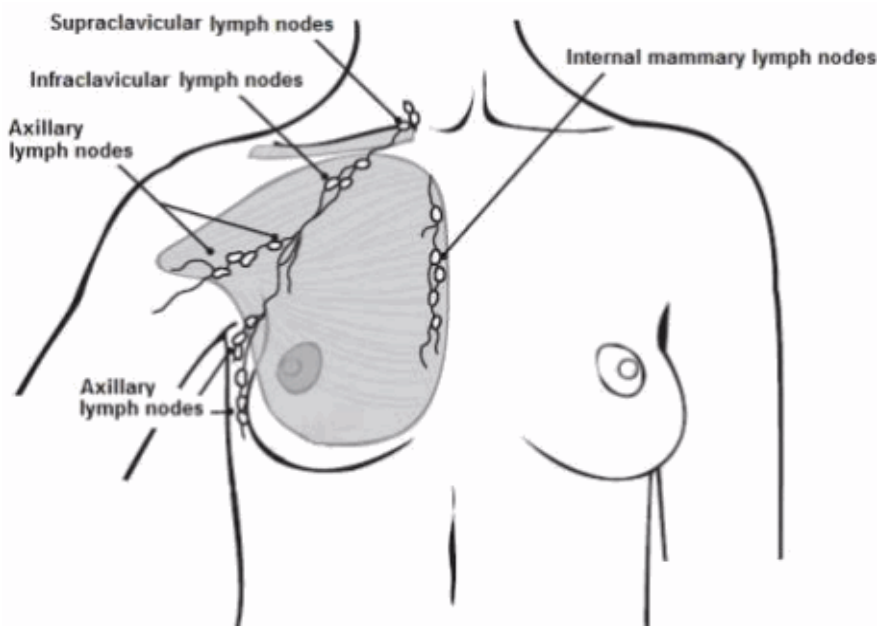

Figure 1.2 The location of the lymph nodes around the breast. Lymph nodes are important in the body's immunity but the presence of breast cancer cells in them is an indicator of the extent of metastasis around the body. Image from American Cancer Society.

1.5 The cell cycle

The appreciation of breast cancer, from initiation to histopathological and clinical outcomes, requires an understanding of the highly ordered and regulated complex sequence of events of the cell cycle. The cell cycle is the universal machinery by which cells in all organisms grow and divide. Triggered by external mitogenic stimuli, its processes, as seen in Figure 1.3, comprise four critical phases that can be grouped into two categories. The first group is the interphase which comprises 3 of the 4 critical phases: The G1, G2 and S phases. G1 and G2 are preparatory stages for cell progression into S and M phase, respectively. The fate of a cell to become quiescent or commit to further cycles of division is decided at the early stage of the G1-phase. Quiescent cells are metabolically active cells in a state of rest (G0) from the cell cycle. The S phase is the period of chromosomal duplication due to DNA replication. The second category, the mitotic or M-phase is subdivided into several distinctive phases which lead to nuclear division and cytokinesis. The M-phase is the final stage of the cell cycle that produces two genetically identical daughter cells from a parent cell (Shackelford *et al.*, 1999; Pinheiro and Sunkel, 2012).

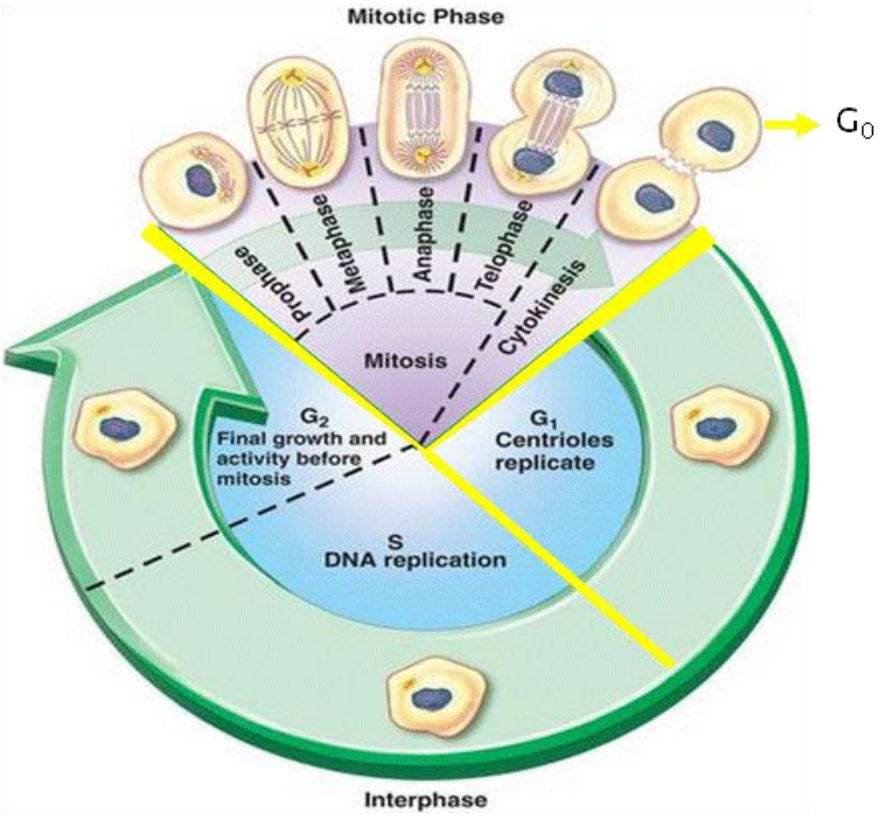

Figure 1.3 The four phases of the cell cycle. The cycle begins from interphase G_1 through to cytokinesis of the M phase. Intersections G1/S, G2/M and M/G1 (thick unbroken lines) indicate checkpoints with proteins that monitor and maintain genetic stability. Cells not committed to enter the cycle remain quiescent, G0. Image from Rausch and Kortleever (2011).

A cells progression through the four phases of the cell cycle is via a sequence of transient phosphorylations setup by complexes of catalytic cyclin-dependent kinases (CDKs) and their corresponding regulatory cyclins i.e. cyclin:CDK complex. These major regulatory proteins of the cell cycle overlap due to their fluctuating concentrations at various points in the cell cycle, as seen in Figure 1.4.

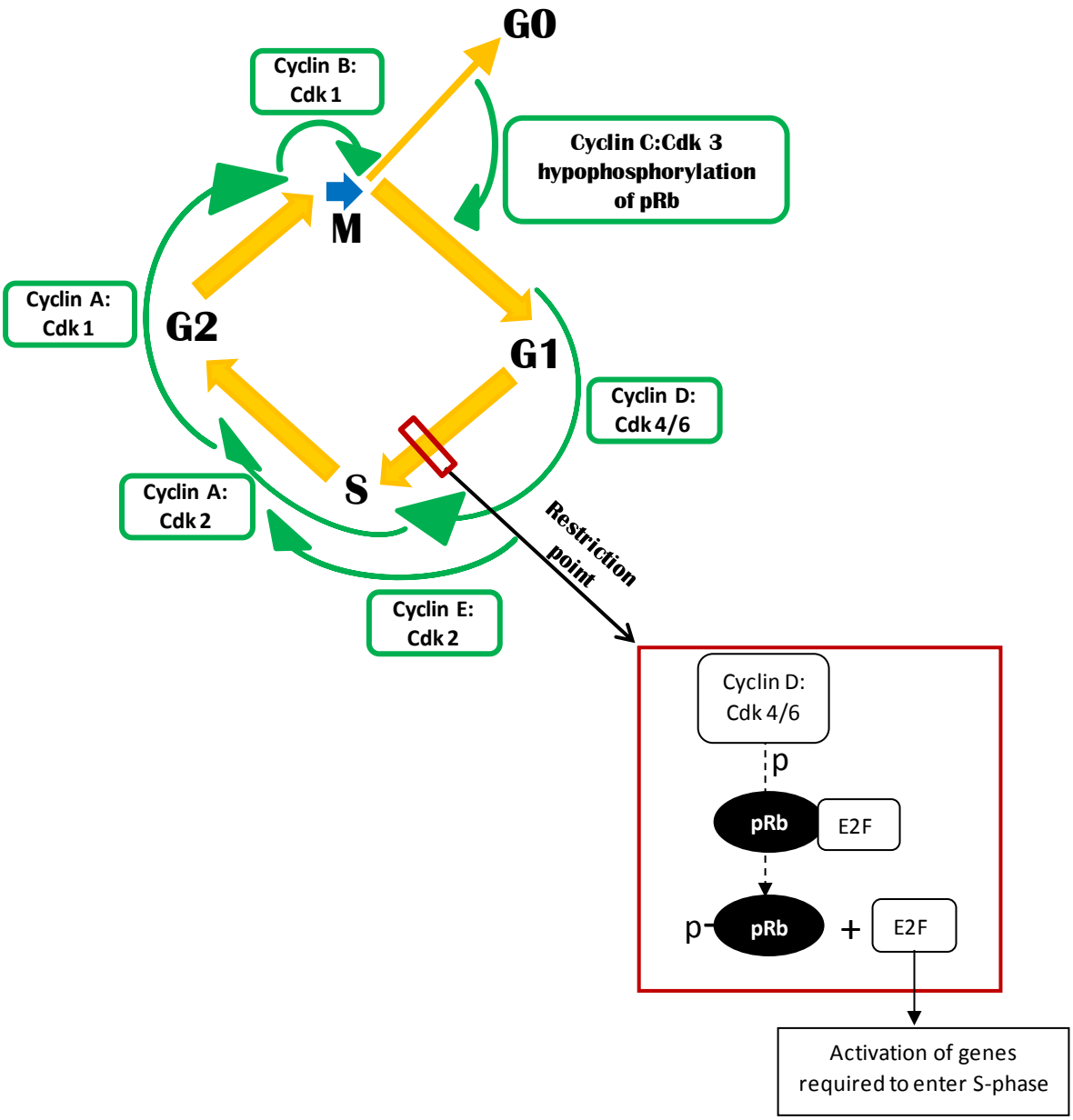

Figure 1.4 The cell cycle showing the order of Cyclin/CDK complexes in the phosphorylation cascade. The phosphorylation cascade helps to relay and regulate the cell from one stage of the cell cycle to the next, through checkpoints like the restriction point. Image from Townsend *et al* (2007).

The activation or inactivation of each complex depends on the addition or removal of phosphate from the two conserved phosphorylation sites of CDK (activating and inhibitory phosphate groups): addition of phosphate groups to CDKs inactivates cyclins:CDKs complexes while removal of inhibitory phosphate groups from CDKs by a Cdcs (phosphatases that belong to the Cdc25 family) activates cyclin:CDK. CDKs catalyze the covalent binding of ATP-derived phosphate to proteins that contribute to regulating the progression of the cell cycle. G0 to G1 transition is negatively regulated by unphosphorylated pRb. The re-entry of cells at G0 into the cell cycle at early G1, is dependent on the hypo-phosphorylation of pRb by cyclin C:CDK3 complex. Cell

progression through G1 is supported by growth factor-mediated induction of cyclin D which complexes with CDK4/6 to phosphorylate (inactivate) pRb. The pRb is a transcriptional repressor of the E2F (a transcription factor required for S-phase initiation) it is bound to resulting in inhibition of G1 to S transition. E2F is released to complex with other proteins which activate the genes required at the G1/S checkpoint and S-phase (which are also controlled by cyclin E:CDK2 and cyclin A:CDK2) by Cyclin D:CDK4/CDK6 hyper-phosphorylation of pRb at the restriction point (a point in late G1 at which the absence of growth factor stimulation does not inhibit cell cycle progression) (Figure 5). Cyclin A:CDK2 mainly controls the S-phase; G2/M checkpoint and the M-phase are controlled by cyclin A:CDK1 and cyclin B:CDK1, respectively. CDK1 is also known as Cdc2. Cells that divide are at a greater risk of acquiring mutations than cells that do not. Hence, to maintain genetic stability, the cell cycle has checkpoints occurring at G1/S, G2/M or M/G1. The events at these checkpoints in the cell cycle are regulated by several proteins seen in Figure 1.5. Some of these proteins detect errors in the cell's DNA e.g. Rad 9, Rad 1 and Hus 1 (the 9-1-1 complex) recruited by Rad 17 in response to DNA damage, while some generate information through signal transduction pathways (e.g. CHK1, CHK2). Also, some proteins (e.g. p53, pRB) act as response elements to halt the progression of a cell in the cycle either for repair or apoptosis (if DNA damage is irreparable). (Pagano *et al.*, 1992; Weinberg, 1995; Dyson, 1998; Kohn, 1999; Shackelford *et al.*, 1999; Zhu and Gooderham, 2006).

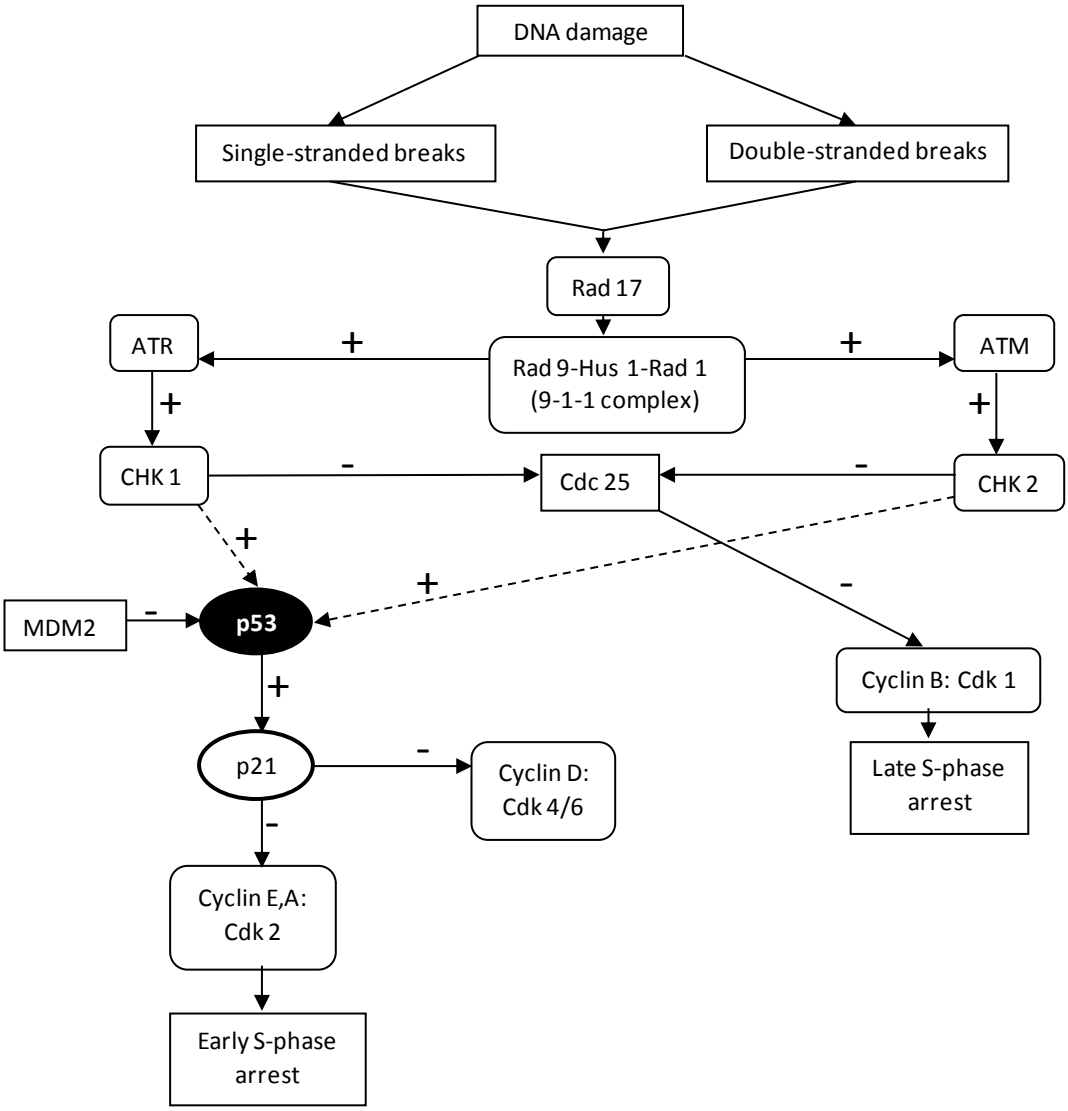

Figure 1.5 The cell cycle checkpoint signalling pathway. Sensor proteins (Rad 17 and 9-1-1 complex) detect DNA damage (single and double-stranded breaks) in chromatin. This facilitates ATR and ATM-mediated phosphorylation of CHK 1 and CHK 2, respectively. CHK 1 and 2 activate effector proteins e.g. p53, that arrest the cell cycle for DNA repair or apoptosis. Activated p53 induces cyclin kinase inhibitors (CKI) e.g. p21, p16, which negatively regulate cyclins at different stages of the cell cycle. Cdc 25 removes the activating phosphate of Cdk 1, therefore inhibiting progression of the S phase and the cell cycle. Image modified from Oesterreich and Fuqua (1999); Abraham (2001).

DNA damage at early (G_1/S) or late (S/G_2) S-phase initiates the ATM (ataxia telangiectasia mutated) and ATR (ataxia telangiectasia and Rad3-related protein) pathways. These mediators, respectively, activate downstream transducers checkpoint 2 and 1 kinases (CHK2 and CHK1) which phosphorylate (activate) p53. The phosphorylation of p53 disrupts its interactions with MDM2, hence inhibiting the degradation and repression of p53 transcription (Figure 5). Activation of p53 induces expression of CKIs (cyclin kinase inhibitors e.g. p21, p27) which restrain cyclins:CDKs

activity to enable DNA repair. Other important proteins involved in this interconnected regulatory process are p16 and p19 (Forsburg, 2002; Zhu and Gooderham, 2006; Junttila and Evan, 2009). Dysregulation in these proteins lead to cancer development.

1.6 Biology of breast cancer

Breast cancer is a complex heterogeneous disease which shows different histopathologies and clinical prognosis underlined by aberrant genetic, epigenetic and transcriptomic patterns that are distinct (vargo-Gogola and Rosen, 2007; Reis-Filho and Lakhani, 2008). It is initiated in epithelial cells of TDLU (terminal ductal lobular units) (Zhan *et al.*, 2008; Polyak, 2011). The probability of the morphological and physiological atypicality of breast tumours increases when mutations in key regulatory genes and abnormal amplifications in gene expression and gene products accrue (Lee and Muller, 2010; Polyak, 2011). The decision for a normal breast cell to proceed in the cell cycle, the duration of its mitotic division in the cycle and its discontinuation and exit from the cycle are controlled by signals from proteins of key genes grouped into proto-oncogenes and tumour suppressor genes (TSGs) (Murthy *et al.*, 2002).

For the tissues and organs of the human body to survival and develop, proto-oncogenes stimulate cell growth and inhibit cell differentiation and cell death. They do this by encoding certain proteins involved in a stepwise signal transduction cascade: Some of these proteins act as cell surface receptors which when bound to extracellular growth factor molecules, release growth signals into the cell for cell proliferation; some are intracellular proteins which control the transmission of the growth signal through the cytoplasm and others are transcription factors that enter the nucleus and directly turn on genes involved with cell division. In contrast, the proteins encoded by TSGs, at certain checkpoints, inhibit cells from entering or completing the cell cycle. This ensures that cells with damaged DNA either die by apoptosis or are repaired to prevent the passage of mutated DNA copies onto the cell progeny by the parent cell. This way the DNA or genome integrity is maintained and cell transformation is averted (Cavenee and White, 1995; Oliveira *et al.*, 2005; Chial, 2008; Lee and Muller, 2010). Although there is a crucial functional balance between these key regulatory genes to stimulate and inhibit cell proliferation, respectively, a succession of permanent mutations of these genes, in a single cell, can make them defective and initiate the multi-step progression to breast cancer development (Osborne *et al.*, 2004; Kenemans, *et al.*, 2004).

Mutation in one of the two alleles of a proto-oncogene is enough for the gene to be activated into a dominant-acting oncogene that brings about dysregulated gain-of-function of transformed breast cells. This is different for a tumour suppressor gene because its genetic alteration inactivates the purpose of its gene product: loss of function. The 'loss-of-function' effect is a recessive trait in that both functional copies (alleles) of the gene have to be mutated (Osborne *et al.*, 2004; Michor *et al*., 2004; Lee and Muller, 2010; Inoue *et al.*, 2013). This mutational event was discovered by Dr. Alfred Knudson, Jr., while trying to understand the genetic mechanisms behind inherited and acquired paediatric retinoblastoma. In 1971, he developed the classical Knudson's two-hit theory of tumour suppression (Figure 1.6), cited by Cavanee and White (1995), Oesterreich and Fuqua (1999) and Oliveira *et al.* (2005).

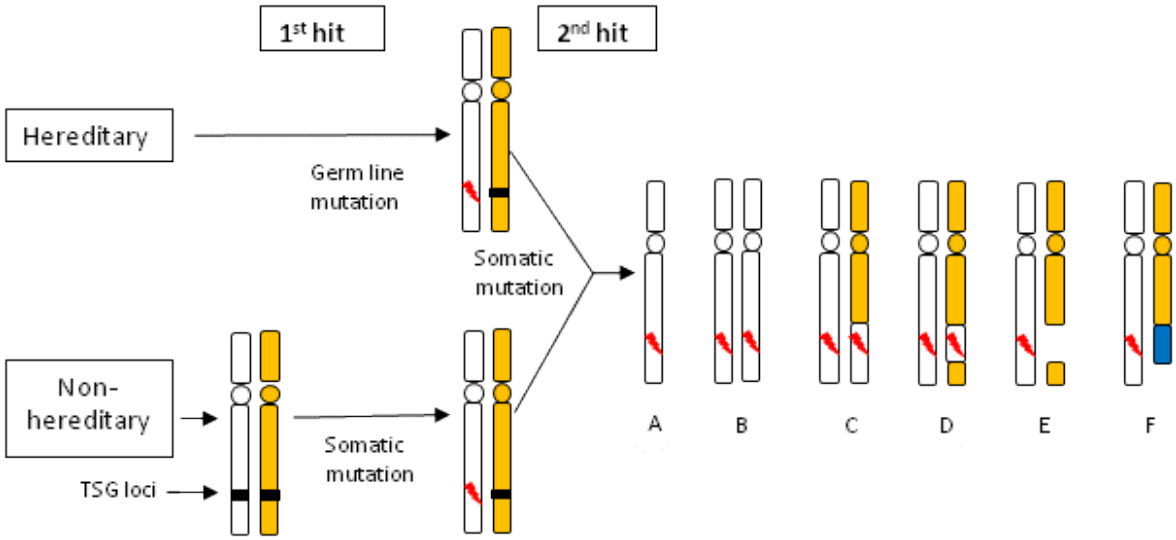

Figure 1.6 Model of the Knudson two-hit theory of inactivation of TSGs (e.g. RB). The white and yellow shapes represent paternally and maternally inherited allele, respectively, while the red lightning bolt shapes represent mutations at the TSG locus. The 1st hit (which could be point mutation or small deletion) of the hereditary and non-hereditary forms of TSG inactivation were germ line and somatic mutations, respectively, occurring at the locus of the first TSG copy. This predisposes a sporadic 2nd hit. The 2nd hit at the locus of the second TSG copy, which causes LOH of the TSG, is a consequence of chromosomal mechanisms: (A) Non-disjunctional loss without mutation reduplication; (B) Non-disjunctional loss with mutation reduplication; (C and D) mitotic recombination; and physical loss of TSG region either by (E) Subchromosomal deletion or (F) An unbalanced translocation. The result of LOH or hemizygosity of TSGs institute the establishment of neoplastic phenotype. Image modified from Devilee *et al* (2001); Oliveira *et al* (2001) and Jozwiak *et al* (2008).

He proposed that retinoblastoma was a consequence of the serial hits or defects of the two alleles of the retinoblastoma (*RB1*) gene which encodes the retinoblastoma tumour suppressor protein (pRb). Dr Knudson's theory applies to all tumour suppressors. Using

the *RB1* gene as a reference, his theory explains that the 'first hit' of both inherited and acquired retinoblastoma require, respectively, germline and somatic mutations of one copy of the gene. If the disorder is inherited, all cells in the body will carry the defective copy and if acquired, only retinal cells will have the defective copy. However, tumour development in the retina does not occur unless a somatic mutation of the second RB1 gene copy, which is independent of the first hit, occurs in both instances. The *RB1* gene copies become homozygous because they are mutated and functionally defective. The loss of heterozygosity (LOH) due to mutation of the second functional copy describes the inactivation of any TSG. The second hit is usually point mutations, gene deletions, mitotic non-disjunction with or without reduplication, chromosomal breaks (or deletions) and in some cases, somatic recombination between the mutated and normal copy of the TSG that leads to replacement of normal gene copy with a mutant copy (Chial, 2008; Tischfield and Shao, 2003; Isola *et al.*, 2003; Murthy *et al.*, 2002).

For oncogenic activation, alteration in the mutant copy is usually point mutations, deletions, gene amplification, chromosomal translocation (Siegel *et al.*, 1994; Chial, 2008). This can also include retroviral transduction and retroviral integration of viruses like the HPVs (Human Papilloma Viruses) and the EBV (Epstein-Barr Virus) (Lawson and Heng, 2010). Examples of proto-oncogenes mutated in breast cancer are: HER-2 (neu or ERBB-2) and c-myc.

On the basis of their function, TSGs can be categorized into gatekeepers, caretakers and landscapers. Gatekeepers directly inhibit tumour growth by inhibiting cell proliferation in the cell cycle and promoting apoptosis. The bi-allelic inactivation of these genes releases the brakes on cell proliferation and differentiation and directly contributes to cancer formation and development. Examples of gatekeeper genes linked to breast cancer are: p53 (or TP53), RB1, BRCA-1 and BRCA-2 genes. Caretakers are not directly involved in the controlling of the cell cycle: they maintain the integrity of the genome by involving in DNA repair. Hence, they are regarded as the 'guardians of the genome'. The inactivation of both alleles of a caretaker gene does not directly initiate neoplasia but results in genome instability which leaves cells at a high risk of further mutations in other genes, including the gatekeepers. Cells that lose heterozygosity in their caretaker genes are said to have a mutator phenotype. Examples of caretakers linked to breast cancer are: BRCA-1, BRCA-2, ATM and PTEN. The landscaper genes also do not directly control the cell cycle. The defects in their genes do not immediately affect cell proliferation but form a cellular or stromal environment that contribute to neoplastic cell transformation. Hence, the interactions between cells and their ECMs (extracellular matrices) are disrupted (Isola

et al., 2003; Loeb, 2001; Michor *et al.*, 2004; Osborne *et al.*, 2004; Oliveira *et al.,* 2005; Hanahan and Weinberg, 2011; Schneider, 2011).

1.6.1 Epigenetics of breast cancer

Proto-oncogenes and TSGs may be the major culprits implicated in breast cancer and other cancers, but there are mechanisms that, when deregulated by an effector, cause cancer without any genetic mutation. These mechanisms can be inherited, self-perpetuating and reversible and respond to developmental and environmental cues. These mechanisms are said to be 'epigenetic' (Riddihough and Zahn, 2010). Epigenetics was defined by Dworkin *et al.* (2009) as the study of how changes in gene expression can be inherited independent of any alterations in the genetic sequence. The deregulation of these mechanisms may include: (1) Inappropriate expression of transcriptional repressors that inhibit the expression of tumour suppressors. (2) Inappropriate negative regulation of mRNA translation by small non-coding RNAs called microRNA. This inhibits the constitutive expression of tumour suppressors to degrade transcriptional activators. (3) Silencing of tumour suppressors by hypermethylation of CpG (cytosine-phosphate-guanine) dinucleotides in the gene promoter. (4) Oncogene activation by ubiquitination of p53 protein, resulting in increased p53 proteolysis and inhibition of its function. (5) Disruption of key phosphorylation sites of tumour suppressor proteins that may result in mislocalization. (6) Permanent tumour suppressor silencing by methylation of histone H3 on lysine 27 (H3K27) (Oesterreich and Fuqua, 1999; Osborne *et al.*, 2004; Oliveira *et al.,* 2005; Dworkin *et al.,* 2009; Huang *et al.,* 2011). Examples of epigenetic effectors of breast tumorigenesis are polycyclic aromatic hydrocarbons (PAHs), hormones, viruses.

PAHs are carcinogens present in cigarette smoke, diet and environmental pollution (e.g. radiation). At the cellular level, PAHs are linked to be the epigenetic cause of breast cancer by repressing the expression of the breast cancer susceptibility gene, BRCA-1 (Jeffy *et al.*, 2002; Pensabene *et al.*, 2012). A Girl or a young woman who has not had her first full-term pregnancy is more susceptible to breast cancer than a woman who has. This is because her breast cells are immature stem cells. At the time of puberty, the breasts are most sensitive that these stem cells divide rapidly and can bind strongly to carcinogens, if exposed. Hence, the inefficient repair of carcinogen-mediated DNA damage by these immature undifferentiated cells affect the risk of breast cancer in later life (Brody and Rudel, 2003; Schkufza *et al.*, 2010).

1.6.2 Hormonal influence of breast cancer

The structure and function of the mammary gland vary from menarche to pregnancy to lactation to involution and to menopause. Very few anatomical changes occur pre-puberty: only a tiny duct of breast tissue at birth. Most of the changes to the anatomy of the breast begin at puberty. Puberty is the beginning of a girl's first menarche and it is when the female breast develops: the mammary epithelial cells proliferate to form branches of many ducts that terminate at the milk-producing alveoli, thus forming terminal ductal-lobular units. These changes to the micro-environment, at puberty, are mainly influenced by exposure to the ovarian steroid hormones, oestrogen and progesterone (Winchester and Winchester, 2006). These hormones have been linked to increased risk of mammary epithelial cell oncogenesis.

Oestrogen (E2 or 17β-estradiol) supports mammary epithelial cell proliferation through growth signal transduction pathways (Osborne *et al.*, 2004; Darbre, 2012) such as the mitogen-activated protein kinase (MAPK) pathway (Zhang and Liu, 2002; Lim *et al.*, 2006), cAMP signalling pathway (Aronica *et al.*, 1994) and the phosphatidylinositol 3 kinase (PI3K) pathway (Sui *et al.*, 2012). Via its cognate nuclear receptors, Estrogen Receptor α and β (ERα and β) (Harvey, 2009), oestrogen controls (genomically or non-genomically) several transcriptional factors and regulators in the G1 to S transition in the cell cycle (Mangelsdorf *et al.*, 1995; Kocanova *et al.*, 2010).

Progesterone (P4 or 4-pregenene-3,20-dione) helps develop normal mammary glands by enabling breast cells to reach a G1 check point, inducing their S-phase progression and preventing senescence. Its proliferative effects may be mediated via its high-affinity receptor isoforms, PR-A and PR-B. These progesterone receptors (PRs) act either as canonical nuclear transcription factors (ligand-activation through binding of the C-terminal or N-terminal motifs to progesterone response elements) or as cytoplasmic signalling molecules that function via the MAPK pathway. However, the effects of the latter have been linked to be the main mechanism of cellular proliferation in progesterone-induced breast cancer (Skildum *et al.*, 2005; Winchester and Winchester, 2006; Lange and Yee, 2008). Progesterone induces genes that are involved in biological processes such as cell adhesion, cell survival and inflammation. However, progesterone-induced inflammation can risk breast cancer development (Cody *et al.*, 2009). Early puberty may result in long term exposure to these hormones which can lead to deregulation of some of these pathways (Schkufza *et al.*, 2010; Lee and Muller, 2010).

1.6.3 Metastasis of breast cancer

Most patients with breast cancer die from its metastasis (Chaffer and Weinberg, 2011). Metastasis is a process by which cancer cells disseminate from their site of initiation to form secondary tumours at local (surrounding breast tissue), regional (to lymph nodes) and distant (other body organs) areas in the body via lymphatic and blood vessels (Weigelt *et al*, 2005). Metastasis of cancer cells can be inefficient because at various stages in the process the cancer cells can be inhibited (e.g. by host immune defence, lack of invasion or detachment factors etc.) (Hunter *et al.*, 2008; Fidler, 2003). Although the axillary lymph nodes are the first site of breast cancer metastasis (Comen and Norton, 2011); the liver, the lungs and the bones are the most common site of metastasis for this type of cancer (Irvin et al, 2011). Chaffer and Weinberg (2011) proposed a two-stage process for metastasis: (1) the physical translocation of a cancer cell into circulation as a result of the pressure from its cell size (supported by the 1929 'mechanical trapping theory' hypothesis by James Ewing, cited by Glinskii *et al.*, 2005) and (2) its progression into a metastatic lesion or secondary tumour (supported by the 1889 'seed and soil' hypothesis by Stephen Paget's, cited by Fidler, 2003). The seed and soil theory states that, 'metastasis depends on the cross-talk between selected cancer cells (the seeds) and specific organ microenvironments (the soil).' These hypotheses encompass distinct sequential steps that lead to the pathogenesis of cancer metastasis (Figure 1.7).

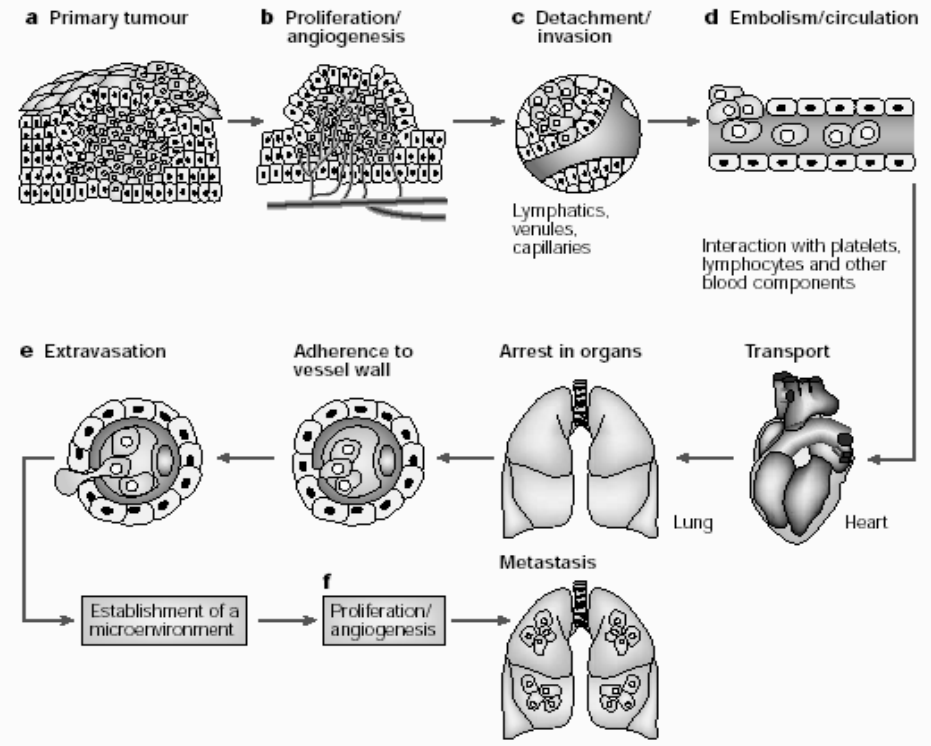

Figure 1.7 Steps in the formation of cancer metastasis. A cancer cell is able to initiate growth and division to form a primary tumour by secretion of vascular-generating angiogenic factors which facilitate extensive vascularisation of the tumour to access nutrients in the blood. As tumour size increases and disrupts adjacent cells, some cancer cells detach and travel through the bloodstream evading the host vessels of a secondary organ where they extravasate into the surrounding tissue of the secondary organ. If microenvironmental conditions are appropriate, they colonize the secondary site and form lesions to establish metastasis. Image modified from Fidler (2003).

Breast cancer metastasis to specific organ sites relies on the effect of the tumour cell-host interactions to homeostatic factors that activate tumour cell proliferation (e.g. EGF, TGF-β, FGF), survival, angiogenesis, invasion (e.g. Epithelial-Mesenchymal Transition (EMT), loss of E-cadherin, epithelial cell polarity and cytokeratin), and metastasis. It also relies, genetically, on the expression of metastatic gene products for basal membrane degradation (e.g. matrix metalloproteinases), migration (e.g. autocrine motility factor) and anchorage-independence (Weber, 2008; Fidler, 2003; Kalluri and Weinberg, 2009).

1.7 Classification of breast cancer

1.7.1 Histopathological classification

As a result of the heterogeneic nature of breast cancer, a classification of the histopathology to determine prognosis and treatment was necessary. Breast cancer can be classified as non-invasive (*in situ*) and invasive or both (Gathani *et al*, 2005; Rakha *et al*, 2010).

1.7.1.1 Non-invasive breast carcinomas

According to the American Cancer Society, non-invasive breast carcinomas are pre-cancerous cells. They are characterised by abnormal cell growth confined within the lining of the breast tissue where they start. They do not metastasize. Examples are DCIS (ductal carcinoma *in situ*) and LCIS (lobular carcinoma *in situ*)**.**

DCIS are the most common earliest forms of non-invasive breast carcinoma that occur inside the milk duct of the breast. DCIS tumours produce lumps. The cells are non-uniform but similar to cells of the breast duct. Tumour necrosis of large area of breast tissue sample is an indication of DCIS progression to becoming IBC. An example of this type of DCIS is comedocarcinoma (Wiechmann and Kuerer, 2008)**.**

LCIS occur inside the lining of the breast lobules and are common in pre-menopausal women. Tumour cells of LCIS are uniform cells similar to cells of the breast lobules and produce no lumps. Although LCIS is not a true cancer, it increases the risk of IBC (Simpson *et al*, 2003).

1.7.1.2 Invasive breast cancers (IBCs)

IBCs are aggressive tumours that can metastasize. Examples are invasive ductal carcinoma (IDC), invasive lobular carcinoma (ILC) (Wiechmann and Kuerer, 2008); less common IBC's (e.g. inflammatory breast cancer, Paget's disease of the nipple, triple negative breast cancer (TNBC), phyllodes tumour and angiosarcoma) and rare breast cancer types (e.g. tubular breast cancer, mucinous breast cancer, medullary breast cancer, and papillary carcinoma) have also been documented by the American Cancer Society.

1.7.2 Molecular Classification

The human mammary epithelium is made up of the *inner luminal cells* and the *basal myoepithilia* (adjacent the basal membrane). These two distinct cells types, which make up the lobules and ducts of the mammary gland, are the originators of most breast cancers. Most breast cancers occur in luminal cells rather than basal myoepithelial cells. The luminal cells line the apical surface of the mammary duct and have secretory properties while the basal myoepithelial cells surround the luminal cells and play a structural role (Figure 1.8) (Deugnier *et al*, 2002; Rakha *et al.*, 2008).

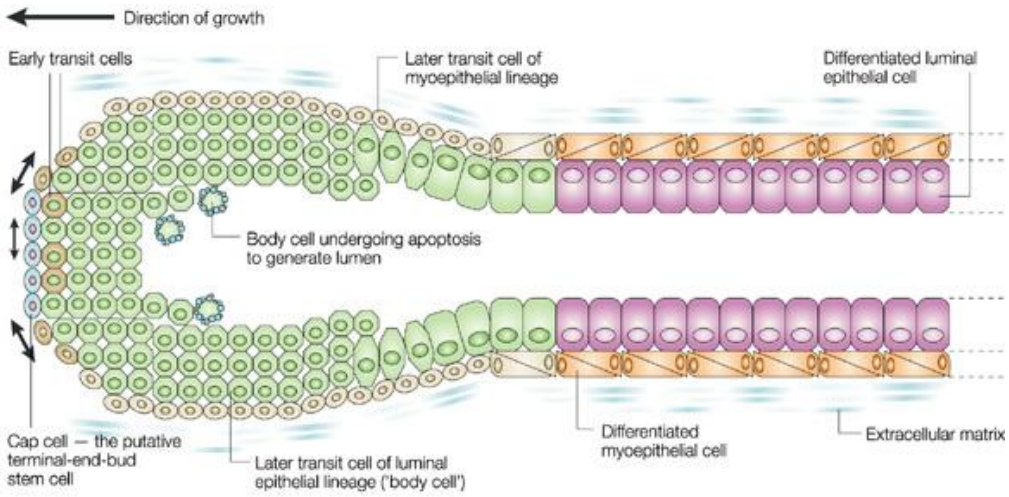

Figure 1.8 The formation of a terminal end bud (TEB) of a developing terminal ductal-lobular unit (TDLU) of the mammary gland. The diagram shows the structural arrangement and orientation (inner luminal and outer myoepithelial layers) of the two distinct cell types of the breast: luminal cells line the lumen of the duct due to their secretory function while surrounded by the contractile myoepithelial cells which are in contact with the basement membrane. The caps cells are putative stem cells that divide, asymmetrically, to generate a new cap cell and an early transit cell of myoepithelial lineage or of luminal lineage (body cell) that would differentiate into terminal luminal or myoepithelial cell. Image modified from Smalley and Ashworth (2003).

Immunohistochemical analysis and advanced molecular diagnostic techniques such as cDNA microarrays, have indicated the existence of four major molecular subtypes of breast cancer based on their hormone receptor (ER, PR) and human epidermal growth factor receptor (HER-2/neu) expressions (Andre and Pusztai, 2006; Cianfrocca and Gradishar, 2006). They are:

1.7.2.1 Luminal A tumours

These are ER+ (and/or PR+) and HER-2/neu-. They are low to moderate histological grade tumours due to their low expression of Ki67 antigen (Alfonso, 2009). This subtype has p53 gene mutations (Yanagawa *et al.*, 2012).

1.7.2.2 Luminal B tumours

These are ER+ (and/or PR+) and HER-2/neu+. They can also be HER2/neu–. Luminal B tumours are high histological grade tumours with high Ki67 expression, large tumour size, lymph node positivity and p53 gene mutations (Schnitt, 2011; Yanagawa *et al.*, 2012). Patients with luminal A or B tumours can respond well to endocrine therapy due to their ER+ status. Hence both luminal tumours have high survival to recurrence ratio compared to HER2 and basal-like tumours (Goldhirsch *et al.*, 2011; Andre and Pusztai, 2006; Voduc *et al.*, 2010).

1.7.2.3 HER2 tumours

These are ER-, PR- but HER-2/neu+. Expression of HER-2 and p53 mutation is high. They are high histological grade, non-luminal, metastatic, lymph node positive tumours (Rakha *et al.*, 2008; Schnitt, 2011; Goldhirsch *et al.*, 2011).

1.7.2.4 Basal-like tumours

They occur in basal epithelial cells. Most basal-like tumours have triple negative immunophenotype (i.e. ER-, PR-, and HER2/neu-). Hence the name, triple negative breast cancer (TNBC). HER-1 and cytokeratin5/6 proteins are highly expressed. Most TNBCs have p53 mutations and dysfunctional BRCA1 gene. Because of the lack of targets for endocrine or hormone therapy, this aggressive subtype poses the worst prognosis and survival rate. They have a high histological grade, metastatic rate (Nielsen *et al.*, 2004; Rakha *et al.*, 2008; Reis-Filho *et al.*, 2011; Schnitt, 2011).

1.8 Cell polarity and scribble (hScrib)

Avascularity, mitotic capacity, structural integrity of cytoskeleton, specialized adherens junctions and cell polarity (apical-basalateral and planar) are a few of the properties epithelial cells possess. Loss of these properties is typical of breast cancer cells (Rubbelke, 1999; Radisky, 2005). Cell polarity is a highly controlled asymmetrical distribution of intracellular organelles, cytoskeleton and cell surface of epithelial cells. It is a phenomenon that is typified by chemically and structurally discrete apical-basal axis

which is significant to the determination of cell type and conserved cell function (Wodarz and Nathke, 2007; Bernd, 2010). The loss of cell polarity is one of the properties of all cancers as the affected cells can overproliferate into tumours that are aggressive and invasive (Dow *et al.*, 2003: Humbert *et al.*, 2003). Epithelial cells are a coordinated group of adherent cell types whose polarity are regulated by proteins localized in appropriate plasma membrane domain (apical or basolateral membrane domain) of the cells (Figure 1.9). The transformation of epithelial breast cells to become invasive and metastatic in nature has been linked to the epithelial-mesenchymal transition (EMT) they undergo. EMT is a biological process that alters the cytoskeletal organization, cell-cell and cell-ECM (extracellular matrix) interaction of polarized epithelial cells to achieve mesenchymal cell phenotype. EMT is induced in the cells by transcription factors e.g. Twist, Slug, Snail, that initiate, through signalling pathways, increased apoptotic resistance, enhanced motility and invasiveness, increased ECM-component secretion, degradation of the basement membrane and loss of expression of the epithelial cell adhesion molecule called E-cadherin. The loss of E-cadherin (a transmembrane glycoprotein) at the adherens junction between neighbouring epithelial cells is significant in breast cancer invasiveness and metastasis (Wijnhoven *et al.*, 2000; Onder *et al*, 2008; Radisky, 2005; Kalluri and Weinberg, 2009; Mendez *et al.*, 2010; Hanahan and Weinberg, 2011). The transformed epithelial breast cells begin to express mesenchymal proteins e.g. N-cadherin, vimentin. In addition to the loss of E-cadherin, proteins that give the cells their polarity are also affected (Qin *et al.*, 2005).

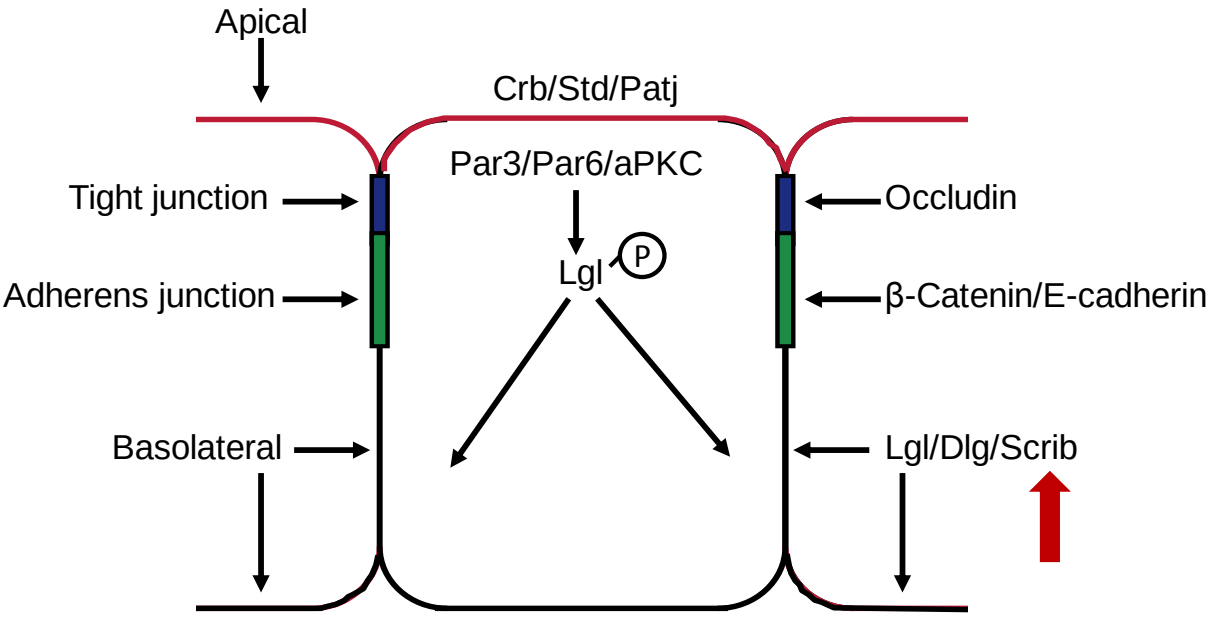

Figure 1.9 The polarity complexes that regulate the apical and basolateral domain of epithelial cells. These complexes interact to inhibit mislocalization from their domains. Crumbs (Crb) complex interacts with Partition (Par) complex to repress Par (at tight junctions) from the sub-apical of the apical domain and vice versa. Likewise, Par complex interacts with Scribble complex to repress Scribble (at the basolateral domain) from the tight junctions of the apical domain. Protein interactions between epithelial cells, at the tight junctions and adherens junctions, involve occludin and β-catenin-E-cadherin complexes, respectively. Image modified from Dollar and Sokol (2007).

These conserved planar polarity proteins, in Figure 1.9, that interact to maintain apical-basal polarity are grouped into three protein complexes: the Scribble or Scrib complex, the PARtition or PAR complex, and the Crumbs or Crb complex. PAR (PAR3/PAR6/atypical protein kinase C (aPKC)) and Crb (Crb/PALS1, STD and PATJ) complexes maintain the apical domain while Scribble (Scribble, DLG and LGL) complex maintain the basolateral domain (Kaplan *et al.,* 2009; Nelson, 2009; Lohia *et al.*, 2012). In the context of breast cancer, studies on Scrib have shown that its knockdown, misfold or mislocalization from cell contact site, in mammary epithelial cells, faults the cell polarity pathway thereby obstructing intercellular adhesion and 3D morphogenesis. In effect, epithelial breast cells with mutant hScrib gene overproliferate and become aggressive and invasive tumours (Dow *et al.*, 2003; Qin *et al.*, 2005). According to the NCBI database, the human Scribble (hScribble or hScrib) gene is a highly conserved gene located on 8q24.3 of the human genome and has two alternative spliced variants (variant 1 and 2). These variants are translated into isoforms **a** (1655aa, MW= 177,594Da) and **b** (1630aa, MW= 174,885Da) respectively, with isoform **a** being the longer of the two isoforms due to the presence of an in-frame exon in transcript variant 1. Large multi-domain hScrib protein localizes in the

basolateral domain of the plasma membrane of epithelial cells. It belongs to a family of LAP (LRRs and PDZ domains) proteins with LRRs (leucine rich repeats) at its amino (N-) terminus, 4 PDZ (PSD-95/Dlg/ZO-1) domains and a carboxyl (C-) terminal domain. Furthermore, hScribble protein belongs to a subfamily of LAP's called LAP4 (4 PDZ domains seen in Figure 1.10) (Bilder *et al.*, 2000; Qin *et al.*, 2005; Osmani *et al.*, 2006; Buday and Tompa, 2010).

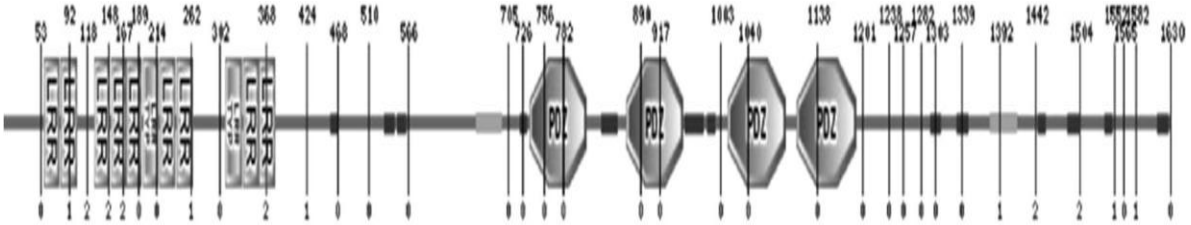

Figure 1.10 The Domain map of hScrib based on a cartoon from a SMART database. It shows the LRRs and four PDZ domains that facilitate hScrib control of signalling pathways such as protein-protein interactions with membrane or cytoskeletal proteins for localisation and signal transduction. Image from Metodieva *et al* (2013).

Signal transduction and protein-protein interactions of hScribble are mediated by its LRRs and PDZ domains respectively (Humbert *et al*, 2003). The PSD (post-synaptic density) complex binds various receptor, cytoskeletal and signalling proteins. DLG is involved in cytoskeletal reorganization. The ZO-1 (Zonal Occludens-1) is a tight junction protein that provides the structural foundation for the epithelial cells. They act as assemblers of a diverse set of junctional protein complexes at the cytoplasmic surface of the intercellular junctions (Albertson *et al.*, 2004; McNeil *et al.*, 2006; Bauer *et al.*, 2010; Buday and Tompa, 2010). The properties of these domains define hScrib's conserved role as a scaffold protein. As a scaffold protein, hScrib acts as a molecular bridge that tethers into close interaction an ordered array of complex signalling proteins. Its allosteric property enables hScribble to efficiently play a role in a diverse array of biological processes such as: 1.) Intercellular adhesion by associating with E-cadherin-β-catenin complex; 2.) Cell proliferation by formation of hScrib (PDZ domains)-APC (adenomatous polyposis coil)-β-catenin protein complex to regulate G1 to S phase progression of the cell cycle; 3.) Epithelial cell polarization (mediated in part by the LRR domain) by hScribble-ARHGEF7 (β-PIX)- PAK1-3 (p21-activated kinases)- GIT protein complex, coordinated through MAPK signal transduction cascade. This represses the Par and Crumbs complexes, limiting extension of the apical domain, consequently regulating orientation and invasiveness of migrating cells i.e. EMT to MET and vice versa (Osmani *et al.*, 2006; Good *et al.*, 2011; Greenwood *et al.*, 2011; Anastas *et al.*, 2012; Lodish *et al.*, 2013:59)

and 4.) Tumour suppression (Bilder *et al.*, 2000; Qin *et al.*, 2005). Although a tumour suppressor, hScrib has been implicated in breast carcinogenesis (Greenwood *et al*, 2011). Therefore this study seeks to understand how the cell polarity and tumour suppressor protein, hScrib, is implicated in invasion and metastasis of triple-negative breast cancer (TNBC).

1.9 Summary and context of study

A study by Metodieva *et al*. (2013) on CD74 overexpression in metastatic triple-negative breast cancers (TNBCs) identified hScrib as a likely target of CD74. The study found changes in hScrib when CD74 was overexpressed. 1.) Localization: hScrib is a peripheral membrane protein but in the presence of CD74 overexpression, translocates to the cytoplasm of the cell. 2.) Pattern of post-translational modification: despite the total amount of hScrib remaining unaffected, the amount of three phosphopeptides at the C-terminal of hScrib decreased significantly in CD74 overexpressing cells. This was due to the change in phosphorylation pattern of four specific serine sites of the phosphopeptides which are at 1306, 1309, 1348 and 1448 positions of the amino acid sequence of hScrib. It was these findings that formed the basis of this research, with the objective of elucidating the mechanisms by which the phosphorylation of hScrib at serine positions 1306, 1309, 1348, and 1448, affects its role in normal and cancer cells. The plan (aim) for achieving this objective include: 1.) Mutating the four serine sites found in the Metodieva *et al*. study to generate mutants that mimic unphosphorylated and phosphorylated hScrib, respectively; 2.) Study the effect of hScrib mutations on cellular localization; 3.) Study the effect of hScrib mutations on cell proliferation and migration/invasion; 4.) Study the effect of hScrib mutations on the cell cycle; 5.) Study the effect of hScrib mutations on interactions with its binding partners.

2. Materials and Methods

2.1 Reagents

Protein A/G magnetic beads, isopropanol, HCl, DMSO, TEMED, Tween 20, Triton X-100, BSA (Bovine Serum Albumin), Formalin (37% wt in ddH_2O), MTT powder, Propidium iodide powder and RNase A solution were from Sigma-Aldrich. MTT solvent (acidic isopropanol) was prepared as a 1.5% (v/v) solution of HCl in isopropanol with 10% Triton X-100. TurboFect, DAPI, dNTP set, DTT, 10X tango buffer and Protease and Phosphatase inhibitor cocktail were from Thermo Scientific. Electrophoresis-grade agarose, SDS, Tris base, glycine, absolute ethanol and methanol were from Fisher Scientific. 6X orange loading dye solution, O'GeneRuler DNA ladder mix and PageRuler Prestained Protein Ladder were from Fermentas. VectaMount was purchased from Vector Laboratories. 30% Bis-acrylamide/acrylamide mix was from National Diagnostics. APS was from Bio Rad. Marvel original dried milk (non-fat).

2.2 Media and enzymes

DMEM and RPMI 1640 cell culture media were purchased from Lonza while FCS was from biosera. Tryptone, NaCl, yeast extract and agar, used for preparing LB 2xYT agars and broths, were purchased from Thermo Scientific. LB (LB broth= 10g tryptone, 10g NaCl, 5g yeast extract; LB agar= 1.5% agar added, H_2O= 1L). 2xYT (2xYT broth= 16g tryptone, 5g NaCl, 10g yeast extract; 2xYT agar= 1.5% agar added, H_2O= 1L). Trypsin, *Pfu* DNA polymerase, *HindIII*, *EcoRI* and *DpnI* were also purchased from Thermo Scientific.

2.3 Antibiotic and antibodies

The antibiotic, kanamycin disulfate salt, was purchased from Sigma-Aldrich. Anti-scribble antibody (Rb mAb to SCRIBBLE) was from abcam while GFP antibody (GFP (B-2) mouse monoclonal IgG_{2a}) and Scrib antibody (Scrib (C-6) mouse monoclonal IgG_{2b}) were purchased from Santa Cruz Biotechnology.

2.4 Buffers

TAE (50X) buffer solution (121g Tris base, 18.6g disodium EDTA, 28.6mL glacial acetic acid in 500mL ddH_2O). 0.5M Tris (12.1g Tris base in 200mL ddH_2O, pH=6.8). 1.5M Tris (36.3g Tris base in 200mL ddH_2O, pH=8.8). Tank (Running) buffer (5X) (15.1g Tris base, 93.8g Glycine, 5% SDS in 1L ddH_2O). Transfer buffer (5X) (15.1g Tris base, 72.1g Glycine in 1L ddH_2O). TBS (10X) (24.2g Tris base, 80g NaCl in 1L ddH_2O, pH=7.6). TBS-T (1X) (100mL TBS, 0.1% Tween 20 in 1L ddH_2O).Transformation buffer (0.59g HEPES (4-(2-hydroxyethyl) piperazine-1-ethanesulfonic acid), 0.55g $CaCl_2.2H_2O$, 4.65g KCl in 100mL ddH_2O, pH= 6.7 + 2.7g $MnCl_2.4H_2O$). Lysis buffer (150mM NaCl, 10% IGEPAL, 100mM Tris, protease and phosphatase inhibitor cocktail). PBS (10X) (80mM Na_2HPO_4, 20mM KH_2PO_4, 1.37M NaCl, 27mM KCl, pH=7.4). PBS (1X) for tissue culturing was prepared by the kitchen staff in the School of Bioscience, University of Essex.

Other materials: Nitrocellulose paper and 0.2mL PCR tubes were from Sigma-Aldrich. The plasmid miniprep kit was from Thermo Scientific (and also QIAGEN). Nalgene 0.20µm syringe filter was also purchased from Thermo Scientific. PVDF was purchased from Merck Millipore.

2.5 Cell line, template and mutation primers

HEK293T cell line was purchased from Thermo Scientific. The recombinant plasmid, pEGFP-C1-Scrib, that was used as a template in SDM was a kind gift from Professor Ian Macara from Vanderbilt University. The mutation primers designed were purchased from Eurofins MWG Operon.

2.6 Bioinformatics

Accession number Q14160, received from Dr. Metodiev from the University of Essex, was used to acquire the cDNA sequence (to design the mutation primers) of hScrib through the ‘tblastn’ program of BLAST (Basic Local Alignment Search Tool) on the NCBI website (http://www.ncbi.nlm.nih.gov/).

DNA sequencing results were run through the ‘blastx’ program of BLAST to validate mutations at the desired sites in the amino acid sequence of hScrib.

Enrichment analysis of statistically analyzed MS/MS data was performed using the KEGG and Wikipathways databases of WebGestalt (Web-based Gene set analysis toolkit). The reference set hsapiens_genome was chosen during the analysis.

2.7 The pEGFP-C1-Scrib recombinant plasmid

The pEGFP-C1-Scrib is a recombinant plasmid comprised of the pEGFP-C1 vector and the wildtype *hScrib* gene. The construct has *hScrib* gene inserted between *HindIII* and *EcoRI* of pEGFP-C1 MCS which is downstream of the C-terminus of the *EGFP* gene (Figure 2.1), thereby enabling GFP-tagged hScrib protein expression when pEGFP-C1-Scrib is transfected. The kanamycin resistant (*KanR*) gene in pEGFP-C1 vector was used as a selective marker.

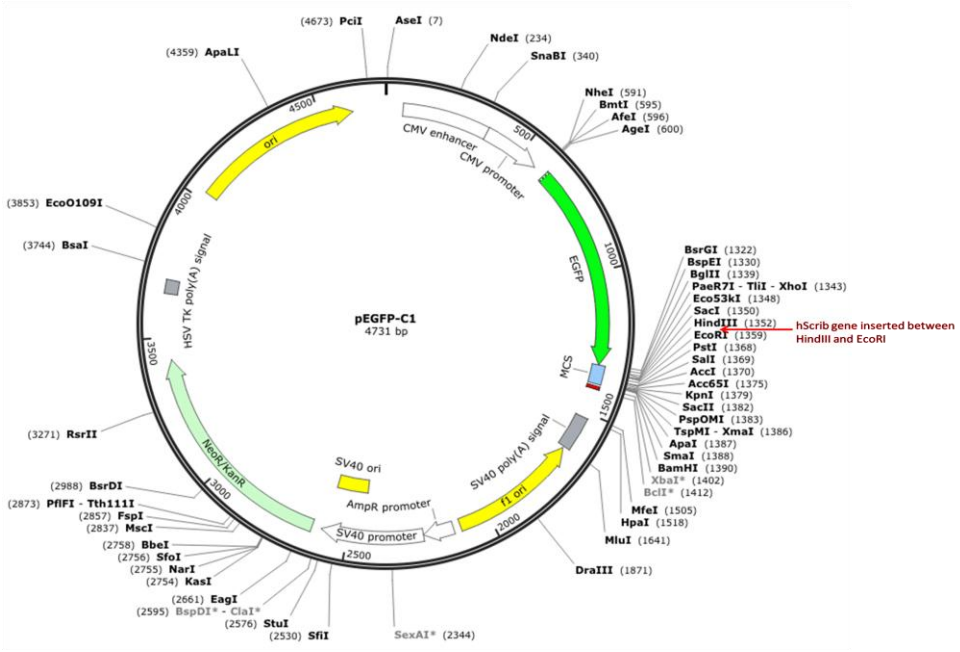

Figure 2.1 Restriction map of the 4.7kb pEGFP-C1 vector made into a recombinant plasmid by the fusion of hScrib gene into the MCS at the C-terminus of EGFP (enhanced green fluorescent protein). The integration of the hScrib gene (indicated by red arrow) was between *HindII* and *EcoRI* of the MCS. With the recombinant pEGFP-C1-Scrib as a template, the introduction of mutations into the hScrib gene was possible. Image was obtained from: http://www.snapgene.com/resources/plasmid_files/fluorescent_protein_genes_and_plasmids/pEGFP-C1/. The nucleotide sequence of the cloning vector can be obtained from: http://www.ncbi.nlm.nih.gov/nuccore/U55763.1.

2.8 Diagnostic restriction enzyme digestion of pEGFP-C1-Scrib

To verify the molecular size of the *hScrib* gene (5201bp) in pEGFP-C1-Scrib (approximately 10kb), a diagnostic restriction enzyme digestion reaction (Table 2.1) was performed. 0.5µg of pEGFP-C1-Scrib was simultaneously digested with *HindIII* and *EcoRI* in 2X tango buffer, which was compatible with both enzymes. The total reaction volume (10µL) was left for 1.5hrs to incubate in a 37^{o}C water bath.

Table 2.1 Diagnostic restriction digest reaction

	Reagent volumes (µL)				
Samples	2X Tango buffer	2X EcoRI	2X HindIII	Milli-Q H_2O	pEGFP-C1-Scrib
EcoRI	2.0	2.0	0.0	5.4	0.6
HindIII	2.0	0.0	2.0	5.4	0.6
EcoRI + HindIII	2.0	2.0	2.0	3.4	0.6

In 2X tango buffer, EcoRI had 100% restriction enzyme activity while HindIII had 50-100% restriction enzyme activity. An EcoRI only and HindIII only sample were prepared to observe what size supercoiled pEGFP-C1-Scrib would be when linearized by either restriction enzyme. It was also to observe which enzyme would produce star activity in the 2X tango buffer. No star activity was observed. 1X tango buffer was not compatible with both enzymes: it was not recommended for EcoRI despite the 50-100% restriction enzyme activity with HindIII. The 2X tango buffer was derived from a stock concentration of 10X tango buffer.

2.9 Antibiotic preparation

To facilitate selection, LB agar and broth were treated with kanamycin antibiotic. 50mg/mL (1000X) stock concentration of kanamycin was prepared by dissolving 0.5g of kanamycin disulfate salt in 10mL of milli-Q water, filter-sterilized with 0.20µm nalgene syringe filter (and a 10mL syringe) and stored at -20^{o}C in 1.0mL aliquots. Kanamycin was used in 1:1000 when preparing selective LB agar and broth.

2.10 Replication, extraction, purification and measurement of pEGFP-C1-Scrib

A glycerol stock of dam^{+} strain of *E.coli* containing pEGFP-C1-Scrib, under aseptic conditions, was streak-plated on a selective LB agar and incubated overnight at 37^{o}C to yield individual colonies. One colony was picked and inoculated in selective LB broth and incubated at 37^{o}C for 12-16hrs while shaking at 250rpm. Replicated pEGFP-C1-Scrib was extracted and purified using a plasmid miniprep kit (Thermo Scientific or QIAGEN) according to manufacturer's instruction. The concentration and purity of pEGFP-C1-Scrib were measured with a Nanodrop 2000 UV absorbance spectrophotometer ($A_{260}/A_{280} \geq 1.8$; $A_{260}/A_{230} \geq 2.2$).

2.11 Design of mutation primers of hScrib

The positions of the four targeted serine residues in the amino acid sequence of hScrib and their corresponding codons were located from the cDNA sequence. These are: ^{1}S

(1306- **TCC**), ^{2}S (1309- **TCT**), ^{3}S (1348- **TCC**) and ^{4}S (1448- **TCC**). The primer pairs were designed to completely overlap and have at least one base substitution in the target codons, flanked on either side by 15 bases. These mutation primers substituted serine for alanine (A) and aspartate (D) (Table 2.2 and 2.3).

Table 2.2 Primers designed to substitute the target serine residues for alanine (A)

PRIMERS	TARGET CODONS	SEQUENCE	
S1306A	TCC	fwd	5' GGCCAGCAGCCGCCC**GCC**CCGCCTTCTCCGGAT 3'
		rvs	5' ATCCGGAGAAGGCGG**GGC**GGGCGGCTGCTGGCC 3'
S1309A	TCT	fwd	5' CCGCCCTCCCCGCCT**GCT**CCGGATGAGCTGCCC 3'
		rvs	5' GGGCAGCTCATCCGG**AGC**AGGCGGGGAGGGCGG 3'
S1348A	TCC	fwd	5' CCTGGGCCTGCAGCC**GCC**CCGGAGCAGCTGTCC 3'
		rvs	5' GGACAGCTGCTCCGG**GGC**GGCTGCAGGCCCAGG 3'
S1448A	TCC	fwd	5' AGGCAGAGCCCGGCG**GCC**CCCCCGCCCCTGGGA 3'
		rvs	5' TCCCAGGGGCGGGGG**GGC**CGCCGGGCTCTGCCT 3'
S[1306+1309]A	TCC & TCT	fwd	5' CCGCCC**GCC**CCGCCT**GCT**CCGGATGAGCTGCCC 3'
		rvs	5' GGGCAGCTCATCCGG**AGC**AGGCGG**GGC**GGGCGG 3'

The base changes on the mutated primers were made on the forward strand and not the reverse strand of hScrib cDNA. Fwd= forward strand; Rvs= reverse strand. S[1306+1309]A also named S-AA implies serine sites S1306 and S1309 were simultaneously mutated to alanine.

Table 2.3 Primers designed to substitute the target serine residues for aspartate (D)

PRIMERS	TARGET CODONS	SEQUENCE	
S1306D	TCC	fwd	5' GGCCAGCAGCCGCCC**GAC**CCGCCTTCTCCGGAT 3'
		rvs	5' ATCCGGAGAAGGCGG**GTC**GGGCGGCTGCTGGCC 3'
S1309D	TCT	fwd	5' CCGCCCTCCCCGCCT**GAT**CCGGATGAGCTGCCC 3'
		rvs	5' GGGCAGCTCATCCGG**ATC**AGGCGGGGAGGGCGG 3'
S1348D	TCC	fwd	5' CCTGGGCCTGCAGCC**GAC**CCGGAGCAGCTGTCC 3'
		rvs	5' GGACAGCTGCTCCGG**GTC**GGCTGCAGGCCCAGG 3'
S1448D	TCC	fwd	5' AGGCAGAGCCCGGCG**GAC**CCCCCGCCCCTGGGA 3'
		rvs	5' TCCCAGGGGCGGGGG**GTC**CGCCGGGCTCTGCCT 3'
S[1306+1309]D	TCC & TCT	fwd	5' CCGCCC**GAC**CCGCCT**GAT**CCGGATGAGCTGCCC 3'
		rvs	5' GGGCAGCTCATCCGG**ATC**AGGCGG**GTC**GGGCGG 3'

The base changes on the mutated primers were made on the forward strand and not the reverse strand of hScrib cDNA. Fwd= forward strand; Rvs= reverse strand. S[1306+1309]D also named S-DD implies serine sites S1306 and S1309 were simultaneously mutated to aspartate.

2.12 Site-directed mutagenesis of *hScrib*

The site-directed mutagenesis (SDM) performed was a QuikChange mutagenesis method developed and described by Stratagene (La Jolla, CA). It was also PCR-mediated with the conditions set up in a thermocycler (Table 2.4).

Table 2.4 PCR program setup

STEPS		TEMPERATURE (°C)	TIME	NO. OF CYCLES
	Pre-heat lid	105		
	Initial denaturation	94	4 mins	1
1	Denaturation	94	45 s	15
2	Annealing	60	1 min	
3	Extension	68	20 mins	
	Final extension	68	5 mins	1
	Final hold	4	∞ (indefinite)	

The PCR reaction mix (Table 2.5) was set up on ice, in 0.2mL PCR tubes. Total volume of each mix was 50µL.

Table 2.5 PCR reaction setup to generate *hScrib* mutants (A and D)

REAGENTS	S1306	S1309	S1348	S1448	NOP	NOT S1306	NOT S1309	NOT S1348	NOT S1448
10X Pfu Buffer with $MgSO_4$	5.0	5.0	5.0	5.0	5.0	5.0	5.0	5.0	5.0
DMSO (6%)	3.0	3.0	3.0	3.0	3.0	3.0	3.0	3.0	3.0
dNTP (0.2mM)	1.0	1.0	1.0	1.0	1.0	1.0	1.0	1.0	1.0
WT template (50ng)	N	N	N	N	N	-	-	-	-
Fwd Primer (0.8µmol/L)	0.4	0.4	0.4	0.4	-	0.4	0.4	0.4	0.4
Rvs Primer (0.8µmol/L)	0.4	0.4	0.4	0.4	-	0.4	0.4	0.4	0.4
Milli-Q H_2O	N	N	N	N	N	39.2	39.2	39.2	39.2
Pfu DNA polymerase (2.5U)	1.0	1.0	1.0	1.0	1.0	1.0	1.0	1.0	1.0

This table shows the PCR reaction set up. Controls: NOP (No Primer added) was used to check for contamination of template with primers, NOT (No Template added) was used to check for contamination of primers with template. N= volume of milli-Q water added to the reaction and volume of template DNA (equivalent to 50ng) added to the reaction. PCR reactions for S[1306+1309]A and S[1306+1309]D were performed using positively validated S1306A and S1306D hScrib mutant plasmids as templates with corresponding 1309A and 1309D primers, respectively. High Fidelity *Pfu* DNA polymerase was added last after a manual hotstart (hotstart on the thermocycler was turned off). Due to high GC content in the template and primer pairs (>72%) which could cause secondary structures and favour primer dimer formation, DMSO was added. 10X *Pfu* Buffer with $MgSO_4$ and dNTP (#R0181, Lot: 00135644) were from Thermo Scientific while DMSO was from Sigma Aldrich. Total volume of PCR mix= 50µL.

2.13 Dpn1 digestion

To remove the template (pEGFP-C1-Scrib) following completion of the PCR, 1µL of *Dpn1* was added to the PCR products and incubated for 4hrs in a 37^{o}C water bath.

2.14 Gel electrophoretic verification of PCR product

Agarose gel electrophoresis was performed on the PCR products, post-*DpnI*. 5µL of each PCR product was mixed with 1µL 6X orange loading dye solution and loaded into the wells of a 0.8% EtBr-infused agarose gel prepared with TAE buffer. 0.6µg pEGFP-C1-Scrib (control) and 2.5µL DNA molecular marker (O'GeneRuler DNA ladder mix) were also loaded. The gel was run in TAE buffer at 100V for 50mins. DNA bands were visualised under a long-wave UV source and imaged (Meyers *et al.*, 1976; Sambrook and Russell, 2001).

2.15 Optimization of SDM protocol

Some of the expected mutants were generated but it was difficult to produce other expected mutants, especially mutants containing more than one mutation. In addition, there was the absence of bands of PCR products and smears from *Dpn1* digestion when samples were run on agarose gel.

One reason put forward was the presence of DMSO. Due to high GC content in the template and primer pairs, there was the possibility of secondary structures (e.g. hairpin loops) and primer dimerization in the template and primers. DMSO was used to prevent these secondary structures (Capriotti and Capriotti, 2012). By binding to the primer pairs and in the minor and major grooves of the template DNA, DMSO interferes with the hydrogen bonding between bases of the primer pairs and between bases of the double helix structure of the template to enable the separation of dsDNA into ssDNA, with less energy, and favour primer-template specificity at the annealing step (Hardjasa *et al.*, 2010).

The absence of any visible bands, post-*Dpn1*, suggested that PCR products were not formed and hence the absence of primer-template hybridization. If no pcr products were formed, then the synthetic primer pairs were not used and should be seen as low molecular weight bands. However, the absence of the low molecular weight bands of the primer pairs in the samples and NOT control suggested that the primer pairs did not dimerize but remained single-stranded whilst not annealing to the template. Detection of ssDNA is very poor because very low affinity of EtBr for ssDNA (Sambrook and Russell, 2001).

The higher the GC contents of the primers (ranged from 57.9% to 84.6%), the higher the melting temperature (T_m) of the primers. Based on the T_m of each primer pair (ranged from 75.7^{o}C to 86.6^{o}C), a new annealing temperature (T_a) was decided. Due to the range of T_m's, too high T_a could cause insufficient or no specific primer-template hybridization and too low T_a could produce non-specific products from mis-match of base pairs. The initial T_a of 60^{o}C was low and provided not enough binding energy to overcome the energy, due to the presence of DMSO, which kept the primers and template single-stranded and caused the *Pfu* DNA polymerase to stall in catalyzing the extension phase of the program. By increasing the T_a to the extension temperature of 68^{o}C, there was enough binding energy to facilitate annealing with the added advantage of immediate extension of the

hybrids at that temperature. This theory facilitated the optimization of the initial three-step cycling program to a two-step cycling program (Table 2.6).

Table 2.6 Optimized PCR program setup

STEPS		TEMPERATURE (ºC)	TIME	NO. OF CYCLES
	Pre-heat lid	105		
	Initial denaturation	95	4 mins	1
1	Denaturation	95	45 s	15
2	Annealing + Extension	68	20 mins	
	Final extension	68	5 mins	1
	Final hold	4	∞ (indefinite)	

2.16 Transformation of PCR products

The PCR products were transformed in chemically competent *E.coli* cells that were prepared (with transformation buffer) according to the protocol used by the proteomics laboratory at the University of Essex. The PCR products were mixed with competent cells (1:10) and incubated in ice for 30mins before heat shocking in a 42^{o}C water bath for 45secs and cooling in ice for 5mins. 500µL of 2xYT broth was asceptically added to the samples and incubated at 37^{o}C in a shaker set at 250rpm for 1hr. The cells were pelleted at 25 ^{o}C and 10000 rpm for 2mins. 400µL of supernatant was discarded and the pellet resuspended in the remaining 100µL supernatant. The samples were spread-plated onto selective LB agar plates and incubated at 37 ^{o}C for 12-16hrs. 0.5µL GFP and pEGFP-C1-Scrib plasmids were also transformed alongside the samples to gauge transformation efficiency and as positive controls. The colonies derived were inoculated in selective LB broth and incubated at 37^{o}C in a shaker set at 250rpm for 12-16hrs. The extraction, purification and measurement of the plasmids were performed, as stated in Section 2.10.

2.17 DNA sequencing of *hScrib* mutant plasmids

For validation of mutation, samples of plasmids (derived from transformation) and mutation primers, according to the sample requirement of the company, were sent to either GATC biotech or Source BioScience for DNA sequencing.

2.18 Tissue culturing, transfection and harvesting.

Human embryonic kidney cell line HEK293T was grown at 37^{o}C and 6% CO_2, in either DMEM or RPMI 1640 cell culture medium supplemented with 10% FCS. The cells were passaged with trypsin every 48 hrs. Transient transfections were performed using TurboFect according to the manufacturer's instruction. However, the reverse transfection protocol option was preferred to the conventional transfection because of inconsistency in transfection efficiency due to detachment of cells from the monolayer when the transfection mix was added. Pending requirement for analysis, the transfected cells were harvested by washing the cells with PBS and storing at -80^{o}C.

2.19 Protein sample preparation for Western blotting

Samples of the transfected cells were mixed with 50µL of pre-chilled lysis buffer and incubated on ice for 15mins to permeabilize. The samples were cleared in a centrifuge (pre-cooled to 4 ^{o}C) for 15mins at 14000rpm. Following centrifugation, the supernatant of the samples were collected and total protein concentration was measured by dye-binding assay (1µL of sample, on nitrocellulose paper, was stained with amido dye and destained in destain solution). Samples with darker spots were diluted with 2X SDS loading buffer while lighter spots were diluted with 5X SDS loading buffer. Following this, the protein samples were reduced for 5mins in 15mM DTT and at 100 ^{o}C before centrifuging at 25 ^{o}C and 14000rpm for 30secs.

2.20 Protein separation by SDS PAGE prior to Western blotting

SDS PAGE gel layers to be cast were prepared as shown in Tables 2.7 and 2.8. 20µL of the reduced samples and 3.5µL of molecular weight marker (PageRuler Prestained Protein Ladder) were loaded and ran in tank buffer for 50mins at 180V.

Table 2.7 Resolving gel (9%)

Reagents	Volume (mL)
1.5M Tris-HCl pH 8.8	2.50
30% Bis-acrylamide/acrylamide mix	3.00
Milli-Q H_2O	4.50 (to 10mL)
APS	0.10
TEMED (added last)	0.01

Resolving gel was cast first. The volumes are for two mini gels to run A-mutant and D-mutant hScrib protein samples.

Table 2.8 Stacking gel (4%)

Reagents	Volume (mL)
0.5M Tris-HCl pH 6.8	2.50
30% Bis-acrylamide/acrylamide mix	1.30
Milli-Q H_2O	6.20 (to 10mL)
APS	0.10
TEMED (added last)	0.01

Stacking gel was cast after the resolving gel. Loading wells were made in the stacking gel. The volumes are for two mini gels to run A-mutant and D-mutant hScrib protein samples.

2.21 Western blot

The SDS PAGE-resolved protein samples were transblotted (for 1hr at 100V) with transfer buffer onto PVDF membranes. Membranes were blocked with 5% non-fat dried milk in TBS buffer and incubated on a rocker, at room temperature for 45mins. After blocking, the membranes were incubated overnight at 4 ^{o}C with two primary antibodies in 1:500 ratio (5% non-fat milk, 0.1% Tween-20, 10µL mouse GFP Ab, 10µL rabbit scrib Ab, 10mL TBS). Following overnight incubation, the membranes were washed thrice with TBS-T (once every 5mins on a rocker) and incubated, in dark boxes, at room temperature for 45mins with two secondary antibodies in 1:10000 ratio (2.5% non-fat milk, 0.1% Tween-20, 1µL anti-mouse GFP Ab, 1µL anti-rabbit scrib Ab, 10mL TBS). The membranes were washed a further three times with TBS-T before the proteins were visualized with ODYSSEY infrared imaging system (LI-COR Corporation).

2.22 Staining, fixation and imaging of transfected HEK293T cells

HEK293T cells were transfected on coverslips and washed with 1mL PBS. PBS was removed and replaced with 500µL of 3.7% formalin in PBS before incubating the cells at room temperature for 15mins. Formalin was aspirated and replaced with 500µL of 0.5% Triton in PBS. Triton was aspirated after incubating the cells at room temperature for 5mins. Following this, the samples were washed with 500µL of 0.1% BSA in PBS. BSA was aspirated and 500µL of DAPI in PBS (1:1000) was added. The cells were covered in aluminium foil and incubated on a rocker, at room temperature for 15mins. After incubation, the coverslips were air-dried ‘cell side up’. A drop of Vectamount was placed on the coverslips, mounted onto microscope slides and left to set overnight at 4^{o}C.

Nikon A1-R confocal microscope was used to capture images of the localization of the GFP-tagged hScrib protein samples expressed in the cells.

2.23 Cell-based assays

2.23.1 MTT assay

Cells were seeded at $1.5x10^4$cell/well, in a 96-well plate, on the day of transfection and incubated overnight at 37^0C in 6% CO_2. 0.01g MTT powder was dissolved in 2mL PBS to prepare 5mg/mL MTT solution which was filter-sterilized, wrapped in aluminium foil and stored at 4^oC before use. 20µL MTT solution was added to the samples and incubated at 37^oC for 4hrs. After incubation, the cell culture medium was aspirated and 300µL MTT solvent was added. The samples were covered in aluminium foil and incubated on a rocker, at room temperature for 15mins. Within 1hr, the absorbances of the samples were measured on a SpectraMAX Plus Microplate reader (with SoftMAX Pro software) set at 570nm with a 630nm reference.

2.23.2 Wound healing assay

Cells were seeded at $0.9x10^5$cell/well on the day of transfection and incubated overnight at 37^0C in 6% CO_2. After incubation, a horizontal scratch was made across the cell monolayer .The cell culture medium was aspirated and 1mL fresh cell culture medium was added. Large stitched images (0% overlap) of the gap closures were acquired, in the brightfield, at T= 0 and T= 24hrs with Eclipse Ti-E widefield microscope (Nikon) while the gap closures were quantified with Java's Image J software using the polygon selection tool (Liang *et al.*, 2007; Yue *et al.*, 2010; Riahi *et al.*, 2012; Treloar and Simpson, 2013). The migration rate of the cells to closing the gap was expressed as a percentage of wound closure:

$$\% \text{ wound closure} = [(A_{t=0} - A_{t=n})/A_{t=0}] \times 100$$

Where $A_{t=0}$ is the mean area of the wound after making the scratch and $A_{t=n}$ is the mean area of the wound healed (or gap closure) after 24 hours.

2.23.3 Flow cytometric assay and analysis

Samples from the wound healing experiment were collected and pelleted at room temperature and 3000 rpm for 5mins to remove old cell culture medium. 0.1% BSA in 50µL of PBS was used to wash the cells which were subsequently pelleted. 25µL of the supernatant was retained to re-suspend the cells. The cells were fixed with 1mL of ice cold 100% ethanol added dropwise while

vortexing. The fixed cells were left overnight at -20^{o}C. Subsequently, the cells were pelleted and resuspended in 200µL of RNase A-containing PI solution (25µg/mL PI and 100µg/mL RNase A solution in PBS) to eliminate the interference of RNA (Nunez, 2001). To facilitate nucleic acid staining, the resuspended cells were incubated for 4hrs in a dark cupboard at room temperature. After incubation, the cells were run through a BD Accuri C6 flow cytometer set to run at 10,000 events. The results from these runs were analysed with a FCS express 4 software program created by DeNovo Software Company.

2.24 Co-Immunoprecipitation (Co-IP) assay

The whole-culture synchronization method was used (Cooper *et al*, 2006; Rosner *et al*, 2013). Eight already harvested and frozen sample cultures of seven synchronous HEK293T cell line and one asynchronous HEK293T cell line were used. Two of the sample cultures were untransfected control samples (HEK293T and HEK293T(Noc)) while the other six were transfected with the following *hScrib* mutants: S[1348+1448]A, S[1348+1448]D, and recently generated mutants P1 (Glu1293stop) and P3 (Gly1624Stop). Volume of samples and buffers used are shown in Table 2.9.

Table 2.9 Volumes used in the Co-IP assay

Sample	Treatment	Harvested in	Lysis buffer (mL)	Vol. of cell lysate used for CoIP (mL)	Vol. of 1XPBS used to dilute CoIP cell lysate (mL)	Vol. Of cell lysate used for WB (mL)
HEK293T	None	150mm petri dish	1.00	0.70	0.70	0.30
S[1348+1448]A (Noc)	Nocodazole (100ng/µL)	100mm petri dish	0.50	0.45	0.45	0.05
S[1348+1448]D (Noc)	Nocodazole (100ng/µL)	100mm petri dish	0.50	0.45	0.45	0.05
S[1348+1448]A (dThdNoc)	Thymidine block + nocodazole (100ng/µL)	15mL centrifuge tube	0.50	0.45	0.45	0.05
S[1348+1448]D (dThdNoc)	Thymidine block + nocodazole (100ng/µL)	15mL centrifuge tube	0.50	0.45	0.45	0.05
P1 C-term big (Noc)	Nocodazole (100ng/µL)	15mL centrifuge tube	0.50	0.45	0.45	0.05
P3 C-term small (Noc)	Nocodazole (100ng/µL)	15mL centrifuge tube	0.50	0.45	0.45	0.05
HEK293T(Noc)	Nocodazole (100ng/µL)	15mL centrifuge tube	1.00	0.70	0.70	0.30

Each transfected cell sample, except HEK293T control, was synchronized by treating with either nocodazole alone or both nocodazole and thymidine. Apart from the HEK293T and HEK293T(Noc) controls, the same volume of lysis buffer was added to each culture dish or centrifuge tube used to collect the samples. Not all the cell lysate obtained from each sample was used in the co-immunoprecipitation (Co-IP) experiment. Some of the lysate was used in a western blot (WB) experiment.

These frozen sample cultures, in lysis buffer, were incubated at room temperature for 5mins on a fine PCR rotator and spun down in a pre-cooled centrifuge at 4^{o}C and 14,000rpm for 20mins. The cell lysates obtained after centrifugation were split (for CoIP and Western blot use) (Table 2.9). Cell lysates for CoIP were diluted (1:1) with PBS and probed with antibody: 3µg of Scrib (C-6) mouse monoclonal antibody were added to HEK293T and HEK293T(Noc) while 3µg of GFP (B-2) mouse monoclonal antibody were added to the other six samples. The probed samples were incubated at room temperature for 30mins on a rotator. 18µL of Protein A/G magnetic beads was added to each sample and incubated at room temperature for 1hr on the rotator. After incubation, the samples were placed on magnetic tube racks, to aggregate the beads, before removing the flowthrough. The magnetic beads were washed, four times, with 1mL wash buffer (0.1% triton in PBS) and aggregated to remove the wash buffer. After the fourth wash, the magnetic beads were resuspended in 1mL of PBS and split equally for western blot (WB) and mass spectrometry (MS) analysis. The flowthroughs of samples for MS and WB were discarded and the magnetic beads were stored at 4^{o}C pending usage. During usage (for samples required for MS), 20µL of solution containing trypsin and 1M urea was added to the magnetic beads and incubated overnight at 30^{o}C.

2.25 Mass spectrometry

Subsequent to Co-IP and trypsin digestion of the proteins into peptides, was the identification of the digested proteins with an electrospray ionization mass spectrometer which has a hybrid LTQ (Linear Trap Quadrupole)/Orbitrap Velos device coupled to a nanoscale HPLC (High Performance Liquid Chromatography) to ionize the peptides and enable high resolution of the peptide ions based on m/z (mass:charge). The mass spectrometer set-up (Greenwood *et al.*, 2012) was performed by Dr. Metodiev (Supervisor) to generate LC-MS/MS spectral counts and corresponding intensity values of the peptide ions. Both measures of relative protein abundance can be used in proteomic analysis.

3. The effect of hSCRIB mutations on cellular localization

3.1 Introduction

A significant feature of breast cancer cells is the loss of epithelial cell polarity (Chatterjee *et al.,* 2012; Royer and Lu, 2011; Bilder *et al.,* 2000). Cell morphology, physiology, regulation of EMT and cell proliferation are influenced by cell polarity (Greenwood *et al.*, 2011; Chaffer and Weinberg, 2011; Royer and Lu, 2011). Cell polarity is regulated by conserved, planar polarity protein complexes localized in the plasma membrane domain of the cells. The presence and localization of these protein complexes are important in mediating the apical and basolateral architecture of epithelial cells (Humbert *et al.,* 2003). Operating in the basolateral domain is the Scrib complex consisting of hScribble (hScrib), hDLG and LGL proteins (Kaplan *et al.,* 2009).

Breast cancer subtypes such as triple-negative breast cancer (TNBC) are difficult to treat because of the absence of established receptor markers to target. However, new molecules have been identified to be expressed in this breast cancer cells of which hScrib is implicated (Rakha *et al.*, 2008; Greenwood *et al.*, 2011). The hScrib is a scaffold protein whose function at intercellular junctions, to maintain cell polarity, affects cytoskeletal and tissue organization. Studies have shown that the mutation of the *hScrib* gene may affect the expression and mislocalization of its gene product from its typical basolateral domain, at the periphery of the plasma membrane, consequently disrupting the regulation of cell polarity. Epithelial breast cells lose cell proliferative and orientation control and become aggressive malignant tumours as a result (Dow *et al.*, 2003; Qin *et al.*, 2005; Metodieva *et al.*, 2013). This indicates that the effect of hScrib protein in epithelial cells is significant to the suppression of tumours. Hence, it is identified as a tumour suppressor (Bilder *et al.*, 2000).

In a study, it was found that hScrib was deregulated in metastatic breast tumour cells by the overexpression of CD74 (Metodieva *et al.*, 2013): hScrib localized to the cytoplasm and the pattern of post-translational modifications (PTMs) of hScrib was affected, despite the total amount of the protein remaining unchanged. Following a combined genomic-scale proteomic screen, four phosphoserine hotspots (S1306, S1309, S1348 and S1448) at the C-terminal part of hScrib protein were identified to be significantly affected by CD74 overexpression. Therefore, by respectively substituting these four serines with alanine (to

mimic unphosphorylated state of hScrib) and with aspartate (to mimic phosphorylated state of hScrib); this experiment aims to study the effect of hScrib (a functional human homolog of *Drosophila melanogaster* tumour suppressor DmScribble) mutations on cellular localization.

3.2 Molecular size of *hScrib* in pEGFP-C1-Scrib

To initiate this study, gel verification, by diagnostic restriction enzyme digestion (Section 2.8), of the molecular size of wildtype *hScrib* in pEGFP-C1-Scrib was performed and gel image of bands (Figure 3.1) was captured under UV light.

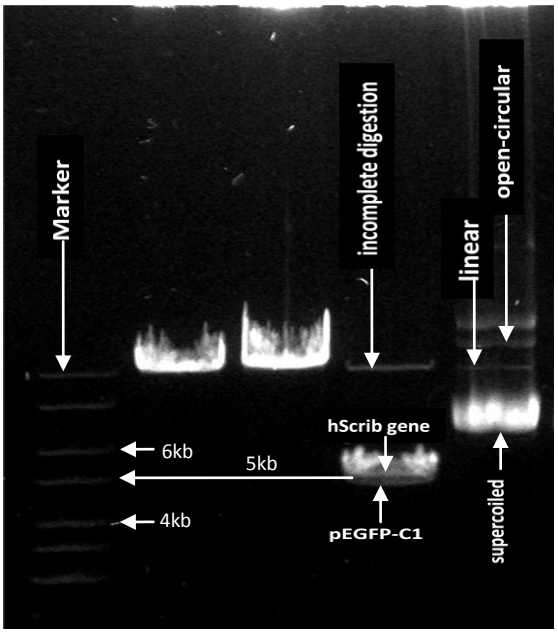

Figure 3.1 Gel electrophoresis image of diagnostic restriction enzyme digest of pEGFP-C1-Scrib. From left to right: Lane 1= Marker; Lane 2= EcoRI; Lane 3= HindIII; Lane 4= EcoRI + HindIII; Lane 5= supercoiled pEGFP-C1-Scrib (0.3µg) as control. The loading volume for all samples, except marker (2.5µL), was 6.6µL. Supercoiled pEGFP-C1-Scrib was used as control to indicate the size of the recombinant plasmid when not digested by enzymes.

The gel image above shows that in lane 5 there are different band sizes of undigested pEGFP-C1-Scrib which corresponds to the different conformations (supercoiled or covalently close-circular, linear and open-circular) it assumes (Jiang *et al.*, 2010). Lanes 2 and 3 each show a single band representing pEGFP-C1-Scrib digested by *EcoRI* and *HindIII*, respectively. Using lane 5 as a reference, these two lanes (2 and 3) show that when pEGFP-C1-Scrib is digested, its conformation becomes linear from supercoiled: its band size also changes to approximately 10kb from about 7kb (marker as reference). These observations are also true in lane 4 except there is more than one linear band of different sizes due to *EcoRI* + *HindIII* simultaneous digestion of pEGFP-C1-Scrib. *EcoRI* +

HindIII simultaneous digestion of pEGFP-C1-Scrib was expected to yield two bands but the presence of a third low abundance band with a size similar to lane 2 indicates digestion that could not be complete within the incubation time due to the 50-100% restriction activity of *HindIII* in the 2X tango buffer. However, the two closely similar lower band sizes in lane 4 indicate, to a large extent, a good double digestion. Using the marker (Lane 1) as a reference, one of the bands in lane 4 is just under 5kb and the other band is just over 5kb. This suggests that the latter, with a possible molecular size of 5.2kb (5201bp), may be the *hScrib* gene. Verification of the *hScrib* gene would be by DNA sequencing.

3.3 The *hScrib* mutants generated

After estimation of the molecular size of *hScrib* gene (in pEGFP-C1-Scrib) with diagnostic restriction enzyme digestion, pEGFP-C1-Scrib was used as template in the SDM process (Chapter 2.12). The mutants generated (Table 3.1) were validated by DNA sequencing.

Table 3.1 Validated hScrib mutants generated

	Positively validated hScrib mutant proteins									
	Single mutation				Double mutation				Triple mutation	
A-mutants	S1306A	S1309A	S1348A	S1448A	S[1306+1309]A		S[1348+1448]A		S-AA(1348A)	S-AA(1448A)
D-mutants	S1306D	S1309D	S1348D	S1448D	S[1306+1309]D		S[1348+1448]D		S-DD(1348D)	S-DD(1448D)
	New hScrib mutants validated									
	P1 (big C-term del)		P3 (small C-term del)		P4	P6	P7	P8	P9	P10
	E1293Stop		G1624Stop		C1297S	S1445A	S1445D	P1449A	S[1445+1448]A	S[1445+1448]D

This table shows the hScrib mutants that were confirmed by DNA sequencing (except P3 (E1293Stop)) to have the expected site mutation(s). P1 (E1293Stop) was also confirmed by mass spectrometry as well as P3 (G1624Stop). S[1306+1309]A and S[1306+1309]D are double mutations of hScrib also known as S-AA and S-DD, respectively. They were used as templates to generate the triple hScrib mutants.

The results were acquired through the 'blastx' program of BLAST which also verified the protein to be hScrib of human origin. Quality of the sequence results were examined on a chromatogram as shown for some of the mutants in Figures 3.2a, b, c, d, e and f.

Wildtype (**S1448**): 5’ AGG CAG AGC CCG GCG **TCC** CCC CCG CCC CTG GGA 3’

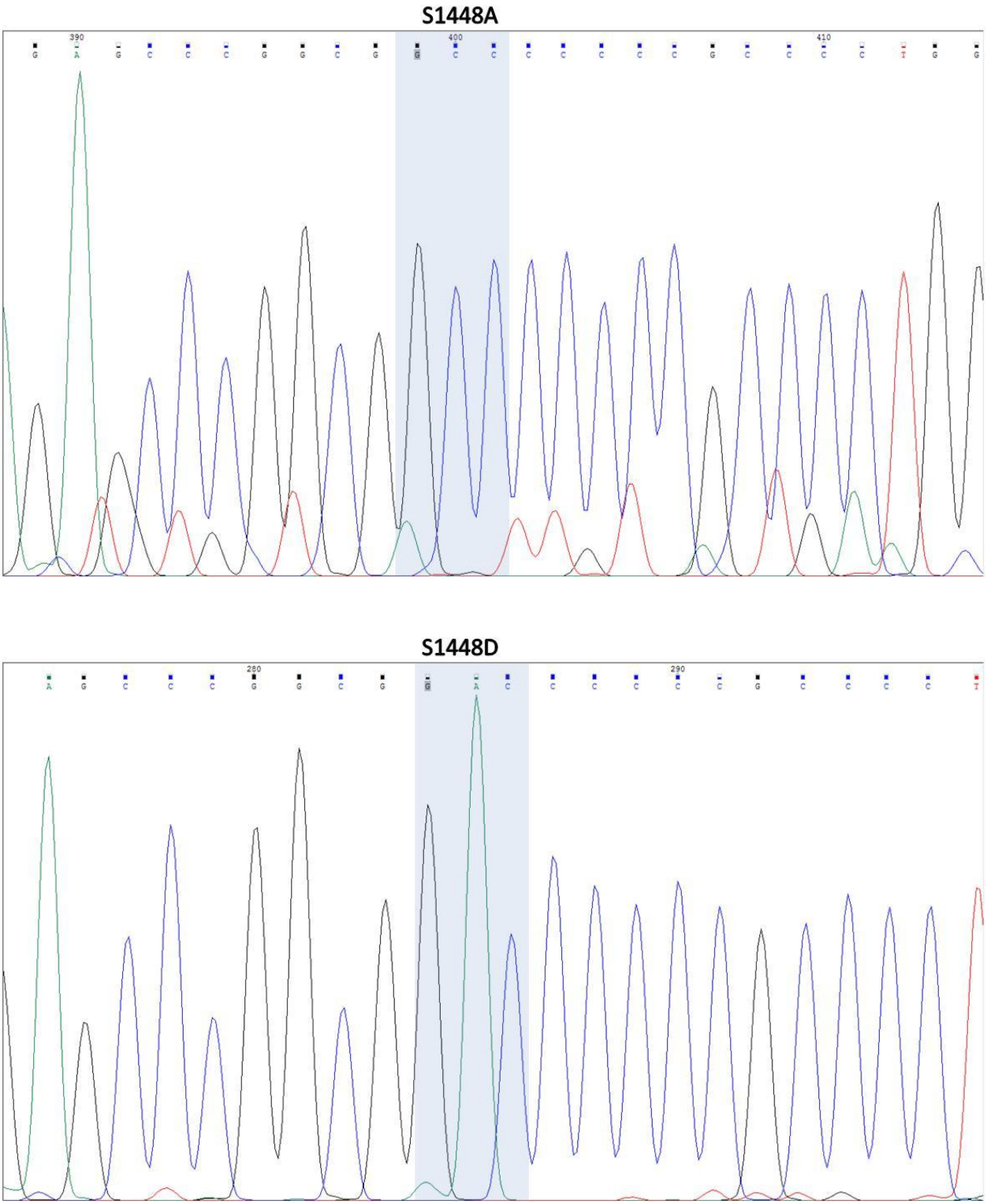

Figure 3.2a Chromatogram results of hScrib mutants S1448A and S1448D using Chromas Lite 2.1.1 software. The chromatograms show four different peak colours for each of the four bases: C = blue, A = green, T = red and G = black. The codon that was mutated is highlighted. The wildtype codon position, S1448, is highlighted above.

Wildtype (**S[1348+1448]**): 5’ CCT GGG CCT GCA GCC **TCC** CCG GAG CAG CTG TCC
--- AGG CAG AGC CCG GCG **TCC** CCC CCG CCC CTG GGA 3’

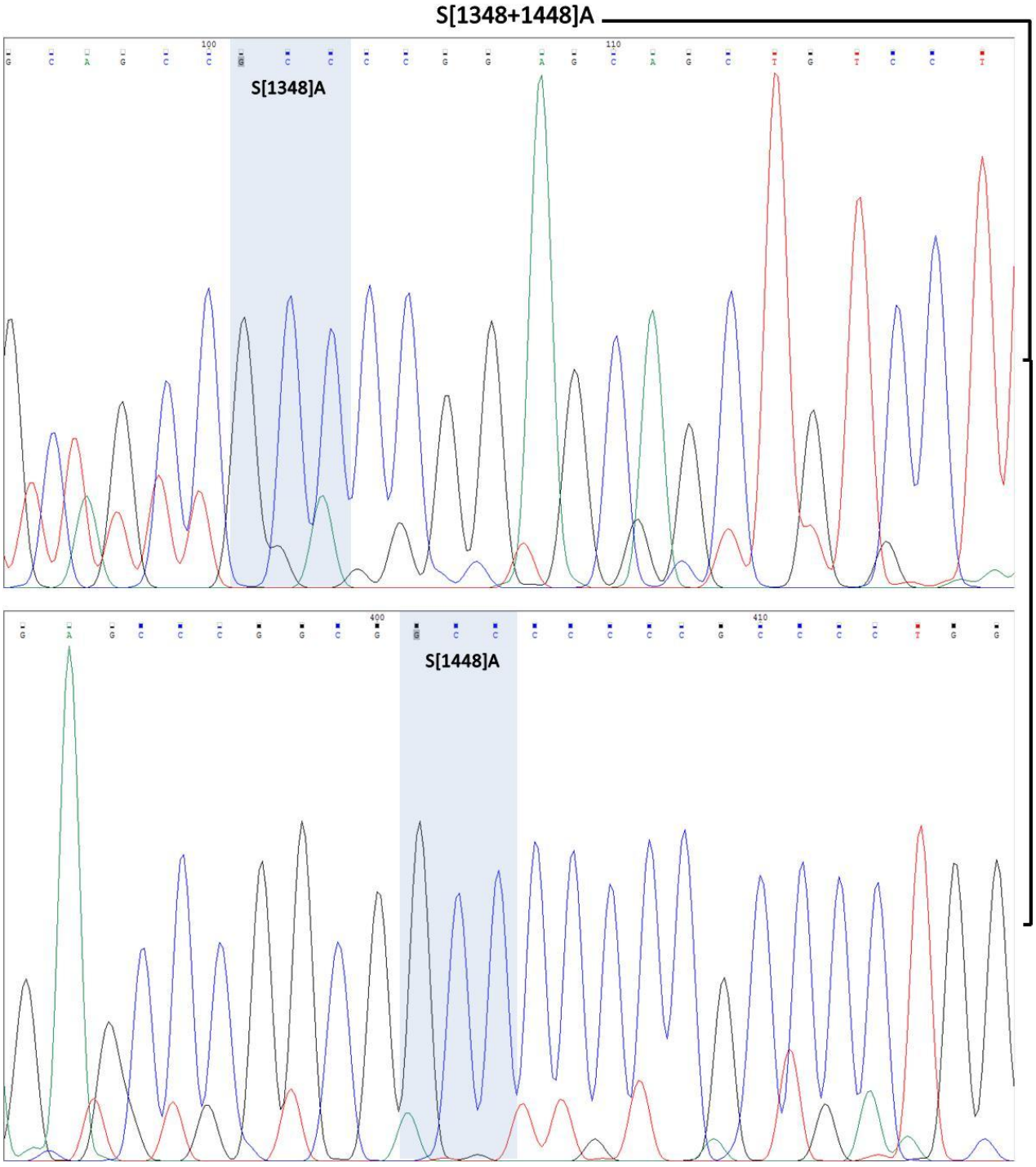

Figure 3.2b Chromatogram results of hScrib mutants S[1348+1448]A using Chromas Lite 2.1.1 software. The chromatograms show four different peak colours for each of the four bases: C = blue, A = green, T = red and G = black. The codons that were mutated are highlighted. The wildtype codon positions, S1348 and S1448, are highlighted above.

Wildtype (**S[1348+1448]**): 5’ CCT GGG CCT GCA GCC **TCC** CCG GAG CAG CTG TCC
--- AGG CAG AGC CCG GCG **TCC** CCC CCG CCC CTG GGA 3’

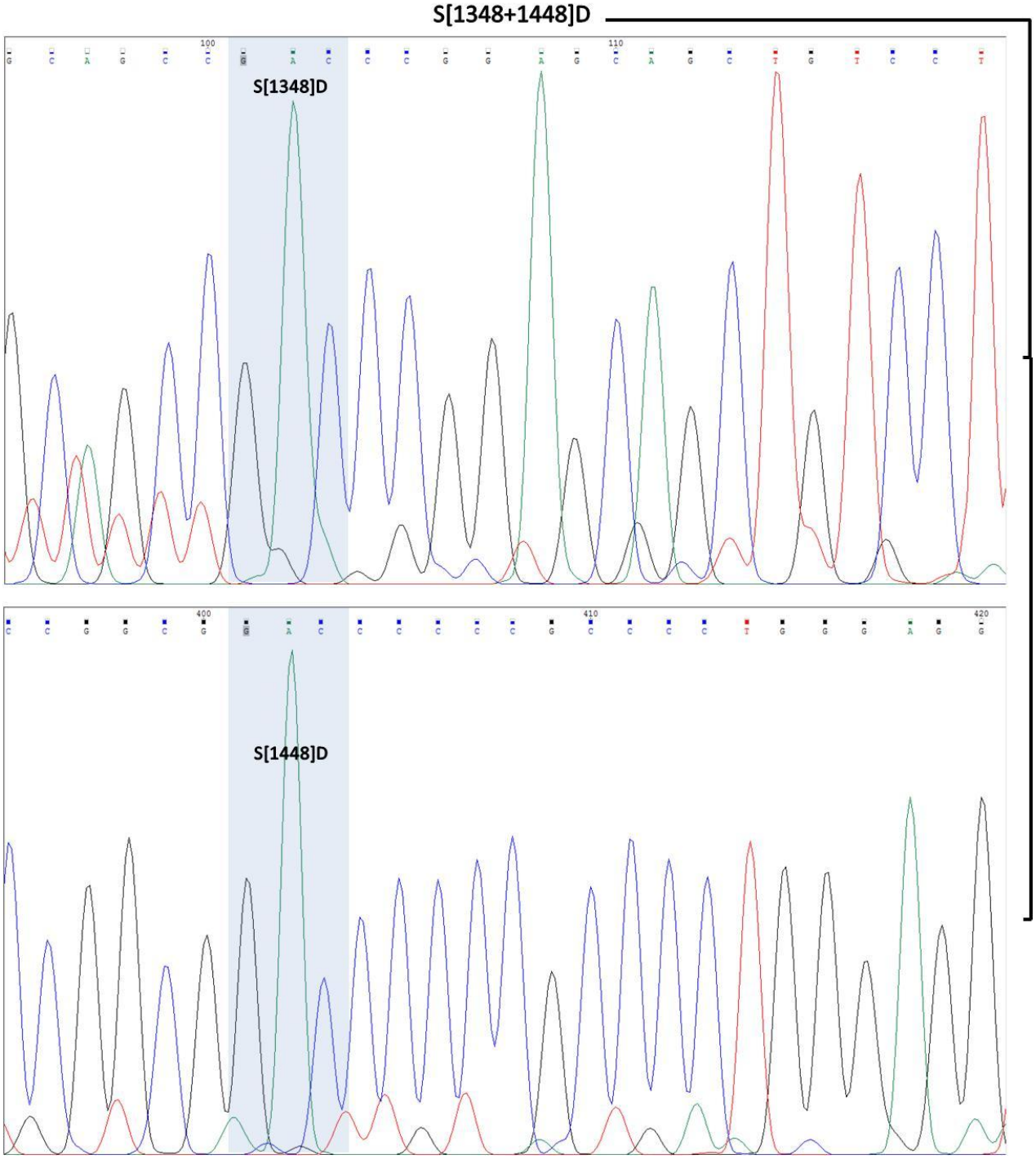

Figure 3.2c Chromatogram results of hScrib mutants S[1348+1448]D using Chromas Lite 2.1.1 software. The chromatograms show four different peak colours for each of the four bases: C = blue, A = green, T = red and G = black. The codons that were mutated are highlighted. The wildtype codon positions, S1348 and S1448, are highlighted above.

Wildtype (**S1445**): 5' C CCC ACC TCA AGG CAG **AGC** CCG GCG TCC CCC CC 3'

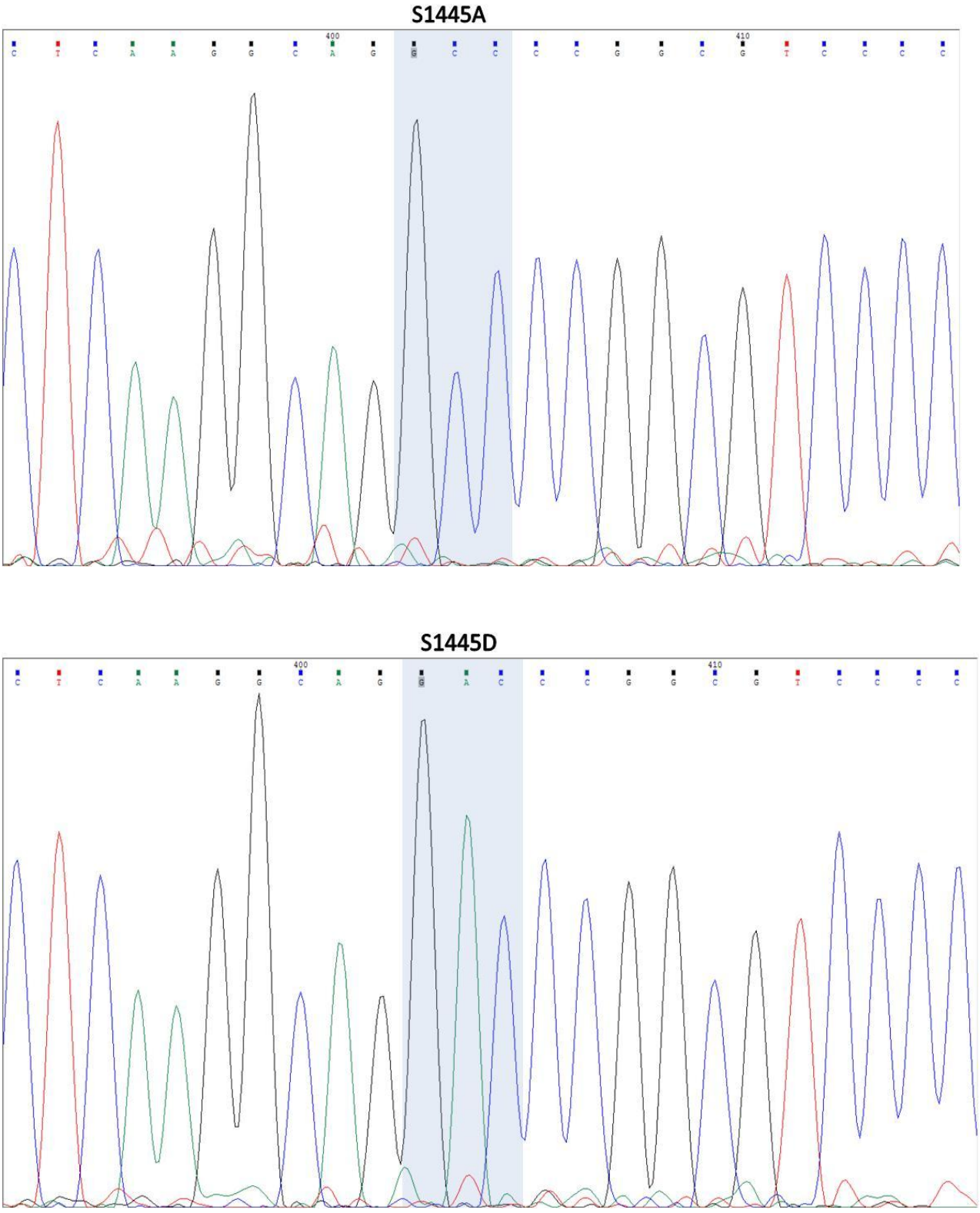

Figure 3.2d Chromatogram results of hScrib mutants S1445A (P6) and S1445D (P7) using Chromas Lite 2.1.1 software. The chromatograms show four different peak colours for each of the four bases: C = blue, A = green, T = red and G = black. The codon that was mutated is highlighted. The wildtype codon position, S1445, is highlighted above.

Wildtype (**S[1445+1448]**): 5’ C CCC ACC TCA AGG CAG **AGC** CCG GCG TCC CCC CC

--- AGG CAG AGC CCG GCG **TCC** CCC CCG CCC CTG GGA 3’

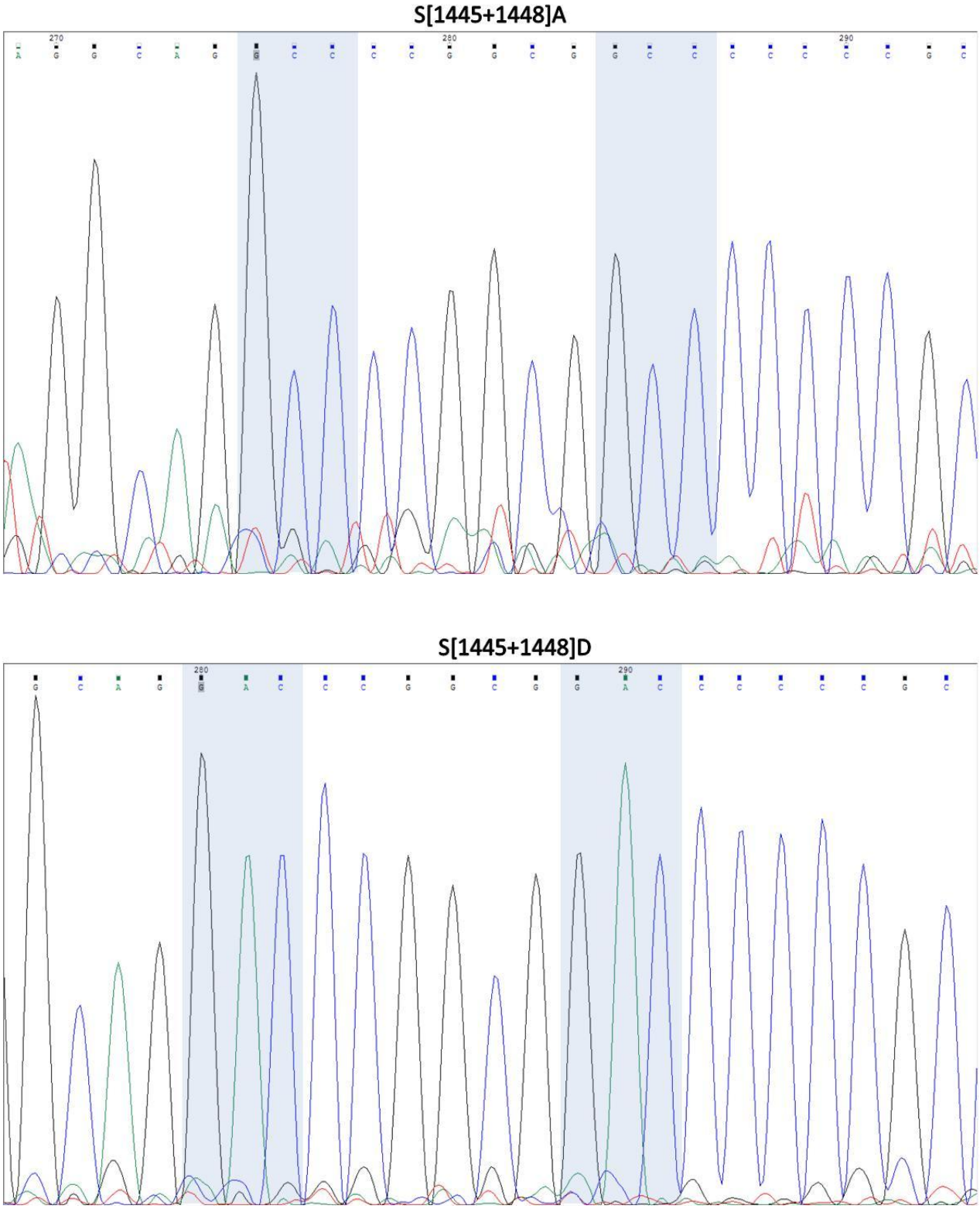

Figure 3.2e Chromatogram results of hScrib mutants S[1445+1448]A (P9) and S[1445+1448]D (P10) using Chromas Lite 2.1.1 software. The chromatograms show four different peak colours for each of the four bases: C = blue, A = green, T = red and G = black. The codons that were mutated are highlighted. The wildtype codon positions, S1445 and S1448, are highlighted above.

Wildtype (**C1297**): 5’ GG AAG ATG GCT GAA TCT CCC **TGC** TCC CCT AGT GGC CAG CAG 3’

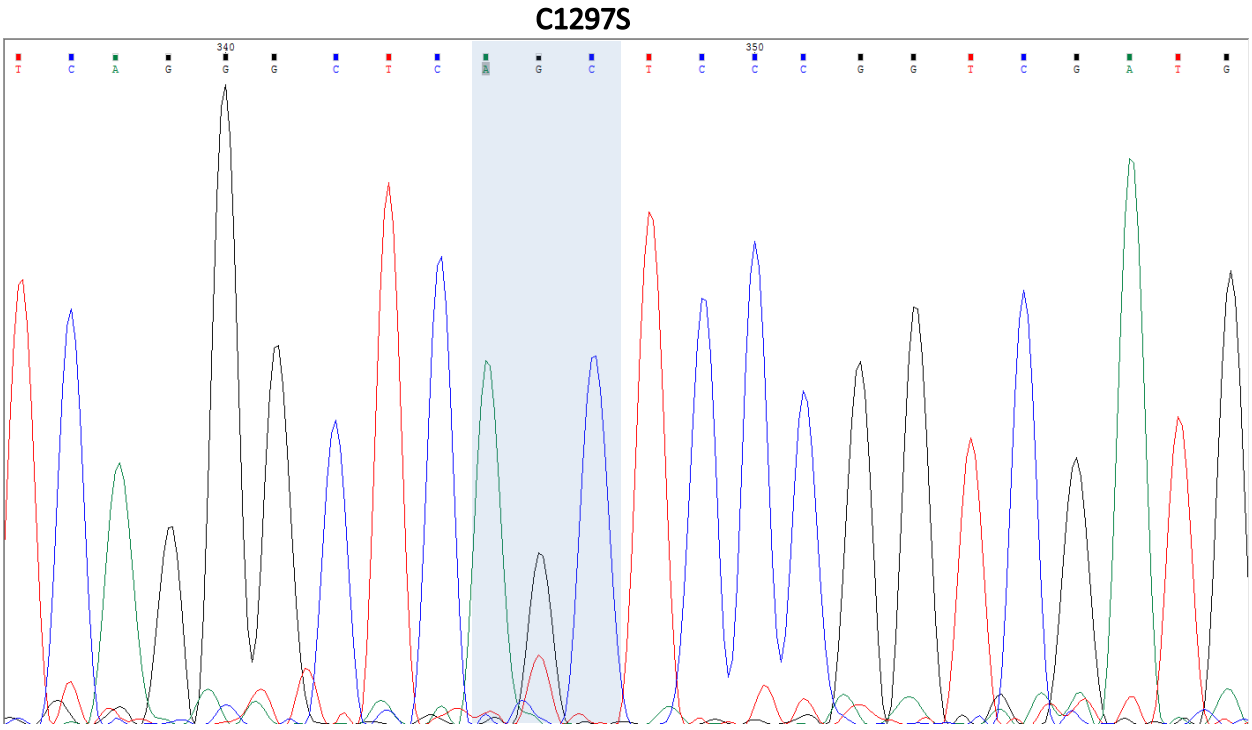

Wildtype (**P1449**): 5’ AG AGC CCG GCG TCC **CCC** CCG CCC CTG GGA GG 3’

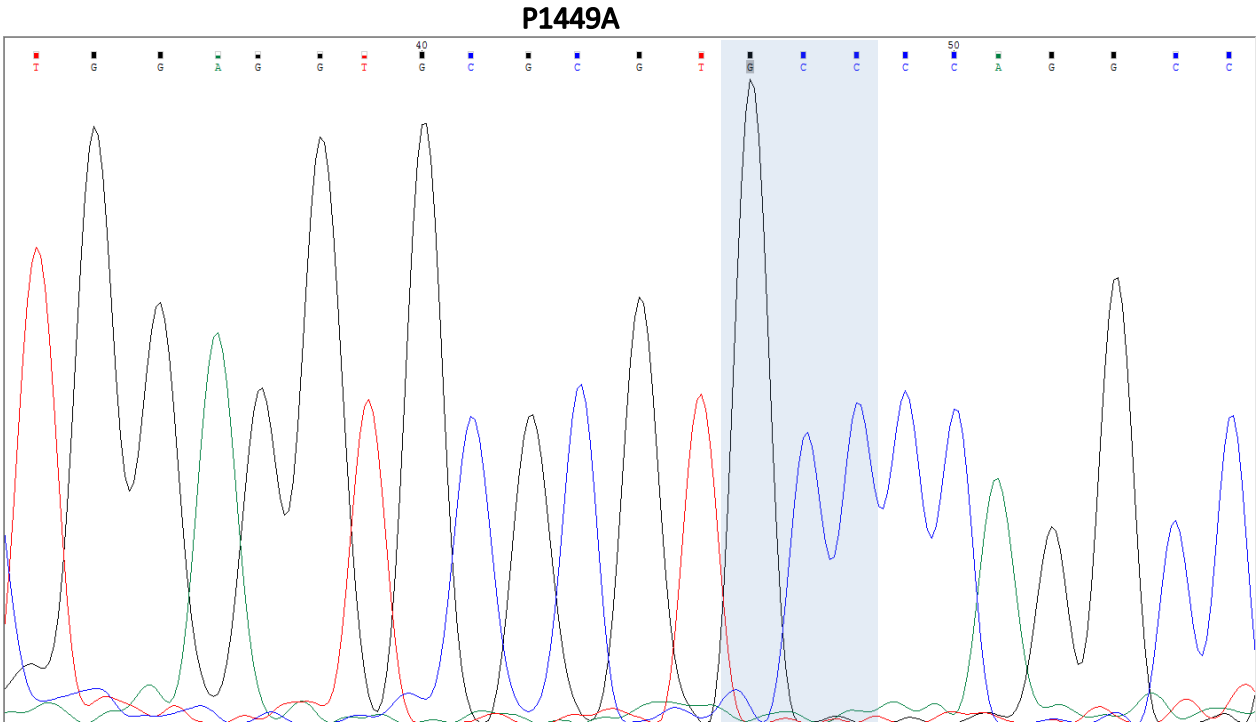

Figure 3.2f Chromatogram results of hScrib mutants C1297S (P4) and P1449A (P8) using Chromas Lite 2.1.1 software. The chromatograms show four different peak colours for each of the four bases: C = blue, A = green, T = red and G = black. The codons that were mutated are highlighted. The wildtype codon positions, C1297 and P1449, are highlighted above.

3.4 Expression of hScrib mutant proteins

Phosphorylation is a reversible PTM mechanism that is significant and prevalent in cells, occurring mostly on threonine, serine and tyrosine residues. Since these affected hotspots are serine sites, will the expression of hScrib be affected by the unphosphorylation and/or phosphorylation states of each of these selected phosphoserine sites? To answer this question, each of the four serine site was substituted for an alanine residue and an aspartate residue. Alanine (A) was considered a neutral amino acid (small side chain with no functional group) because it cannot be ionized. Thus it was used to mimic unphosphorylated hScrib. Aspartate (D) was used to mimic phosphorylated hScrib because its side chain consists of a carboxylic functional group (-COOH) that can become ionized (deprotonated) just as serine amino acid when it is phosphorylated. To test the expression of these phosphorylation states, the validated hScrib mutants (Table 3.1) were transfected in HEK293T cell line (Chapter 2.18) and imaged, live, on Eclipse Ti-E widefield microscope (Nikon), to capture their expression (Figures 3.3a and b).

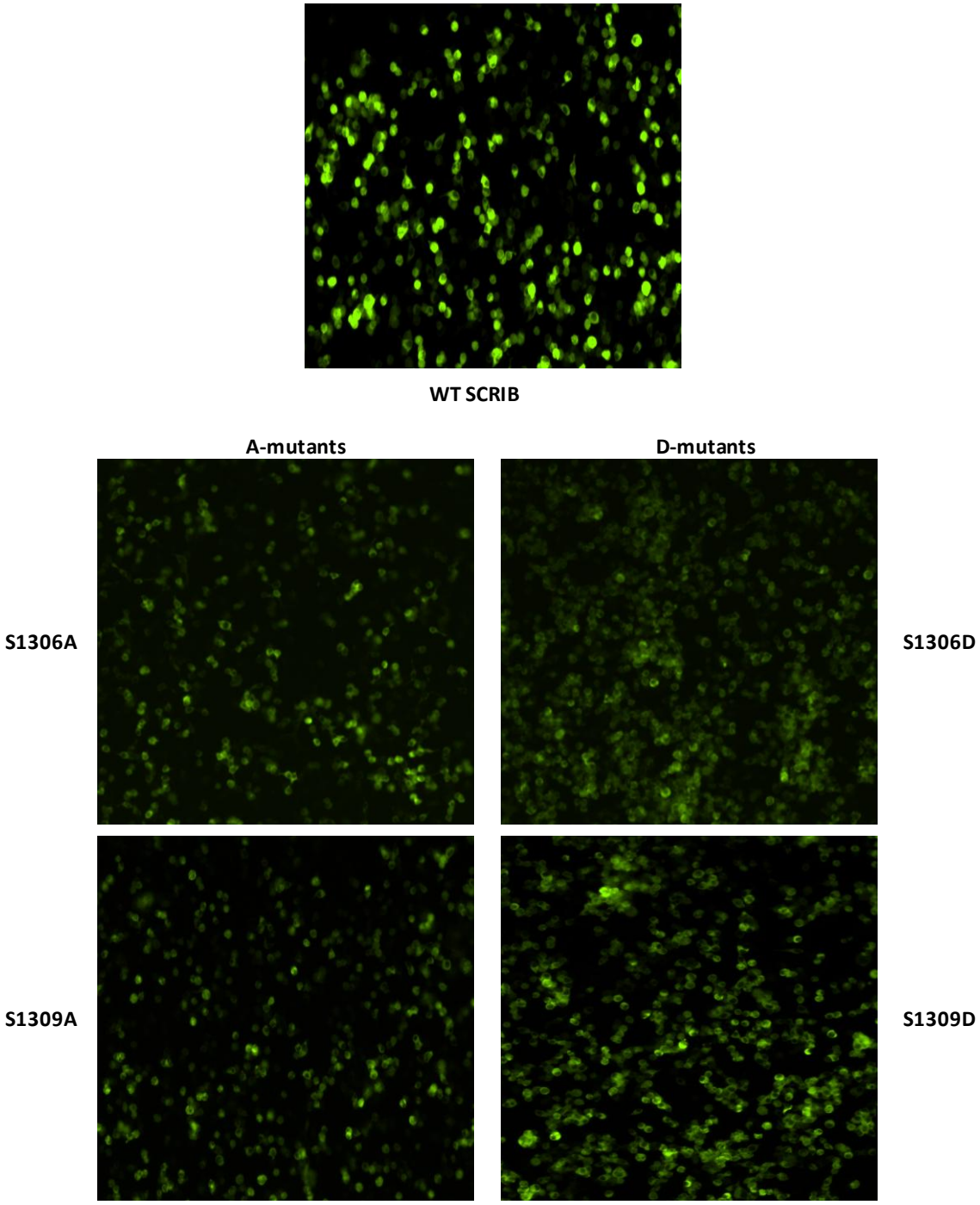

Figure 3.3a. Widefield images of live HEK293T cell lines transfected with WT *hScrib* and *hScrib* mutant DNA. The green fluorescence signal is due to the expression of EGFP tagged to hScrib. This was detected by FITC filter. **WT**= wildtype hScrib (positive control); **S1306A**= mutant hScrib protein with single amino acid change of serine site S1306 to alanine; **S1309A**= mutant hScrib protein with single amino acid change of serine site S1309 to alanine; **S1306D**= mutant hScrib protein with single amino acid change of serine site S1306 to aspartate; **S1309D**= mutant hScrib protein with single amino acid change of serine site S1309 to aspartate. Scale bar: 10 µm.

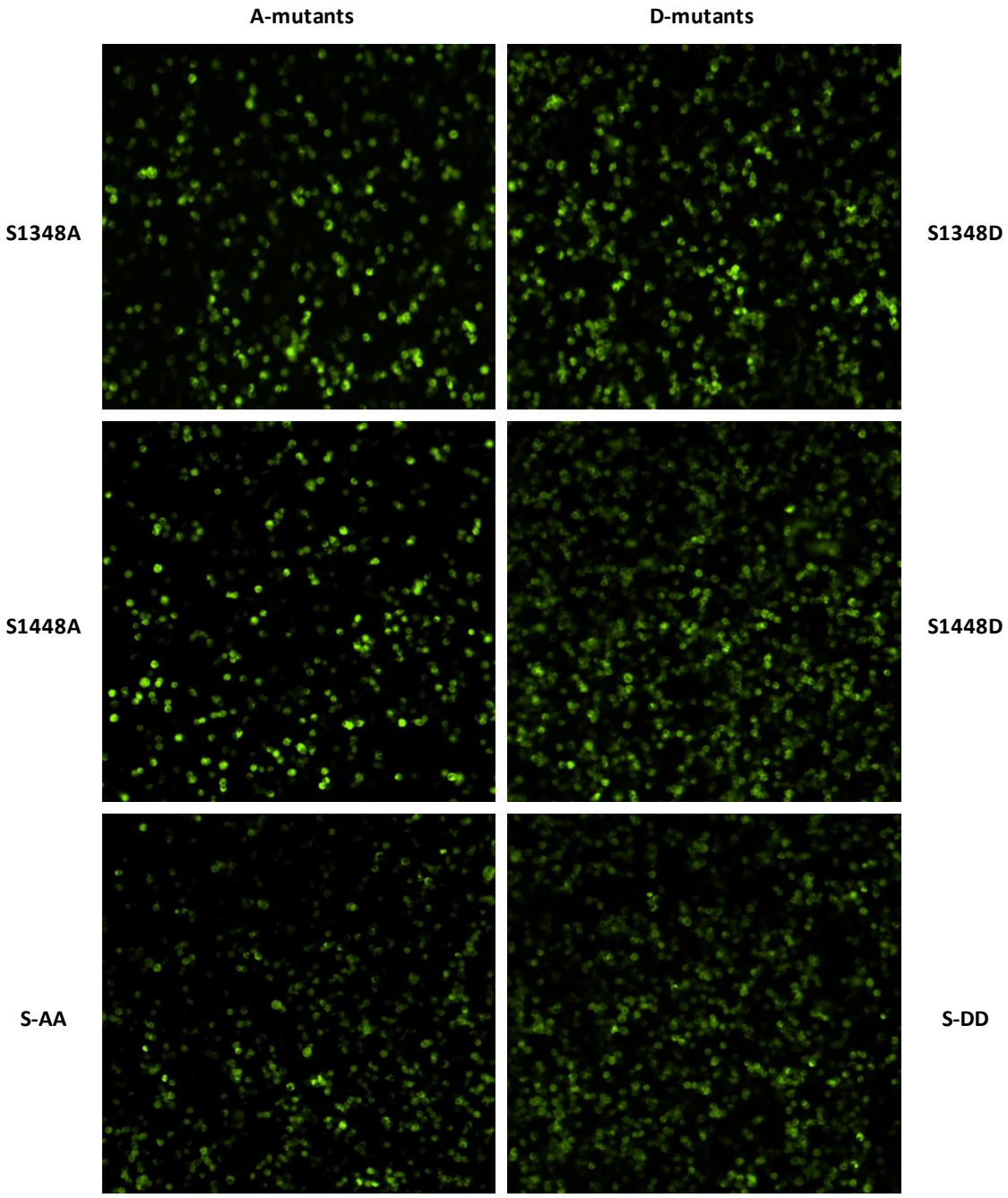

Figure 3.3b. Widefield images of live HEK293T cell lines transfected with *hScrib* mutant DNA. The green fluorescence signal is due to the expression of EGFP tagged to hScrib. This was detected by FITC filter. **S1348A**= mutant hScrib protein with single amino acid change of serine site S1348 to alanine; **S1448A**= mutant hScrib protein with single amino acid change of serine site S1448 to alanine; **S-AA**= double residue substitution of serine sites S1306 and S1309 to alanine; **S1348D**= mutant hScrib protein with single amino acid change of serine site S1348 to aspartate; **S1448D**= mutant hScrib protein with single amino acid change of serine site S1448 to aspartate; **S-DD**= double residue substitution of serine sites S1306 and S1309 to aspartate. Scale bar: 10 µm.

The widefield images observed (above), show good expression of the mutant hScrib proteins that is no different to the WT.

In relation to abundance, Western blotting (Chapter 2.21) was performed. By observation, the Western blot results (Figures 3.4a, b and c) show good abundances. However, due to the absence of the use of a loading control to normalize the level of protein detected in the samples, a constant level of abundance (protein amount) between the different samples loaded cannot be inferred. Therefore, it cannot be said that the mutant hScrib proteins were expressed at the same level in the HEK293T cell line. In spite of this, the western blots show that each mutant hScrib protein has the same molecular size as WT hScrib (≈175kDa) and not truncated; EGFP= 32.7kDa. The low abundance of S1306A was loss of protein that may have been through contamination after live imaging or poor sample preparation)

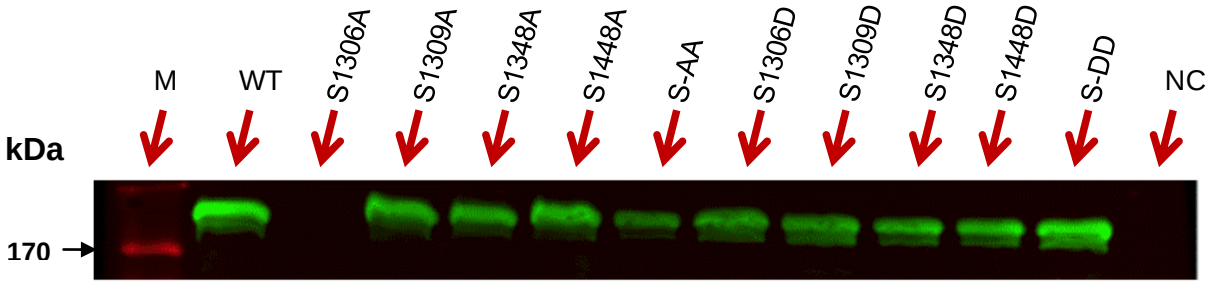

Figure 3.4a Western blots showing the abundance of non-native WT and mutant hScrib proteins. Each sample is tagged to EGFP which is recognized by anti-GFP antibody and detected as green fluorescence at 800nm wavelength. Anti-scribble antibody recognises the hScrib epitope which is detected at 700nm as red fluorescence (not shown). Each mutant protein had the same band size equal to the molecular weight of the WT= 175kDa. **M**= protein marker; **WT**= wildtype hScrib (positive control); **S1306A**= mutant hScrib protein with single amino acid change of serine site S1306 to alanine; **S1309A**= mutant hScrib protein with single amino acid change of serine site S1309 to alanine; **S1348A**= mutant hScrib protein with single amino acid change of serine site S1348 to alanine; **S1448A**= mutant hScrib protein with single amino acid change of serine site S1448 to alanine; **AA**= double residue substitution of serine sites S1306 and S1309 to alanine; **S1306D**= mutant hScrib protein with single amino acid change of serine site S1306 to aspartate; **S1309D**= mutant hScrib protein with single amino acid change of serine site S1309 to aspartate; **S1348D**= mutant hScrib protein with single amino acid change of serine site S1348 to aspartate; **S1448D**= mutant hScrib protein with single amino acid change of serine site S1448 to aspartate; **DD**= double residue substitution of serine sites S1306 and S1309 to aspartate; **NC**= untransfected sample (negative control).

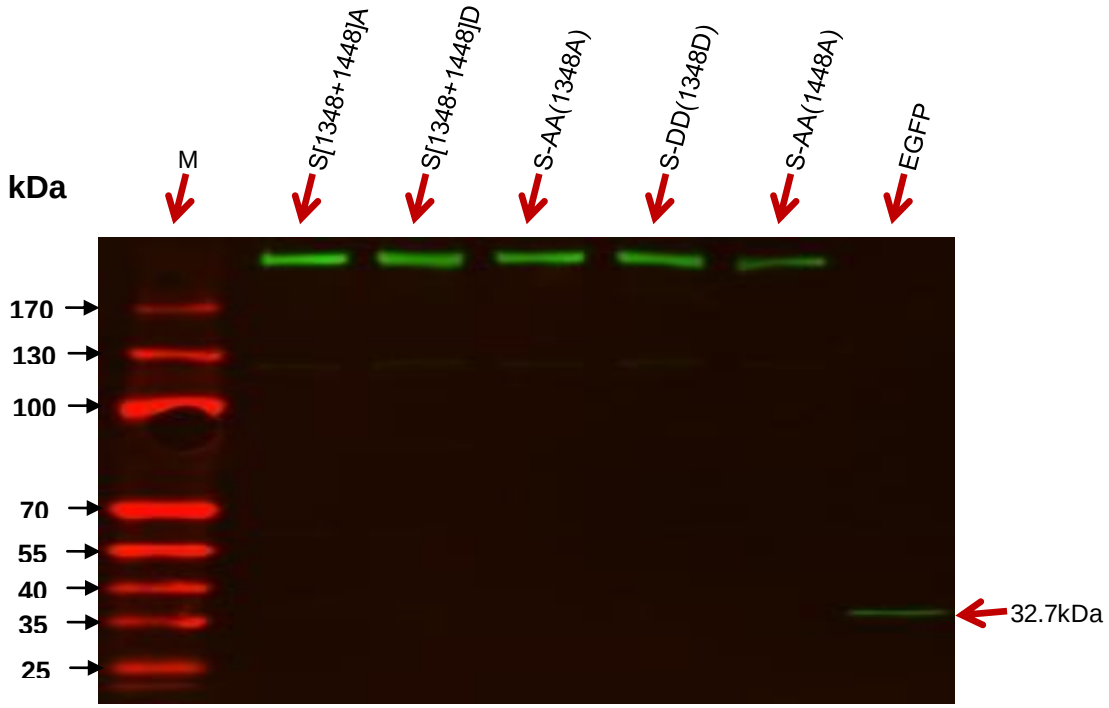

Figure 3.4b Western blots showing the abundance of non-native mutant hScrib proteins and EGFP. These were double and triple mutated hScrib samples. Each mutant protein is tagged to the C-terminal of EGFP to visualize and identify whether a mutation would truncate the protein, but all the samples have the same band size equal to the molecular weight of the WT hScrib = 175kDa. **S[1348+1448]A**= double substitution of serine residues at sites S1348 and S1448 to alanine; **S[1348+1448]D**= double substitution of serine residues at sites S1348 and S1448 to aspartate; **S-AA(1348A)**= triple substitution of serines at S1306, S1309 and S1348 to alanine; **S-DD(1348D)**= triple substitution of serines at S1306, S1309 and S1348 to aspartate; **S-AA(1448A)**= triple substitution of serines at S1306, S1309 and S1448 to alanine; **EGFP**= enhanced green fluorescent protein is 32.7kDa in molecular weight.

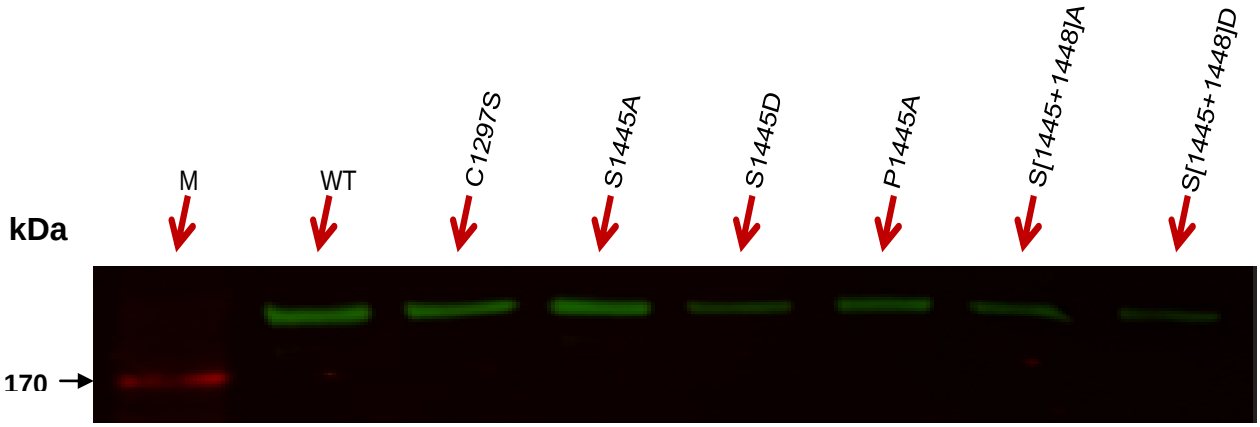

Figure 3.4c Western blots showing the abundance of non-native WT and mutant hScrib proteins. These samples are new single and double mutations of hScrib at positions other than the four selected serine hotspots. All the samples had the same band size equal to the molecular weight of the WT= 175kDa. **WT**= wildtype hScrib; P4= **C1297S**= single substitution of a cysteine residue at site C1297 to serine; P6= **S1445A**= single substitution of a serine residue at site S1445 to alanine; P7= **S1445D**= single substitution of a serine residue at site S1445 to aspartate; P8= **P1449A**= single substitution of a serine residue at site P1449 to alanine; P9= **S[1445+1448]A**= double substitution of serine residues at sites S1445 and S1448 to alanine; P10= **S[1445+1448]D**= double substitution of serine residues at sites S1445 and S1448 to aspartate.

From these analyses, it may be said that the expression of hScrib is not affected by the unphosphorylation or phosphorylation of the hScrib hotspots (including the newly mutated positions in hScrib) but their level of expression may not be the same. Samples would need to be run with a loading control.

3.5 Localization of mutant hScrib proteins

If hScrib expression is not affected, does unphosphorylation or phosphorylation of the hotspots affect its cellular localization? To answer this question, a more detailed picture of the typical localization of hScrib in a cell was required. By using confocal fluorescent microscopy, images of transiently transfected HEK293T cells were analysed (Figures 3.5a and b). These confocal images were not to show expression but the destination point of hScrib (visualized with the aid of the EGFP-tag). To minimize spectral crossover and enable nucleus and cytoplasm differentiation and visualisation, DAPI (emission wavelength= 455nm) fluorochrome was used to stain the DNA of the nucleus while the FITC filter detected EGFP (emission wavelength= 509nm).

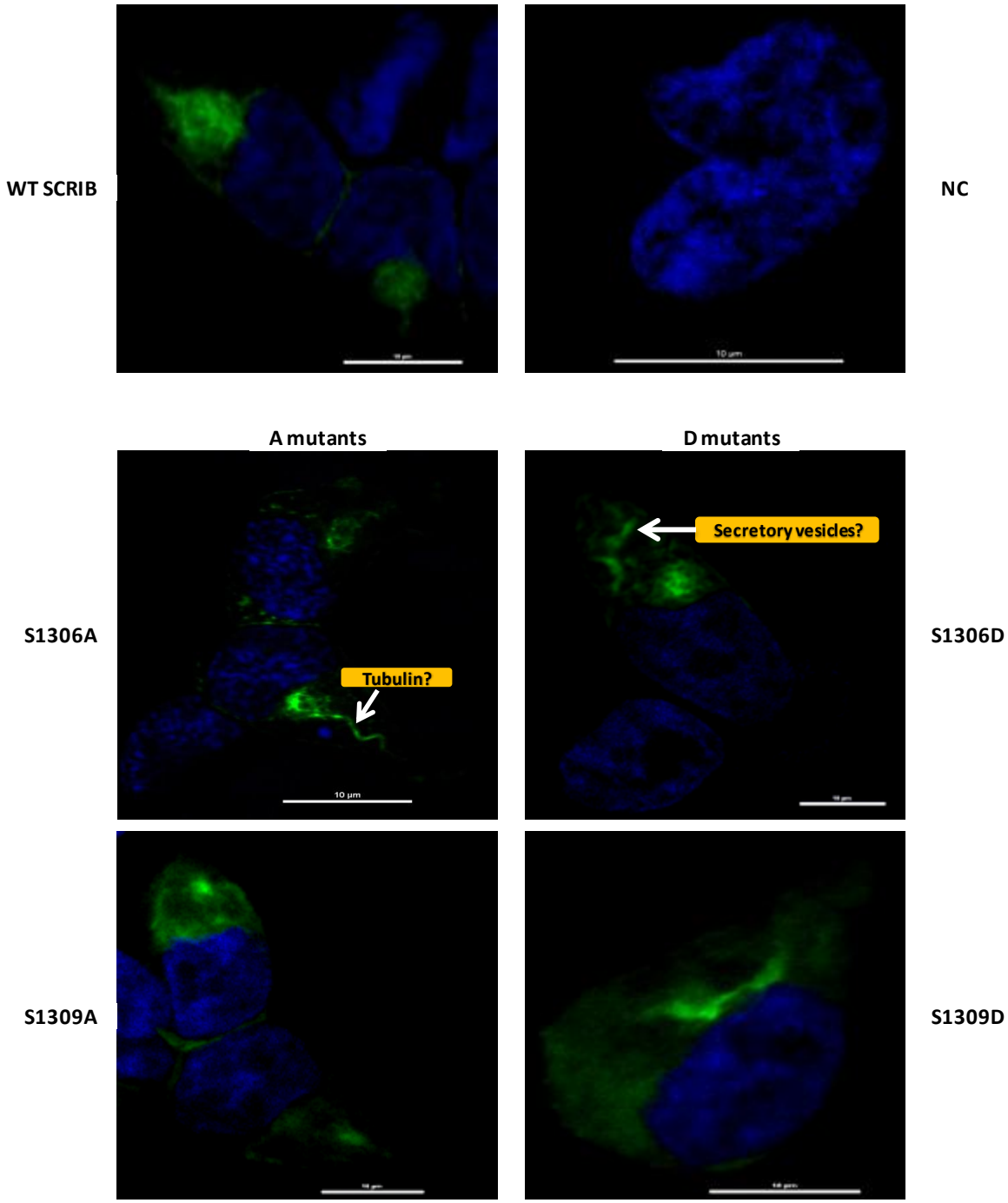

Figure 3.5a Confocal images of fixed HEK293T cell lines transfected with mutant hScrib plasmid DNA. To identify the nucleus, the cells DNA was stained blue with DAPI fluorochrome and the green fluorescence signal from the EGFP tag was detected by FITC filter. This was to observe the cellular localisation of hScrib; **WT**= wildtype hScrib (positive control); **NC**= negative control (untransfected sample). **S1306A**= mutant hScrib protein with single amino acid change of serine site S1306 to alanine; **S1306D**= mutant hScrib protein with single amino acid change of serine site S1306 to aspartate;**S1309A**= mutant hScrib protein with single amino acid change of serine site S1309 to alanine; **S1309D**= mutant hScrib protein with single amino acid change of serine site S1309 to aspartate. Scale bar: 10 µm.

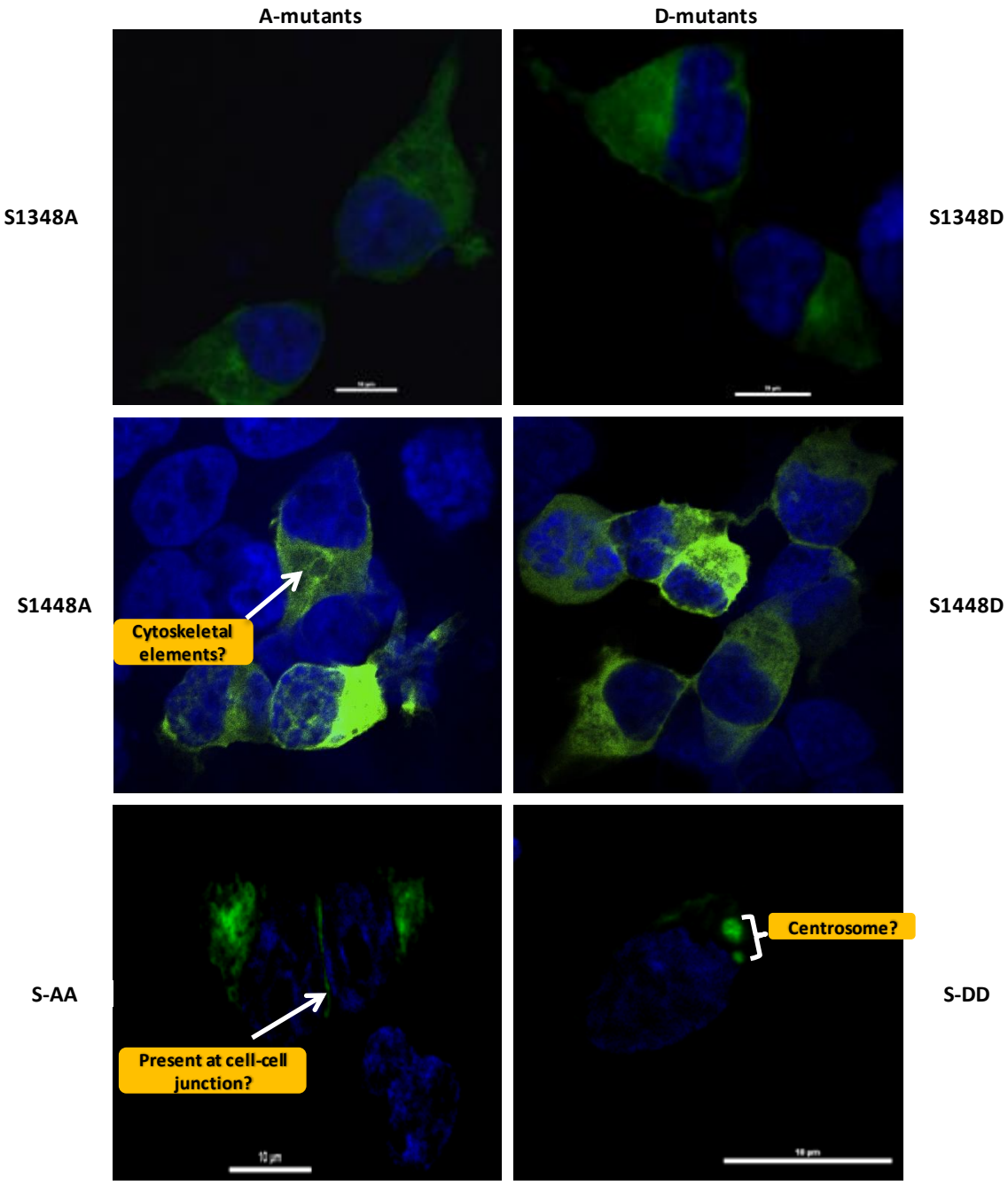

Figure 3.5b Confocal images of fixed HEK293T cell lines untransfected and transfected with WT and mutant hScrib plasmid DNA. To identify the nucleus, the cells DNA was stained blue with DAPI fluorochrome and the green fluorescence signal from the EGFP tag was detected by FITC filter. This was to observe the cellular localisation of hScrib; **S1348A**= mutant hScrib protein with single amino acid change of serine site S1348 to alanine; **S1348D**= mutant hScrib protein with single amino acid change of serine site S1348 to aspartate **S1448A**= mutant hScrib protein with single amino acid change of serine site S1448 to alanine; **S1448D**= mutant hScrib protein with single amino acid change of serine site S1448 to aspartate; **AA**= double residue substitution of serine sites S1306 and S1309 to alanine; **DD**= double residue substitution of serine sites S1306 and S1309 to aspartate. Scale bar: 10 µm.

In comparison to the WT, which show the presence of hScrib at cytoplasmic and at cell-cell contact site, the confocal images of the mutants show different localization phenotypes. A-mutants all showed cytoplasmic localization of hScrib. However, S1306A showed fragmented localization at the plasma membrane between cells and strong localization (thus interaction) to a structure in the cytoplasm (see arrow) with a tail-like extension away from the nucleus. This structure may be the protein tubulin. S-AA show localization at cell-cell contact. D-mutants also show cytoplasmic localization of hScrib. However, S1306D show localization at cell-cell contact (same as S1448D) but fragments of localization within the cytoplasm. S-DD show strong localization to two perinuclear structures (see arrow) that may be centrioles of a centrosome.

3.6 Discussion

To understand the disorganization, invasion and metastasis of cells in breast cancer, it is important to know what proteins contribute to the maintenance of cell shape and polarity, tissue organization and development and cell physiology. This is because the effective regulation of these cell properties, inhibit the establishment of breast cancer and its properties. A key protein in the regulation of epithelial cell and tissue polarity and organisation is a component of the Scribble complex (hScrib/Hugl/hDlg) called hScribble (Dow *et al.*, 2003; Royer and Lu, 2011). This known tumour suppressor protein found to be expressed in invasive and metastatic TNBC (Greenwood *et al.*, 2011), was also found to be deregulated or mislocalized from its basolateral plasma membrane domain in mammary epithelial tumours (Dow *et al.*, 2003; Ivanov *et al.*, 2010).

Further quantitative proteomic analysis discovered that PTM patterns of four phosphoserine sites in the C-terminal part of this hScribble changed significantly with CD74 overexpression (Metodieva *et al*, 2013). The changes in these phosphorylation sites may be a significant reason for hScribble involvement in breast cancer invasion and metastasis. Therefore this experiment studied how changes in serine phosphorylation status at these sites affect the expression and localization of hScribble in a cultured cell line.

The widefield images and Western blot results confirmed good expression of the hScribble mutants (both unphosphorylated and phosphorylated). This may indicate: (1) the unphosphorylation and phosphorylation of each hotspot is not a signal for proteosomal degradation of hScribble tumour suppressor protein seen in cancer caused by Human Papilloma Viruses (Lawson and Heng, 2010; Royer and Lu, 2011). This is because it was

found that some oncoproteins of HPV (such as E6) interact with the PDZ domains of polarity proteins e.g. Dlg, Patj (component of the Crumbs polarity complex), especially the phosphorylated forms, to disrupt cell cycle regulation. If it were, it would suggest that such PTM state is an underlying incentive for the loss of cell polarity and the aggressive invasion and metastasis of breast cancer (Zhan *et al.*, 2008). (2) The mutated hotspots of hScribble are not signals for apoptosis of the cells as a result of hScribble expression being toxic or non-functionally accumulating in the cytosol (Coleman *et al.*, 2001; Norman *et al.*, 2012). (3) Each phosphorylation hotspot, either unphosphorylated or phosphorylated, facilitates a different conformational change in hScribble protein to localize and/or recognize and interact allosterically with other protein complexes to alter cell behaviour e.g. apical-basal polarity, cell cycle regulation, epithelial-mesenchymal transition (EMT) etc, via signalling pathways such as the MAPK (Good *et al.*, 2011; Vaira *et al.*, 2011; Metodieva *et al.*, 2013).

Images of A-mutants S1306A, S1309A and S-AA show the possibility that unphosphorylated hScrib localize to cell-cell contact site. A-mutant S1306A also shows the possibility that unphosphorylated hScrib may likely interact with a cytoskeletal element called tubulin. Tubulin is a polymerized microtubular protein involved in cell motility (Hammond *et al.*, 2009) and hence may promote cell invasion in breast cancer. There is a large presence of hScribble in the cytosol in some of the A-mutants e.g. S1309A, A1348A, S1448A, S-AA and D-mutants e.g. S1306D to S1448D. This may be the interaction of hScribble with other cytoskeletal elements e.g. intermediate filaments (IFs). Interacting to these cytoskeletal elements, at different phosphorylation states, induces different cellular activities. IFs are cytoskeletal fibres that are more abundant in the cell than microtubules of tubulin. They associate with plasma membrane proteins to give mechanical support to the cell in cell-cell and cell-ECM contact (Lodish *et al.*, 2000:19.6). An example of IF these hScrib mutant proteins may be interacting with are cytokeratins and vimentin. Cytokeratins (acidic keratin type 1 and basic keratin type 2) are IFs known to be highly expressed in basal-like breast tumours such as TNBC (Eerola *et al.*, 2008). Vimentin is a type III IF known to induce a mesenchymal phenotype in epithelial cells, thus altering the morphology, adhesion and motility of epithelial cells (Mendez *et al.*, 2010): the result of EMT.

The fragments of hScrib in the cytoplasm, seen in S1306D of Figure 3.5a, is an indication that hScrib protein may be interacting with cytoskeletal elements to rearrange the distribution of molecules within the cell (Hammond *et al.*, 2009). This event may be involved in the alteration of apical-basal cell polarity. The doubly phosphorylated D-mutant of hScrib, (S-DD), was also intriguing as it showed strong localization to what looked like

centrosome which is involved in mitosis. This is an indication of hScrib's involvement in the cell cycle. The centrosome consists of a pair of centrioles made up of tubulin and perpendicular to one another. The centrioles not only play a role in cytokinesis, they organise microtubular spindles which contributes to the fidelity of chromosomal segregation during mitosis. In addition, centrioles may also regulate cell-cycle progression, thus suggesting a signalling role for centrioles (Marshall, 2006). If this is true, then hScrib protein in the doubly phosphorylated state may be acting as a scaffold to concentrate and coordinate the tubular centrioles and other signalling molecules to enable the regulation of cell-cycle progression.

Based on the results of the experiment, it is not suffice to infer that any of the identified phosphorylation hotspots of hScrib in phosphorylated or unphosphorylated state is a contributor to the invasion of breast cancer. Due to the heterogeneity of the cell lines used, more confocal images of the mutant proteins would be analysed. Also combinations of phosphorylation states where three and four phosphoserine hotspots are mutated in the hScrib gene e.g. S-AA(1348A), S-AAAA, S-DD(1348D), S-DD(1448D) and S-DDDD, would be studied. Furthermore, experiments to analyse the protein-protein interactions of hScrib in different phosphorylation state would be carried out to understand what role hScrib plays in breast cancer.

Summary of the localization study of hScrib is tabled below (Table 3.2).

Table 3.2 Summary of hScrib localization study

Methods	Objective	A-mutants					D-mutants				
SDM DNA sequencing	Generation of validated hScrib mutants	**S1306A**	**S1309A**	**S1348A**	**S1448A**	**S-AA**	**S1306D**	**S1309D**	**S1348D**	**S1448D**	**S-DD**
Transfection Widefield imaging Western blot	Expression	Good	Good	Good	Good	Good	Good	Good	Good	Good	Good
Transfection Confocal imaging	Localization	Cytoplasmic tail-like structure (possibly tubulin)	Cell-cell contact	Cytoplasmic presence	Possibly cytoskeletal elements	Cell-cell contact	Cytoplasmic presence (possibly secretory vesicles)	Cytoplasmic presence	Cytoplasmic presence	Cytoplasmic presence	Cytoplasmic structures (possibly centrioles)
		Cell-cell contact (minimal)	Cytoplasmic presence		Cytoplasmic presence	Cytoplasmic presence					Cytoplasmic presence

4. The effect of hSCRIB on cell proliferation and migration

4.1 Introduction

In humans, hScribble or hScrib protein is a product of an important tumour suppressor gene, *hScrib*, with the role of inhibiting tissue overproliferation seen in tumours. Its tumour suppressive function is facilitated by its scaffolding property to enable its interaction with a diverse set of proteins (Albertson *et al.*, 2004; McNeil *et al.*, 2006; Bauer *et al.*, 2010; Buday and Tompa, 2010) to regulate epithelial cell polarity which is essential for coordinated cell proliferation, migration and maintenance of intercellular adhesion (Dow *et al.*, 2003).

Cell proliferation is cell division through the universal cell cycle machinery, a highly ordered and regulated complex sequence of events that comprises four critical phases: G_1, G_2, S and M phases (Shackelford *et al.*, 1999; Pinheiro and Sunkel, 2012), with the initiation and termination of each phase being controlled by proteins at checkpoints G_1/S, G_2/M or M/G_1. In cancer cells, this machinery is 'hijacked' to cause loss of control of cell proliferative function which leads to an abnormal mass of cells. These abnormal cells may acquire further mutations, with the potential to migrate unregulated (Chow, 2010) and invade surrounding tissue. This 'gain of function' may be a result of the loss of function of tumour suppressor proteins like hScrib designated at certain cell cycle stages (Osborne *et al.*, 2004; Lee and Muller, 2010). The function of hScrib is compromised when mutations of the *hScrib* gene cause loss of expression or mislocalization of its gene product. These mutations lead to the loss of cell polarity which induces lack of control of cell proliferation and abnormal migration of cancer cells (Dow *et al.*, 2003; Qin *et al.*, 2005; Hanahan and Weinberg, 2011; Feigin *et al.*, 2014).

In the context of breast cancer, the changes in the phosphorylation state of hScrib protein responsible for the occurrence of such cellular transformation are unknown, even though proteomic analysis from a recent study (Metodieva *et al.*, 2013) discovered that the post-translational patterns of four phosphoserine sites in the C-terminal part of hScrib protein changed significantly in TNBC overexpressing CD74. The changes in these phosphorylation sites may be significant to the involvement of hScrib in tumourigenesis

and breast cancer invasion and metastasis. Therefore, this experiment aims to study the effects of hScrib mutations on cell proliferation and migration by determining which mutant/s of hScrib protein, previously designed from the four phosphoserine sites, is/are involved cell proliferation and migration.

4.2 Proliferation in hScrib transfected HEK293T cells

The mutation of the *hScrib* gene may cause loss of expression or mislocalization of its gene product, hScrib protein. These changes lead to the loss of cell polarity, which is known to induce the lack of control of cell proliferation and migration in cancer cells (Dow *et al.*, 2003; Qin *et al.*, 2005). However, what changes in the amino acid sequence of hScribble protein responsible for such cellular transformation to occur are unknown even though proteomic analysis from a recent study (Metodieva *et al.*, 2013) discovered that the post translational patterns of four phosphoserine sites in the C-terminal part of scribble changed significantly with TNBC overexpressing CD74. The changes in these phosphorylation sites may be significant to the involvement of hScrib in breast cancer invasion and metastasis. A feature of cancer cells is their abnormal, progressive proliferation (Humbert *et al.*, 2003; Fidler, 2003). The proliferation rate of HEK293T cells transfected with A or D-mutants of hScrib were determined by MTT assay (Chapter 2.23). This is a colorimetric approach that utilizes the level of absorbance of the purple formazan produced in the mitochondria of living cells as a measure of cell proliferation (Price and McMillan, 1990; van de Loosdrecht *et al.*, 1994; Freimoser *et al.*, 1999; Chapdelaine, 2012). Untransfected HEK293T cell lines was used as a reference for over proliferating breast cancer cells in this assay while wildtype (WT) hScrib-transfected HEK293T cells were used as a reference of inhibition of cell proliferation. As a result of the WT hScrib tagged to GFP, GFP-transfected HEK293T cells were included to rule out the effect GFP may have on the result of the WT and mutants in the assay (Table 4.1).

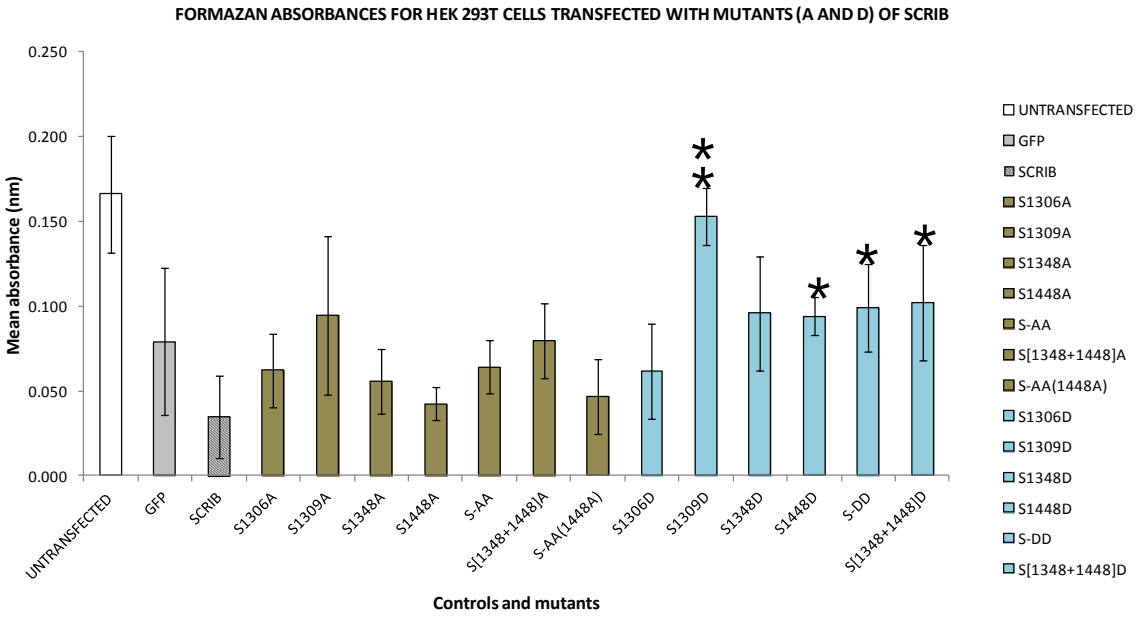

Figure 4.1 Absorbance of formazan produced by untransfected and transfected HEK293T cell line. The graph showed that there was just about more formazan produced by the D-mutants than the A-mutants. The results are expressed as mean ± stdev, $p<0.05$. The asterisks indicate the level of significant difference between the proliferation rate of WT-transfected cells and mutants. Mutants without the sign were not significant.

Figure 4.1 shows a bar chart of the mean absorbances of each mutant and controls after 4 hours of MTT reduction to formazan. Although this experiment was not repeated (only one experiment with triplicates), it shows that the intensity of MTT conversion was more in the untransfected or untreated cells than any other samples: The untreated cells proliferated about 5 times more than WT hScrib; 4 times more than S-AA(1448A); 3 times more than S1306A, S1348A, S-AA and S1306D; twice more than S1309A, S[1348+1448]A, S1348D, S1448D, S-DD and S[1348+1448]D; except S1448A (6 times less than untreated) and S1309D(8.2% less than untreated).

Statistically, Student's t-test that was performed showed no significant difference in proliferation rate between the untreated control and one A-mutant (S1309A) and four D-mutants (S1309D, S1348D, S-DD and S[1348+1448]D). As expected, there was a significant difference in the proliferation rate between the untreated control and WT hScrib control. Student's t-test to determine whether GFP, tagged to the WT and hScrib mutants, affected their proliferation rate showed no significant difference in proliferation rate between GFP and GFP-tagged WT and hScrib mutants. However, between WT hScrib and its mutants, only D-mutants S1309D, S1448D, S-DD and S[1348+1448]D showed significant difference in proliferation rate as shown in asterisks in Figure 4.1. S1309D was

the most significant (2 asterisks). All other mutants, without the asterisk, were not significant. Therefore, this data suggests that D-mutants proliferate more than A-mutants.

4.3 Migration in hScrib transfected HEK293T cells

Cell migration is highly regulated. This is because it is a very intricate cellular event that is involved in several functional processes in the body e.g. embryogenesis, angiogenesis, organogenesis, tissue repair, immune response, and wound healing. It has also been proposed to be involved significantly in the invasion of cancer cells (Riahi *et al.*, 2012) as this is required in the early stages of tumour metastasis (Fidler, 2003). A typical cell migration process involves a regulated modification of cell polarity for an epithelial cell to assume a mesenchymal phenotype. However, in invasive breast cancers like TNBC, this process is abnormal (Yamaguchi et al., 2005; Etienne-Manneville, 2008). As a polarity protein, known to be involved in regulated cell migration, the mutation or loss of expression of hScrib cause abnormal cell migration (Etienne-Manneville, 2008; Qin *et al.*, 2005). To study the effects of hScrib on cell migration, a wound healing or *in vitro* scratch assay (Chapter 2.23) was conducted.

The mean areas (mm^2) from T=0 to T=24hrs indicate reduction of the cell-free zones (gap closure). However, Due to the non-uniform scratch areas made in each sample at T=0, the mean areas do not show how fast the scratch was covered in each sample. Therefore, the migration rate of the cells to closing the scratch was expressed as a percentage of wound closure as seen in Table 4.1:

Table 4.1 Migration rate of transfected cells after 24 hours

	Mean (0)	Mean (24)	Wound closure (%)
UNTRANSFECTED	0.246	0.015	93.9
GFP	0.246	0.215	12.6
SCRIB	0.256	0.224	12.5
S1306A	0.245	0.214	12.8
S1309A	0.257	0.222	13.6
S1348A	0.249	0.227	9.0
S1448A	0.277	0.205	26.1
S-AA	0.259	0.182	29.8
S[1348+1448]A	0.255	0.169	33.6
S-AA(1448A)	0.254	0.121	52.3
S1306D	0.254	0.235	7.5
S1309D	0.254	0.223	12.2
S1348D	0.242	0.204	16.0
S1448D	0.271	0.210	22.7
S-DD	0.249	0.192	22.9
S[1348+1448]D	0.245	0.198	19.3

This table shows the area of the scratch covered after 24 hours as a percentage wound closure for each sample to represent a measure of cell migration rate.

Table 4.1 shows that after 24 hours, the percentage of the scratch area covered by the untransfected cells (93.9%) was more than all other samples with approximately 13 times cell migration rate than the least migratory sample i.e. S1306D (7.5%). The least migratory of the A-mutant samples was S1348A with 9% migratory rate.

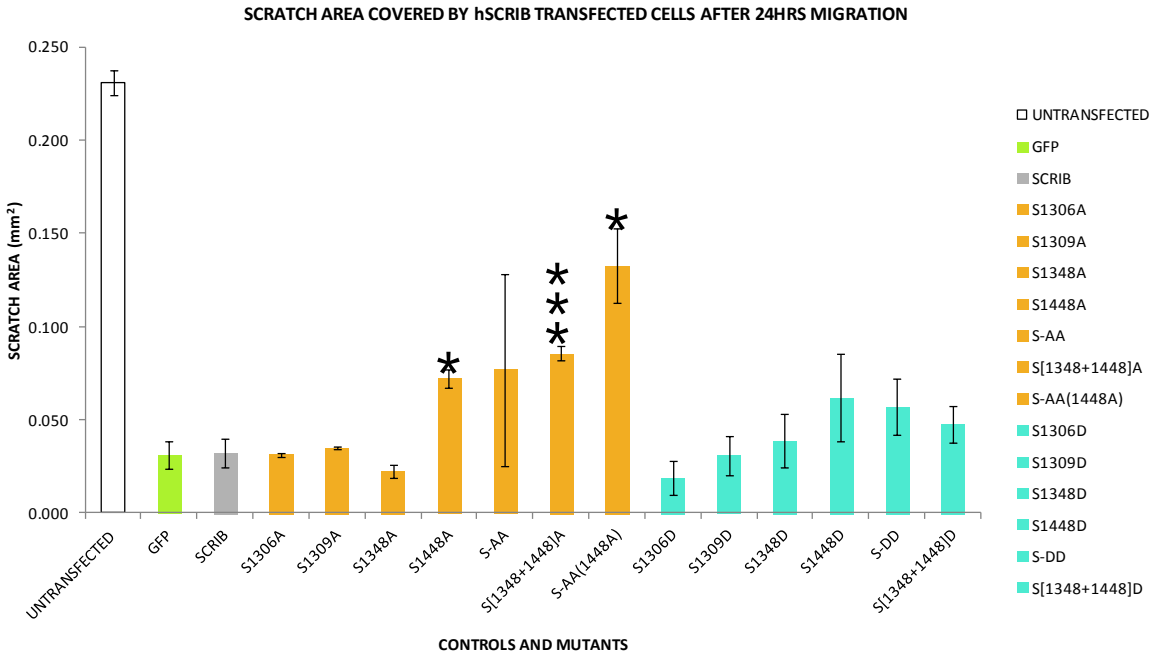

Figure 4.2 Wound closure of untransfected and transfected HEK293T cell line. The graph showed that after 24 hours, only S1448A, S-AA, S[1348+1448]A and S-AA(1448A) covered more than a quarter of the scratched area or cell-free zone. All the D mutant samples covered less than a quarter of the scratch area. The results are expressed as mean ± stdev, $p<0.05$. The asterisks indicate the level of significant difference between the migration rate of WT-transfected cells and mutants. Mutants without the sign were not significant.

Figure 4.2 illustrates graphically that only S1448A, S-AA, S[1348+1448]A and S-AA(1448A) of the A-mutant samples covered more than a quarter (i.e. 25%) of the scratch area. Student's t-test showed significant difference in migration rate between WT hScrib and S1448A, S[1348+1448]A and S-AA(1448A) as shown in asterisks in Figure 4.2. S[1348+1448]A was the most significant (3 asterisks). All other mutants, without the asterisk, were not significant. Therefore, comparing the A and D-mutant samples, this data suggests that A-mutant-transfected cells migrated more the D-mutant-transfected cells.

However, As more than 25% scratch area was covered by cells transfected with S1448A, S-AA, S[1348+1448]A and S-AA(1448A), a second wound healing assay with these four mutants was conducted to confirm their effect on the migratory rate of cells. D-mutant counterpart S1448D, S-DD and S[1348+1448]D were also tested. The migration rate of cells transfected with these mutants were calculated (Table 4.2).

Table 4.2 Migration rate of cells transfected with selected hScrib mutants after 24 hours

	Mean (0)	Mean (24)	Wound closure (%)
UNTRANSFECTED	12.278	4.520	63.2
SCRIB	12.540	12.379	1.3
S1448A	9.958	9.643	3.2
S-AA	10.684	9.820	8.1
S[1348+1448]A	11.065	9.018	18.5
S-AA(1448A)	11.107	10.113	8.9
S1448D	12.874	12.696	1.4
S-DD	12.714	12.507	1.6
S[1348+1448]D	11.982	11.337	5.4

This table shows the percentage wound closure of the samples selected for the second wound healing assay. These percentages represent a measure of cell migration rate.

Table 4.2 shows that once again, after 24 hours, the percentage of the scratch area covered by the untransfected cells (63.2%) was more than all other samples. The migration rate of cells transfected with S1448D (1.4%) and S-DD (1.6%) is similar to WT hScrib (1.3%) while cell transfected with S[1348+1448]D (5.4%) covered 3 to 4 times more scratch area than WT hScrib, S1448D and S-DD. Of the A-mutants, S[1348+1448]A (18.5%) had the highest migration rate: about 6 times more scratch area than A1448A (3.2%) and about twice more than S-AA (8.1%) and S-AA(1448A) (8.9%). Comparing these A and D-mutant counterparts, S1448A covered twice the scratch area of both WT hScrib and A1448D; S-AA migrated about 5 times more than S-DD; S[1348+1448]A migrated 3 times more than S[1348+1448]D while the scratch area covered by S-AA(1448A) was 7 times more than WT hScrib, 3 times more than S1448A and 6 times more than S1448D and S-DD. Figure 4.3 shows this graphically.

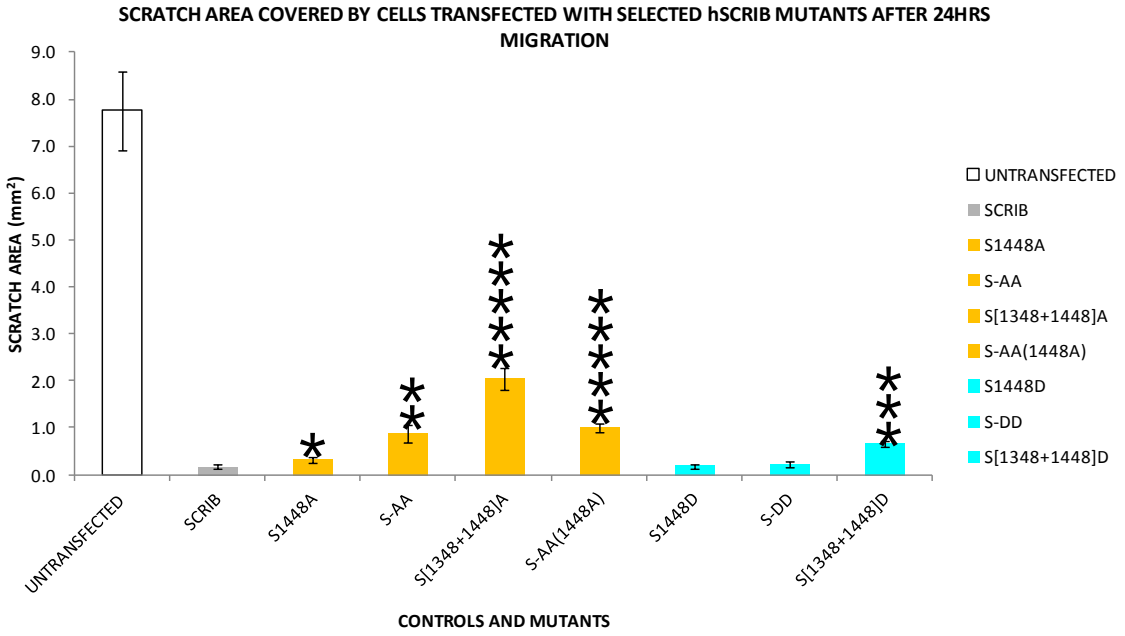

Figure 4.3 Wound closure of untransfected and transfected HEK293T cell line. The graph showed again that after 24 hours, cells transfected with the selected A mutants migrated faster than cells transfected with their D mutant counterpart. The results are expressed as mean ± stdev, $p<0.05$. The asterisks indicate the level of significant difference between the migration rate of WT-transfected cells and mutants. Mutants without the sign were not significant.

When Student's t-test was applied, there was significant difference in migration rated between WT hScrib and the A-mutants, but also S[1348+1448]D. A[1348+1448]A and S-AA(1448A) were the most significant (5 asterisks). All other mutants, without the asterisk, were not significant. Further Student's t-test's to test the cell migration difference between A-mutants and D-mutants of the same serine position presented significant differences, with A and D-mutants of the serine positions 1348+1448 displaying greater significant differences. Within the A-mutants, there was greater significant difference between S1448A and S[1348+1448]A than with the other A-mutant samples. There was no significant difference between S-AA and S-AA(1448A). Overall, the A-mutants migrated more than the D-mutants.

Figures 4.4 and 4.5 below show the brightfield images of the wound closure captured at T=0 and 24hrs.

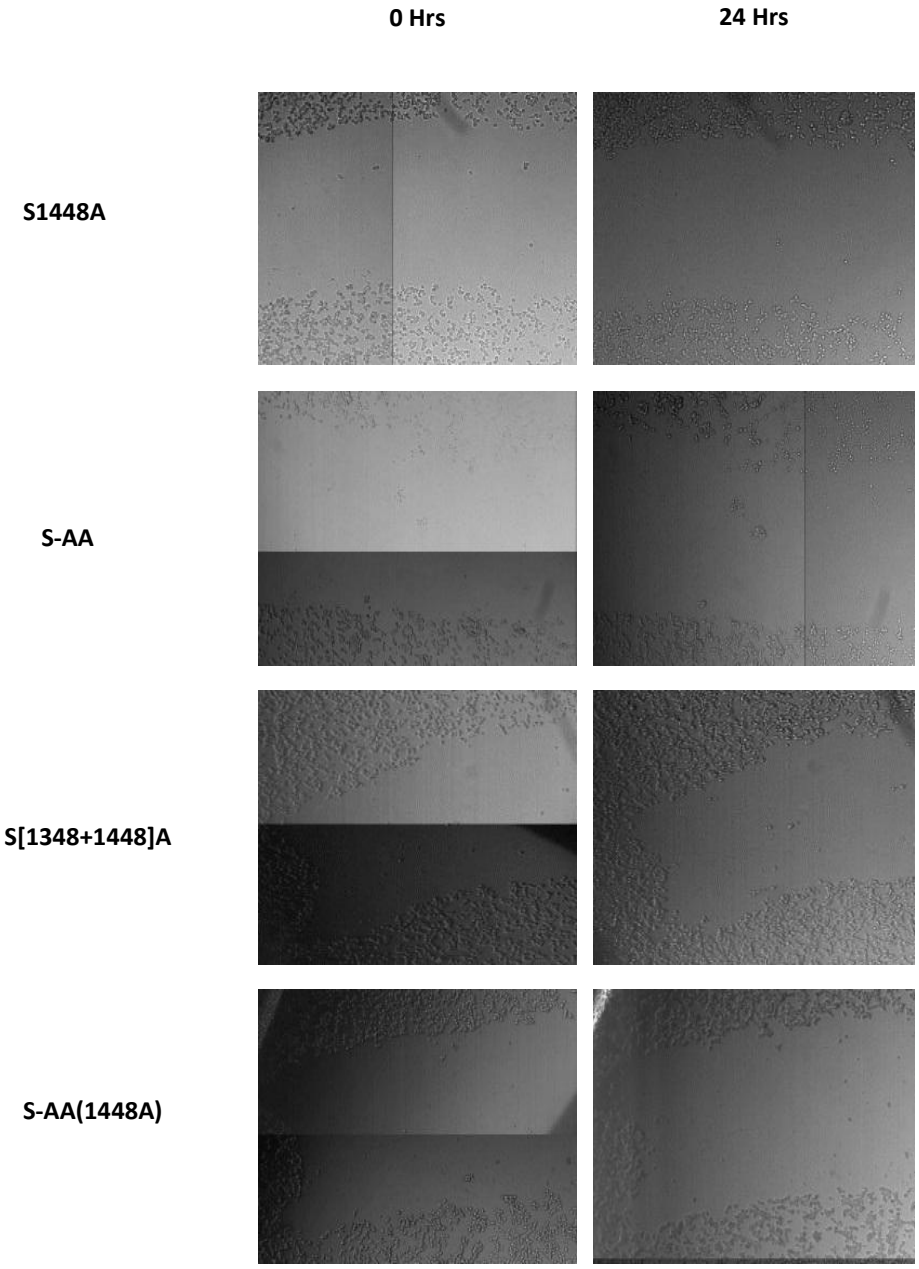

Figure 4.4 Brightfield images of wound closure of HEK293T cell lines transfected with A-mutants. The images shown are representative of a full scratch acquired as large stitched images from an automated Nikon widefield microscope. Scale bar= 100µm.

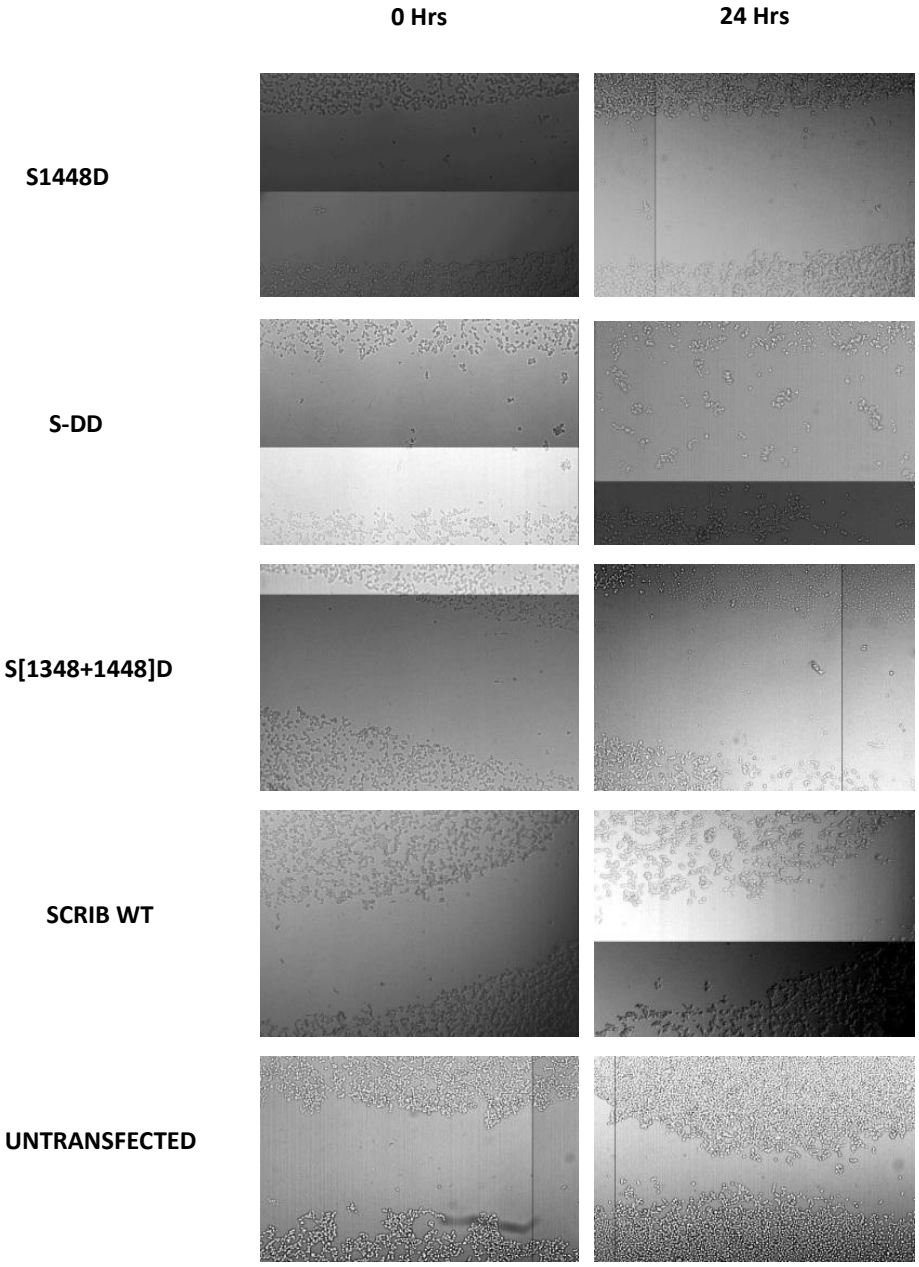

Figure 4.5 Brightfield images of wound closure of HEK293T cell lines untransfected and transfected with D-mutants and wt scrib. The untransfected cells were used as a control to model *in vivo* cell migration in breast cancer epithelial cells while wt scrib was used as a control to model *in vivo* restriction of cell migration. The images shown are representative of a full scratch acquired as large stitched images from an automated Nikon widefield microscope. For each sample, a polygon selection tool in imagej software was used to create regions of interest in the stitched scratch images to enable calculation of the areas. Scale bar= 100µm.

4.4 Discussion

Amongst other molecules, hScrib was found to be expressed in breast cancer subtypes such as TNBC (Triple-negative Breast Cancer) (Metodieva *et al.*, 2013). It implicates this known tumour suppressor and cell polarity protein in contributing to the propagation of breast tumour cells and their invasion. The changes to the phosphorylation pattern found to occur in four phosphoserine sites of hScrib, called hotspots, may be a reason for this implication. Therefore, experiments were set out to study what effects the changes in the hotspots have on hScrib function to restrict proliferation and regulate migration in epithelial cells of the breast: cell proliferation assay (MTT) and a cell migration assay (wound healing assay).

The result of the MTT assay showed that all except S1306D of the D-mutants had a proliferation rate above 50% and all except S1309A of the A-mutants had a proliferation rate below 50%. This suggests that the phosphorylation of positions 1309, 1448, 1306+1309, 1348+1448 and the phosphorylation or unphosphorylation of 1309 may result in a conformational change in the hScribble protein structure, which will expose its PDZ domains to interact with certain binding partners involved in driving the cell cycle progressively e.g. (cyclins) (Humbert et al., 2003). The Student's t-test on: (1) the proliferation rate between untreated and the treated samples and (2) the proliferation rate between WT hScrib and the mutants would suggest, as a means of screening the mutants, that S1309D, S-DD and S[1348+1448]D are candidates that may indicate the implication of hScribble in the over proliferative behaviour of breast cancer cells. This is because Student's t-test 1 (*t*test 1) showed no significant difference in proliferation rate between the aforementioned D-mutants and the untreated sample but a significant difference in proliferation to WT hScrib in Student's t-test 2 (*t*test 2). S1309A and S1348D showed no significant difference in proliferation rate in both *t*test 1 and 2 which suggests an uncertainty in the ability of such mutations to cause overproliferation in breast cancer cells.

There were two wound healing assays conducted. The result of the first wound healing assay showed that all except S1448A, S-AA, S[1348+1448]A and S-AA(1448A) of the A-mutants had above 25% recovery of the wounded area while none of the D-mutants did. This suggests that the unphosphorylation of positions 1448, 1306+1309, 1348+1448 and 1306+1309+1448 may contribute to the ability of breast cancer cells to become invasive. Considering the first Student's t-test (*t*test 1) (not shown) to test the difference in cell migration between untreated and treated samples showed a significant difference but the second Student's t-test (*t*test 2) to test the cell migration difference between WT hScrib and hScrib mutants showed a significant difference in the migration rate for A-mutants S[1348+1448]A and S-AA(1448A) (Figure 4.2). To screen mutant hScrib candidates with

the cell migration potential, a second wound healing assay was conducted with S1448A, S-AA, S[1348+1448]A and S-AA(1448A). D-mutant counterpart S1448D, S-DD and S[1348+1448]D were also tested. The result of the second wound healing assay showed cells transfected with 1448 of the A-mutants and the D-mutant, respectively, had below 8% wound recovery compared to S-AA, S[1348+1448]A and S-AA(1448A) of the A-mutants. This suggests that double and triple unphosphorylation state of hScrib at serine positions 1306+1309, 1348+1448 and 1306+1309+1448 may pose significantly to the capacity of breast cancer cells to metastasize. Although *t*test 1 (not shown) to test the difference in cell migration between untreated and treated samples showed a significant difference, *t*test 2 (not shown) to test the cell migration difference between WT hScrib and hScrib mutants revealed a significant difference in migration rate for all A-mutants and S[1348+1448]D (Figure 4.3). However, the *p*-value of S[1348+1448]A and S-AA(1448A) showed greater significance than the *p*-value of the other significant samples (similar to the first wound healing conducted).

The results from the analysis suggest S[1348+1448]A may be a candidate for breast cancer invasion. S[1348+1448]A may be involved in a cascade of events that may involve the facilitation of a modified epithelial cell polarity to support a mesenchymal phenotype which is a feature of invasive breast cancer cells (Radisky, 2005; Etienne-Manneville, 2008; Yarrow et al., 2004; Chaffer and Weinberg, 2011; Metodieva *et al.*, 2013).

Findings of the cell migration and proliferation studies of hScrib are summarized in Table 4.3

Table 4.3 Summary of hScrib Cell migration and proliferation study

Methods	Objective	**A-mutants**	**D-mutants**
Wound healing assay Widefield imaging	Cell migration	Increased cell migration represented by increased rate of wound closure	Decreased cell migration represented by reduced rate of wound closure
MTT assay Spectrophotometry	Cell proliferation	Decreased cell proliferation represented by reduced absorbance of formazan	Increased cell proliferation represented by increase in the absorbance of formazan

5. The effect of hSCRIB on cell cycle

5.1 Introduction

Protein complexes that are known to control polarity at the cellular and tissue level also contribute to the regulation of cell proliferation, in addition to other cellular functions such as cell apoptosis, and the establishment of intercellular junctions (Qin *et al.*, 2005; Huang and Muthuswamy, 2010; Macara and McCaffrey, 2013). One such polarity protein complex is the Scribble complex which comprises the proteins: hScrib, hDlg and Hugl (human homologues of the *Drosophila melanogaster* scrib, disc large and lethal giant larvae). The effects these proteins have on cellular activities depend on their subcellular localization e.g. the localization of hScrib at the basolateral region of epithelial cells is crucial for maintaining cell polarity and regulation of cell proliferation (Dow *et al.*, 2003; Grifoni *et al.*, 2004; Takizawa *et al.*, 2006; Feigin *et al.*, 2014).

Mutation of any of these proteins cooperates with oncogenic Ras signalling to cause cell overproliferation, but only with the mutation of hScrib do the Ras-induced overproliferated cells become metastatic (Qin *et al.*, 2005; Chatterjee *et al.*, 2012). This outlines hScrib as a very important tumour suppressor protein against breast cancers and other cancers which are known to display, among others, the characteristic cell overproliferation due to excessive cell division (Hanahan and Weinberg, 2011; Royer and Lu, 2011). Although the loss of hScrib function (which may result from the loss of its expression level or subcellular localization) may be associated with the aberrant proliferative nature of cancers, it seems likely that there may also be an association between inappropriate post-translational modification e.g. phosphorylation of hScrib and cell overproliferation (Zhan *et al.*, 2008; Anastas *et al.*, 2012; Metodieva *et al.*, 2013).

Cell proliferation is cell division governed by a checkpoint-monitoring, four-phased cell cycle which sometimes could incur errors. After confocal images from Chapter 3 suggested that hScrib might be involved in the cell cycle, screening assays (MTT and wound healing) were used to select candidates of hScrib with different phosphorylation statuses (unphosphorylated (Alanine, A) and phosphorylated (Aspartate, D)). These candidates originated from the four serine hotspots found in hScrib, by proteomic screening, to have altered post translational patterns in triple-negative breast cancer

(TNBC) overexpressing CD74 (Metodieva *et al.*, 2013). To understand the effects of hScrib on the cell cycle, a flow cytometric assay was performed and analysis was done to generate a cell cycle model using FCS express 4 software program created by DeNovo Software Company.

5.2 Reason for conducting flow cytometry

In Chapter 3, it was reported that confocal images of the localization of hScrib in transfected HEK293T cell line (used as a model of triple-negative breast cancer cells) suggested that hScrib might be involved in the cell cycle. This was supported by a Nagasaka *et al.* (2006) study which demonstrated that hScrib negatively regulates G1 to S phase progression in the cell cycle by localizing at the basolateral membrane in epithelial cells. However, this study only used GFP-fused hScrib domain and deletion constructs and it did not look at how the phosphorylation pattern of hScrib affected the cell cycle. With hScrib implicated in breast cancer progression (Greenwood *et al.*, 2012), could the changes in the pattern of phosphorylation of four serine sites, identified to be affected by CD74 overexpression in TNBC, be a contributor to the lack of inhibitive control exhibited in the cell cycle by breast cancer cells. To investigate this reasoning, a flow cytometric experiment and analysis was conducted on mutants of hScrib selected as possible candidates of breast cancer proliferation and invasion through MTT and wound healing assay screenings that were conducted and reported in Chapter 4. WT hScrib was used as a control.

5.3 The cell cycle model and results of the flow cytometry

Analysis of the flow cytometry result involved the introduction of a model that fits the histograms generated by the Accuri C6 flow cytometer to enable better analysis and comparison of the G1, S and G2/M phases between A and D-mutants, between hScrib mutants within each group and between hScrib mutants and control. The model used was from FCS express 4 created by DeNovo Software Company. The expression of GFP-fused hScrib and its mutants was detected by the FL1 channel (FITC) while the fluorescence intensity (which indicates DNA content) of the PI-stained DNA was detected by the FL2 channel.

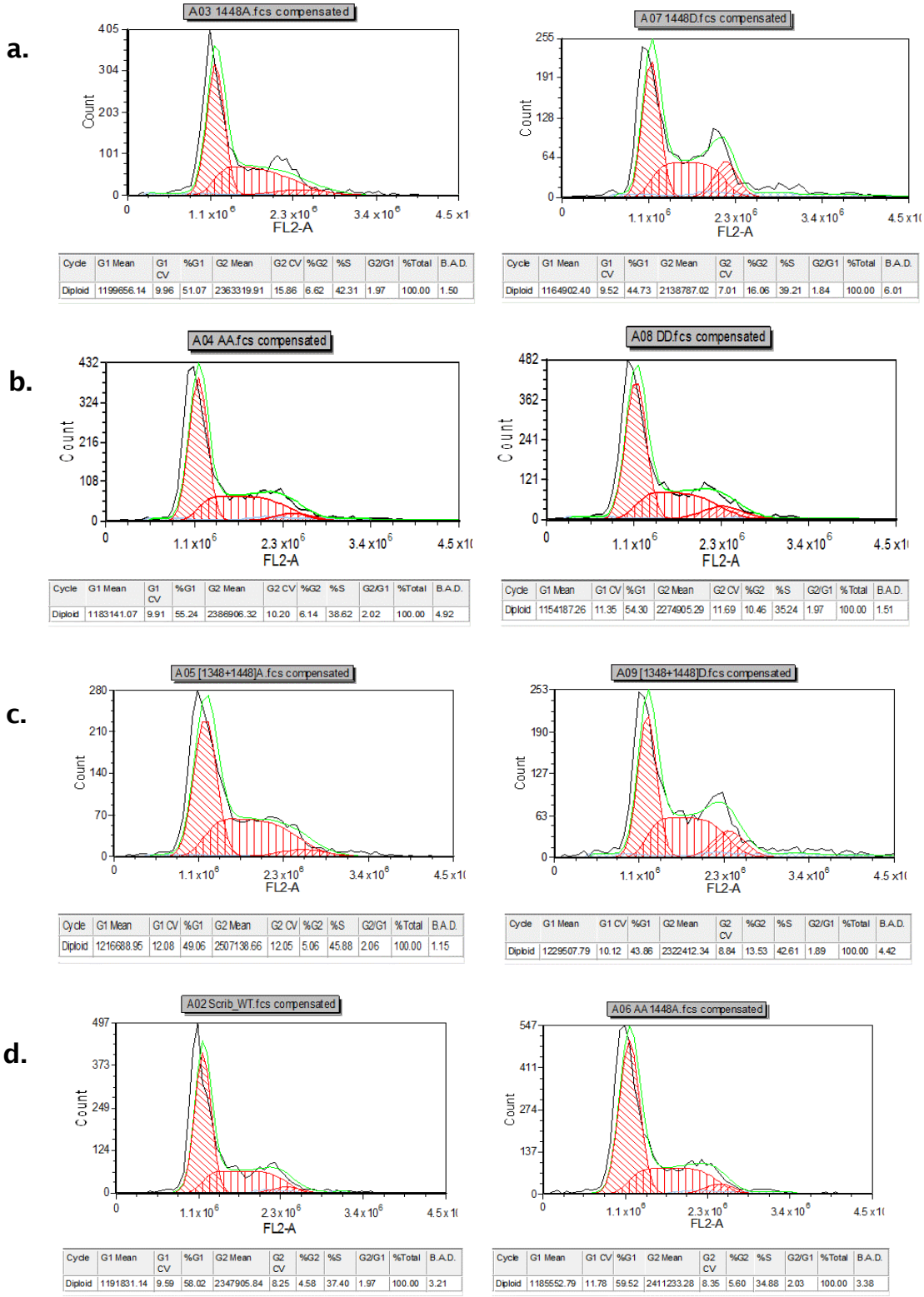

Figure 5.1 Gated histograms with a model of the distribution of $FITC^{+}$+PI^{+} HEK293T cell line population transfected with wt hScrib and selected candidates of A and D mutants of hScrib. The same gating was applied to each sample and adjusted to find the model to fit their histograms. The x-axis (FL2-A) represents the total fluorescence intensity measured by the channel detecting PI-stained DNA of cell population that were positively expressing the respective hScrib. The y-axis (count) represents the number of cells under each cell cycle phase depicted by three red-patterned curves under the histogram. The histograms are in the order of A Vs D: **a.** 1448A and 1448D mutant hScrib. **b.** AA and DD mutant hScrib. **c.** [1348+1448]A and [1348+1448]D mutant hScrib. **d.** hScrib WT control and AA1448A. These mutants and control were ordered in this manner to enable easy comparison of their cell cycle phases. However, comparison was also made between mutants and control and between mutants of the same group. The results here are representative of the experiment conducted in duplicate for each mutant and control.

The histograms show a gated HEK293T cell population that not only had their DNA stained with propidium iodide (PI), but also positively expressed the respective hScrib DNA's they were transfected with. Therefore, the cell population are $FITC^{+}$+PI^{+}. The gating was to exclude untransfected cell population ($FITC^{-}$+PI^{+}), and as much as possible, cell aggregates, cell doublets and debris that developed during sample preparation. The edges of the histograms are traced, with as much fit as possible, by a green line which implies the application of a multicycle mathematical model (the polynomial S-fit model of Dean and Jett integrated by Phoenix Flow Systems in DeNovo Software) to the histograms. This was followed by the formation of three differently red-patterned curves under each green trace to compartmentalize the G1, S and G2/M phases. The same gate was used for all samples. By manually adjusting the gate to determine which of the six different multicycle models will fit the histograms, the best model with good S phase confidence and low B.A.D (background, aggregates and debris) was used to resolve what percentage of $FITC^{+}$+PI^{+} cell population were in the respective cell cycle phases. The peaks of G1 and G2 phases represent the average number of cells that had the maximum fluorescence intensity in the G1 and G2 phases, respectively. Hence, the G1 and G2 mean displayed in the DNA model summary statistic table under each histogram. The coefficient of variation (CV) determines the accuracy of DNA content measurement in the cell cycle and the quality of the histogram. It is a measure of the spread of DNA from cells under the G1 and G2 curves- the G1 more importantly. The smaller the CV, the better the estimated percentage of cells in each cell cycle phase (Carroll *et al.*, 2007:226; Ormerod, 2008). Expressed in Table 5.1, in tabular form, is a summary of the cell cycle results.

Table 5.1 Cell cycle model summary

	% G1				% S				% G2				χ^2	
	1	2	mean % G1	stdev % G1	1	2	mean % S	stdev % S	1	2	mean % G2	stdev % G2	1	2
SCRIB	58.02	58.37	58.20	0.25	37.40	36.86	37.13	0.38	4.58	4.78	4.68	0.14	0.80	0.62
S1448A	51.07	55.61	53.34	3.21	42.31	37.40	39.86	3.47	6.62	6.99	6.81	0.26	0.75	0.59
S-AA	55.24	63.36	59.30	5.74	38.62	30.49	34.56	5.75	6.14	6.15	6.15	0.01	0.45	0.31
S[1348+1448]A	49.06	49.04	49.05	0.01	45.88	46.38	46.13	0.35	5.06	4.58	4.82	0.34	0.45	0.76
S-AA(1448A)	59.52	58.26	58.89	0.89	34.88	37.21	36.05	1.65	5.60	4.54	5.07	0.75	0.67	0.69
S1448D	44.73	42.31	43.52	1.71	39.21	41.25	40.23	1.44	16.06	16.45	16.26	0.28	0.74	0.65
S-DD	54.30	56.80	55.55	1.77	35.24	32.83	34.04	1.70	10.46	10.37	10.42	0.06	0.82	0.44
S[1348+1448]D	43.86	44.10	43.98	0.17	42.61	41.87	42.24	0.52	13.53	14.03	13.78	0.35	0.79	0.39

Each mutant sample and control (WT hScrib) was duplicated. Student *t*test (not shown) was used to statistically analyse a two-tailed paired null hypothesis that there would be no significant difference between wt scrib and the scrib mutants on the percentage of cells in the G1, S and G2 phases of the cell cycle. Statistical significance was established at $p<0.01$. Stdev= standard deviation; χ^2= chi-square; %S= percentage of cells in the synthesis phase of the cell cycle; %G1= percentage of cells in the first preparatory or gap stage of the cell cycle, before the S phase; %G2= percentage of cells in the second preparatory or gap stage of the cell cycle, after the S phase but before the mitosis (M) phase.

The Chi-Square (χ^2) is an indication of how well the mathematical model is fitting the histogram. The smaller the χ^2, the better the fit of the model to the histogram. Although the result of each repeat of the samples have low χ^2, they also have high CV values (>3%). This may be due to inadequate data analysis, improper staining conditions or inadequacies in sample preparation to minimize large number of dead cells, cell doublets, clumps and debris. Also, the use of cultured cells which have heterogeneous DNA content may play a part in the high CV values of the samples (Pozarowski and Darzynkiewicz, 2004; Ormerod, 2008). From Table 5.1, the percentage of cells in the G1 phase that were transfected with S[1348+1448]A and S[1348+1448]D were significantly lower than other samples, with S[1348+1448]D (43.98±0.17%; $p<0.01$) more significantly lower than S[1348+1448]A (49.05±0.01%; $p<0.01$) (p values not shown). The percentage of cells in the S phase that were transfected with S[1348+1448]A (46.13±0.35%; $p<0.01$) were significantly higher than other A-mutants, D-mutants and WT hScrib. The percentage of cells in the G2 phase that were transfected with WT hScrib is the lowest compared to the mutant samples. However, this was not statistically significant when compared to the A-mutants (4.68±0.14% vs 6.81±0.26%, 6.15±0.01%, 4.82±0.34% and 5.07±0.75%; $p<0.01$). Comparing WT hScrib or A-mutants to the D-mutants, there was a significant difference

as more than 10% of cells transfected with D-mutants progressed to the G2 phase i.e. two to three times more D-mutant-transfected cells in the G2 phase than the A-mutants and WT hScrib (Figure 5.2).

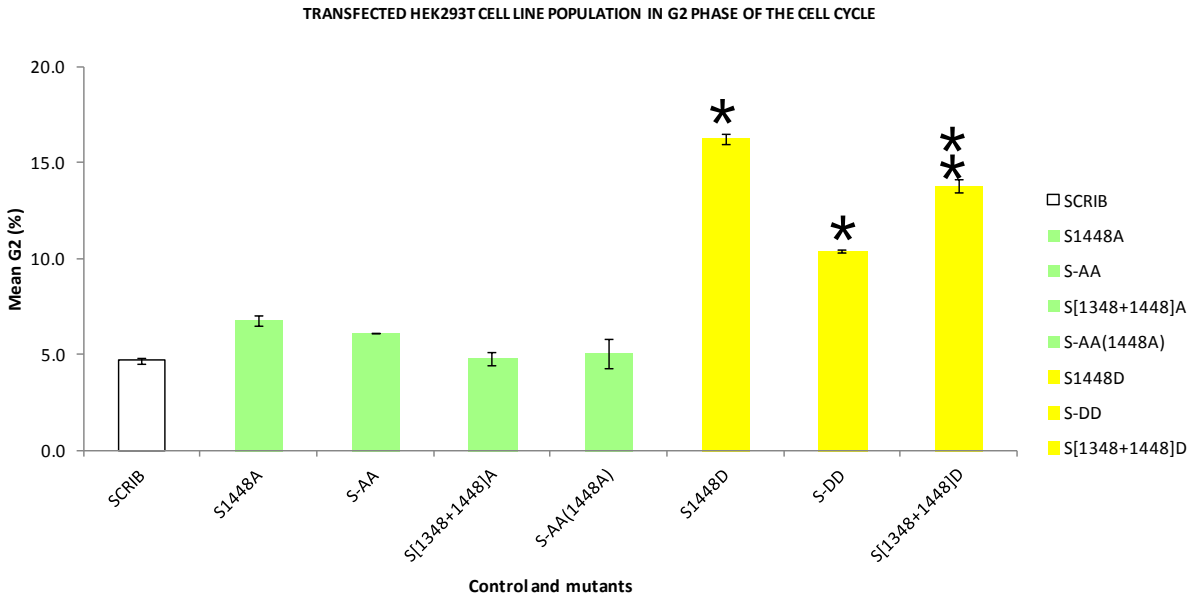

Figure 5.2 Bar graph of HEK293T cell lines, transfected with hScrib samples, in the G2 phase of the cell cycle. The graph shows that more cells entered the G2 phase of the cell cycle when transfected with D-mutants of hScrib than when transfected with A-mutants of hScrib or WT hScrib. Hence the probability that the cells would complete the cell division process. This supports the MTT proliferation assay in Chapter 3 that suggested that D-mutants proliferated more than the A-mutants of hScrib. The results are expressed as mean ± stdev, $p<0.01$. The error bars show the variability about the percentage mean for control and mutant sample. The asterisks indicate the level of significant difference of cells in the G2 phases of the cell cycle between WT-transfected cells and mutants. Mutants without the sign were not significant.

The results, taken together, suggest D-mutants favour progression through the cell cycle thereby supporting cell proliferation, while A-mutants inhibit cell cycle progression to favour cell migration.

5.4 Discussion

The cell cycle controls cell proliferation. Breast cancer is initiated by inappropriate cell proliferation and hence a disease of the cell cycle (Collins *et al*, 1997; Sandal, 2002; Sa and Das, 2008). After employing the MTT and wound healing assays as screening processes, some hScrib A-mutants and their D-mutant counterpart were selected to study their effects on the cell cycle. As it was shown in Chapter 4 that the D-mutants in the MTT assay proliferated more than the A-mutants, it was also shown through the analysed flow

cytometry results that D-mutants enabled progression of more cells into the G2/M phase (Figure 5.2) and therefore support cell proliferation. If D-mutants of hScrib support cell cycle progression, it indirectly suggests what phosphorylation state hScrib acts to restrict cell cycle progression and hence enact its tumour suppressive role (Chow A.Y. 2010) i.e. the serine hotspots identified have to be unphosphorylated. It also suggests that unphosphorylated hScrib may be functioning at the G1 restriction point or at the G1/S phase border to repress the cell cycle (Nagasaka *et al.*, 2006).

To contribute to the regulation of signalling pathways such as polarity, proliferation, migration and apoptosis, hScrib possesses a scaffold structure. This enables hScrib, by facilitating close interaction of proteins, to act as a molecular bridge to bring about the formation of complexes of proteins that establish cell signalling networks that are effective and specific to the respective signalling pathway. While enabling and moderating the signal strength of the cell signalling networks, the scaffolding property of hScrib also minimizes the crosstalk between these signalling networks. This is especially significant in the mitogen-activated protein a kinase (MAPK) pathway via which hScrib is likely to exert its tumour suppressive role in the cell cycle (Levchenko *et al.*, 2000; Dhanasekaran *et al.*, 2007).

The MAPK pathways are a family of protein kinases involved in phosphorylation cascades that control or are involved in multiple cellular activities e.g. cell growth, cell proliferation, cell differentiation, survival and apoptosis. The cell cycle mechanism of cell proliferation is controlled by the MAPK (mitogen-activated protein kinase) pathways which have been reported to be responsible for cancers and other human diseases (Seger and Krebs, 1995; Wada and Penninger, 2004; Zhan *et al.*, 2008; Kim and Choi, 2010; Good *et al.*, 2011; Greenwood *et al.*, 2012). Of these MAPK pathways, the ERK signalling pathways (ERK1/2 and ERK5) have been implicated in the cell cycle (Chuderland and Seger, 2005; Wang and Tournier, 2006): the classical ERK1/2 activation via the Ras/Raf/MEK/ERK signal transduction cascade and the ERK5 activation via the Ras-WNK1/MEKK/MEK5/ERK5 signal transduction cascade (Wang and Tournier, 2006; Moniz and Jordan, 2010). ERK1/2 and EKR5 are third tier protein kinases that are phosphorylated by MEK1/2 and MEK5, respectively. MEK1/2 activate ERK1/2 translocation to the nucleus while MEK5 activates EKR5 phosphorylation which activates further downstream reactions. Ultimately, both signal transduction cascades activate protein kinases like RSK (ribosomal S6 kinase) and transcription factors like E2F, c-Myc, c-Fos, Sap1 and NF-kB, TCF (ternary complex factor), SRF (serum response factor), c-Jun etc, to encode genes required for progression through G1, DNA replication of the S phase and subsequent cell cycle phases (Sears *et al*., 2000; Zhang and Liu, 2002;

Nashimoto and Nashida, 2006; Cude *et al*., 2007; Chen and Thorner, 2007; Gabay *et al*., 2014; Lodish *et al*., 2013: 741 and 887).

How D-mutants of hScrib enabled G2/M phase cell progression may come from the understanding of hScrib control of ERK activation. This is because hScrib has been found to control ERK activation. A study published in 2010, by Nagasaka *et al*, discovered that hScrib has two kinase interaction motif sites (N-terminal KIM and C-terminal KIM) with two corresponding downstream phospho-acceptor sites (S853 and S1448) that influence the effect of ERK by either (i) inhibiting upstream MEK phosphorylation of ERK or (ii) dephosphorylating activated ERK (phospho-ERK): ERK1/2 phosphorylated by MEK1/2 is activated for nuclear translocation but in the presence of hScrib, phospho-ERKs bind to the ERK docking sites (N-terminal KIM and C-terminal KIM) of hScrib and lose their phosphate to the phospho-acceptor sites on hScrib which becomes phosphorylated. Either way, hScrib controls when ERK is activated and translocated to the nucleus. ERK kinase function is inhibited and cell cycle progression is suppressed (Ramos, 2008; Nagasaka *et al.*, 2010).

A statistical *ttest G2* (not shown) was conducted to compare the difference in the percentage of cells that entered the G2/M phase between WT hScrib and the selected hScrib D-mutants. It showed a highly significant percentage of cells transfected with the selected hScrib D-mutants entered G2/M phase, especially the D-mutants with the mutated S1448 site i.e. S1448D and S[1348+1448]D. This was because a further *ttest G2 D-mutant* (not shown) to test, among the hScrib D-mutants, the difference in percentage of cells that entered G2/M phase showed a significant difference between phosphorylated S1448 site D-mutants (S1448D and S[1348+1448]D) and non-phosphorylated S1448 site D-mutants (DD). It could be that S1448 site phosphorylation (with or without S1348) changed hScrib conformation which compromised the orientation of the C-terminal KIM site and affected the interaction with ERK. Another reason could be that phosphorylation of the C-terminal phospho-acceptor S1448 site may have, rather than alter hScrib conformation, reduced the strong ERK-binding affinity of the C-terminal KIM site to weaken the interaction (Durek *et al.*, 2009; Wu *et al.*, 2009; Nagasaka *et al.*, 2010; Sun *et al.*, 2010). As Nagasaka *et al.* (2010) revealed ERK to be the main protein that phosphorylates hScrib at S1448, the presence of an already phosphorylated S1448 site may have prevented phospho-ERK from binding and phosphorylating hScrib at the S1448 site. The consequence of these events occurring due to a mutated S1448 mean ERK is free to remain phosphorylated and activated by MEK1/2 and activated ERK cannot be regulated by hScrib phosphorylation. The ERK phosphorylation levels increase thus encouraging phospho-ERK translocation to the nucleus. Besides being significantly

different from WT hScrib and A-mutants, D-mutant DD i.e. S[1306+S1309]D, was also significantly different from the phosphorylated S1448 site D-mutants (S1448D and S[1348+1448]D). This could be due to its phosphorylation status which may have affected the conformation of the C-terminal KIM docking site downstream of its phosphorylated position. This conformational change may have caused weak interaction with ERK, not enough to repress G2/M cell entry but also not enough to reduce the amount of free phospho-ERK to translocate to the nucleus (Durek *et al.*, 2009; Sun *et al.*, 2010). These potentially inappropriate phosphorylations may be an incentive for initiation of oncogenic cell proliferation.

The ERK1/2 signalling may not necessarily be the only pathway to G2/M cell progression as a study by Cude *et al*. (2007) found that G2/M cell cycle progression is via the ERK5 (or BMK1) signalling pathway. MEK5-phosphorylation of ERK5 recruits and activates RSK2 (ribosomal S6 kinase 2) to mediate the release of NFkB from the cytosolic inactive IkB:NF-kB complex by phosphorylation of IkB for degradation. NF-kB translocation to the nucleus activates its DNA-binding ability to transcribe molecules required for G2-M transition. ERK5 functions similar to ERK1/2: (i) it can be stimulated by Ras (although enhanced by WNK1) and (ii) ERK5 can phosphorylate ERK1/2 substrates like Sap1, c-myc, RSK (Nashimoto and Nashida, 2006) and probably hScrib (via KIM sites). If this is the case, at G2/M phase, phosphorylation of hScrib in the manner represented by the D-mutant samples, either diminishes in its ability to interact with ERK5 to execute its inhibitive role on the cell cycle or re-configures hScrib to support ERK5 recruitment of RSK2 via its scaffolding structure (Durek *et al.*, 2009; Wu *et al.*, 2009; Good *et al.*, 2011). Besides the mediation of G2/M cell cycle progression by the ERK5 or ERK1/2 signalling pathways, both signalling pathways may also mediate G1/S transition and S phase progression by inducing cyclin D1 expression for cyclin D1-cdk4/6 complex hyperphosphorylation (inactivation) of tumour suppressor pRb (retinoblastoma protein) at G1 restriction point and cyclin A expression to facilitate transcription of molecules required for DNA replication (Guttridge *et al.,* 1999; Nagasaka *et al.*, 2010; Nashimoto and Nashida, 2006; Cude *et al*., 2007; Moniz and Jordan, 2010).

From a statistical *ttest G1* (not shown) conducted to compare the difference in the percentage of cells that arrested in G1 phase between WT hScrib and the hScrib mutants, it was found that the percentage of cells arrested in G1 when transfected with S[1348+1448]A or S[1348+1448]D was significantly lower than WT hScrib. Other mutants showed no significant difference. In addition, a *ttest S* (not shown) conducted to compare the percentage of cells arrested in the S phase between WT hScrib and the hScrib mutants showed the percentage of S[1348+1448]A transfected cells arrested in S phase

was significantly higher than WT hScrib. Other mutants showed no significant difference. Taken together, these suggest that S[1348+1448]D may be responsible for G2/M transition but S[1348+1448]A could be responsible for both G1/S transition and progression through the S phase. S[1348+1448]A may be an inappropriate phosphorylation state that engage in interactions that support the actions of cyclin D1-cdk4/6, cyclin E-cdk2 and cyclin A-cdk2 complexes (Woo and Poon, 2003) to enable G1/S transition and the nucleic acid replication and transcription for S phase progression. Also, from the statistical *ttest G1* conducted, it is possible that unphosphorylation of hScrib (other than S[1348+1448]A) enable G1 arrest by direct interaction with APC (Takizawa *et al*., 2006).

APC (adenomatous polyposis coli) is a tumour suppressor that negatively regulates G1 to S phase cell cycle progression by binding to β-catenin (Ishidate *et al*., 2000; Wang *et al*., 2008). Beta(β) catenin is a transcriptional co-activator of the Armadillo-domain subfamily of proteins found in the nucleus and at the intercellular adherens junction complexing with other cell-adhesion molecules like E-cadherin, p120 catenin, etc (Anastasiadis and Reynolds, 2000; McCrea and Gu, 2010; Lohia *et al*., 2012). β-catenin is regulated by the Wnt signal transduction pathway that is responsible for cell fate determination, apoptosis and also cell proliferation. APC binding to β-catenin promotes proteosome-mediated degradation of β-catenin, when β-catenin is in excess in the cytoplasm or nucleus (Henderson, 2000; Benchabane and Ahmed, 2009; MacDonald *et al*., 2009). This downregulatory mechanism of β-catenin by APC is facilitated by the interaction of APC with a member of the Scribble complex of polarity proteins, hDlg (Ishidate *et al*., 2000). hScrib is a member of the Scribble complex that is known to interact with hDlg at the basolateral membrane region to maintain cell polarity. hScrib-hDlg complex associate with cell junctional complexes to maintain cell-cell contact (Bilder *et al*., 2000; Nakagawa and Huibregtse, 2000; Dow *et al*., 2003). If the localization of hScrib at the basolateral membrane (which contributes to maintenance of cell polarity) is responsible for the G1 arrest of cells in the cell cycle (Nagasaka *et al*., 2006), then it is likely facilitated by hScrib-hDlg complex in the basolateral membrane recruiting APC from the cytoplasm to bind to and chaperone excess cytoplasmic or nuclear β-catenin for degradation in the cytoplasm. In addition to hScrib KIM site-dependent inactivation of ERK, proteins involved in G1 to S transition e.g. c-Myc, c-Fos, E2F, c-cdk4/6, cdk2, cyclin D1, cyclin E, etc, are downregulated. Hence cell proliferation is terminated. Phosphorylation of hScrib, as seen in Figure 5.2, may disrupt the localization and interaction of hScrib with its binding partners at the basolateral membrane to maintain cell polarity and the adherens junction: hScrib localizes to the cytoplasm and is unable control the ERK signal transduction

pathway and enable APC-mediated proteosomal degradation of β-catenin. Thus cell proliferation is unchecked.

The results so far suggest that although phosphorylation of hScrib enables G2/M transition, it does not facilitate the completion and exit from M phase as this requires its dephosphorylated. It is also possible that dephosphorylation of serine sites 1448 (most likely) and 1348 may be required for exit from M phase. However, these possibilities are only speculations until confirmed by results from the analysis of mass spectrometry Co-IP and WB Co-IP, which are pending.

The findings of the cell cycle study of hScrib is summarized in Table 5.2

Table 5.2 Summary of hScrib Cell cycle study

Method	Objective	**A-mutants**	**D-mutants**
Flow cytometry	Cell cycle progression	G1 arrest	G2/M arrest

6. Protein-protein interactions of hSCRIB

6.1 Introduction

Proteins are the basic functional unit of a cell and hence living systems in the human body. They are dynamic as their functions are diverse. How proteins function determine how cells are organized and what their specific roles are. The diverse function of a protein, most likely, is through the formation of molecular networks by its interaction with other proteins within the cell to form protein complexes and/or cause cascades (Berg *et al.*, 2002:3; Spirin and Mirny, 2003). One important cell behaviour governed by the formation of protein-protein interactions is in the maintenance of cell polarity (Humbert *et al.*, 2003; Chatterjee and McCaffrey, 2014).

Polarity at the cellular and tissue level contribute to the regulation of cell migration, cell proliferation, apoptosis, establishment of intercellular junctions, tissue organization and tumour suppression (Qin *et al.*, 2005; Huang and Muthuswamy, 2010; Macara and McCaffrey, 2013; Chatterjee and McCaffrey, 2014). Known to be involved in facilitating these cell behaviours is the Scribble complex which comprises the proteins: hScrib, hDlg and Lgl. These components are also tumour suppressors (Su *et al.*, 2012), of which one of the components, hScrib, was the focus of study.

The hScrib was implicated in the invasion and metastasis of triple-negative breast cancer (TNBC) due to its protein interactions (Greenwood *et al.*, 2012; Metodieva *et al*., 2013). Therefore, this experiment aims to study the effect of hScrib mutations on interactions with its binding partner so that the molecular mechanism by which hScrib provides a tumour-suppressive function could be understood. By identifying the protein binding partners of hScrib when phosphorylated and unphosphorylated at given C-terminal serine sites of hScrib, a signalling pathway can be developed.

Breast cancer, or any other cancer, is a disease of the cell cycle (Collins *et al*, 1997; Sandal, 2002) and a confocal image in chapter 3 (Figure 3.4b, S-DD) suggested hScrib may be involved in the cell cycle. At what stage of the cell cycle remains unknown. Therefore, to begin to identify the binding partners involved with hScrib in cell migration and at stages of the cell cycle, a co-immunoprecipitation (CoIP) assay that incorporated cell synchronization was performed. This was complemented with the use of a nanoscale

electrospray ionization hybrid LTQ/Orbitrap Velos mass spectrometer (MS) to identify the proteins from CoIP that were proteolytically treated before MS analysis. Computational predictions of probable interactions of hScrib with other proteins were applied to aid in developing the biological pathway/s through which it prevents or may be involved in invasion of breast cancer (Zahiri *et al.*, 2013).

6.2 Statistical analysis of MS results

The mass spectrometer was used to measure the protein abundances of two conditions that were set up in the Co-IP assay: a negative control condition with a non-specific antibody and an experimental condition with GFP antibody to target GFP in the GFP-tagged S[1306+1309]A and S[1306+1309]D mutants of hScrib used as baits, respectively. The result from the mass spectrometer was a proteomic dataset presented in Microsoft Excel spreadsheet. It contained 1195 identified proteins with their abundances in both conditions (dataset not shown). Each experimental condition (labelled aa-p1 to aa-p3 and dd-p1 to dd-p3 to represent S[1306+1309]A and S[1306+1309]D pull-down, respectively) and the negative control condition of S[1306+1309]D pull-down (labelled dd-n1 to dd-n3) was in triplicate. The negative control condition for S[1306+1309]A pull-down was in duplicate (aa-n1 to aa-n2). Due to huge variations in the intensity values within the two conditions and to avoid the risk of false positive results during analysis, a spectral counting (MS/MS) approach (Heinecke *et al.*, 2010) was adopted: each replicate was summed up e.g. aa-n1 + aa-n2, and the value of the total sum of the replicates in each condition was calculated i.e. Σ(aa-n1 + aa-n2).

For a biologically validated result, it was important to identify differences in protein abundances that show statistical significance when the hScrib mutants, used as bait, were expressed. This was in addition to minimizing the false discovery rate (FDR). To achieve these, a combination of statistical methods was applied: 1.) G-test of goodness-of-fit = 2Σ [O*ln (O/E)] of one nominal variable (protein abundance) with two conditions (negative control and experimental). The G-test measures, for each protein in the data, how far their observed MS/MS Count (O) is likely to be from their expected theoretical MS/MS Count (E) if null hypothesis is to be true. Therefore, it is also called a log-likelihood ratio test. In the G-test, all summed up MS/MS Counts with abundance of 0 were assigned a value of 1 to enable statistical computation i.e. spectral count + 1.

However, the G-statistic values obtained do not prove statistical significance without comparing with 2.) The chi-squared distribution (CHIDIST) from Microsoft Excel. With a degree of freedom (n-1) of 1 i.e. 2 conditions minus 1, CHIDIST provides a measure, via

probability values (p-value), of how significant the G-statistic values are. In spite of this, stringency in the statistical significance was required because of the multiple gene set tested at the same time. Therefore, the question was asked: what is the probability that the p-value for each protein show true significance or non-significance? This question prompted the use of a multiple testing correction method called 3.) Bonferroni correction.

The p-value of each protein was multiplied by the total number of identified proteins (1195) in the dataset to give an adjusted p-value (adjP). From the result of this operation, all corrected p-values of 1 and above were assigned the value of 1. This was to prevent the probability of a type 1 error or false-positive result (Bland and Altman, 1995; Noble, 2009; Heinecke *et al.*, 2010). Hence, with a set threshold of $p<0.05$, the null hypothesis that there would be no significant difference in protein abundances between the negative control condition and the experimental conditions, were evaluated.

These calculations produced two gene lists (Tables 6.1a and 6.1b and 6.2a and 6.2b) that showed, in decreasing order of significance, the proteins with significant difference in their abundance, when S[1306+1309]A and S[1306+1309]D hScrib mutant were expressed and used as bait.

Table 6.1a Significant binding partners of S[1306+1309]A hScrib

Uniprot	Protein names	Gene symbol	Adj. P-value
P04264	Cytokeratin-1	KRT1	9.90E-67
P35527	Cytokeratin-9	KRT9	6.36E-57
P35908	Cytokeratin-2e	KRT2E	4.43E-49
P13645	Cytokeratin-10	KRT10	1.20E-46
Q14160	Protein scribble homolog	SCRIB	1.74E-46
P08670	Vimentin	VIM	1.02E-29
P17812	CTP synthase 1	CTPS1	4.85E-25
P08779	Cytokeratin-16	KRT16	1.18E-20
Q13085	Acetyl-Coenzyme A carboxylase alpha	ACACA	7.18E-19
P13647	Cytokeratin-5	KRT5	1.05E-17
P02538	Cytokeratin-6A	KRT6A	2.45E-13
Q9Y383	RNA-binding protein Luc7-like 2	LUC7L2	1.00E-12
P00761	TRYP_PIG		1.23E-11
P50213	Isocitrate dehydrogenase [NAD] subunit alpha, mitochondrial	IDH3A	5.90E-11
Q9Y2X7	G protein-coupled receptor kinase-interactor 1	GIT1	1.26E-10
Q96N67	Dedicator of cytokinesis protein 7	DOCK7	4.22E-10
P02769	(Bos taurus) Bovine serum albumin precursor		5.29E-10
Q9UJS0	Solute carrier family 25 (Mitochondrial aspartate-glutamate car	SLC25A13	8.35E-10
C9JP52	TBC1 domain family member 5	TBC1D5	1.11E-09
P61513	Ribosomal protein L37a	RPL37A	3.82E-09
P12277	Creatine kinase, brain	CKB	5.50E-09
Q16352	Internexin neuronal intermediate filament protein, alpha varia	INA	5.97E-09
Q9Y2H2	Inositol polyphosphate 5-phosphatase F	INPP5F	1.56E-08
P27708	Dihydroorotase and Glutamine-dependent carbamoyl-phospha	CAD	1.90E-08
P07900	Heat shock protein HSP 90-alpha	HSP90A	5.28E-08
P08708	Ribosomal protein S17	RPS17	7.33E-08
Q9U6Y5	Green fluorescent protein	GFP	7.88E-08
P02533	Cytokeratin-14	KRT14	1.36E-07
Q86YZ3	Hornerin	HRNR	4.41E-07
Q14155	Rho guanine nucleotide exchange factor (GEF) 7	ARHGEF7	1.90E-06
P42285	Superkiller viralicidic activity 2-like 2	SKIV2L2	1.90E-06
P15924	Desmoplakin	DSP	2.01E-06
O14654	Insulin receptor substrate 4	IRS4	7.41E-06
P25098	Beta-adrenergic receptor kinase 1	ADRBK1	1.02E-05
P07197	Neurofilament medium polypeptide	NEFM	2.08E-05
P22314	Ubiquitin-like modifier-activating enzyme 1	UBA1	2.89E-05
Q9UJV9	DEAD (Asp-Glu-Ala-Asp) box polypeptide 41	DDX41	4.60E-05
Q6NZY4	Zinc finger CCHC domain-containing protein 8	ZCCHC8	1.11E-04
P62937	Peptidylprolyl isomerase A (Cyclophilin A)	PPIA	1.19E-04

In order of adjusted p-value (Bonferroni correction), this table shows 39 out of the 79 proteins that present significant differential expression when HEK293T cell line was transfected with S[1306+1309]A mutant of hScrib and thus expressed. Based on spectral count + 1, it was possible to determine the G-test, p-value and, for stringency, an adjusted p-value at a threshold of significance of $p<0.05$. Highlighted in yellow is the hScrib protein identified by the mass spectrometer. Each protein has a uniprot accession code to enable identification of the gene of each protein in any bioinformatics database.

Table 6.1b Significant binding partners of S[1306+1309]A hScrib (contd.)

Uniprot	Protein names	Gene symbol	Adj. P-value
P62750	Ribosomal protein L23a	RPL23A	1.44E-04
B1ARM6	Centrosomal protein 170kDa	CEP170	1.78E-04
O94776	Metastasis-associated 1-like 1	MTA2	2.06E-04
P01860	Ig gamma-3 chain C region	IGHG3	2.06E-04
Q8TA86	Retinitis pigmentosa 9 protein (autosomal dominant)	RP9	2.06E-04
P07195	L-lactate dehydrogenase B chain	LDHB	2.36E-04
P52701	DNA mismatch repair protein Msh6	MSH6	3.64E-04
Q9BVP2	Guanine nucleotide-binding protein-like 3 (nucleolar)	GNL3	4.23E-04
P05141	solute carrier family 25 (mitochondrial carrier; adenine nucleot	SLC25A5	4.78E-04
P10809	Heat shock 60 kDa protein (Chaperonin), mitochondrial	HSPD1	5.05E-04
Q14257	Reticulocalbin-2	RCN2	5.85E-04
Q9NVI7	ATPase family, AAA domain-containing protein 3A	ATAD3A	9.41E-04
Q5D862	Filaggrin-2	FLG2	1.47E-03
Q92616	General control of amino acid synthesis 1-like protein 1 (yeast)	GCN1L1	1.76E-03
E9PBD4	Dolichol-phosphate mannose synthase	DPM1	2.43E-03
Q14839	Chromodomain-helicase-DNA-binding protein 4	CHD4	4.07E-03
Q01130	arginine/serine-rich splicing factor 2	SFRS2	4.07E-03
P19474	Tripartite motif-containing protein 21	TRIM21	4.07E-03
P26368	U2 small nuclear RNA auxiliary factor 2	U2AF2	4.07E-03
Q9Y580	RNA-binding motif protein 7	RBM7	4.95E-03
P62249	Ribosomal protein S16	RPS16	5.79E-03
P62277	Ribosomal protein S13	RPS13	5.96E-03
Q9BU76	Multiple myeloma tumor-associated protein 2	MMTAG2	6.60E-03
Q15084	Protein disulfide-isomerase A6	PDIA6	6.65E-03
P61978	Heterogeneous nuclear ribonucleoprotein K	HNRNPK	1.01E-02
P49327	Fatty acid synthase	FASN	1.11E-02
P62269	Ribosomal protein S18	RPS18	1.21E-02
Q9Y3C1	HBV pre-S2 trans-regulated (nucleolar) protein 3	NOP16	1.50E-02
P62861	Ribosomal protein S30	FAU	1.68E-02
Q13547	Histone deacetylase 1	HDAC1	1.80E-02
Q69YN4	Protein virilizer homolog	KIAA1429	1.80E-02
P00558	Phosphoglycerate kinase 1	PGK1	1.80E-02
P13797	Plastin-3	PLS3	1.80E-02
Q9UQ35	Serine/arginine-rich splicing factor-related nuclear matrix prot	SRRM2	1.80E-02
Q92945	KH type-splicing regulatory protein	KHSRP	2.47E-02
O15027	SEC16 homolog A	SEC16A	2.59E-02
P00338	L-lactate dehydrogenase A chain	LDHA	2.72E-02
P42766	Ribosomal protein L35	RPL35	2.87E-02
P35580	Myosin, heavy chain 10, non-muscle	MYH10	2.95E-02
P63173	Ribosomal protein L38	RPL38	3.19E-02

A continuation of the previous table. In order of adjusted p-value (Bonferroni correction), this table shows the remaining 40 of the 79 proteins that present significant differential expression when HEK293T cell line was transfected with S[1306+1309]A mutant of hScrib and thus expressed. Based on spectral count + 1, it was possible to determine the G-test, p-value and, for stringency, an adjusted p-value at a threshold of significance of $p<0.05$.

Table 6.2a Significant binding partners of S[1306+1309]D hScrib

Uniprot	Protein	Gene symbol	Adj. P-value
P04264	Cytokeratin-1	KRT1	9.35E-176
P35527	Cytokeratin-9	KRT9	3.66E-131
P35908	Cytokeratin-2e	KRT2E	2.67E-91
P13645	Cytokeratin-10	KRT10	3.09E-84
P08779	Cytokeratin-16	KRT16	8.16E-58
Q14160	Protein scribble homolog	SCRIB	2.53E-57
P13647	Cytokeratin-5	KRT5	5.61E-46
P02538	Cytokeratin-6A	KRT6A	2.44E-34
P17812	CTP synthase 1	CTPS1	4.83E-28
Q13085	Acetyl-Coenzyme A carboxylase alpha	ACACA	1.40E-20
P15924	Desmoplakin	DSP	3.17E-18
P02533	Cytokeratin-14	KRT14	3.70E-18
P61513	Ribosomal protein L37a	RPL37A	1.07E-17
P00761	TRYP_PIG		2.41E-16
Q9Y2X7	G protein-coupled receptor kinase-inter	GIT1	1.60E-15
P27708	Dihydroorotase and Glutamine-depend	CAD	4.51E-15
P07197	Neurofilament medium polypeptide	NEFM	1.00E-14
C9JP52	TBC1 domain family member 5	TBC1D5	1.36E-14
O14654	Insulin receptor substrate 4	IRS4	2.11E-13
Q96N67	Dedicator of cytokinesis protein 7	DOCK7	1.31E-12
P50213	Isocitrate dehydrogenase [NAD] subuni	IDH3A	1.51E-12
Q14155	Rho guanine nucleotide exchange facto	ARHGEF7	4.42E-12
Q9Y2H2	Inositol polyphosphate 5-phosphatase F	INPP5F	5.99E-12
Q16352	Internexin neuronal intermediate filam	INA	1.49E-11
Q86YZ3	Hornerin	HRNR	3.06E-11
Q9UJS0	Solute carrier family 25 (Mitochondrial a	SLC25A13	5.28E-11
Q9U6Y5	Green fluorescent protein	GFP	1.27E-10
P42285	Superkiller viralicidic activity 2-like 2	SKIV2L2	1.42E-09
P62269	Ribosomal protein S18	RPS18	1.50E-09
Q92616	General control of amino acid synthesis	GCN1L1	1.92E-09
P78527	DNA-dependent protein kinase catalytic	PRKDC	2.20E-09
Q8TA86	Retinitis pigmentosa 9 protein (autoson	RP9	4.05E-09
Q04695	Cytokeratin-17	KRT17	4.80E-08
P01860	Ig gamma-3 chain C region	IGHG3	5.59E-08
P62249	Ribosomal protein S16	RPS16	7.92E-08
P25098	Beta-adrenergic receptor kinase 1	ADRBK1	9.82E-08
Q6NZY4	Zinc finger CCHC domain-containing pro	ZCCHC8	1.33E-07
Q02413	Desmoglein-1	DSG1	2.07E-07
Q9Y383	RNA-binding protein Luc7-like 2	LUC7L2	2.51E-07
Q9NVI7	ATPase family, AAA domain-containing	ATAD3A	3.29E-07
P62861	Ribosomal protein S30	FAU	3.34E-07
P08708	Ribosomal protein S17	RPS17	4.57E-07
P42766	Ribosomal protein L35	RPL35	4.69E-07
P19474	Tripartite motif-containing protein 21	TRIM21	7.66E-07
P62750	Ribosomal protein L23a	RPL23A	9.19E-07
Q14257	Reticulocalbin-2	RCN2	1.49E-06

In order of adjusted p-value (Bonferroni correction), this table shows 46 out of the 92 proteins that present significant differential expression when HEK293T cell line was transfected with S[1306+1309]D mutant of hScrib and thus expressed. Based on spectral count + 1, it was possible to determine the G-test, p-value and, for stringency, an adjusted p-value at a threshold of significance of $p<0.05$. Highlighted in yellow is the hScrib protein identified by the mass spectrometer. Each protein has a uniprot accession code to enable identification of the gene of each protein in any bioinformatics

Table 6.2b Significant binding partners of S[1306+1309]D hScrib (contd.)

Uniprot	Protein	Gene symbol	Adj. P-value
P52701	DNA mismatch repair protein Msh6	MSH6	1.49E-06
B1ARM6	Centrosomal protein 170kDa	CEP170	2.72E-06
O14980	Exportin-1	XPO1	2.78E-06
Q69YN4	Protein virilizer homolog	KIAA1429	2.83E-06
P08670	Vimentin	VIM	2.89E-06
P62266	Ribosomal protein S23	RPS23	9.71E-06
O94776	Metastasis-associated 1-like 1	MTA2	1.05E-05
P62937	Peptidylprolyl isomerase A (Cyclophilin	PPIA	1.05E-05
Q9Y580	RNA-binding motif protein 7	RBM7	3.02E-05
P11142	Heat shock 70 kDa protein 8	HSPA8	3.46E-05
Q15007	Wilms tumor 1-associating protein	WTAP	3.85E-05
P62273	Ribosomal protein S29	RPS29	5.52E-05
Q9BVP2	Guanine nucleotide-binding protein-lik	GNL3	9.77E-05
Q96HS1	Phosphoglycerate mutase family memb	PGAM5	1.00E-04
Q8N5F7	NF-kappa-B-activating protein	NKAP	1.42E-04
Q9UQ35	Serine/arginine-rich splicing factor-rela	SRRM2	1.42E-04
O95831	Apoptosis-inducing factor 1, mitochond	AIFM1	2.47E-04
Q9Y3C1	HBV pre-S2 trans-regulated (nucleolar)	NOP16	2.50E-04
P62277	Ribosomal protein S13	RPS13	2.69E-04
P63173	Ribosomal protein L38	RPL38	4.33E-04
P12277	Creatine kinase, brain	CKB	5.19E-04
B4DE59	Junction plakoglobin	JUP	5.19E-04
O43592	Exportin, tRNA (nuclear export receptor	XPOT	6.06E-04
Q9BU76	Multiple myeloma tumor-associated pr	MMTAG2	9.93E-04
Q9Y2Z0	Protein 40-6-3	SUGT1	1.10E-03
Q9UJV9	DEAD (Asp-Glu-Ala-Asp) box polypeptic	DDX41	1.90E-03
P22061	L-isoaspartyl protein carboxyl methyltra	PCMT1	1.90E-03
P62847	Ribosomal protein S24	RPS24	2.47E-03
	Chromosome 11 open reading frame 48	C11orf48	4.19E-03
Q9UG63	ATP-binding cassette, sub-family F (GCN	ABCF2	4.90E-03
Q14161	ARF GTPase-activating protein GIT2	GIT2	4.90E-03
Q5D862	Filaggrin-2	FLG2	5.40E-03
P18621	Ribosomal protein L17	RPL17	5.63E-03
P23246	Splicing factor, proline- and glutamine-r	SFPQ	8.63E-03
P31689	DnaJ (Hsp40) homolog, subfamily A, me	DNAJA1	1.20E-02
Q13547	Histone deacetylase 1	HDAC1	1.29E-02
O15027	SEC16 homolog A	SEC16A	1.61E-02
Q9NR30	DEAD/H(Asp-Glu-Ala-Asp/His)box polyp	DDX21	2.17E-02
P06493	Cyclin-dependent kinase 1	CDC2	2.17E-02
O75052	Nitric oxide synthase 1 (neuronal) adapt	NOS1AP	2.17E-02
Q15052	Rac/Cdc42 guanine nucleotide exchange	ARHGEF6	2.17E-02
P84090	Enhancer of rudimentary homolog (Dros	ERH	2.52E-02
Q8N1N4	Cytokeratin-78	KRT78	2.52E-02
P04792	Heat shock 27 kDa protein 1	HSPB1	3.01E-02
Q6P2Q9	p220	PRPF8	3.93E-02
P62829	Ribosomal protein L23	RPL23	4.07E-02

A continuation of the previous table. In order of adjusted p-value (Bonferroni correction), this table shows the remaining 46 of the 92 proteins that present significant differential expression when HEK293T cell line was transfected with S[1306+1309]D mutant of hScrib and thus expressed. However, the red highlighted row with Gene Name C11orf48 has no uniprot accession code. Based on spectral count + 1, it was possible to determine the G-test, p-value and, for stringency, an adjusted p-value at a threshold of significance of $p<0.05$.

6.3 Bioinformatics analysis of results with WebGestalt

Respectively, the two gene lists were put through enrichment analysis via a web-based gene set analysis toolkit (WebGestalt). To enter these lists, 'hsapiens' i.e. *Homo sapiens* (human), as organism of interest was selected, 'hsapiens_uniprot_swissprot_accession' was selected to specify the gene type ID and the list of uniprot codes for S[1306+1309]A and S[1306+1309]D were respectively copied and pasted into the 'upload gene list' box.

Once each gene list was entered, a GO (Gene Ontology) Slim Classification that gives an overview of the categories of the Biological Process, the Molecular Function and the Cellular Component classification the proteins in the given gene lists were observed. This overview is in the form of a bar chart for each classification where each category in a classification is represented by bars and the height of each bar represents the number of proteins, from the list, that were observed in the category. The bars are in order of decreasing height. There were only 70 out of 79 proteins in the list for S[1306+1309]A (Tables 6.1a and 6.1b) that could be clearly mapped to unique Entrez Gene IDs in the GO database while the other 9 could not. Only 91 uniprot codes could be entered into WebGestalt, for S[1306+1309]D (Tables 6.2a and 6.2b), because C11orf48 has no code. 83 out of the 91 proteins could be clearly mapped to unique Entrez Gene IDs in the GO database while the other 8 could not. There are 13 Biological Processes and 15 Molecular Functions identified by WebGestalt from both lists. WebGestalt also identified 18 Cellular Components categories for S[1306+1309]A compared to 16 for S[1306+1309]D.

To enable comparison between categories of S[1306+1309]A and S[1306+1309]D pull-downs, these bars have been merged together (Figures 6.1, 6.2 and 6.3).

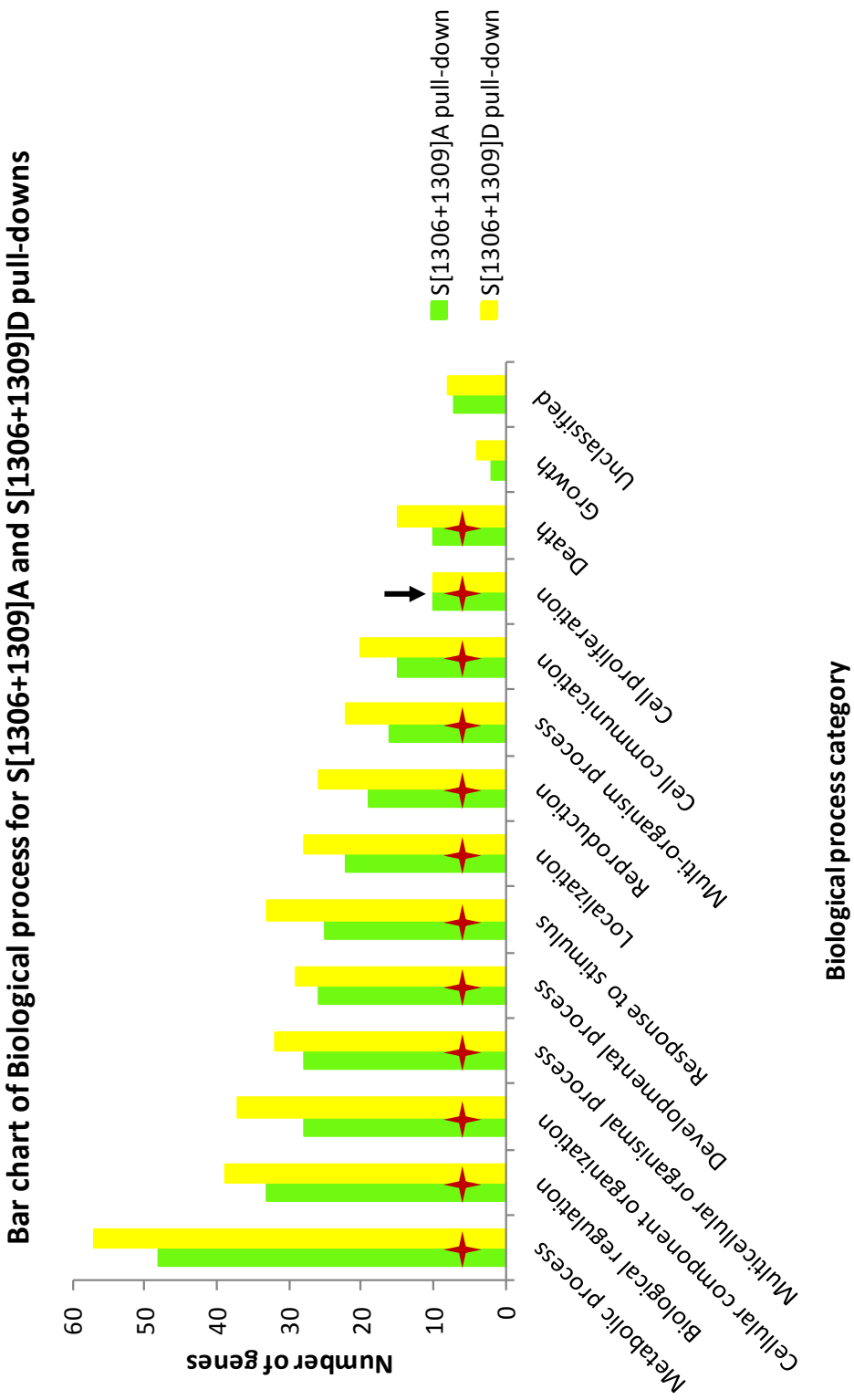

Figure 6.1 Bar chart of the categories, under the GO Slim classification of biological processes, when S[1306+1309]A and S[1306+1309]D were expressed. The green and yellow bars represent a category that S[1306+1309]A and S[1306+1309]D pull-downs were observed in, respectively. The height of each bar represents the number of genes in the given gene lists observed in that category. Only 7 genes out of the 70 and 8 genes out of 83 were mapped as unclassified in S[1306+1309]A and S[1306+1309]D pull-downs, respectively. The black arrow indicates the category in which the same number of proteins pull-down by S[1306+1309]A and S[1306+1309]D, respectively, were observed. The red coloured 4-point stars indicate the categories that contain proteins which showed significance between the pull-downs (Figure 6.3).

Figure 6.1 shows that, in general, the number of proteins pulled down by S[1306+1309]D, in each biological process category, was more compared to S[1306+1309]A. However, Figure 6.1 also shows that the same number of proteins was observed in the biological

process of cell proliferation in S[1306+1309]A and S[1306+1309]D pull-downs, respectively (black arrow).

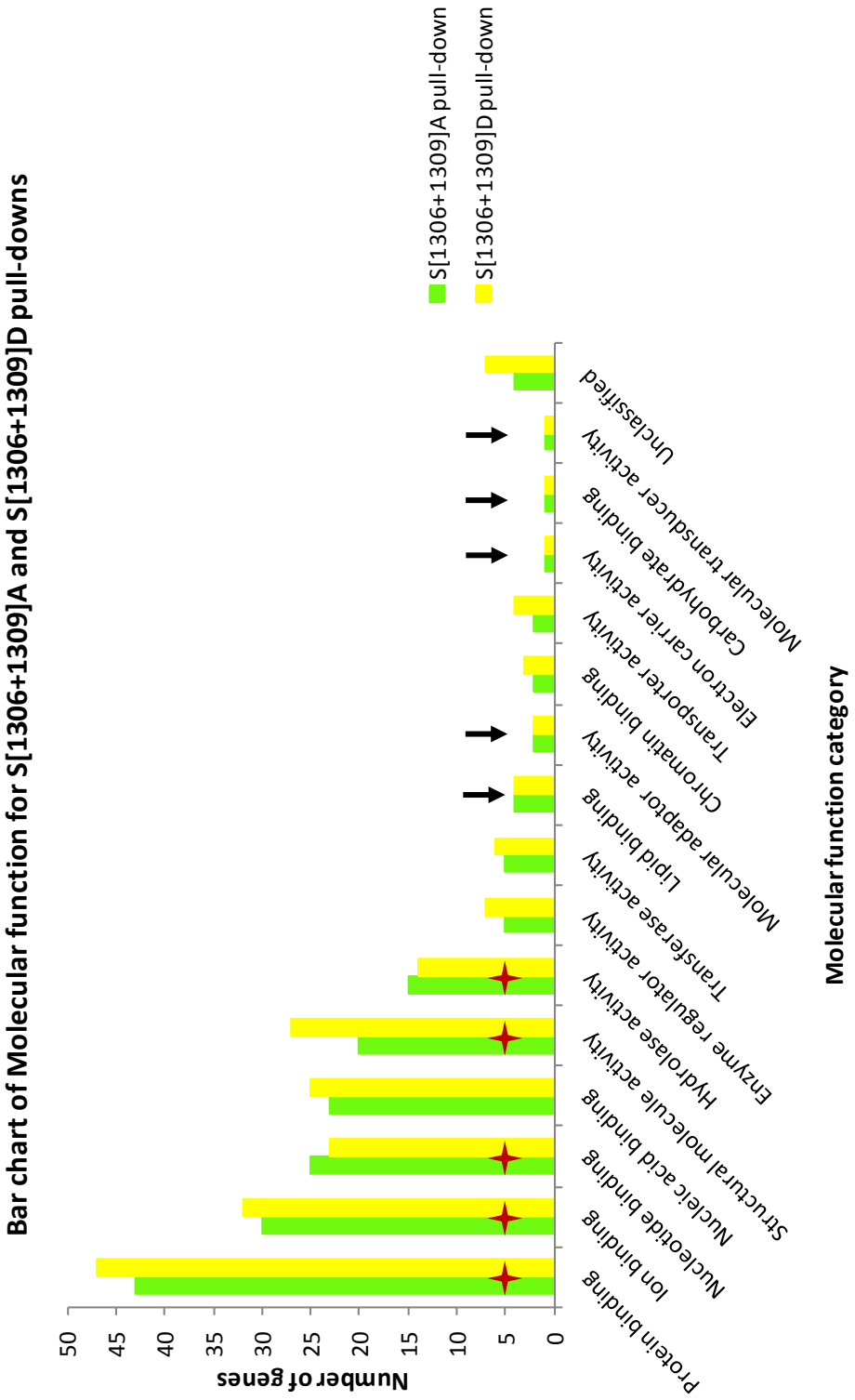

Figure 6.2 Bar chart of the categories, under the GO Slim classification of molecular function, when S[1306+1309]A and S[1306+1309]D were expressed. The green and yellow bars represent a category that S[1306+1309]A and S[1306+1309]D pull-downs were observed in, respectively. The height of each bar represents the number of genes in the given gene lists observed in that category. Only 4 genes out of the 70 and 7 genes out of 83 were mapped as unclassified in S[1306+1309]A and S[1306+1309]D pull-downs, respectively. The black arrows indicate the categories in which the same number of proteins pull-down by S[1306+1309]A and S[1306+1309]D, respectively, were observed. The red coloured 4-point stars indicate the categories that contain proteins which showed significance between the pull-downs (Figure 6.3).

Figure 6.2 shows that there are 5 molecular function categories with the same number of proteins observed in S[1306+1309]A and S[1306+1309]D pull-downs, respectively (black arrow). These are: lipid binding, molecular adaptor activity, electron carrier activity, carbohydrate binding and molecular transducer activity. There were more proteins

observed in nucleotide binding and hydrolase activity in S[1306+1309]A pull-down compared to S[1306+1309]D pull-down. Proteins from S[1306+1309]D pull-down were observed more in the other 8 molecular function categories than S[1306+1309]A pull-down.

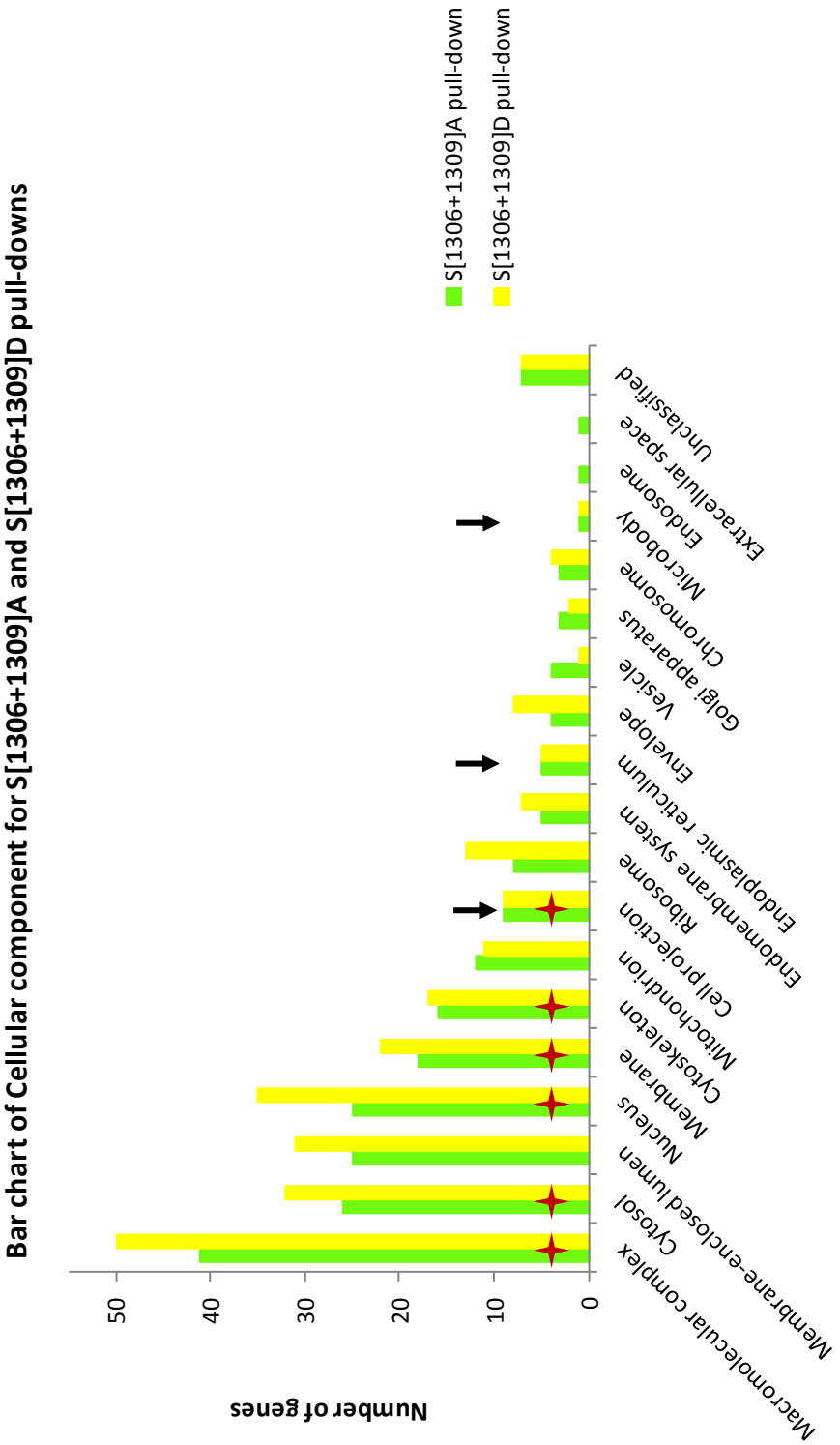

Figure 6.3 Bar chart of the categories, under the GO Slim classification of cellular component, when S[1306+1309]A and S[1306+1309]D were expressed. The green and yellow bars represent a category that S[1306+1309]A and S[1306+1309]D pull-downs were observed in, respectively. The height of each bar represents the number of genes in the given gene lists observed in that category. Only 7 genes out of the 70 and 7 genes out of 83 were mapped as unclassified in S[1306+1309]A and S[1306+1309]D pull-downs, respectively. The black arrows indicate the categories in which the same number of proteins pull-down by S[1306+1309]A and S[1306+1309]D, respectively, were observed. The red coloured 4-point stars indicate the categories that contain proteins which showed significance between the pull-downs (Figure 6.3).

In Figure 6.3, only proteins from S[1306+1309]A pull-down were observed in the endosome and extracellular space. Proteins from S[1306+1309]A pull-down were observed more in mitochondrion, vesicle and golgi apparatus. Cell projection, endoplasmic reticulum (ER) and microbody are the only cellular component categories where the same number of proteins from S[1306+1309]A and S[1306+1309]D pull-downs, respectively (black arrow), were observed. The remaining 10 cellular components show that there were more proteins observed from S[1306+1309]D pull-down than from S[1306+1309]A pull-down.

An important biological validation of the result was identifying proteins abundances that show statistical significance between S[1306+1309]A and S[1306+1309]D pull-downs i.e. when S[1306+1309]A assumed the negative control condition and S[1306+1309]D assumed the experimental condition. The spectral counting approach was also used. Each replicate of S[1306+1309]A (aa-p1 to aa-p3) and S[1306+1309]D (dd-p1 to dd-p3) were summed up, respectively, and the value of the total sum of the replicates in each assumed condition was calculated i.e. Σ(aa-p1 + aa-p2 + aa-p3). The same statistical methods and stringency in statistical significance were applied and the same threshold of significance ($p<0.05$) was set to test the null hypothesis that there would be no significant difference in protein abundances between the S[1306+1309]A and S[1306+1309]D pull-downs. The result was a third gene list of six proteins that showed significant difference in their abundance (Table 6.3). The result was the same when performed in the reverse i.e. where S[1306+1309]D= negative control condition, S[1306+1309]A= experimental condition.

Table 6.3 Proteins with significant abundance when S[1306+1309]A and S[1306+1309]D pull-downs were compared statistically

Uniprot	Protein	Gene symbol	Adj. P-value
P35579	Myosin, heavy chain 9, non-muscle	MYH9	6.90E-31
P35580	Myosin, heavy chain 10, non-muscle	MYH10	3.37E-17
Q14160	Protein scribble homolog	SCRIB	3.26E-08
O14950	Myosin regulatory light chain 12B	MYL12B	1.96E-04
P60660	Smooth muscle and non-muscle myosi	MYL6	1.62E-02
P07197	Neurofilament medium polypeptide	NEFM	4.10E-02

In increasing order of adjusted p-value (Bonferroni correction), this table shows 6 proteins that present significant differential expression when comparing the expressions of HEK293T cell line transfected S[1306+1309]A and S[1306+1309]D mutants of hScrib, respectively. Based on spectral count + 1, it was possible to determine the G-test, p-value and, for stringency, an adjusted p-value at a threshold of significance of $p<0.05$. Highlighted in yellow is the hScrib protein identified by the mass spectrometer. Each protein has a uniprot accession code to enable identification of the gene of each protein in any bioinformatics database.

This gene list was run through WebGestalt and all six proteins were mapped and GO Slim Classification was performed. There are 12 Biological Processes, 5 Molecular Functions and 6 Cellular Components identified by WebGestalt. These are indicated with red 4-point stars in Figures 6.1, 6.2 and 6.3. Table 6.4 contains the list of categories in each classification the proteins from Table 6.3 were observed in.

Table 6.4 List of categories that contain proteins with significant abundance between the pull-downs

Biological Process	No. of proteins	Molecular Function	No. of proteins	Cellular Component	No. of proteins
Metabolic process	2	Protein binding	5	Macromolecular complex	6
Biological regulation	5	Ion binding	4	Cytosol	3
Cellular component organization	5	Nucleotide binding	2	Nucleus	1
Multicellular organismal process	6	Structural molecule activity	2	Membrane	3
Developmental process	6	Hydrolase activity	3	Cytoskeleton	5
Response to stimulus	5			Cell projection	3
Localization	4				
Reproduction	2				
Multi-organism process	1				
Cell communication	2				
Cell proliferation	2				
Death	1				

Table 6.4 shows that all six proteins, in Table 6.3, are observed in two biological processes: multicellular organismal process and developmental process. Only 1 of 6 proteins was observed in multi-organism process and death.

The 12 biological processes occur through 5 molecular function categories that the six proteins were observed in. Most of these proteins are observed in protein binding (5) and ion binding (4). Half of these proteins were observed in hydrolase activity.

For these 5 molecular functions to occur, these proteins were present in 6 cellular components. All six proteins form macromolecular complex and half of them are present in the cytosol, membrane and cell projection (for motility). Only 1 protein is present in the nucleus.

GO Slim Classification show that one protein can be involved in and also be found in one or more than one process and cellular component.

As part of the enrichment analysis, over-represented (or under-represented) proteins in each gene list were searched for using Gene Ontology (GO) Analysis. The reference set selected for enrichment analysis was hsapiens_genome. For enrichment evaluation analysis, hypergeometric statistical method was selected and due to testing multiple genes sets at the same time, a multiple test adjustment of p-values based on Benjamini and Hochberg (1995), BH, was selected. To enable identification of the 10 pathways with the most significant p-values, the significance level was left on the 'Top 10' default option before running the enrichment analysis. The result of running GO analysis is a GO analysis tree which displays enriched gene numbers in red (significant), their non-enriched parents in black and non-significant genes in brown (Zhang et al., 2005).

GO analysis identified for S[1306+1309]A and S[1306+1309]D pull-downs, respectively, 10 enriched categories under biological process, molecular function and cellular component, respectively. These categories are represented in Venn diagrams (Figures 6.4, 6.5 and 6.6).

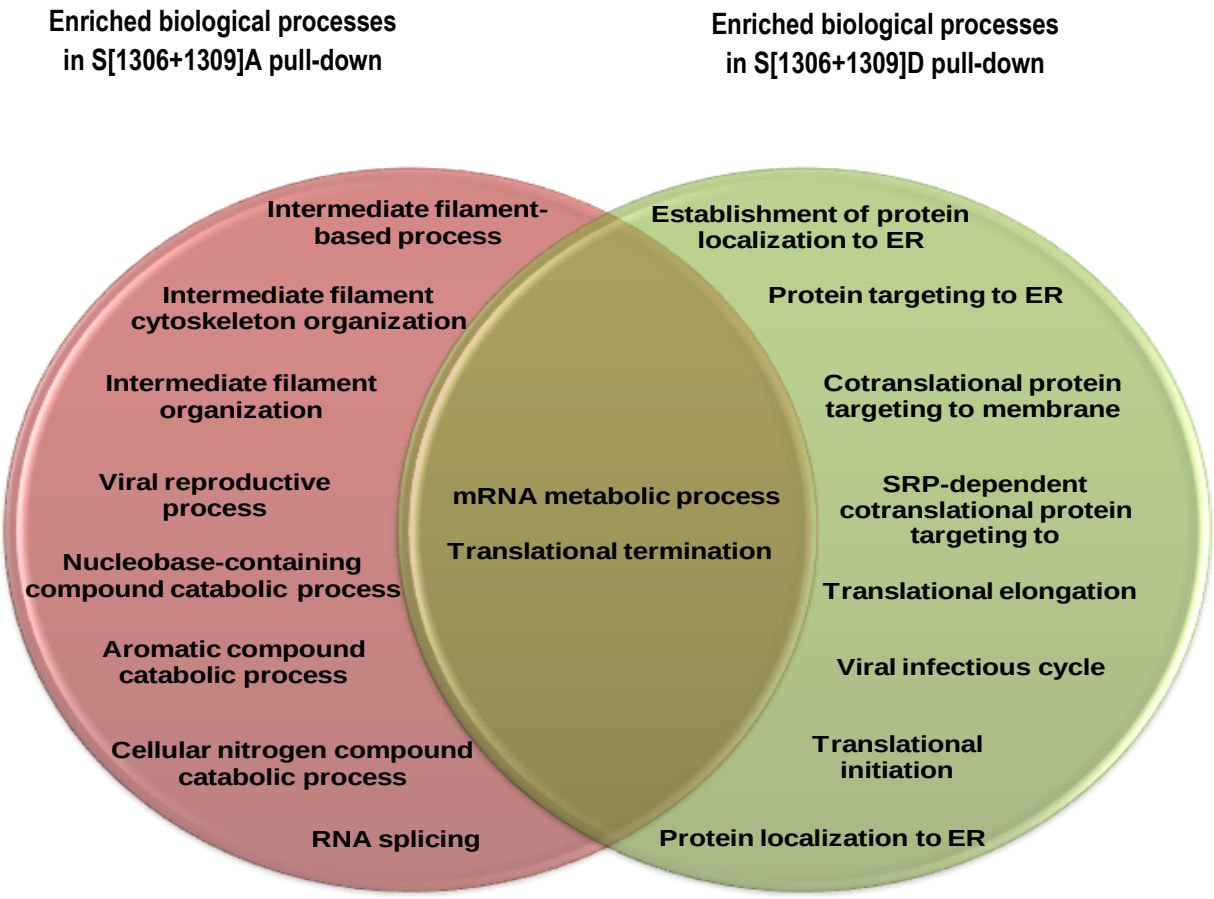

Figure 6.4 Venn diagram of significantly enriched biological processes in S[1306+1309]A and S[1306+1309]D pull-downs. There are 10 significantly enriched biological processes in both pull-downs.

Figure 6.4 shows that there are 10 significantly enriched biological processes for both pull-downs. Intermediate filament-based process (adjP=1.58e-08) and Intermediate filament cytoskeleton organization (adjP=1.58e-08) were the most significantly enriched in S[1306+1309]A pull-down while while translational termination (adjP=1.06e-11) and mRNA metabolic process (adjP=1.06e-11) were the most significantly enriched in S[1306+1309]D pull-down. Although translational termination and mRNA metabolic process are the common biological processes in both pull-downs, they are more significant in S[1306+1309]D than S[1306+1309]A pull-down. The list for both pull-downs, outside the Venn diagram intersection, is in order of significance.

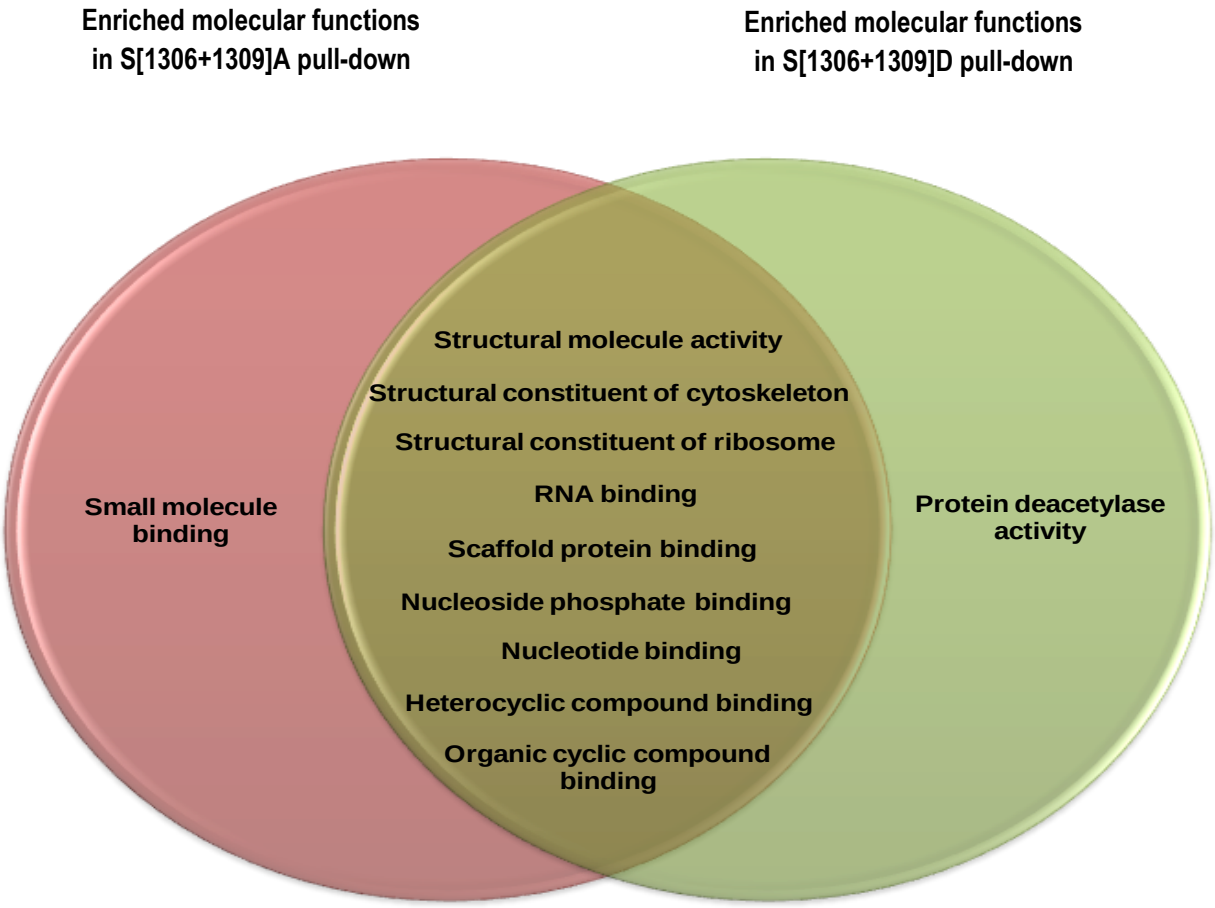

Figure 6.5 Venn diagram of significantly enriched molecular functions in S[1306+1309]A and S[1306+1309]D pull-downs. There are 10 significantly enriched molecular functions in both pull-downs.

Figure 6.5 also shows 10 significantly enriched molecular functions for both pull-downs but 9 molecular functions are common to both pull-downs. Structural constituent of cytoskeleton (adjP=1.06e-11) was most significantly enriched molecular function in S[1306+1309]A pull-down (although 18 times less significant than that from S[1306+1309]D pull-down) while structural molecule activity (adjP=7.89e-17) was the most significant in S[1306+1309]D pull-down. Small molecule binding and protein deacetylase activity are enriched in S[1306+1309]A and S[1306+1309]D, respectively.

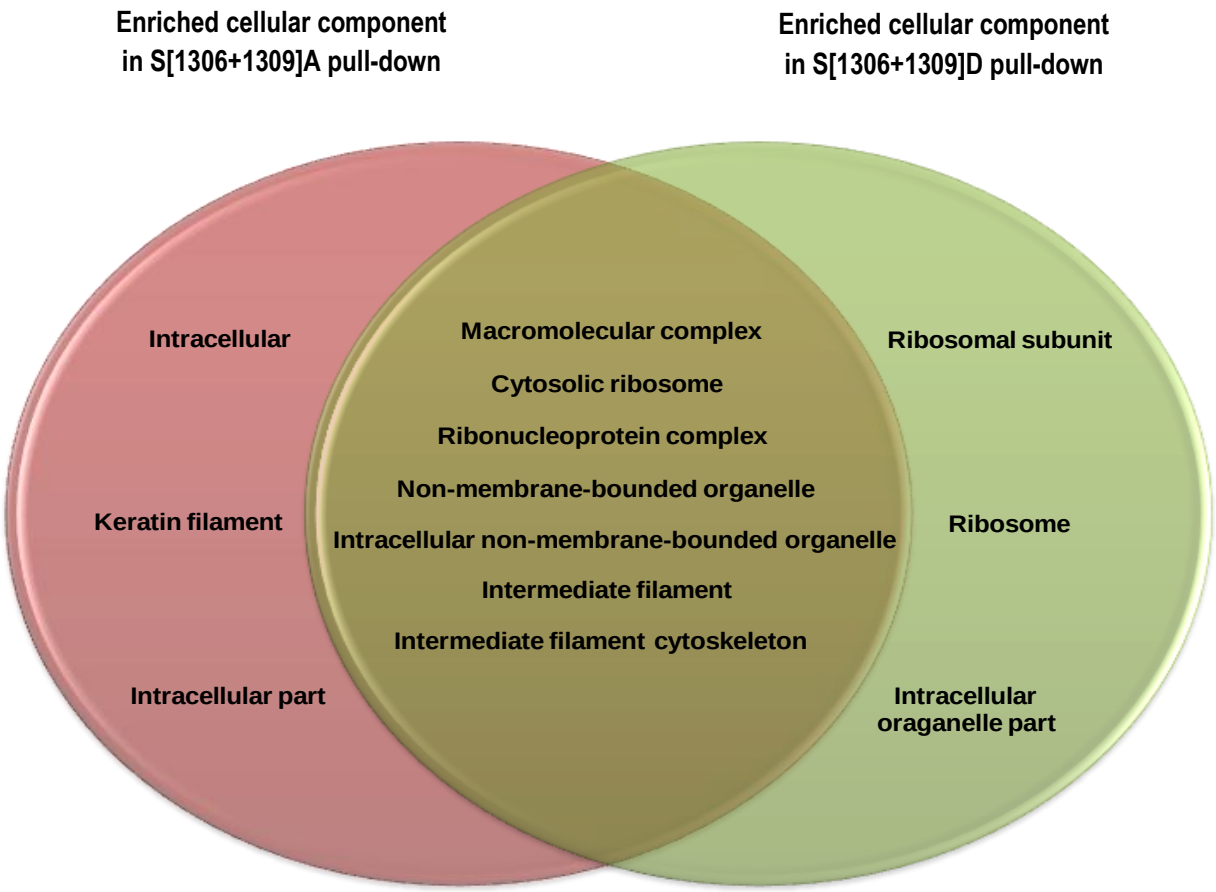

Figure 6.6 Venn diagram of significantly enriched cellular component in S[1306+1309]A and S[1306+1309]D pull-downs. There are 10 significantly enriched cellular components in both pull-downs.

Figure 6.6 also shows 10 significantly enriched cellular components for both pull-downs. 7 cellular components are common to both pull-downs. Although common to both pull-downs, macromolecular complex (adjP=3.76e-10) and intermediate filament (adjP=3.76e-10) were the most significantly enriched in S[1306+1309]A pull-down. Macromolecular complex (adjP=4.76e-13) and cytosolic ribosomes (adjP=4.76e-13) were the most significantly enriched in S[1306+1309]D. The intermediate filament for S[1306+1309]A pull-down comprised 12 intermediate filament encoding genes (NEFM, KRT5, KRT14, KRT1, KRT2, KRT9, VIM, KRT10, DSP, KRT6A, KRT16 and INA), most of which are keratin (KRT) filaments enriched in S[1306+1309]A pull-down only. The intermediate filament for S[1306+1309]D pull-down comprised 14 intermediate filament encoding genes (the same 12 intermediate filaments as above and keratin filaments KRT17 and KRT78). The cytosolic ribosomes comprised 12 cytosolic ribosomes encoding genes (RPL35, RPS16, RPL23, RPL17, RPS29, RPL38, RPS24, RPL37A, RPS18, RPS23, RPS13, and RPL23A), all of which are part of the ribosomal subunit enriched in S[1306+1309]D pull-down only.

Comparing the GO classification of both pull-downs suggest that although S[1306+1309]A and S[1306+1309]D pull-downs may share 2 common biological processes (mRNA metabolic process and translational termination), 9 molecular functions and 7 cellular components, they facilitate different cellular behaviour.

When the third gene list was run for GO enrichment analysis, 10 enriched categories were identified under biological processes, molecular function and cellular component, respectively (Table 6.5).

Table 6.5 List of categories from GO analysis that are significantly enriched between the pull-downs

Biological Process	No. of proteins	Molecular Function	No. of proteins	Cellular Component	No. of proteins
Taxis	5	ADP binding	2	Synapse	4
Chemotaxis	5	Calmodulin binding	2	Neuromuscular junction	3
Cell development	6	Actin filament binding	2	Protein complex	6
Cell part morphogenesis	5	Hydrolase activity, acting on acid anhydrides	3	Cytoskeletal part	5
Cell projection morphogenesis	5	Hydrolase activity, acting on acid anhydrides, in phosphorus-containing anhydrides	3	Actin cytoskeleton	4
Cell morphogenesis involved in differentiation	5	Motor activity	3	Actin filament bundle	3
Neuron projection development	5	Microfilament motor activity	2	Actomyosin	3
Cell morphogenesis involded in neuron differentiation	5	ATPase activity	3	Myosin complex	4
Neuron projection morphogenesis	5	ATPase activity, coupled	3	Myosin II complex	3
Axonogenesis	5	Actin-dependent ATPase activity	3	Stress fiber	3

There were five most significantly enriched categories under biological process: taxis (adjP=2.30e-05), chemotaxis (adjP=2.30e-05), neuron projection morphogenesis (adjP=2.30e-05), cell morphogenesis involved in neuron differentiation (adjP=2.30e-05) and axonogenesis (adjP=2.30e-05). MYH9, MYL6, MYH10, MYL12B and SCRIB were found in the list of enriched taxis and chemotaxis locomotion in response to chemical stimulus.

Under molecular function, the actin-dependent ATPase activity (adjP=1.16e-07) was the most significantly enriched with MYH9, MYL6 and MYH10 involved in this activity.

Under cellular component, myosin complex (adjP=1.26e-07) of the cytoskeletal macromolecular complex was the most significantly enriched followed by myosin II complex (adjP=1.00e-06) involving MYH9, MYH10 and MYL12B.

From the GO analysis enrichment result on the third gene list, it suggests that these proteins in the gene list may be involved in formation of cellular projections or processes, in response to chemical stimulus, to facilitate cell movement. They accomplish this biological process as macromolecular myosin complexes, which require actin-dependent ATPase enzyme activity.

With 3 gene lists created, what biological pathways would be enriched? To identify the biological pathways, the candidate proteins in the individual gene list were ran through the KEGG (Figure 6.7) and Wikipathways Analysis (Figure 6.8) databases, respectively.

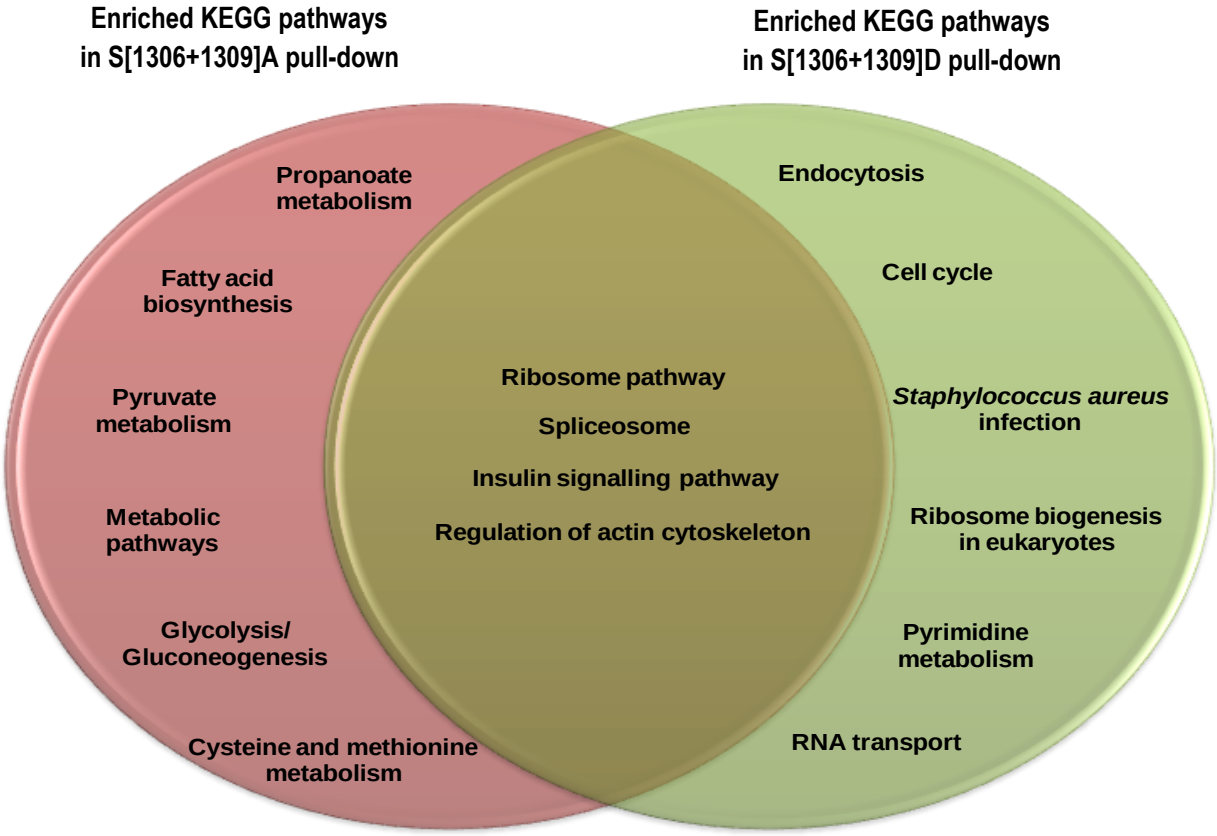

Figure 6.7 Venn diagram of significantly enriched KEGG pathways in S[1306+1309]A and S[1306+1309]D pull-downs. There are 10 significantly enriched pathways in both pull-downs.

Figure 6.7 shows that the cell cycle pathway is enriched only in S[1306+1309]D pull-down. This supports the results from Chapter 4 and 5 that suggested D-mutants of hScrib may be involved in cell proliferation. Results also from Chapter 4 suggest A-mutants of hScrib may be involved in cell migration. This requires the actin cytoskeleton regulation (Lambrechts *et al*., 2004) which is also a pathway enriched in S[1306+1309]D pull-down as seen in the Venn diagram intersection above. Also common to both pull-downs is the ribosome pathway. It was the most significant pathway of both pull-downs. The pathway list for both pull-downs, outside the Venn diagram intersection, is in order of significance.

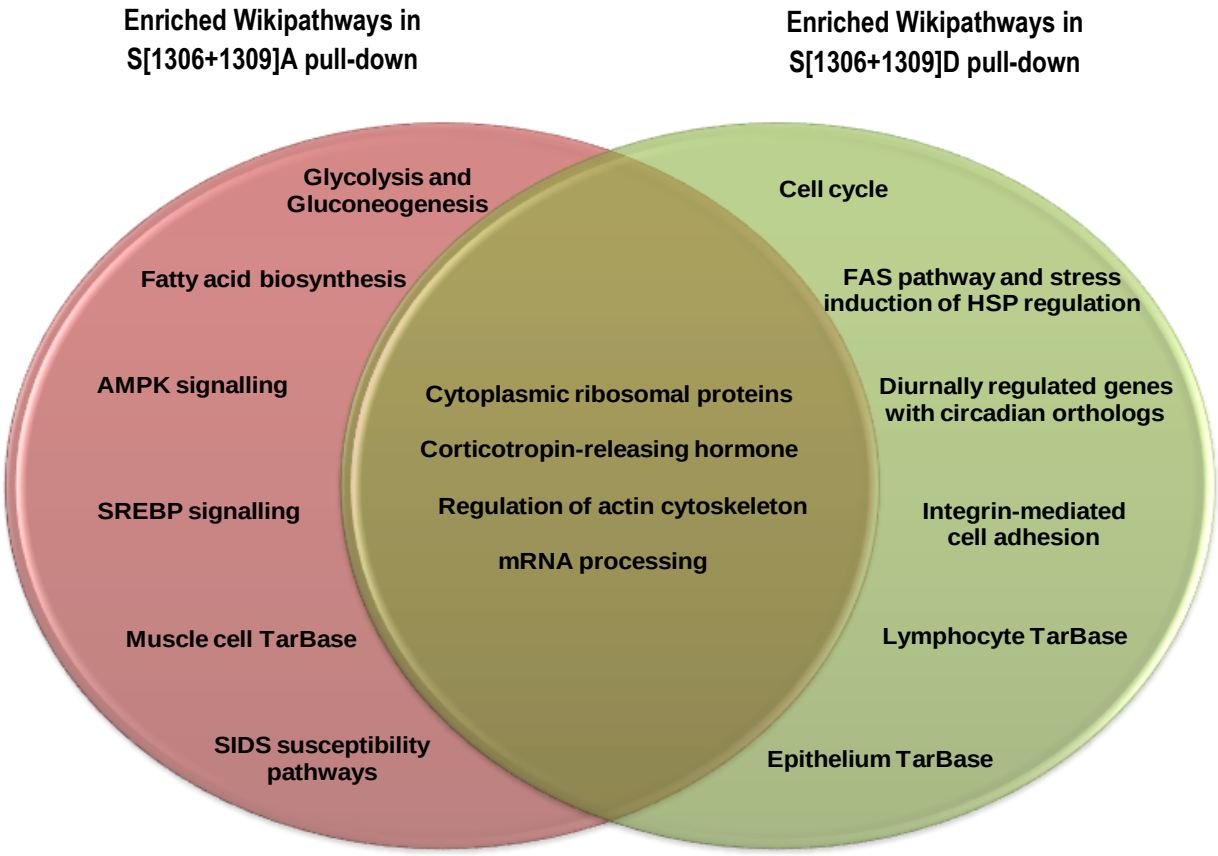

Figure 6.8 Venn diagram of significantly enriched Wikipathways in S[1306+1309]A and S[1306+1309]D pull-downs. There are 10 significantly enriched pathways in both pull-downs.

Wikipathways analysis in Figure 6.8 supports the KEGG pathway analysis in Figure 6.7 by suggesting that D-mutants support cell proliferation and A-mutants support cell migration but both cellular behaviours may require the regulation of actin cytoskeleton.

According to the flow chart in Figure 6.9, S[1306+1309]A pulled down GIT1, MYH10 and ARHGEF7 while S[1306+1309]D pulled down GIT1, ARHGEF6 and ARHGEF7. These proteins are enriched in the enriched pathway of regulation of actin cytoskeleton. S[1306+1309]D also pulled down HDAC1, CDK1 and PRKDC proteins enriched in the enriched cell cycle pathway. hScrib was not in the list of enriched proteins involved in these enriched pathways.

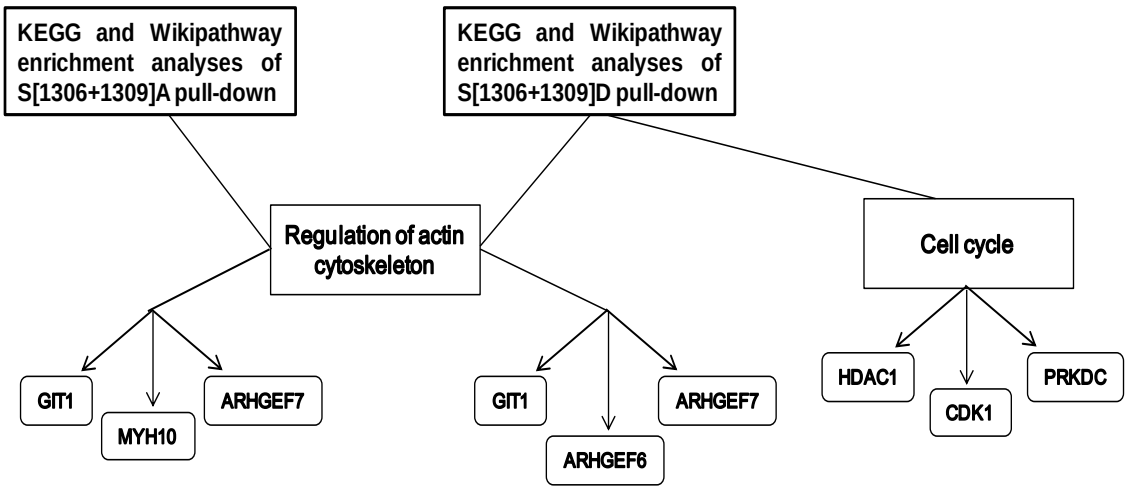

Figure 6.9 Flow chart of KEGG and Wikipathway enrichment analysis of S[1306+1309]A and S[1306+1309]D pull-downs, their respectively enriched pathways and proteins involved.

When the third gene list was run in KEGG analysis, 3 significantly enriched pathways were identified (Figure 6.10): 1.) Tight junction (adjP=1.67e-6) 2.) Regulation of actin cytoskeleton (adjP=3.53e-6) 3.) Viral myocarditis (adjP=3.88e-5). The tight junction pathway was the most significantly enriched. All 3 pathways did not list hScrib as one of the enriched proteins.

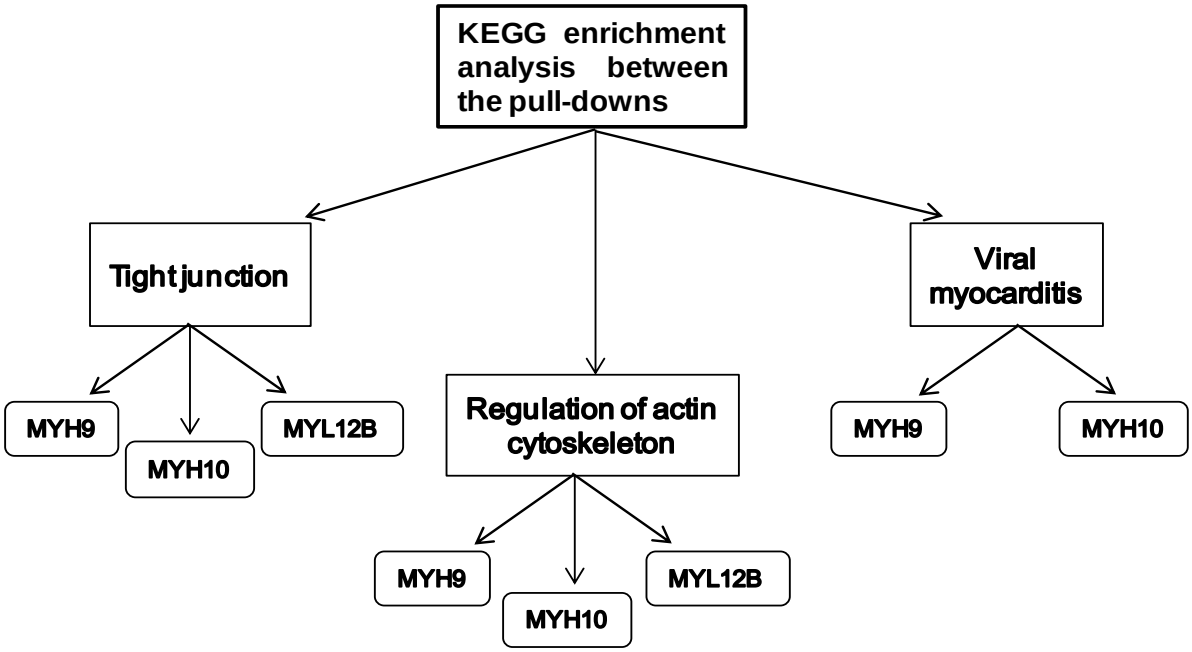

Figure 6.10 Flow chart of KEGG enrichment analysis between S[1306+1309]A and S[1306+1309]D pull-downs, the pathways enriched and the proteins involved.

However, when run in Wikipathways analysis database, only the TSH (thyroid-stimulating hormone) pathway (Figure 6.11) was identified and was found to have 2 enriched proteins which include hScrib and MYL12B.

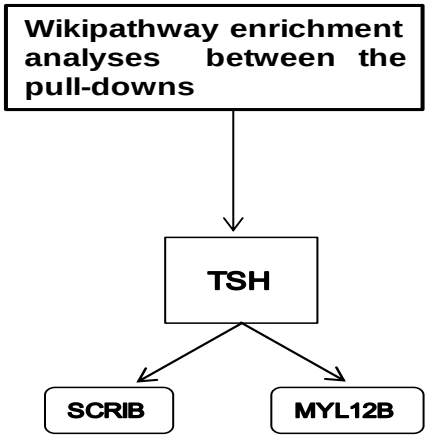

Figure 6.11 Flow chart of Wikipathway enrichment analysis between S[1306+1309]A and S[1306+1309]D pull-downs, the pathway enriched and the proteins involved.

The third gene list (Table 6.3) contains proteins with statistically significant differences in abundance between the S[1306+1309]A and S[1306+1309]D pull-downs. Figure 6.12 shows their relative abundances.

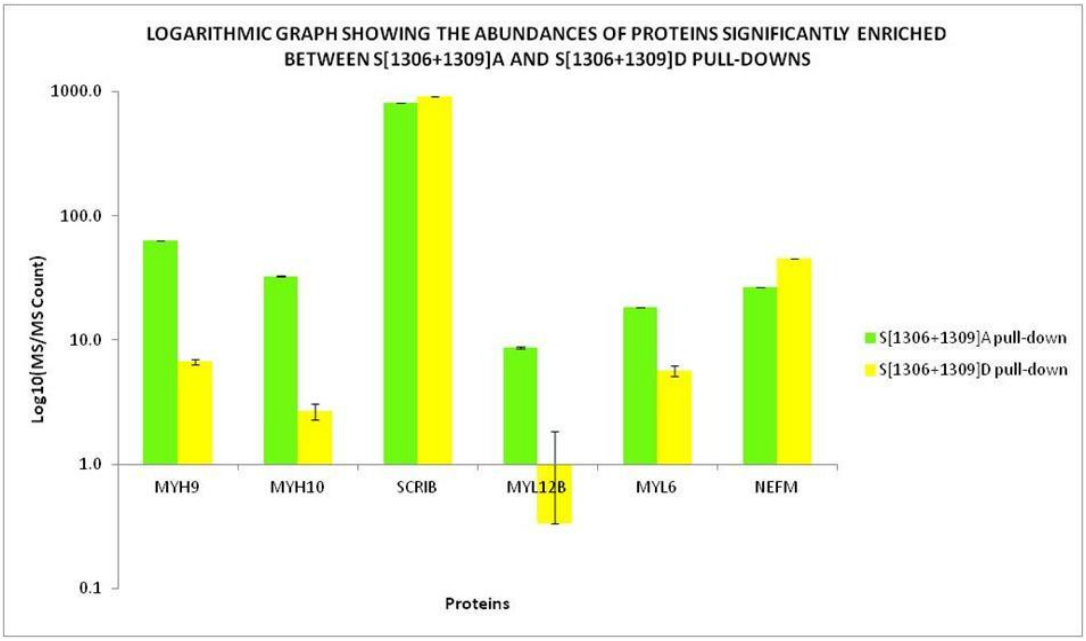

Figure 6.12 Logarithmic bar graph proteins that were identified in both the S[1306+1309]A and S[1306+1309]D pull-downs but showed significant differences in their abundance between the pull-downs. Bar graph y-axis was to a log scale of 10 with log transformed error bars calculated as (uncertainty)/ (mean MS/MS Count). Log graph was used to display variations abundance, between pull-downs, of each of the protein identified to be a significant binding partner of both S[1306+1309]A and S[1306+1309]D.

Figure 6.12 shows that MYH9, MYH10, MYL12B and MYL6 were significantly pulled down with S[1306+1309]A than with S[1306+1309]D: 89.5% more MYH9, 91.8% more MYH10, 96.2% more MYL12B and 69.1% more MYL6 were pulled down with S[1306+1309]. S[1306+1309]D pulled down 40.7% more NEFM than S[1306+1309]A. 10.7% more S[1306+1309]D was pulled down than S[1306+1309]A, but this may be due to loss of some S[1306+1309]A in the washing steps of the Co-IP assay.

Statistical analysis of the results from S[1306+1309]A and S[1306+1309]D pull-downs were performed separately to determine the biological pathways (Figure 6.7 and 6.8) affected by S[1306+1309]A and S[1306+1309]D and the proteins involved as a result. However, there were a few pathways similar to both S[1306+1309]A and S[1306+1309]D. This was why both pull downs were statistically compared (Table 6.3) to identify the biological pathway/s specific to S[1306+1309]A and S[1306+1309]D, respectively. It was by determining the proteins that were more abundant in S[1306+1309]A than in S[1306+1309]D and vice versa (Figure 6.12).

6.4 Discussion

It is true that the complex and diverse biological processes that occur in the cells of a human body are as a result of the dynamic nature of a group of subcellular biomolecules called proteins. The diverse bio-processes are credited to unique attributes of proteins which include the ability of a protein to interact with another and also the ability to form macromolecular complexes. These attributes facilitate the establishment of a network of transduction or cascade of a biological signal (Berg *et al.*, 2002:3; Spirin and Mirny, 2003) to establish cell properties such as cell polarity which contributes to the regulation of cell proliferation, cell migration, apoptosis, tissue organization and tumour suppression (Humbert *et al.*, 2003; Qin *et al.*, 2005; Huang and Muthuswamy, 2010; Chatterjee and McCaffrey, 2014) to name a few. Abnormalities in protein interactions cause unregulated cell properties which could lead to diseases such as cancer (Dow *et al.*, 2003; Qin *et al.*, 2005). Therefore identifying protein binding partners under given conditions, would give insights into the cellular function of the protein-protein interactions, an understanding of the disease that could arise because of or without the protein-protein interaction and enable discovery of novel drug targets to aid treatment in disease cases such as cancer.

In cancer, loss of epithelial cell polarity is a common characteristic (Chatterjee *et al.*, 2012; Royer and Lu, 2011; Bilder *et al.*, 2000). Cell polarity complex proteins such as the Scribble complex (hScrib, hDlg and Lgl) are affected. One component of the Scribble

complex, hScrib, was the focus of study because it was implicated in an aggressive form of breast cancer called TNBC (Greenwood *et al.*, 2012; Metodieva *et al.*, 2013). This polarity protein is also a tumour suppressor (Su *et al.*, 2012). By using mass spectrometry and bioinformatics toolkits, the aim was finding the binding partners of hScrib, at different phosphorylations states, to identify which pathway/s its uses to establish cell polarity, tumour suppression and breast cancer invasion and metastasis. Using the toolkits (GO, KEGG and Wikipathways) in WebGestalt on hScrib double mutants S[1306+1309]A and S[1306+1309]D pull-downs, it was found that regulation of actin cytoskeleton occurred more with expressed S[1306+1309]A while cell cycle pathway occurred with expressed S[1306+1309]D. It was also found that there were 6 proteins (MYH9, MYH10, SCRIB, MYL12B, MYL6 AND NEFM) significantly enriched between S[1306+1309]A and S[1306+1309]D pull-downs and 4 of the proteins (MYH9, MYH10, MYL12B and MYL6) were more abundant in the S[1306+1309]A pull-down. These proteins are involved in the tight junction and regulation of actin cytoskeleton pathways.

The tight junction pathway allows intercellular adhesion while providing partitioning between the membranes of adjacent epithelial cells. This partitioning or barrier regulates the paracellular traffic of substances across the epithelium and keeps membrane proteins (claudins and occludins) and other proteins (e.g. ZO-1, -2 and -3) at the apical domain of a cell from membrane proteins (E-cadherin) and other proteins (p120-catenin, β-catenin and α-catenin) at the basolateral domain of the cell (Hartsock and Nelson, 2008; Anderson and Van Itallie, 2009; McCaffrey and Macara, 2012). MYH10, MYH9 and MYL12B were found in the tight junction pathway (Figure 6.13). Tight junction is established through Rho (ras homolog family member A)/ ROCK (Rho-associated coiled-coil containing protein kinase) inhibition of Rac. Rho/ROCK phosphorylatory suppression of the phosphatase activity of MLCP (protein phosphatase regulatory subunit) on MLC (which includes MYL12B) increases the levels of phosphorylated MLC to activate myosin II (MYH9 and MYH10). Myosin II actively binds to stress fibres of stably polymerized actin (also mediated by Rho/ROCK) to form actomyosin contraction (Amano *et al.*, 2010). This re-organization of the actin cytoskeleton allows interaction of actin cytoskeleton with proteins that support tight junction formation and hence contribute to cell adhesion.

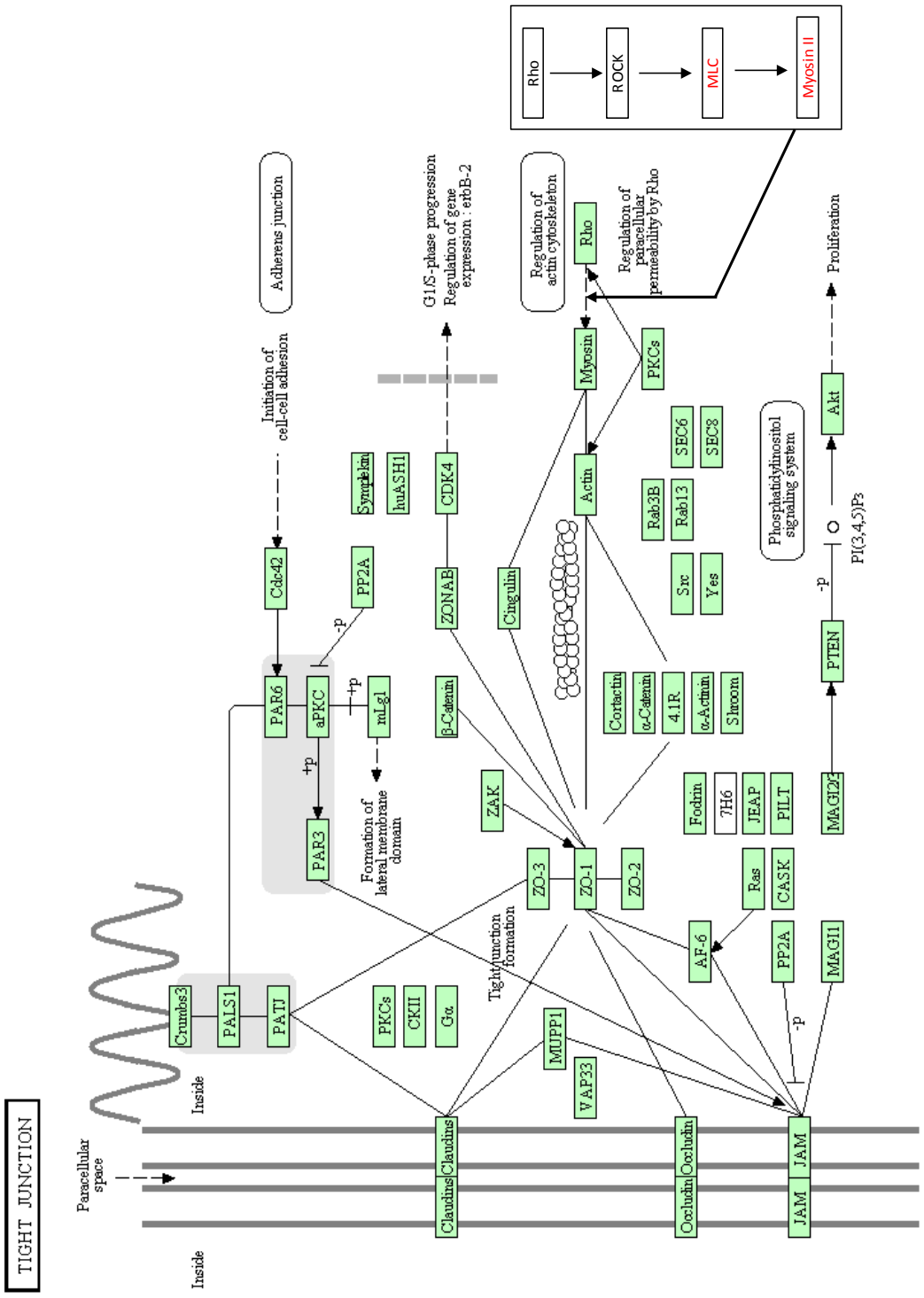

Figure 6.13 Establishment of the tight junction pathway through regulation of the actin cytoskeleton. Black arrows show the direction of signalling cascades. The big black bent arrow connector indicates the reactions that link regulation of actin cytoskeleton by Rho/ROCK to tight junction formation in epithelial cells. Rho/ROCK facilitate rearrangement of actin cytoskeleton assembly to enable interaction with tight junction transmembranes (claudins, occludins and junctional adhesion molecules (JAMs)) via zonal occludens complex (Zo-1, -2 and -3) to form and maintain the tight junctions between cells. Image adapted from http://www.kegg.jp/pathway/hsa04530+4627+4628+103910

Correlating with these enriched pathway proteins were 12 intermediate filament encoding genes (from GO cellular component analysis in Figure 6.6) found to be enriched. These proteins are part of the components of the cytoskeleton. This suggests that the enriched pathway proteins initiate the downstream formation and disassembly of macromolecular complex of the intermediate filaments. This may also suggest how the interaction of vimentin (VIM) (one of the 12 enriched intermediate filament genes) with hScrib translocates hScrib to the plasma membrane to regulate vesicle and organelle localization, maintain intercellular interaction and also control cell migration (Phua *et al.*, 2009). The identification of these enriched proteins suggest that the effect of S[1306+1309]A is upstream of its identified protein partners involved in the regulation of actin cytoskeleton pathway to facilitate the establishment and maintenance of cell polarity or cause cell invasion in breast cancer .

Actin cytoskeleton is required for maintaining cell shape. This is important as, in the processes of cell-cell contact, intracellular transport, cell migration and proliferation (via cell cycling), the cytoskeleton is required to disassemble and re-organize at certain stages (Lodish et al., 2000:18.1; Heng and Koh, 2010). Both S[1306+1309]A and S[1306+1309]D pulled down proteins (GIT1, ARHGEF7 and MYH10 for S[1306+1309]A; GIT1, ARHGEF7 and ARHGEF6 for S[1306+1309]D) that were enriched in regulation of the actin cytoskeleton pathway. Through this pathway, GIT1, ARHGEF7 and MYH10 mediate focal adhesion of migrating cells via RTK (receptor tyrosine kinase) and GPCR (G-protein coupled receptor) in response to chemotactic stimuli (Figure 6.14). It was found, through the Biological General Repository for Interaction Datasets (BioGRID), that GIT1 and ARHGEF7 interact. GIT1 and ARHGEF7 (red arrows) interaction mediate focal adhesion by inducing focal adhesion assembly (actin polymerization) at the leading edge of the cell through PAK (protein (Cdc42/Rac)-activating kinases) (blue arrow) phosphorylation of ARHGEF7 and ARHGEF7 inhibition of RhoGEF of the Rho/ROCK tight junction initiation pathway. This enables migrating cells to make cell-ECM (extracellular matrix) contact with their lamellipodia (or filopodia) at the leading edge, therefore contributing to the maintenance of anterior-posterior polarity (Phua *et al.*, 2009).

A study on GIT1 found GIT1-ERK1/2(phosphorylated) interaction in focal adhesion caused cell migration while GIT1-PXN (paxillin) interaction caused focal adhesion disassembly (Zhang et al., 2009). ARHGEF7 mediates actin organization and focal adhesions (Wozniak *et al.*, 2004; Yu *et al.*, 2015). A study by Sun and Bamji (2011) also found ARHGEF7 to form cadherin-β-catenin-hScrib-ARHGEF7 complexes to mediate actin polymerization to regulate localization of vesicles and constitutes apico-basal polarity (Iden and Collard, 2008). Chahdi and Raufman (2013) found ARHGEF7 to directly interact

with β-catenin and initiate cell proliferation in colon cancer but through hScrib (possibly unphosphorylated)-hDlg-APC complex interactions, as discussed in Chapter 5, β-catenin is degraded leading to G1 arrest of the cell cycle (Ishidate *et al*., 2000).

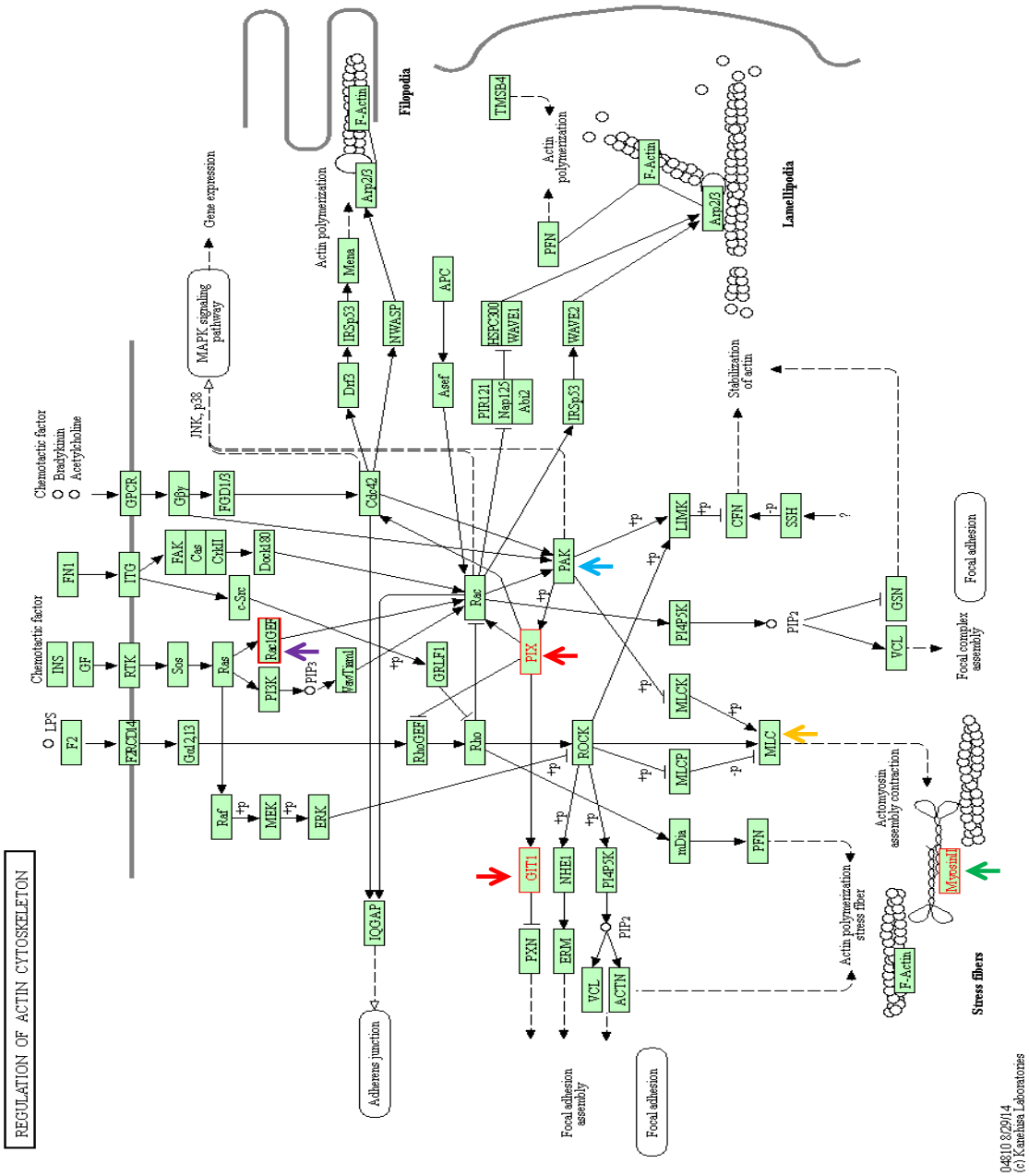

Figure 6.14 Regulation of actin cytoskeleton pathway. Black arrows show the direction of a signalling cascade. The blue arrow identifies PAK (protein-activated kinase) to be activated by both Cdc42 (cell division cycle 42) and Rac. PAK, subsequently phosphorylates PIX (ARHGEF7) (1st red arrow) which then activates GIT1 (G protein-coupled receptor kinase interactor 1) (2nd red arrow) to inhibit PXN and facilitate interactions that lead to focal adhesion assembly at the front of the lamellipodia. As new cell-ECM contact is established at the anterior of the migrating cell, old cell-ECM contact is terminated by contraction of the posterior of the cell from the ECM which requires the formation of ATP-dependent assembly of polymerized actin microfilament and myosin complex II (green arrow), regulated by phosphorylation of MLC (orange arrow which includes MYL12B) through PAK inhibitory phosphorylation of MLCK. This mechanism aids controlled directional migration of cells. When proliferation, rather than migration, is required, ARHGEF6 acts as Rac1GEF (purple arrow) to activate Rac1 (member of Rac subfamily) which transduces the signal for cell proliferation via the MAPK signalling pathway. While regulation of actin cytoskeleton is used for migration and proliferation, it could also lead to invasion of breast cancer cells if, in the case of hScrib, the wrong phosphorylation state is established. Image adapted from http://www.kegg.jp/pathway/hsa04810+4627+4628+103910

MYH10 was one of the proteins identified to be more abundant in the S[1306+1309]A pull-down than in the S[1306+1309]D pull-down. MYH10, MYH9 and MYL12B were found to be involved in regulation of the actin cytoskeleton pathway. MYH10 and MYH9 interact (BioGRID). MYH10 mediates focal adhesion by forming myosin II complex (green arrow) with MYH9 and effecting actomyosin assembly contraction to retract the trailing edge of migrating cells from the ECM. The actin-dependent ATPase activity of the myosin II complex catalyzes this energy-dependent process which is activated by phosphorylation of MYL12B (orange arrow) (Kondo *et al.*, 2012). MYL12B (member of myosin regulatory light chain, MLC) of myosin II complex is activated when PAK inhibits MLCK (myosin light chain kinase) by phosphorylation. The inactivation of MLCK releases MYL12B to be phosphorylated. Activated MYL12B translocates to the regulatory site on myosin II complex. This phosphorylates and activates the ATPase activity of myosin II leading to association of myosin II complex with polymerized actin microfilaments. MYH10 was found to mediate centrosome re-orientation and centriole migration during ciliogenesis (Avasthi and Marshall, 2012; Hong *et al.*, 2015). MYH9 is a motor protein whose association with F-actin, a polymerized form of G-actin, produces intracellular contractile forces to power retraction (pull back) in cell migration and cytokinesis (Betapudi, 2010; Elliot *et al.*, 2015).

Regulation of actin cytoskeleton, in the case of S[1306+1309]D, does not require the myosin II complex component MYH10, but ARHGEF6 as well as GIT1 and ARHGEF7 (Figure 6.14). While GIT1 and ARHGEF7 mediate focal adhesion, for cell ECM interaction, ARHGEF6 acts as a guanine nucleotide exchange factor for Rac1 (a member of Rac subfamily). It exchanges bound GDP for GTP to activate Rac1 GTPase activity. Hence, Rac1GEF (purple arrow). Activating Rac1 signals the induction of the MAPK signalling pathway for cell proliferation which occurs via the cell cycle pathway. Proteins found to be enriched in the cell cycle pathway were HDAC1, CDK1 and PRKDC. Studies show that HDAC1 is known to repress gene transcription by mediating condensation of the chromatin to enable G2 to M phase transition in the cell cycle. This occurs when the expression level of HDAC1 gradually increases from late G1 phase as pRb1, at cell cycle restriction point, becomes hyper-phosphorylated (deactivated) and HAT, which mediates gene transcription by chromatin remodelling, almost reaches peak expression levels. Without the HDAC1, cells arrest in G1 or G2 phase (Ropero and Esteller, 2007; Senese *et al.*, 2007; Haberland *et al.*, 2009). CDK1 (or Cdc 2), an M-phase promoting factor (MPF) that phosphorylates RB1, cyclins A and B for G1/S and G2/M transition (Xi, et al., 2015) was enriched. HDAC1 and CDK1 proteins are complemented by PRKDC, a kinase that binds to DNA and serves as a molecular sensor for DNA double-stranded breaks and

repair. Without the repair of DNA double-stranded breaks, PRKDC interactions with ARHGEF6 and p53 (tumour suppressor protein) induce apoptosis in the cell (Maiti, 2010). PRKDC also localizes to centrosomes and kinetochores during metaphase and at midbody during cytokinesis to prevent abnormal nuclear morphology after mitosis (Anderson and Lees-Miller, 1992; Jette and Lees-Miller, 2015). The cell cycle pathway was the second most significantly enriched when S[1306+1309]D was expressed.

The most significantly enriched pathway was the ribosome pathway which comprised 12 enriched genes that encode cytosolic ribosomes (Figure 6.6). These cytosolic ribosomes may form macromolecular complexes to facilitate translational termination of, possibly, certain structural constituents of the cytoskeleton, that enable the structural molecule activity associated with S[1306+1309]A pull-down. In addition to translational termination in the ribosome pathway was the cellular metabolic process of mRNA metabolic process (also part of the ribosome pathway), performed by 23 enriched cytosolic-ribosome-encoding genes. The mRNA metabolic process involves mRNA splicing, translational initiation, polypeptide formation and polypeptide folding. The genes involved in this process seem to be linked to cell cycle regulation (Kondoh *et al*., 1996; Gerecitano, 2014; Bansal *et al*., 2014).

Figure 6.12 showed SCRIB to be more abundant (10.7%) with S[1306+1309]D pull-down than S[1306+1309]A pull-down but Figure 6.11 identified involvement of SCRIB and MYL12B in the TSH (thyroid-stimulating hormone) signalling pathway (Figure 6.15). The TSH pathway is a major pathway, used by almost every cell in the body, required for cellular metabolic processes such as the cell proliferation (Goel et al., 2011; Brent, 2012). In the regulation of actin cytoskeleton and tight junction pathway, the light chain motor protein regulator, MYL12B, was phosphorylated. In the TSH pathway MYL12B is dephosphorylated. Since the 10.7% increase in abundance of S[1306+1309]D is significant, it would suggest that the expression of S[1306+1309]D may indirectly lead to the inactivation (dephosphorylation) of MYL12B by phosphorylated inhibition of ROCK via ERK signalling pathway, to increase the dephosphorylation activity by MLCP on MLC (which includes MYL12B). This action would inhibit cell migration and induce expression of transcription factors that promote cell proliferation via the cell cycle.

The findings of the protein-protein interaction study of hScrib are summarized in Table 6.6.

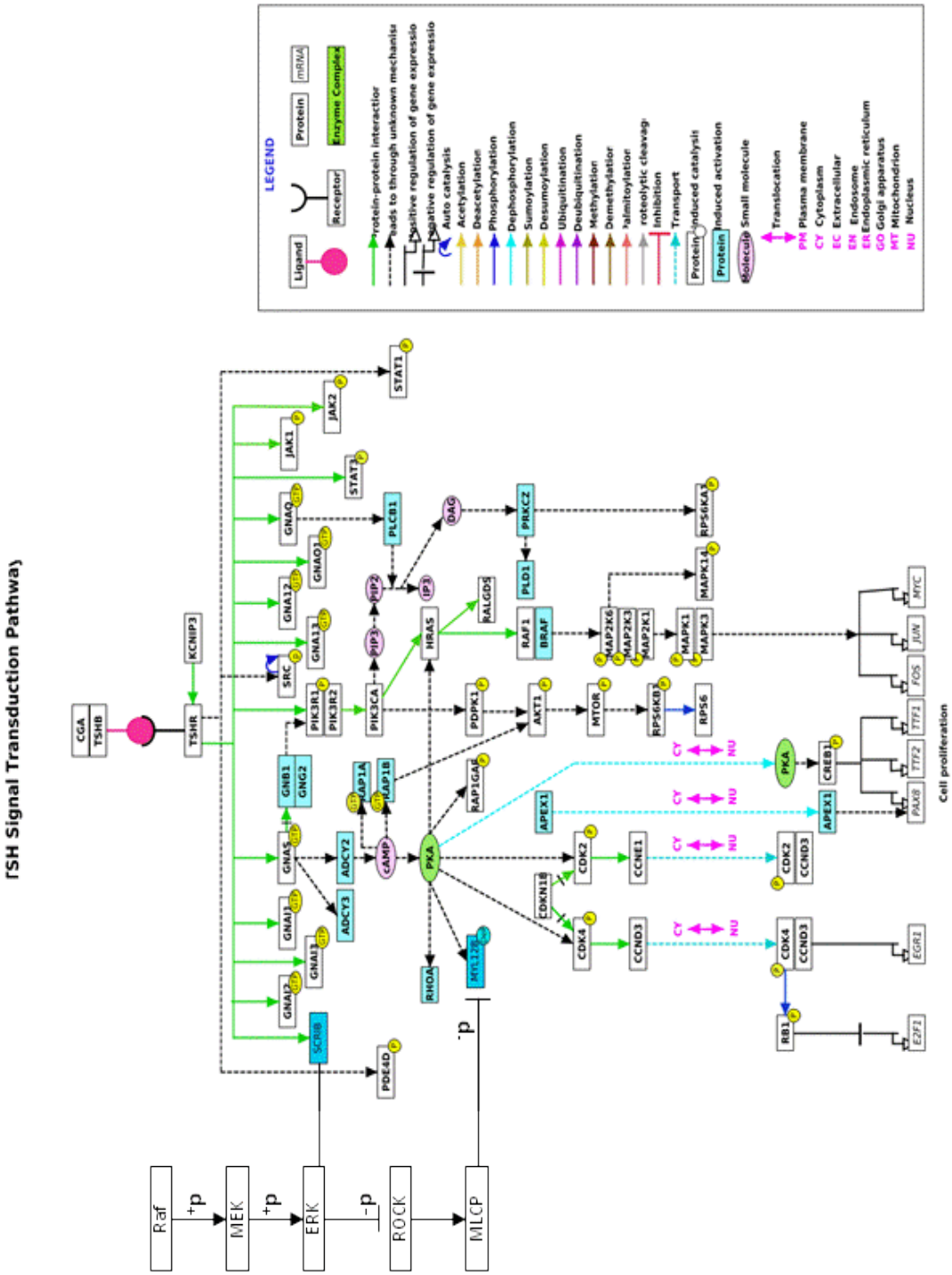

Figure 6.15 The involvement of SCRIB and MYL12B in the TSH signalling pathway. The TSH pathway is used by virtually every cell for metabolic processes including the cell proliferation process. What the different coloured arrows illustrate is depicted in the legend shown in this image. From the pathway, SCRIB is involved in a protein-protein interaction with intracellular domain of the TSH receptor. This SCRIB is S[1306+1309]D and through the ERK signalling, indirectly initiates the dephosphorylation of MYL12B (a member of MLC). This inhibits cell migration to enable cell proliferation to occur. Image adapted from http://www.kegg.jp/pathway/hsa04810+4627+4628+103910

Table 6.6 Summary of hScrib protein-protein interaction study

Methods	Objective	**S[1306+1309]A**	**S[1306+1309]D**
Co-immunoprecipitation Mass spectrometry Statistics (G-test, χ^2 distribution, Bonferroni correction) WebGestalt	Protein binding partners and pathways:		
	Tight junction	MYH9, MYH10, MYL12B	MYH9, MYH10, MYL12B
	Regulation of actin cytoskeleton	GIT1, MYH10, ARHGEF7	GIT1, ARHGEF6, ARHGEF7
	Cell cycle		CDK1, HDAC1, PRKDC
	TSH signal transduction		SCRIB, MYL12B-dephosphorylated
	Cellular Process	**Invasion**	**Proliferation**

7. Concluding remarks, limitations, relevance and future studies

S[1306+1309]A and S[1306+1309]D are some of the mutants of hScrib designed to mimic unphosphorylated (A) and phosphorylated (D) hScrib protein, respectively, in the cell. They were designed by site-directed mutagenesis to study how changes in the phosphorylation pattern of serine sites at the C-terminal of hScrib implicate hScrib in the invasion of breast cancer.

The confocal images (Figures 3.4a and 3.4b) of HEK cells transfected with the generated hScrib mutants showed hScrib had varied localization. Besides being present at cell to cell contact, hScrib, when unphosphorylated, localized to a tail-like cell structure suggested to be microtubules and when phosphorylated, localized to two structures proximal to the nucleus that were believed to be centrioles of a centrosome. This prompted the use of biochemical assays to test whether hScrib affected cell proliferation and cell migration, common features that are uncontrollable in breast cancer cells.

Wound healing and MTT assays were conducted in Chapter 4 to test cell migration and cell proliferation, respectively. The results suggested significant cell migration with unphosphorylated hScrib and significant cell proliferation with phosphorylated hScrib. To get more credible proof of this comparison, cell cycle assays were conducted (Chapter 5). This would give more detail, through cell cycle analysis, of which mimicked phosphorylation state of hScrib would support progressive transition of cells in the cell cycle and to what stage i.e. G1, S or G2/M. The results showed that cells transfected with D-mutants of hScrib arrested more in the G2/M phase than cells transfected with A-mutants of hScrib, which arrested more in the G1 phase of the cell cycle. Although there were no significant differences between the number A-mutant and D-mutant transfected cells arrested in the S phase, this was further proof of phosphorylated hScrib progressive transition of cells in the cell cycle.

To consolidate this proof, proteins that interact with hScrib in the different phosphorylation states had to be identified and their function in relation to hScrib profiled. hScrib was used as bait, in a CoIP assay, to pull down potential candidates of hScrib. The captured proteins were analysed for abundance and identified using a mass spectrometer. To avoid false positive results, stringent statistical analysis was performed on these candidates and the significance of their abundances with and without bait hScrib was determined. Three gene lists of significantly abundant protein partners were created and ran in a

bioinformatics toolkit called WebGestalt to search for the enrichment of these proteins and the pathway/s that they would significantly be involved in. Using the mass spectrometry dataset from S[1306+1309]A and S[1306+1309]D pull-downs, S[1306+1309]A expression was found to be involved in cell migration and tight junction formation by potentially interacting with proteins such as GIT1, ARHGEF7, MYL12B to effect the regulation of actin cytoskeleton through downstream effectors of MYH9, MYH10 and intermediate filaments. The actions of regulating actin cytoskeleton through the Cdc42/Rac (cell migration of anterior-posterior polarity) (Figures 6.14) and Rho/ROCK (tight junction of planar and apico-basal polarity) (Figures 6.13) contribute to maintaining epithelial cell polarity and morphology while suppressing cell proliferation. However, it is known that cancer cells can use either the Rho/ROCK-dependent or the Rac-dependent migration to invade (Amano *et al.*, 2010). Therefore, it is possible that uncontrolled expression of S[1306+1309]A of hScrib could encourage this. A possible molecular mechanism is illustrated below (Figure 7.1).

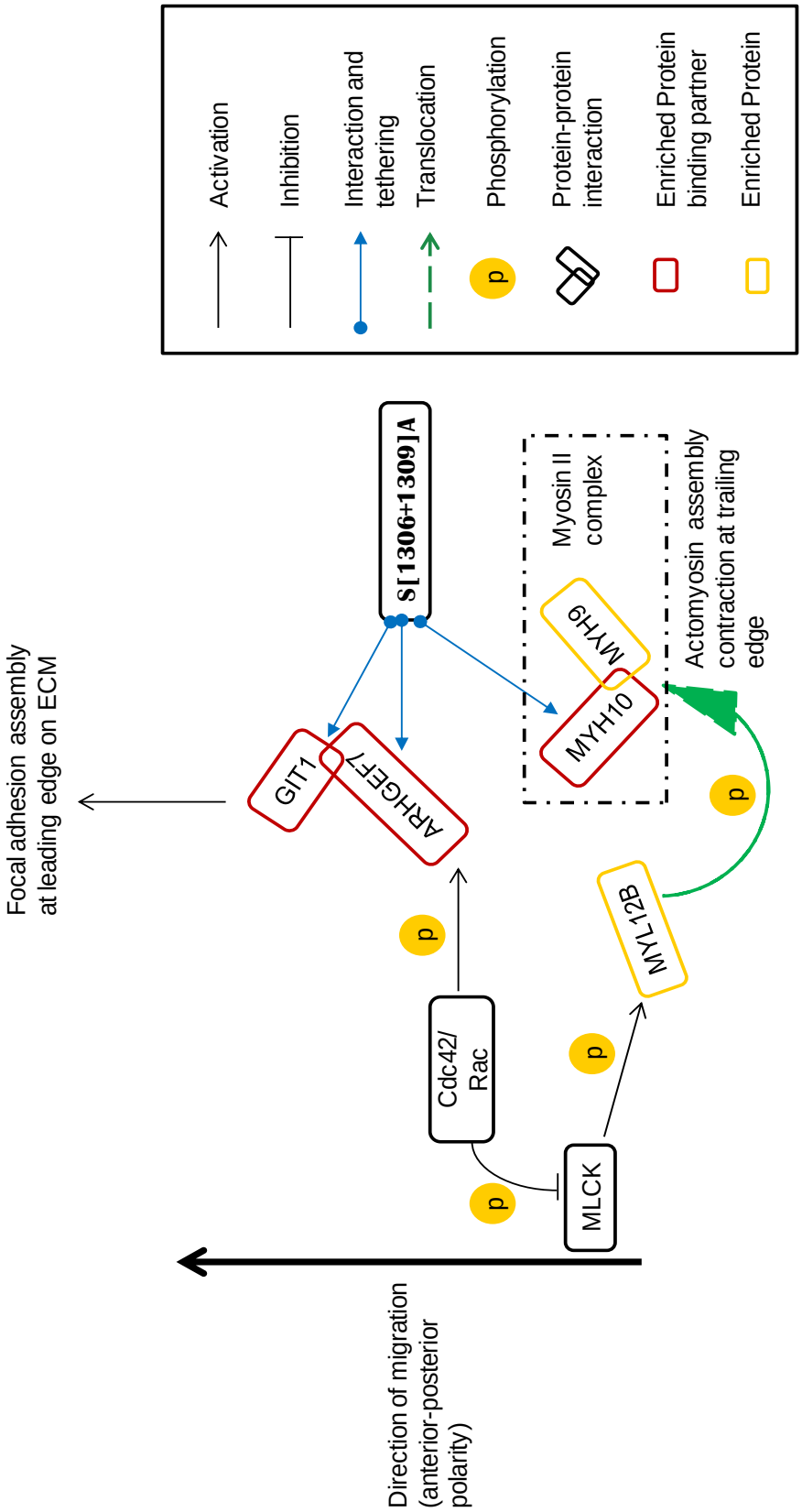

Figure 7.1 The possible molecular mechanism of breast cancer cell migration/invasion involving unphosphorylated hScrib S[1306+1309]A. S[1306+1309]A interacts with and tethers GIT1, ARHGEF7 and MYH10. GIT1 and ARHGEF7 interact and through Cdc42/Rac phosphorylation of ARHGEF7 facilitate focal adhesion assembly at the leading edge. MYH10 interacts with MYH9 to form myosin II complex. Through Cdc42/Rac inhibition of MLCK, MYL12B is phosphorylated and translocates to the regulatory subunit of myosin II complex to activate the actin-dependent ATPase activity (assembling myosin II filaments) of myosin II complex, facilitating actomyosin contraction to retract the trailing edge. This mechanism leads to cell motility and hence cell invasion.

Conversely, S[1306+1309]D expression was found to be involved, via the thyroid-stimulating hormone signalling pathway, in cell proliferation by potentially interacting with proteins such as HDAC1, CDK1, PRKDC and indirectly inactivating MYL12B, the light chain regulator for ATP-driven actomyosin assembly contraction of cell movement. This suggests that cell proliferation also requires the regulation of actin cytoskeleton but for the purpose of cell cycling and not motility. This is because S[1306+1309]D expression enriched GIT1, ARHGEF6 and ARHGEF7, which contribute to regulating the cytoskeletal elements in the cell. By directly inactivating MYL12B via the ERK signalling, HDAC1, CDK1, PRKDC can function in the S and G2/M phases of the cell cycle pathway, hence suggesting that phosphorylated hScrib facilitates G2 to M phase transition (Figure 5.2) of cells while suppressing cell migration through regulation of actin cytoskeleton. In the event of DNA double-stranded breaks (sensed by PRKDC), S[1306+1309]D may enable ARHGEF6-PRKDC interaction to enable ARHGEF6-PRKDC-p53 interaction to facilitate cell apoptosis (if DNA break is irreparable).

However, uncontrolled expression of S[1306+1309]D or S[1306+1309]D not facilitating ARHGEF6-PRKDC interaction may be exploited by breast cancer cells to favour tumour formation. A possible molecular mechanism is illustrated below (Figure 7.2).

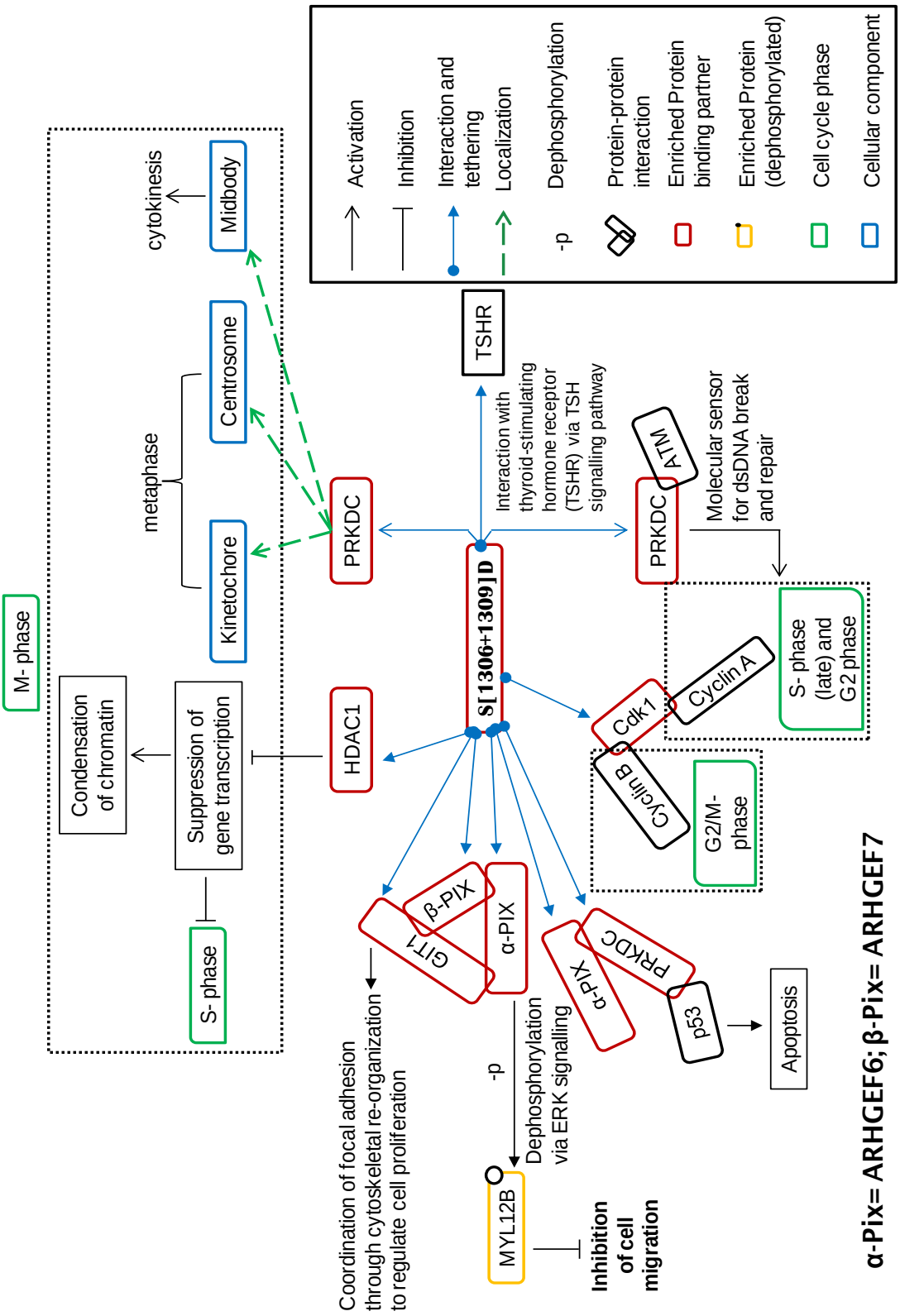

Figure 7.2 The possible molecular mechanism of breast cancer cell proliferation involving phosphorylated hScrib S[1306+1309]D. The binding of thyroid-stimulating hormone (TSH) to its receptor initiates a signal transduction beginning with the thyroid-stimulating hormone receptor (TSHR) interaction with S[1306+1309]D which tethers it and proteins HDAC1, PRKDC and Cdk1. These proteins contribute to facilitating various phases of the cell cycle pathway for cell proliferation. Also, S[1306+1309]D interacts and tethers GIT1, ARHGEF7 and ARHGEF6. ARHGEF6, via ERK signalling, dephosphorylates MYL12B. MYL12B, unable to translocate, enables GIT1-ARHGEF7-ARHGEF6 interaction to reorganize the cytoskeleton during cell cycling to facilitate cell proliferation.

The molecular mechanisms (Figure 7.1 and 7.2) show that the action of the binding partners of both unphosphorylated and phosphorylated hScrib appear to be antagonistic than complementary in that cell migration and proliferation may not occur simultaneously.

Summary of the overall research is tabled below in Table 7.1.

Table 7.1 Summary of overall study

Methods	Objective	**A-mutants**	**D-mutants**
SDM DNA sequencing	Generation of validated hScrib mutants		
Transfection Widefield imaging Western blot	Expression	Good	Good
Transfection Confocal imaging	Localization	Intracellular tail-like structure (possibly tubulin)	Possibly centrioles
		Possibly cytoskeletal elements	Possibly cytoskeletal elements
		Cell-cell contact	
Wound healing assay Widefield imaging	Cell migration	Increased cell migration represented by increased rate of wound closure	Decreased cell migration represented by reduced rate of wound closure
MTT assay Spectrophotometry	Cell proliferation	Decreased cell proliferation represented by reduced absorbance of formazan	Increased cell proliferation represented by increase in the absorbance of formazan
Flow cytometry	Cell cycle progression	G1 arrest	G2/M arrest
Co-immunoprecipitation Mass spectrometry Statistics (G-test, χ^2 distribution, Bonferroni correction) WebGestalt	Protein binding partners and pathways:		
	Tight junction	MYH9, MYH10, MYL12B	MYH9, MYH10, MYL12B
	Regulation of actin cytoskeleton	GIT1, MYH10, ARHGEF7	GIT1, ARHGEF6, ARHGEF7
	Cell cycle		CDK1, HDAC1, PRKDC
	TSH signal transduction		SCRIB, MYL12B-dephosphorylated
	Cellular Process	**Invasion**	**Proliferation**

Limitations

Although, conclusions have been drawn, the overall study was not without limitations:

Serine is a polar and uncharged residue with hydroxyl functional group (-OH) that can be phosphorylated when deprotonated (hydrogen donor). The choice of mutation model, substituting serine for alanine (A) and aspartate (D), to mimic unphosphorylation and phosphorylation hScrib, respectively, is limited. This is because alanine is hydrophobic and non-polar and due to its hydrophobicity would affect the conformity of hScrib as unphosphorylated hScrib. Aspartate may be polar, but it is a charged acidic residue that can not only be deprotonated, but also forms strong ionic bonds which may also affect the conformity of hScrib as phosphorylated hScrib. These slight changes in conformity that occur due to these deliberate substitutions to mimic hScrib phosphorylation states, may affect how hScrib interacts with its binding partners *in vitro* and hence, the pull-down.

The use of HEK293T cell line was because it was easily transfectable. However, results obtained and conclusions drawn from the assays performed with this cell line may not be directly representative of what may occur in breast cancer cells in the study of invasion and proliferation.

Western blot is a good detection system of protein of choice but errors that affect its result could be incurred due to the many steps and buffers it involves. These include trapped air bubbles during electro-transblotting or antibody probing. Protein of interest could be lost by poor sample preparation and if transfer time is too much or insufficient. There is the probability of secondary antibody reaction to label a non-specific protein. Western blot is not quantitative i.e. amount of protein detected cannot be determined.

The reproducibility of the wound healing assay is limited due to the variability in the size and shape of the gap made in each experiment. This makes comparison between experiments difficult. The creation of a mechanical scratch with a scratch tool may cause injury to the cells: cell contents and debris from the scratch tool are released into the gap. This is hard to control. Although the wound healing assay was conducted to study cell migration, during the course of the assay cells that migrate into the gap also proliferate. This is may interfere with the measurement of migrating cells and interfere with the process.

MTT assay is not reproducible. It measures metabolic activity and not cell viability. Contact inhibition may occur and cells no longer become in their most active phase of

growth i.e. log phase. As it is an absorbance-based assay, MTT assay is not very sensitive at picking out minor changes in formazan colour intensity.

The flow cytometry analyses, with PI staining method, used a single time point to measure cellular DNA content and show the percentage of cells in G1, S and G2/M phases of the cell cycle. However, it does not provide information about the rate at which the transfected cells progress through the cell cycle i.e. cell cycle kinetics. This is an indication of how fast the cells are proliferating, as an increased rate is common in breast cancer and other cancers.

Co-IP was used to capture potential binding partners of hScrib, when unphosphorylated and phosphorylated. However, it may be difficult to capture and detect *in vitro*, low-affinity binding partners as well as potential binding partners that have very low level of expression. There could also be non-specific interaction, due to the mutation model adopted, that may lead to false positive results.

Relevance of study

The findings of this research bear relevance in the Cell biology area of tissue homeostasis because it shows hScrib may contribute to determining cell proliferation as well as apoptosis through the possible molecular mechanism shown in Figure 7.2. Through the illustrated possible mechanisms of action of hScrib (with its binding partners) in regulating cell migration and proliferation, respectively, an insight into the possibility of designing therapeutic drugs that may target certain hScrib phosphorylation and binding sites (and also binding partners) of hScrib that may influence tumour formation and invasion of breast cancer may be established.

Cell polarity is the asymmetric distribution of intracellular organelles, cytoskeleton and cell surface of epithelial cells. The research findings suggest that the scaffolding structure of hScrib (unphosphorylated) enables the positioning (through regulation of actin cytoskeleton) of certain binding partners to interact, hence, mediating anterior-posterior polarity to regulate cell motility and apical-basal polarity to maintain tight junction. This also suggests that the study by Metodieva *et al*., 2013: where CD74 interacts with hScrib and hScrib translocates from cell-to-cell contacts at the plasma membrane to the cytoplasm causing enhanced motility and invasiveness of breast cancer cells, may be a consequence contributed by inappropriate unphosphorylation of one or more of the selected C-terminal serine site in hScrib.

By hScrib (phosphorylated) scaffolding structure mediating binding partners ARHGEF6 and PRKDC interaction, to enable their interaction with p53 to facilitate apoptosis (due to irreparable DNA double-stranded breaks) at S and G2/M phases of the cell cycle, it exemplifies hScribs function as a TSG. However, this TSG function of hScrib may be related to tumour formation and progression when hScrib (phosphorylated) does not enable ARHGEF7-PRKDC interaction to occur to facilitate apoptosis with p53. This contributes to favouring G2 to M phase transition of the affected cells with no means of halting or exiting the cell cycle, therefore establishing an abnormal mass of breast epithelial cells. This is a finding that contributes to increased knowledge of tumourigenesis and progression.

Future studies

There is progress towards getting a clear picture as to how hScrib is involved in the invasion of breast cancer and developing a mechanism/s for its tumour suppressive and cell polarity functions. Bioimaging studies would be conducted with constructed S[1306+1309]A tagged differently to S[1306+1309]D and co-transfected to distinguish their cellular localization and correlate the result to the pathways they are involved in. Colocalization studies of the protein partners of S[1306+1309]A and S[1306+1309]D would be performed to identify any direct interactions and where in the cell these interactions between hScrib and a protein partner occurs. To build a bigger picture requires further work to be done by using breast cancer cell lines (e.g. MCF7, MDA-231) with the hScrib mutants (Metodieva *et al.*, 2013) and the other C-terminal amino acid sites in the hScrib protein newly validated (Table 3.1). This could reveal one or more of the generated phosphorylation patterns of hScrib are responsible for hScribs involvement in breast cancer invasion, tumourigenesis and progression. Also more mass spectrometry combined with bioinformatics (WebGestalt and BioGRID) would be conducted with the end result of identifying candidate biomarkers and new drug targets for the treatment of breast cancer.

Reference List

1. Abraham, R.T. (2001). **Cell cycle checkpoint signalling through the ATM and ATR kinases**. *Genes and Development*, 15, 2177-2196.

2. Albertson, R. Chabu, C. Sheehan, A. And Doe, C.Q. (2004). **Scribble protein domain mapping reveals a multistep localization mechanism and domains necessary for establishing cortical polarity**. *Journal of Cell Science,* 117(25), 6061-6070.

3. Alfonso, A.R. (2009). **Molecular classification of breast cancer tumours from patients treated with doxorubicin and docetaxel**. *The Journal of the International Federation of Clinical Chemistry and Laboratory Medicine,* 20(4), 1-3.

4. Amano, M. Nakayama, M. And Kaibuchi, K. (2010). **Rho-kinase/ROCK: a key regulator of the cytoskeleton and cell polarity**. *Cytoskeleton*, 67(9), 545-554.

5. Anastas, J.N. Biechele, T.L. Robitaille, M. Muster, J. Allison, K.H. Angers, S. And Moon, R.T. (2012). **A protein complex of SCRIB, NOS1AP and VANGL1 regulates cell polarity and migration, and is associated with breast cancer progression**. *Oncogene,* 31, 3696-3708.

6. Anastasiadis P.Z. And Reynolds, A.B. (2000). **The p120 catenin family: complex roles in adhesion, signaling and cancer**. *Journal of Cell Science*, 113, 1319-1334.

7. Anderson, C.W. And Lees-Miller, S.P. (1992). **The nuclear serine/threonine protein kinase DNA-PK**. *Critical Reviews in Eukaryotic Gene Expression*, 2(4), 283-314.

8. Anderson, J.M. And Van Itallie, C.M. (2009). **Physiology and function of the tight junction**. *Cold Spring Harbor Perspectives in Biology*, 1(2), 1-16.

9. Andre, F. And Pusztai, L. (2006). **Molecular classification of breast cancer: implications for selection of adjuvant chemotherapy**. *Nature Clinical Practice Oncology,* 3(11), 621-632.

11. Aronica, S.M. Kraus, W.L. And Katzenellenbogen, B.S. (1994). **Estrogen action via the cAMP signalling pathway: stimulation of adenylate cyclise and cAMP-regulated gene transcription**. *Proceedings of the National Academy of Sciences of the United States of America,* 91(18), 8517-8521.

12. Avasthi, P. And Marshall, W.F. (2012). **Stages of ciliogenesis and regulation of ciliary length**. *Differentiation; Research in Biological Diversity*, 83(2), S30-S42.

13. Banerjee, S. Kumar, J. Apte-Deshpande, A. And Padmanabhan, S. (2010). **A novel prokaryotic vector for identification and selection of recombinants: direct use of the vector for expression studies in E.coli**. *Microbial Cell Factories*, 9(30), 1-8.

14. Bansal, H. Yihua, Q. Iver, S.P. Ganapathy, S. Proia, D.A. Penalva, L.O. Uren, P.J. Suresh, U. Carew, J.S. Karnad, A.B. Weitmen, S. Tomlinson, G.E. Rao, M.K. Kornblau, S.M. And Bansal, S. (2014). **WTAP is a novel oncogenic protein in acute myeloid leukemia**. *Leukemia*, 28(5), 1171-1174.

15. Bauer, H. Zweimueller-Mayer, J. Steinbacher, A. Lametschwandtner, And Bauer, H.C. (2010). **The dual role of Zonula Occludens (ZO) proteins**. *Journal of Biomedicine and Biotechnology,* 2010(2010), 1-11.

16. Benchabane, H. And Ahmed, Y. (2009). **The adenomatous polyposis coli tumor suppressor and Wnt signalling in the regulation of apoptosis**. *Advances in Experimental Medicine and Biology*, 656, 75-84.

17. Benjamini, Y. And Hochberg, Y. (1995). **Controlling the false discovery rate: a practical and powerful approach to multiple testing**. *Journal of the Royal Statistical Society. Series B (Methodological)*, 57(1), 289-300.

18. Berg, J.M. Tymoczko, J.L. and Stryer, L. (2002) **Protein Structure and Function**. In: Biochemistry, 5th edition. Chapter 3. New York. W.H. Freeman. URL http://www.ncbi.nih.gov/books/NBK21154/ 20.01.16.

19. Bernd, K. (2010). **Epithelial cells: cell polarity**. URL http://www.bio.davidson.edu/people/kabernd/BerndCV/Lab/EpithelialInfoWeb/Polarity.html 14.03.13

20. Betapudi, V. (2010). **Myosin II motor proteins with different functions determine the fate of lamellipodia extension during cell spreading**. *PLoS ONE*, 5(1), 1-14.

21. Bilder, D. Li, M. And Perrimon, N. (2000). **Cooperative regulation of cell polarity and growth by drosophila tumour suppressors**. *Science,* 289(5476), 113-116.

22. Blackford, A.N. And Grand, R.J.A. (2009). **Adenovirus E1B 55-kilodalton protein: multiple roles in viral infection and cell transformation**. *Journal of Virology*, 83(9), 4000-4012.

23. Bland, J.M. And Altman, D.G. (1995). **Multiple significance tests: the Bonferroni method**. *BMJ*, 310, 170.

24. Brent, A.G. (2012). **Mechanisms of thyroid hormone action**. *The Journal of Clinical Investigation*, 122(9), 3035-3043.

25. Brody, J.G. And Rudel, R.A. (2003). **Environmental pollutants and breast cancer**. *Environmental Health Perspectives*, 111(8), 1007-1019.

26. Buday, L. And Tompa, P. (2010). **Functional classification of proteins and related molecules**. *The FEBS Journal,* 277(21), 4348-4355.

27. Cancer Research UK. (2015). *Breast cancer incidence (invasive) statistics*. Available at: http://www.cancerresearchuk.org/health-professional/cancer-statistics/statistics-by-cancer-type/breast-cancer/incidence-invasive#heading-One [Accessed 29 Aug, 2016].

28. Cancer Research UK. (2015). *Breast cancer statistics*. [online] Available at: http://www.cancerresearchuk.org/health-professional/cancer-statistics-by-cancer-type/breast-cancer#heading-Three [Accessed 26 Aug, 2016].

29. Cancer.org. (2016). *What is breast cancer?* [online] Available at: http://www.cancer.org/cancer/breastcancer/detailedguide/breast-cancer-what-is-breast-cancer [Accessed 26 Aug, 2016].

30. Capriotti, K. And Capriotti, J.A. (2012). **Dimethyl Sulfoxide**. *The Journal of Clinical and Aesthetic Dermatology*, 5(9), 24-26.

31. Carroll, S. Naeiri, M. and Al-Rubeai, M. (2007) **Monitoring of Growth, Physiology, and Productivity of Animal Cells by Flow Cytometry**. In: *Animal Cell Biotechnology: Methods and Protocols* (ed Portner, R.) 2nd edition. pp 223-238. New Jersey. Humana Press Incorporation. URL https://books.google.co.uk/books?id=oqs7CyFj0FUC&pg=PA226&lpg=PA226&dq=coefficient+of+variation+of+cultured+cells+in+cell+cycle&source=bl&ots=eaRy6lLPSw&sig=Z7KRQ4R2KmZSUJkHy7y6Xs7FZ1I&hl=en&sa=X&ei=tnwuVcWlHoPpaonGgPAO&ved=0CFQQ6AEwBg#v=onepage&q=coefficient%20of%20variation%20of%20cultured%20cells%20in%20cell%20cycle&f=false 22.04.15.

32. Cavenee, W.K. And White, R.L. (1995). **The genetic basis of cancer**. *Scientific American,* 272(3), 72-79.

33. Chaffer, C.L. And Weinberg, R.A. (2011). **A perspective on cancer cell metastasis**. *Science,* 331(6024), 1559-1564.

34. Chahdi, A. And Raufman, J.P. (2013). **The Cdc42/Rac nucleotide exchange factor protein β_1Pix (Pak-interacting exchange factor) modulates β-catenin transcription activity in colon cancer cells: evidence for direct interaction of β_1Pix with β-catenin**. *The Journal of Biological Chemistry*, 288(47), 34019-34029.

35. Chalfie, M. Tu, Y. Euskirchen, G. Ward, W.W. And Prasher, D.C. (1994). **Green fluorescent protein as a marker for gene expression**. *Science*, 263(5148), 802-805.

36. Chapdelaine, J.M. (2011). **MTT reduction- a tetrazolium-based colorimetric assay for cell survival and proliferation**. URL http://www.moleculardevices.com/Documents/general-documents/mkt-appnotes/microplate-appnotes/Maxline_AppNote_05_MTT.pdf 04.03.2014.

37. Chatterjee, S.J. And McCaffrey, L. (2014). **Emerging role of cell polarity proteins in breast cancer progression and metastasis**. *Breast Cancer: Targets and Therapy*, 6, 15-27.

38. Chatterjee, S. Seifried, L. Feigin, M.E. Gibbons, D.L. Scuoppo, C. Lin, W. Rizvi, Z.H. Lind, E. Dissanayake, D. Kurie, J. Ohashi, P. And Muthuswamy, S.K. (2012). **Dysregulation of cell polarity proteins synergize with oncogenes or the microenvironment to induce invasive behavior in epithelial cells**. *PLoS One*, 7(4), 1-13.

39. Chen, R.E. And Thorner, J. (2007). **Function and regulation in MAPK signalling pathways**. *Biochimica et Biophysica Acta*, 1773(8), 1311-1340.

40. Chew, H.K. (2001). **Adjuvant therapy for breast cancer**. *Western Journal of medicine*, 174(4), 284-287.

41. Chial, H. (2008). **Proto-oncogenes to oncogenes to cancer**. *Nature Education,* 1(1), 33.

42. Chuderland, D. And Seger, R. (2005). **Protein-protein interactions in the regulation of the extracellular signal-regulated kinase**. *Molecular Biotechnology*, 29(1), 57-74.

43. Chow, A.Y. (2010). **Cell cycle control by oncogenes and tumor suppressors: Driving the transformation of normal cells into cancerous cells**. *Nature Education,* 3(9), 7.

44. Cianfrocca, M. And Gradishar, W. (2009). **New molecular classifications of breast cancer**. *Cancer Journal for Clinicians,* 59(5), 303-313.

45. Cody, J. Haslam, S. And Schwartz, R. (2009). **Research: progesterone leads to inflammation, a breast cancer risk factor**. URL http://msutoday.msu.edu/news/2009/research-progesterone-leads-to-inflammation-a-breast-cancer-risk-factor/ 01.01.13.

46. Comen, E.A. And Norton, L. (2011). **Breast cancer tumor size, nodal status and prognosis: biology trumps anatomy**. *Journal of Clinical Oncology*, 29(19), 2610-2612.

47. Collins, K. Jacks, T. And Pavletich, N.P. (1997). **The cell cycle and cancer**. *Proceedings of the National Academy of Sciences*, 94(7), 2776-2778.

48. Cooper, S. Iyer, G. Tarquini, M. And Bissett, P. (2006). **Nocodazole does not synchronize cells: implications for cell-cycle control and whole-culture synchronization**. *Cell and Tissue Research*, 324(2) 237-242.

49. Coradini, D. Casarsa, C. And Oriana, S. (2011). **Epithelial cell polarity and tumorigenesis: new perspectives for cancer detection and treatment**. *Acta Pharmacologica Sinica,* 32, 552-564.

50. Cude, K. Wang, Y. Choi, H-J. Hsuan, S-L. Zhang, H. Wang, C-Y. And Xia, Z. (2007). **Regulation of the G2-M cell cycle progression by the ERK5-NFkB signaling pathway**. *The Journal of Cell Biology*, 177(2), 253-264.

51. Darbre, P.D. (2012). **Molecular mechanisms of oestrogen action on growth of breast cancer cells in culture**. *Hormone Molecular Biology and Clinical Investigation,* 9(1), 65-85.

52. De la Torre, M. Heldin, P. And Bergh, J. (1995). **Expression of the CD44 glycoprotein (lymphocyte-homing receptor) in untreated human breast cancer and its relationship to prognostic markers**. *Anticancer Research,* 15(6B), 2791-2795.

53. Deugnier, M. Teuliere, J. Faraldo, M.M. Thiery, J.P. And Glukhova, M.A. (2002). **The importance of being a myoepithelial cell**. *Breast Cancer Research*, 4(6), 224-230.

54. Devilee, P. Cleton-Jansen, A-M. And Cornelisse, C.J. (2003). **Ever since knudson**. *Trends in Genetics,* 17(10), 569-573.

55. Dhanasekaran, D.N. Kashef, K. Lee, C.M. Xu, H. And Reddy, E.P. (2007). **Scaffold proteins of MAP-kinase modules**. *Oncogene*, 26, 3185-3202.

56. Dollar, G.L. and Sokol, S.Y. (2007) **WNT signalling in embryonic development.** In: *Wnt signalling and the establishment of cell polarity*, pp 61-66. California. Elsevier. URL https://books.google.co.uk/books?id=tNgIlRfdrGoC&pg=PA63&lpg=PA63&dq=scribble+basolateral+domain+by+dollar+and+sokol&source=bl&ots=1SOhNkbgaG&sig=iKi8QY7ohiruB3tVAgp3d3lycfg&hl=en&sa=X&ved=0CC8Q6AEwAmoVChMI6rz50e-LyQIVxusUCh1smwGu#v=onepage&q=scribble%20basolateral%20domain%20by%20dollar%20and%20sokol&f=false 28.11.13.

57. Dow, L.E. Brumby, A.M. Muratore, R. Coombe, M.L. Sedelies, K.A. Trapani, J.A. Russell, S.M. Richardson, H.E. And Humbert, P.O. (2003). **hScrib is a functional homologue of the *Drosophila* tumour suppressor Scribble**. *Oncogene,* 22, 9225-9230.

58. Durek, P. Schudoma, C. Weckwerth, W. Selbig, J. And Walther, D. (2009). **Detection and characterization of 3D-signature phosphorylation site motifs and their contribution towards improved phosphorylation site prediction in proteins**. *BMC Bioinformatics*, 10(117), 1-17.

59. Dworkin, A.M. Huang, T.H-M. And Tolan, A.E. (2009). **Epigenetic alterations in the breast: implications for breast cancer detection, prognosis and treatment**. *Seminars in Cancer Biology,* 19(3), 165-171.

60. Dyson, N. (1998). **The regulation of E2F by pRB-family proteins**. *Genes and Development,* 12(15), 2245-2262.

61. Elliot, H. Fischer, R.S. Myers, K.A. Desai, R.A. Gao, L. Chen, C.S. Adelstein, R.S. Waterman, C.M. And Danuser, G. (2015). **Myosin II controls cellular branching morphogenesis and migration in three dimensions by minimizing cell-surface curvature**. *Nature Cell Biology*, 17(2), 137-147.

62. Ellis, H. And Mahadevan, V. (2013). **Anatomy and physiology of the breast**. *Surgery (Oxford),* 31(1), 11-14.

63. Etienne-Manneville, S. (2008). **Polarity proteins in migration and invasion**. *Oncogene,* 27, 6970-6980.

64. Ezhevsky, S.A. Nagahara, H. Vocero-Akbani, A.M. Guis, D.R. Wei, M.C. **And Dowdy, S.F. (1997). Hypo-phosphorylation of the retinoblastoma protein (pRb) by cyclin D:Cdk 4/6 complexes results in active pRb**. *Proceeding of the National Academy of Sciences of the United States of America*, 94(20), 10699-10704.

65. Feigin, M.E. Akshinthala, S.D. Araki, K. Rosenberg, A.Z. Muthuswamy, L.B. Martin, B. Lehmann, B.D. Berman, H.K. Pietenpol, J.A. Cardiff, R.D. And Muthuswamy, S.K. (2014). **Mislocalization of the cell polarity protein Scribble promotes mammary tumourigenesis and is associated with basal breast cancer**. *Cancer Research*, 74(11), 3180-3194.

66. Feigin, M.E. And Muthuswamy, S.K. (2009). **ErbB receptors and cell polarity: new pathways and paradigms for understanding cell migration and invasion**. *Experimental Cell Research,* 315(4), 707-716.

67. Fidler, I.J. (2003). **The pathogenesis of cancer metastasis: the 'seed and soil' hypothesis revisited**. *Nature Reviews Cancer,* 3, 453-458.

68. Freimoser, F.M. Jakob, C.A. Aebi, M. And Tuor, U. (1999). **The MTT [3-(4,5-dimethylthiazol-2-yl)-2,5-diphenyltetrazolium bromide] assay is a fast and reliable method for colorimetric determination of fungal cell densities**. *Applied and Environmental Microbiology,* 65(8), 3727-3729.

69. Forsburg, S.L. (2002). **Dr Forsburg's all-purpose cell cycle lecture notes**. URL http://www-bcf.usc.edu/~forsburg/cclecture.html%20 03.01.12.

70. Gabay, M. Li, Y. And Felsher, D.W. (2014). **MYC activation is a hallmark of cancer initiation and maintenance**. *Cold Spring Harbor Perspectives in Medicine*, 4(6), 1-14.

71. Garcea, R.L. And Imperiale, M.J. (2003). **Simian virus 40 infection of humans**. *Journal of Virology*, 77(9), 5039-5045.

72. Gathani, T. Bull, D. Green, J. Reeves, G. Beral, V. And the million women study collaborators. (2005). **Breast cancer histological classification: agreement between the office for national statistics and the National Health Service breast screening programme**. *Breast Cancer Research*, 7(6), 1090-1096.

73. Gerecitano, J. (2014). **SINE (selective inhibitor of nuclear export)--translational science in a new class of anti-cancer agents**. *Journal of Haematology and Oncology*, 7, 67.

74. Glinskii, O.V. Huxley, V.H. Glinsky, G.V. Pienta, K.J. Raz, A. And Glinsky, V.V. (2005). Mechanical entrapment is insufficient and intercellular adhesion is essential for metastatic cell arrest in distant organs. *Neoplasia,* 7(5), 522-527.

75. Goel, R. Raju, R. Maharudraiah, J. Kumar, G.S.S. Ghosh, K. Kumar, A. Lakshmi, P.T. Sharma, R. Balakrishnan, L. Pan, A. Kandasamy, K. Christopher, R. Krishna, V. Mohan, S.S. Harsha, H.C. Mathur, P.P. Pandey, A. And Prasad, T.S.K. (2011). **A signalling network of thyroid-stimulating hormone**. *Journal of Proteomics and Bioinformatics*, 4, 1-8.

76. Goldhirsch, A. Wood, W.C. Coates, A.S. Gelber, R.D. Thurlimann, B. Senn, H.J. And Panel members. (2011). **Strategies for subtypes- dealing with the diversity of breast cancer: highlights of the St Gallen International Concensus on the Primary Therapy of Early Breast Cancer 2011**. *Annals of Oncology,* 22(8), 1736-1747.

77. Good, M.C. Zalatan, J.G. And Lim, W.A. (2011). **Scaffold proteins: hubs for controlling the flow of cellular information**. *Science,* 332(6030), 680-686.

78. Graham, F.L. Smiley, J. Russell, W.C. And Nairn, R. (1977). **Characteristics of a human cell line transformed by DNA from human adenovirus type 5**. *Journal of General Virology*, 36(1), 59-74.

79. Greenwood, C. Metodieva, G. Al-Janabi, K. Lausen, B. Alldridge, L. Leng, L. Bucala, R. Fernandez, N. And Metodiev, M.V. (2012). **Stat1 and CD74 overexpression is co-dependent and linked to increased invasion and lymph node metastasis in triple-negative breast cancer**. *Journal of Proteomics,* 75(10), 3031-3040.

80. Grifoni, D. Garoia, F. Schimanski, C.C. Schmitz, G. Laurenti, E. Galle, P.R. Pession, A. Cavicchi, S. And Strand, D. (2004). **The human protein Hugl-1 substitutes for *Drosophila* Lethal giant larvae tumour suppressor function *in vivo***. *Oncogene*, 23, 8688-8694.

81. Guttridge, D.C. Albanese, C. Reuther, J.Y. Pestell R.G. And Baldwin, A.S. Jr (1999). **NF-kappaB controls cell growth and differentiation through transcriptional regulation of cyclin D1**. *Molecular and Cellular Biology*, 19(8), 5785-5799.

82. Haberland, M. Montgomery, R.L. And Olson, E.N. (2009). **The many roles of histone deacetylases in development and physiology: implications for disease and therapy**. *Nature Reviews Genetics*, 10(1), 32-42.

83. Hanahan, D. Weinberg, R.A. (2011). **Hallmarks of cancer: the next generation**. *Cell*, 144(5), 646-674.

84. Hardjasa, A. Ling, M. Ma, K. And Yu, H. (2010). **Investigating the effects of DMSO on PCR fidelity using a restriction digest-based method**. *Journal of Experimental Microbiology and Immunology*, 14, 161-164.

85. Hartsock, A. And Nelson, W.J. (2008). **Adherens and tight junctions: structure, function and connections to the actin cytoskeleton**. *Biochimica et Biophysica Acta*, 1778(3), 660-669.

86. Harvey, B. (2009). **Novel aspects of oestrogen actions**. *Journal of physiology,* 587(21), 5017.

87. Heinecke, N.L. Pratt, B.S. Vaisar, T. And Becker, L. (2010). **PepC: proteomics software for identifying differentially expressed proteins based on spectral counting**. *Bioinformatics*, 26(12), 1574-1575.

88. Heng, Y-W. And Koh, C-G. (2010). **Actin cytoskeleton dynamics and the cell division cycle**. *The International Journal of Biochemistry and Cell Biology*, 42(10), 1622-1633.

89. Henderson, B.R. (2000). **Nuclear-cytoplasmic shuttling of APC regulates β-catenin subcellular localization and turnover**. *Nature Cell Biology*, 2(9), 653-660.

90. Hong, H. Kim, J. And Kim, J. (2015). **Myosin heavy chain 10 (MYH10) is required for centriole migration during the biogenesis of primary cilia**. *Biochemical and Biophysical Research Communications*, 461(1), 180-185.

91. Huang, L. And Muthuswamy, S.K. (2010). **Polarity protein alterations in carcinoma: a focus on emerging roles for polarity regulators**. *Current Opinion in Genetics and Development*, 20(1), 41-50.

92. Huang, Y. Nayak, S. Jankowitz, R. Davidson, N.E. And Oesterreich, S. (2011). **Epigenetics in breast cancer: what's new?** *Breast Cancer Research,* 13(6), 225-235.

93. Humbert, P.O. Grzeschik, N.A. Brumby, A.M. Galea, R. Elsum, I. **And Richardson, E. (2008). Control of tumourigenesis by the scribble/dlg/lgl polarity module**. *Oncogene*, 27, 6888-6907.

94. Humbert, P. Russell, S. And Richardson, H. (2003). **Dlg, Scribble and Lgl in cell polarity, cell proliferation and cancer**. *BioEssays*, 25(6), 542-553.

95. Hunter, K.W. Crawford, N.P.S. And Alsarraj, J. (2008). **Mechanisms of metastasis**. *Breast Cancer Research,* 10(1), 1-10.

96. Iden, S. And Collard, J.G. (2008). **Crosstalk between small GTPases and polarity proteins in cell polarization**. *Nature Reviews Molecular Cell Biology*, 9, 846-859.

97. Inoue, K. Fry, E.A. And Taneja, P. (2013). **Recent progress in mouse models for tumour suppressor genes and its implications in human cancer**. *Clinical Medicine Insights: Oncology,* 7, 103-122.

98. Irvin Jr, W. Muss, H.B. And Mayer, D.K. (2011). **Symptom management in metastatic breast cancer**. *The Oncologist,* 16(9), 1203-1214.

99. Ishidate, T. Matsumine, A. Toyoshima, K. And Akiyama, T. (2000). **The APC-hDLG complex negatively regulates cell cycle progression from the G0/G1 to S phase**. *Oncogene*, 19(3), 365-372.

100. Isola, J. Kallioniemi, D.A. Tanner, D.M. And Nevanlinna, D.H. **Somatic genetic changes of BRCA1 and BRCA2 in breast cancer**. Academic Dissertation. University of Tampere, Institute of Medical Technology, Finland, June 2003.

101. Ivanov, A.I. Young, C. Beste, K.D. Capaldo, C.T. Humbert, P.O. Brenwald, P. Parkos, C.A. And Nusrat, A. (2010). **Tumor suppressor scribble regulates assembly of tight junctions in the intestinal epithelium**. *The American Journal of Pathology*, 176(1), 134-145.

102. Jeffy, B.D. Chirnomas, R.B. And Romagnolo, D.F. (2002). **Epigenetics of breast cancer: polycyclic aromatic hydrocarbons as risk factors**. *Environmental and Molecular Mutagenesis,* 39(2-3), 235-244.

103. Jette, N. And Less-Miller, S.P. (2015). **The DNA-dependent protein kinase: a multifunctional protein kinase with roles in DNA double strand break repair and mitosis**. *Progress in Biophysics and Molecular Biology*, 117(2-3), 194-205.

104. Jiang, Y. Rabbi, M. Mieczkowski, P.A. And Marszalek, P.E. (2010). **Separating DNA with different topologies by atomic force microscopy in comparison with gel electrophoresis**. *Journal of Physical Chemistry B*, 114(37), 12162-12165.

105. Jozwiak, J. Jozwiak, S. And Wlodarski, P. (2008). **Possible mechanisms of disease development in tuberous sclerosis**. *The Lancet Oncology,* 9(1), 73-79.

106. Junttila, M.R. And Evan, G.I. (2009). **p53- a Jack of all trades but master of none**. *Nature Reviews Cancer,* 9(11), 821-829.

107. Kalluri, R. And Weinberg, R. (2009). **The basics of epithelial-mesenchymal transition**. *The Journal of Clinical Investigation,* 119(6), 1420-1428.

108. Kaplan, N.A. Liu, X. And Tolwinski, N.S. (2009). **Epithelial polarity: interactions between junctions and apical-basal machinery**. *Genetics,* 1-20.

109. Kenemans, P. Verstreaten, R.A. And Verheijen, R.H.M. (2004). **Oncogenic pathways in hereditary and sporadic breast cancer**. *Maturitas,* 49(1), 34-43.

110. Kim, E.K. And Choi, EJ. (2010). **Pathological roles of MAPK signaling pathways in human diseases**. *Biochimica et Biophysica Acta*, 1802(4), 396-405.

111. Knipe, D.M. and Howley, P.M. (2007) **Fields Virology**. In: *Cell Transformation by Viruses*, 5th edition. Volume 1. pp 231-235. Philadelphia. Lippincott Williams and Wilkins. URL https://books.google.co.uk/books?id=5O0somr0w18C&pg=PA233&lpg=PA233&dq=sv40+gene+and+E1A&source=bl&ots=FrnEfdX3bw&sig=puNc1fR_vHutpVZFLxYeC7880JU&hl=en&sa=X&ved=0CEkQ6AEwCGoVChMIl_Ly1Y-syAIVR6weCh1T-wse#v=onepage&q=sv40%20gene%20and%20E1A&f=false 02.10.15.

112. Kocanova, S. Mazaheri, M. Caze-Subra, S. And Bystricky, K. (2010). **Ligands specify estrogen receptor alpha nuclear localization and degradation**. *BioMed Central Cell Biology,* 11(98), 1-13.

113. Kohn, K.W. (1999). **Molecular interaction map of the mammalian cell cycle control and DNA repair systems**. *Molecular Biology of the Cell,* 10, 2703-2734.

114. Kondo, T. Isoda, R. Uchimura, T. Sugiyama, M. Hamao, K. And Hosova, H. (2012). **Diphosphorylated but not monophosphorylated myosin II regulatory light chain localizes to the midzones without its heavy chain during cytokinesis**. *Biochemical and Biophysical Research Communications*, 417(2), 686-691.

115. Kondoh, N. Noda, M. Fisher, R.J. Schweinfest, C.W. Papas, T.S. Kondoh, A. Samuel, K.P. And Oikawa, T. (1996). **The S29 ribosomal protein increases tumor suppressor activity of K rev-1 gene on v-K ras-transformed NIH3T3 cells**. Biochimica et biophysica acta, 1313(1), 41-46.

116. Lambrechts, A. Van Troys, M. And Ampe, C. (2004). **The actin cytoskeleton in normal and pathological cell motility**. *The International Journal of Biochemistry and Cell Biology*, 36(10), 1890-1909.

117. Lange, C.A. And Yee, D. (2008). **Progesterone and breast cancer**. *Women's Health,* 4(2), 151-162.

118. Lawson, J.S. And Heng, B. (2010). **Viruses and breast cancer**. *Cancers,* 2(2), 752-772.

119. Lee, E.Y.H.P. And Muller, W.J. (2010). **Oncogenes and tumour suppressor genes**. *Cold Spring Harbor Perspectives in Biology,* 2(10), 1-18.

120. Levchenko, A. Bruck, J. And Sternberg, P.W. (2000). **Scaffold proteins may biphasically affect the levels of mitogen-activated protein kinase signalling and reduce its threshold properties**. *Proceedings of the National Academy of Sciences*, 97(11), 5818-5823.

121. Liang, C. Park, A.Y. And Guan, J. (2007). ***In vitro* scratch assay: a convenient and inexpensive method for analysis of cell migration *in vitro***. Nature Protocols, 2(2), 329-333.

122. Lim, K.T. Cosgrave, N. Hill, A.D. And Young, L.S. (2006). **Non-genomic oestrogen signalling in oestrogen receptor negative breast cancer cells: a role for the angiotensin II receptor AT1**. *Breast Cancer Research,* 8(3), 1-10.

123. Lin, Y-C. Boone, M. Meuris, L. Lemmens, I. Van Roy, N. Soete, A. Reumers, J. Moisse, M. Plaisance, S. Drmanac, R. Chen, J. Speleman, F. Lambrechts, D. Van de Peer, Y. Tavernier, J. And Callewaert, N. (2014). **Genome dynamics of the human kidney 293 lineage in response to cell biology manipulations**. *Nature Communications*, 5(4767), 1-12.

124. Lodish, H. Berk, A. Kaiser, C.A, Krieger, M. Bretscher, A. Ploegh, H. Amon, A. and Scott, M.P. (2000) **The Eukaryotic Cell Cycle**. In: *Molecular Cell Biology*, 7th edition. New York. W.H. Freeman and Company, pp 721-924.

125. Lodish, H. Berk, A. Zipursky, S.L. Matsudaira, P. Baltimore, D. and Darnell, J. (2000) **Regulation of the Eukaryotic Cell Cycle**. In: *Molecular Cell Biology,* 4th edition. Section 13.6. New York. W.H. Freeman. URL http://www.ncbi.nlm.nih.gov/books/NBK21497/ 30.04.15.

126. Lodish H, Berk, A. Zipursky, S.L. Matsudaira, P. Baltimore, D. and Darnell, J. (2000) **The Actin Cytoskeleton**. In *Molecular Cell Biology*, 4th edition. Section 18.1. New York. W. H. Freeman. URL http://www.ncbi.nlm.nih.gov/books/NBK21493/ 05.04.16.

127. Lodish, H. Kaiser, C.A. Bretscher, A. Amon, A. Berk, A. Krieger, M. Ploegh, H. and Scott, M.P. (2013) **Protein Structure and Function**. In: *Molecular Cell Biology,* 7th edition. pp 59-60. New York. W.H. Freeman.

128. Loeb, L.A. (2001). **A mutator phenotype in cancer**. *Cancer Research,* 61(8), 3230-3239.

129. Lohia, M. Qin, Y. And Macara, I.G. (2012). **The scribble polarity protein stabilizes e-cadherin/p120-catenin binding and blocks retrieval of e-cadherin to the golgi**. *PLoS ONE,* 7(11), 1-12.

130. Longtin, R. (2004). **A forgotten debate: is selenocysteine the 21st amino acid?** *Journal of the National Cancer Institute*, 96(7), 504-505.

131. Louis, N. Evelegh, C. And Graham, L. (1997). **Cloning and sequencing of the cellular-viral junctions from the human adenovirus type 5 transformed 293 cell line**. *Virology*, 233(2), 423-429.

132. Macara, I.G. And McCaffrey, L. (2013**). Cell polarity in morphogenesis and metastasis**. *Philosophical Transactions of the Royal Society of London. Series B, Biological Sciences*, 368(1629), 1-6.

133. MacDonald, B.T. Tamai, K. And He, X. (2009). **Wnt/β-catenin signalling: components, mechanisms, and diseases**. *Developmental Cell*, 17(1), 9-26.

134. Macea, J.R. And Fregnani, J.H.T.G. (2006). **Anatomy of the thoracic wall, axilla and breast**. *International Journal of Morphology,* 24(4), 691-704.

135. Maiti, A.K. (2010). Gene network analysis of oxidative stress-mediated drug sensitivity in resistant ovarian carcinoma cells. *The Pharmacogenomics Journal*, 10(2), 94-104.

136. Mangelsdorf, D. Thummel, C. Beato, M. Herrlich, P. Schutz, G. Limesono, K. Blumberg, B. Kastner, P. Mark, M. Chambon, P. And Evans, R.M. (1995). **The nuclear receptor superfamily: the second decade**. *Cell,* 83(6), 835-839.

137. McCaffrey, L.M. And Macara, I.G. (2012). **Signaling pathways in cell polarity**. *Cold Spring Harbor Perspectives in Biology*, 4(6),1-15.

138. McCrea, P.D. And Gu, M. (2010). **The catenin family at a glance**. *Journal of Cell Science*, 123(5), 637-642.

139. McNeil, E. Capaldo, C.T. And Macara, I.G. (2006). **Zonula Occludens-1 function in the assembly of tight junctions in Madin-Darby Canine Kidney Epithelial Cells**. *Molecular Biology of the Cell,* 17(4), 1922-1932.

140. Mendez, M.G. Kojima, S. And Goldman, R.D. (2010). **Vimentin induces changes in cell shape, motility, and adhesion during the epithelial to mesenchymal transition**. *The FASEB Journal,* 24(6), 1838-1851.

141. Metodieva, G. Nogueira-de-Souza, N.C. Greenwood, C. Al-Janabi, K. Leng, L. Bucala, R. And Metodiev, M.V. (2013). **CD74-dependent deregulation of the tumor suppressor scribble in human epithelial and breast cancer cells**. *Neoplasia*, 15(6), 660-668.

142. Meyers, J.A. Sanchez, D. Elwell, L.P. And Falkow, S. (1976). **Simple agarose gel electrophoresis method for the identification and characterization of plasmid deoxyribonucleic acid**. *Journal of Bacteriology*, 127(3), 1529-1537.

143. Michor, F. Iwasa, Y. And Nowak, M.A. (2004). **Dynamics of cancer progression**. *Nature Reviews Cancer,* 4, 197-205.

144. Moniz, S. And Jordan, P. (2010). **WNK kinase signalling in cancer biology**. *Emerging Signaling Pathways in Tumor Biology*, 43-70.

145. Murthy, S.K. DiFrancesco, L.M. Ogilvie, R.T, And Demetrick, D.J. (2002). **Loss of heterozygosity associated with uniparental disomy in breast carcinoma**. *Modern Pathology,* 15(12), 1241-1250.

146. Nagasaka, K. Nakagawa, S. Yano, T. Takizawa, S. Matsumoto, Y. Tsuruga, T. Nakagawa, K. Minaguchi, T. Oda, K. Hiraike-Wada, O. Ooishi, H. Yasugi, T And Taketani, Y. (2006). **Human homolog of *Drosophila* tumor suppressor scribble negatively regulates cell-cycle progression from G1 to S phase by localizing at the basolateral membrane in epithelial cells**. *Cancer Science*, 97(11), 1217-1225.

147. Nagasaka, K. Pim, D. Massimi, P. Thomas, M. Tomaic, V. Subbaiah, V.K. Kranjec, C. Nakagawa, S. Yano, T. Taketani, Y. Myers, M. And Banks, L. (2010). **The cell polarity regulator hScrib controls ERK activation through a KIM site-dependent interaction**. *Oncogene*, 29(38), 5311-5321.

148. Nakagawa, S. And Huibregtse, J.M. (2000). **Human scribble (Vartul) is targeted for ubiquitin-mediated degradation by the high-risk papilloma virus E6 proteins and the E6AP ubiquitin-protein ligase**. *Molecular Cell Biology*, 20(21), 8244-8253.

149. Nashimoto, S. And Nashida, E. (2006). **MAPK signalling: ERK5 versus ERK1/2**. *EMBO Reports*, 7(8), 782-786.

150. National Cancer Institute. (2016). *Risk Factors*. [online] Available at: http://www.cancer.gov/about-cancer/causes-prevention/risk [Accessed 29 Aug, 2016].

151. National Cancer Institute. (2016). *What is Cancer?*. [online] Available at: http://www.cancer.gov/about-cancer/understanding/what-is-cancer [Accessed 29 Aug, 2016].

152. Nelson, W.J. (2009). **Remodeling epithelial cell organization: transitions between front-rear and apical-basal polarity**. *Cold Spring Harbor Perspectives in Biology,* 1-19.

153. Nielsen, T.O. Hsu, F.D. Jensen, K. Cheang, M. Karaca G. Hu, Z. Hernandez-Boussard, T. Livasy, C. Cowan, D. Dressler, L. Akslen, L.A. Ragaz, J. Gown, A.M. Gilks, C.B. Van de Rijn, M. And Perou, C.M. (2004). **Immunohistochemical and clinical characterization of the basal-like subtype of invasive breast carcinoma**. *Clinical Cancer Research*, 10, 5367-5374.

154. Noble, W.S. (2009). **How does multiple testing correction work?** *Nature biotechnology*, 27(12), 1135-1137.

155. Nunez, R. (2001). **DNA measurement and cell cycle analysis by flow cytometry**. *Current Issues in Molecular Biology*, 3(3), 67-70.

156. Oesterreich, S. And Fuqua, S.A.W. (1999). **Tumor suppressor genes in breast cancer**. *Society for Endocrinology,* 6, 405-419.

157. Oliveira, A.M. Ross, J.S. And Fletcher, J.A. (2005). **Tumor suppressor genes in breast cancer**. *American Society for Clinical Pathology,* 124(1), 16-28.

158. Onder, T.T. Gupta, P.B. Mani, S.A. Yang, J. Lander, E.S. And Weinberg, R.A. (2008**). Loss of E-cadherin promotes metastasis via multiple downstream transcriptional pathways**. Cancer Research, 68(10), 3645-3654.

159. Ormerod, M.G. (2008) Flow cytometry- **A basic introduction**. Chapter 6. URL http://flowbook-wiki.denovosoftware.com/Flow_Book/Chapter_6%3A_DNA_Analysis 13.11.14.

160. Osborne, C. Wilson, P. And Tripathy, D. (2004). **Oncogenes and tumor suppressor genes in breast cancer: potential diagnostic and therapeutic applications**. *The Oncologist,* 9(4), 361-377.

161. Osmani, N. Vitale, N. Borg, J. And Etienne-Manneville, S. (2006). **Scrib controls Cdc42 localization and activity to promote cell polarization during astrocyte migration**. *Current Biology,* 16(24), 2395-2405.

162. Pagano, M. Pepperkok, P. Verde, F. Ansorge, W. And Draetta, G. (1992). **Cyclin A is required at two points in the human cell cycle**. *The EMBO Journal*, 11(3), 961-971.

163. Pensabene, M. Condello, C. De Placido, S. Contegiacomo, A. And Pepe, S. (2012). **Epigenetic factors in hereditary breast cancer**. URL https://www.novapublishers.com/catalog/product_info.php?products_id=22169 06.12.12.

164. Phua, D.C. Humbert, P.O. And Hunziker, W. (2009). **Vimentin regulates scribble activity by protecting it from proteosomal degradation**. *Molecular Biology of the Cell*, 20(12), 2841-2855.

165. Phua, D.C.Y. Humbert, P.O. And Hunziker, W. (2009). **Vimentin regulates scribble activity by protecting it from proteosomal degradation**. *Molecular Biology of the Cell*, 20(12), 2841-2855.

166. Pinheiro, D. And Sunkel, C (2012). **Mechanisms of cell cycle control**. *Journal of the Portuguese Biochemical Society,* 4-15.

167. Polyak, K. (2011). **Heterogeneity of breast cancer**. *The Journal of Clinical Investigation,* 121(10), 3785-3788.

168. Pozarowski, P. And Darzynkiewicz, Z. (2004). **Analysis of cell cycle by flow cytometry**. *Methods in Molecular Biology,* 281, 301-311.

169. Price, P. And McMillan, T.J. (1990). **Use of the tetrazolium assay in measuring the response of human tumor cells in ionizing radiation**. *Cancer Research,* 50(5), 1392-1396.

170. Qin, Y. Capaldo, C. Gumbiner, B.M. And Macara, I.G. (2005). **The mammalian scribble polarity protein regulates epithelial cell adhesion and migration through E-cadherin**. *The Journal of Cell Biology,* 171(6), 1061-1071.

171. Radisky, D.C. (2005). **Epithelial-mesenchymal transition**. *Journal of Cell Science,* 118(19), 4325-4326.

172. Rakha, E.A. Reis-Filho, J.S. And Ellis, I.O. (2008). **Basal-like breast cancer: a critical review**. *Journal of Clinical Oncology,* 26(15), 2568-2581.

173. Rakha, E.A. Reis-Filho, J.S. Baehner, F. Dabbs, D.J. Decker, T. Eusebi, V. Fox, S.B. Ichihara, S. Jacquemier, J. Lakhani, S.R. Palacios, J. Richardson, A. Schnitt, S.T. Schmitt, F.C. Tan, P. Tse, G.M. Badve, S. And Ellis, I.O. (2010). **Breast cancer prognostic classification in the molecular era: the role of histological grade**. *Breast Cancer Research*, 12(4), 1-12.

174. Ramos, J.W. (2008). **The regulation of extracellular signal-regulated kinase (ERK) in mammalian cells**. *The international Journal of Biochemistry and Cell Biology*, 40(12), 2707-2719.

175. Rausch, A. And Kortleever, C. (2011). **Human Physiology**. URL http://humanphysiology2011.wikispaces.com/03.+Cell+Physiology 04.10.13.

176. Reis-Filho, J.S. And Lakhani, S.R. (2008). **Breast cancer special types: why bother?** *Journal of Pathology*, 216(4), 394-398.

177. Riahi, R. Yang, T. Zhang, D.D. And Wong P.K. (2012). **Advances in wound-healing assays for probing collective cell migration**. *Journal of Laboratory Automation,* 17(1), 59-65.

178. Riddihough, G. And Zahn, L.M. (2012). **What is epigenetics?** *Science,* 330, 611.

179. Ropero, S. And Esteller, M. (2007). **The role of histone deacetylases (HDACs) in human cancer**. *Molecular Oncology*, 1(1), 19-25.

180. Rosner, M. Schipany, K. And Hengstschlager, M. (2013). **Merging high-quality biochemical fractionation with a refined flow cytometry approach to monitor nucleocytoplasmic protein expression throughout the unperturbed mammalian cell cycle**. *Nature Protocols*, 8, 602-626.

181. Royer, C. And Lu, X. (2011). **Epithelial cell polarity: a major gatekeeper against cancer?** *Cell Death and Differentiation*, 18(9), 1470-1477.

182. Rubbelke, D.L. (1999). **Tissues of the human body**: an introduction. URL http://www.mhhe.com/biosci/ap/histology_mh/epi1.html 18.02.13.

183. Sa, G. And Das, T. (2008). **Anti cancer effects of curcumin: cycle of life and death**. *Cell Division*, 3, 1-14.

184. Sambrook, J. and Russell, D.W. (2001) **Gel Electrophoresis of DNA and Pulsed-field Agarose Gel Electrophoresis**. In: *Molecular Cloning: A Laboratory Manual.* 3rd edition, Chapter 5. New York. Cold Spring Harbor Laboratory Press.

185. Sandal, T. (2002). **Molecular aspects of the mammalian cell cycle and cancer**. *The Oncologist*, 7(1), 73-81.

186. Sarkar, S. And Mandall, M. (2011). **Breast Cancer: Classification Based on Molecular Etiology Influencing Prognosis and Production**. In*: Breast Cancer-Focusing Tumor Microenvironment, Stem Cells and Metastasis* (eds Gunduz, M. and Gunduz, I.). pp 69-84. Rijika, InTech Europe.

187. Schaack, J. Bennett, M.L. Colbert, J.D. Torres, A.V. Clayton, G.H. Ornelles, D. And Moorhead, J. (2004). **E1A and E1B proteins inhibit inflammation induced by adenovirus**. *Proceedings of the National Academy of Sciences*, 101(9), 3124-3129.

188. Schkufza, L. Coyote, P. Aldsworth, C. Barcellos-Hoff, M.H. Barlow, J. Werb, Z. Yaswen, P. and Huff, K. (2010) ***The Breast Biologues****.* pp 5-18. San Francisco. Bay Area Breast Cancer and the Environment Research Center.

189. Schneider, K.A. (2012) ***Counseling About Cancer: Strategies for Genetic Counseling****,* 3rd edition. 3.4.2. New Jersey, Wiley-Blackwell.

190. Schnitt, S.J. (2010). **Classification and prognosis of invasive breast cancer: from morphology to molecular taxonomy**. *Modern pathology,* 23, 60-64.

191. Sears, R. Nuckolls, F. Haura, E. Taya, Y. Tamai, K. And Nevins, J.R. (2000). **Multiple Ras-dependent phosphorylation pathways regulate Myc protein stability**. *Genes and Development*, 14(19), 2501-2514.

192. Seger, R. And Krebs, E.G. (1995). **The MAPK signaling cascade**. *FASEB Journal*, 9(9), 726-735.

193. Senese, S. Zaragoza, K. Minardi, S. Muradore, I. Ronzoni, S. Passafaro, A. Bernard, L. Draetta, G.F. Alcalay, M. Seiser, C. And Chiocca, S. (2007). **Role for histone deacetylase 1 in human tumour cell proliferation**. *Molecular and Cell Biology*, 24(13), 4784-4795.

194. Shakelford, R.E. Kaufmann, W.K. And Paules R.S. (1999). **Cell cycle control, checkpoint mechanisms and genotoxic stress**. *Environmental Health Perspectives,* 107(1), 5-15.

195. Siegel, P.M. Dankort, D.L. Hardy, W.R. And Muller, W.J. (1994). **Novel activating mutations in the *neu* proto-oncogene involved in induction of mammary tumors**. *Molecular and Cellular Biology,* 14(11), 7068-7077.

196. Simpson, P.T. Gale, T. Fulford, L.G. Reis-Filho, J.S. And Lakhani, S.R. (2003). **The diagnosis and management of pre-invasive breast disease: pathology of atypical lobular hyperplasia and lobular carcinoma *in situ***. *Breast Cancer Research*, 5(5), 258-262.

197. Skildum, A, Faivre, E. And Lange, C.A. (2005). **Progesterone receptors induce cell cycle progression via activation of mitogen-activated protein kinases**. *Molecular Endocrinology,* 19(2), 327-339.

198. Smalley, M. And Ashworth, A. (2003). **Stem cells and breast cancer: a field in transit**. *Nature Reviews Cancer*, 3, 832-844.

199. Spirin, V. And Mirny, L.A. (2003). **Protein complexes and functional modules in molecular networks**. *Proceedings of the National Academy of Sciences of the United States of America*, 100(21), 12123-12128.

200. Su, W-H. Mruk, D.D. Wong, E.W.P. Lui, W-Y. And Cheng, C,Y. (2012). **Polarity protein complex Scribble/Lgl/Dlg and epithelial cell barriers**. Advances in experimental medicine and biology, 763, 149-170.

201. Suami, H. Pan, W. Mann, G.B. And Taylor, G.I. (2008). **The lymphatic anatomy of the breast and its implications for sentinel lymph node biopsy: A human cadaver study**. *Annals of Surgical Oncology,* 15(3), 863-871.

202. Sui, H. Fan, Z-Z. And Li, Q. (2012). **Signal transduction pathways and transcriptional mechanisms of ABCB1/Pgp-mediated multiple drug resistance in human cancer cells**. *The Journal of International Medical Research,* 40(2), 426-435.

203. Sun, Q. Jackson, R.A. Ng, C. Guy, G.R. And Sivaraman, J. (2010). **Additional serine/threonine phosphorylation reduces binding affinity but preserves interface topography of substrate proteins to the c-Cbl TKB domain**. *PLoS One*, 5(9), 1-11.

204. Sun, Y. And Bamji, S.X. (2011). **β-pix modulates actin-mediated recruitment of synaptic vesicles to synapses**. *The Journal of Neuroscience*, 31(47), 17123-17133.

205. Takizawa, S. Nagasaka, K. Nakagawa, S. Yano, T. Nakagawa, K. Yasugi, T. Takeuchi, T. Kanda, T. Huibregtse, J.M. Akiyama, T. And Taketani, Y. (2006). **Human scribble, a novel tumor suppressor identified as a target of high-risk HPV E6 for ubiquitin-mediated degradation, interacts with adenomatous polyposis coli**. *Genes to Cells*, 11(4), 453-464.

206. Thiery, J.P. And Sleeman, J.P. (2006). **Overview of the molecular networks that regulate EMT**. *Nature Reviews Molecular Cell Biology,* 7, 131-142.

207. Thomas, P. And Smart, T.G. (2005). **HEK293 cell line: a vehicle for the expression of recombinant proteins**. *Journal of Pharmacological and Toxicological Methods*, 51(3), 187-200.

208. Tischfield, J.A. And Shao, C. (2003). **Somatic recombination redux**. *Nature Genetics,* 33, 5-6.

209. Townsend, M.C. Beauchamp, R.D. Evers, B.M. and Mattox, K.L. (2007) **Sabiston textbook of Surgery: The Biological Basis of Modern Surgical Practice**, 18th edition. pp 36.

210. Treloar, K.K. Simpson, M.J. (2013). **Sensitivity of edge detection for quantifying cell migration assays**. *PLos ONE*, 8(6), 1-10.

211. Turanov, A.A. Xu, X-M. Carlson, B.A. Yoo, M-H. Gladyshev, V.N. And Hatfield, D.L. (2011). **Biosynthesis of selenocysteine, the 21st amino acid in the genetic code, and a novel pathway for cysteine biosynthesis**. *Advances in Nutrition*, 2, 122-128.

212. Van de Loosdrecht, A.A. Beelen, R.H. Ossenkoppele, G.J. And Langehuijsen, M.M. (1994). **A tetrazolium-based colorimetric MTT assay to quantitate human monocyte mediated cytotoxicity agains leukemic cells from cell lines and patients with acute myeloid leukemia**. *Journal of Immunological Methods,* 174(1-2), 311-320.

213. Vargo-Gogola, T. And Rosen, J.M. (2007). **Modelling breast cancer: one size does not fit all**. *Nature Reviews Cancer,* 7(9), 659-672.

214. Voduc, K.D. Cheang, M.C.U. Tyldesley, S. Gelmon, K. Nielsen, T.O. And Kennecke, H. (2010). **Breast cancer subtypes and the risk of local and regional relapse**. *Journal of Clinical Oncology,* 28(10), 1684-1691.

215. Wada, T. And Penninger, J.M. (2004). **Mitogen-activated protein kinases in apoptosis regulation**. *Oncogene*, 23(16), 2838-2349.

216. Wang, W. And Malcolm, B.A. (1999). **Two-stage PCR protocol allowing introduction of multiple mutations, deletions and insertions using QuikChange site-directed mutagenesis**. *BioTechniques*, 26(4), 680-682.

217. Wang, X. And Tournier, C. (2006). **Regulation of cellular functions by the ERK5 signalling pathway**. *Cellular Signalling*, 18(6), 753-760.

218. Wang, Y. Azuma, Y. Moore, D. Osheroff, N. And Neufeld, K.L. (2008). **Interaction between tumor suppressor adenomatous polyposis coli and topoisomerase IIα: implication for the G2/M transition**. *Molecular Biology of the Cell*, 19(10), 4076-4085.

219. Weber, G.F. (2008). **Molecular mechanisms of metastasis**. *Cancer Letters,* 270(2), 181-190.

220. Weigelt, B. Peterse, J.L. And van't Veer, L.J. (2005). **Breast cancer metastasis: markers and models**. *Nature Reviews Cancer*, 5, 591-602.

221. Weinberg, R.A. (1995). **The retinoblastoma protein and cell cycle control**. *Cell*, 81(3), 323-330.

222. Wiechmann, L. And Kuerer, H.M. (2008). **The molecular journey from ductal carcinoma in situ to invasive breast cancer**. *Cancer*, 112(10), 2130-2142.

223. Wijnhoven, B.P. Dinjens, W.N. And Pignatelli, M. (2000). **E-cadherin-catenin cell-cell adhesion complex and human cancer**. *British Journal of Surgery,* 87(8), 992-1005.

224. Winchester, D.J. and Winchester, D.P. (2006) ***Breast Cancer*** 2nd edition. pp 83-88. Ontario. BC Decker Inc.

225. Wodarz, A. And Nathke, I. (2007). **Cell polarity in development and cancer**. *Nature Cell Biology*, 9(9), 1016-1024.

226. Woo R.A. And Poon, R.Y. (2003). **Cyclin-dependent kinases and S phase control in mammalian cells**. *Cell Cycle*, 2(4), 316-324.

227. Wozniak, M.A. Modzelewska, K. Kwong, L. And Keely, P.J. (2004). **Focal adhesion regulation of cell behaviour**. *Biochimica et Biophysica Acta- Molecular Cell Research*, 1692(2-3), 103-119.

228. Wu, C-J. Kai, T. Rikova, K. Merberg, D. Kasif, S. And Steffen, M. (2009). **A predictive phosphorylation signature of lung cancer**. *PLoS One*, 4(11), 1-9.

229. Xi, Q. Huang, M. Wang, Y. Zhong, J. Liu, R. Jiang, L. Wang, J. Fang, Z. and Yang, S. (2015). **The expression of CDK1 is associated with proliferation and can be a prognostic factor in epithelial ovarian cancer**. *Tumour Biology*, 36(7), 4939-4948.

230. Yamaguchi, H. Wyckoff, J. And Condeelis, J. (2005). **Cell migration in tumors**. *Current Opinion in Cell Biology,* 17(5), 559-564.

231. Yanagawa, M. Ikemot, K. Kawauchi, S. Furuya, T. Yamamoto, S. Oka, M. Oga, A. Nagashima, Y. And Sasaki, K. (2012). **Luminal A and B (HER2 negative) subtypes of breast cancer consist of a mixture of tumors with different genotype**. *BMC Research Notes,* 5, 1-8.

232. Yarrow, J.C. Perlman, Z.E. Westwood, N.J. And Mitchison, T.J. (2004). **A high-throughput cell migration assay using scratch wound healing, a comparison of image-based readout methods**. *BioMed Central Biotechnology,* 4(21), 1472-6750.

233. Yu, H.W. Chen, Y.Q. Huang, C.M. Liu, C.Y. Wang, Y.K. Tang, M.J. And Kuo, J.C. (2015). **β-Pix controls intracellular viscoelasticity to regulate lung cancer cell migration**. *Journal of Cellular and Molecular Medicine*, 19(5), 934-947.

234. Yue, P.Y.K Leung, E.P.Y. Mak, N.K. And Wong, R.N.S. (2010). **A simplified method for quantifying cell migration/wound healing in 96-well plates**. *Journal of Biomolecular Screening,* 15(4), 424-433.

235. Zahiri, J. Bozorgmehr, J.H. And Masoudi-Nejad, A. (2013). **Computational prediction of protein-protein interaction networks: algo-rithms and resources**. *Current Genomics*, 14(6), 397-414.

236. Zhan, L. Rosenberg, A. Bergami, K.C. Yu, M. Xuan, Z. Jaffe, A.B. Allred, C. And Muthuswamy, S.K. (2008). **Deregulation of Scribble promotes mammary tumorigenesis and reveals a role for cell polarity in carcinoma**. *Cell,* 135(5), 865-878.

237. Zhang, B. Kirov, S. And Snoddy, J. (2005). **WebGestalt: an integrated system for exploring gene sets in various biological contexts**. *Nucleic Acid Research*, 33, W741-W748.

238. Zhang, N. Cai, W. Yin, G. Nagel, D.J. And Berk, B.C. (2009). **GIT1 is a novel MEK1-ERK1/2 scaffold that localizes to focal adhesions**. *Cell Biology International*, 34(1), 41-47.

239. Zhang, W. And Liu, H.T. (2002). **MAPK signal pathways in the regulation of cell proliferation in mammalian cells**. *Cell Research,* 12, 9-18.

240. Zheng, L. And Lee, W.H. (2001). **The retinoblastoma gene: a prototypic and multifunctional tumour suppressor**. *Experimental Cell Research*, 264(1), 2-18.

241. Zhu, H. And Gooderham, N.J. (2006). **Mechanisms of induction of cell cycle arrest and cell death by cryptolepine in human lung adenocarcinoma A549 cells**. *Society of Toxicology,* 91(1), 132-138.

Appendix A

Alignment results of DNA sequenced hScrib mutants (in Chapter 3) as displayed by blastx of the basic local alignment search tool (BLAST). Red arrows indicate the position of change made on 'query' sequence. The primers (forward or reverse) were used in the sequencing of the mutants.

ALIGNMENTS OF POSITIVELY VALIDATED hSCRIB MUTANT PROTEINS

Single Mutations (A-mutants)

S1306A + 1448A Reverse primer

SCRIB protein, partial [Homo sapiens]
Sequence ID: gb|AAH14632.2|Length: 832Number of Matches: 1
Related Information
Gene-associated gene details
Map Viewer-aligned genomic context
Range 1: 370 to 605GenPeptGraphics Next Match Previous Match

Alignment statistics for match #1

Score	Expect	Method	Identities	Positives	Gaps	Frame
387bits(995)	4e-125	Compositional matrix adjust.	234/236(99%)	235/236(99%)	0/236(0%)	-3

```
Query  797  LTHGEAVQLLRSVGDTLTVLVCDGFEASTDAALEVSPGVIANPFAAGIGHRNSLESISSI 618
            LTHGEAVQLLRSVGDTLTVLVCDGFEASTDAALEVSPGVIANPFAAGIGHRNSLESISSI
Sbjct  370  LTHGEAVQLLRSVGDTLTVLVCDGFEASTDAALEVSPGVIANPFAAGIGHRNSLESISSI 429

Query  617  DRELSPEGPGKEKELPGQTLHWGPEATEAAGRGLQPLKLDYRALAAVPSAGSVQRVPSGA 438
            DRELSPEGPGKEKELPGQTLHWGPEATEAAGRGLQPLKLDYRALAAVPSAGSVQRVPSGA
Sbjct  430  DRELSPEGPGKEKELPGQTLHWGPEATEAAGRGLQPLKLDYRALAAVPSAGSVQRVPSGA 489

Query  437  AGGKMAEspcspsgqqppappsPDELPANVKQAYRAFAAVPTSHppedapaqpptpgpaa 258
            AGGKMAESPCSPSGQQPP+PPSPDELPANVKQAYRAFAAVPTSHPPEDAPAQPPTPGPAA
Sbjct  490  AGGKMAESPCSPSGQQPPSPPSPDELPANVKQAYRAFAAVPTSHPPEDAPAQPPTPGPAA 549

Query  257  sPEQLSFREXQKYFELEVRVPQAEGPPKRVSLVGADDLRKMQEEEARKLQQKRAQM  90
            SPEQLSFRE QKYFELEVRVPQAEGPPKRVSLVGADDLRKMQEEEARKLQQKRAQM
Sbjct  550  SPEQLSFRERQKYFELEVRVPQAEGPPKRVSLVGADDLRKMQEEEARKLQQKRAQM  605
```

S1309A + 1448A Reverse primer

SCRIB protein, partial [Homo sapiens]
Sequence ID: gb|AAH14632.2|Length: 832Number of Matches: 1
Related Information
Gene-associated gene details
Map Viewer-aligned genomic context
Range 1: 361 to 605GenPeptGraphics Next Match Previous Match

Alignment statistics for match #1

Score	Expect	Method	Identities	Positives	Gaps	Frame
405 bits(1042)	4e-132	Compositional matrix adjust.	242/245(99%)	243/245(99%)	0/245(0%)	-1

```
Query  811  EVNQQSLLGLTHGEAVQLLRSVGDTLTVLVCDGFEASTDAALEVSPGVIANPFAAGIGHR 632
            EVNQQSLLGLTHGEAVQLLRSVGDTLTVLVCDGFEASTDAALEVSPGVIANPFAAGIGHR
Sbjct  361  EVNQQSLLGLTHGEAVQLLRSVGDTLTVLVCDGFEASTDAALEVSPGVIANPFAAGIGHR 420

Query  631  NSLESISSIDRELSPEGPGKEKELPGQTLHWGPEATEAAGRGLQPLKLDYRALAAVPSAG 452
            NSLESISSIDRELSPEGPGKEKELPGQTLHWGPEATEAAGRGLQPLKLDYRALAAVPSAG
Sbjct  421  NSLESISSIDRELSPEGPGKEKELPGQTLHWGPEATEAAGRGLQPLKLDYRALAAVPSAG 480

Query  451  SVQRVPSGAAGGKMAEsxcspsgqqppsppaPDELPANVKQAYRAFAAVPTSHppedapa 272
            SVQRVPSGAAGGKMAES CSPSGQQPPSPP+PDELPANVKQAYRAFAAVPTSHPPEDAPA
Sbjct  481  SVQRVPSGAAGGKMAESPCSPSGQQPPSPPSPDELPANVKQAYRAFAAVPTSHPPEDAPA 540

Query  271  qpptpgpaasPEQLSFRERQKYFELEVRVPQAEGPPKRVSLVGAXDLRKMQEEEARKLQQ  92
            QPPTPGPAASPEQLSFRERQKYFELEVRVPQAEGPPKRVSLVGA DLRKMQEEEARKLQQ
Sbjct  541  QPPTPGPAASPEQLSFRERQKYFELEVRVPQAEGPPKRVSLVGADDLRKMQEEEARKLQQ 600

Query  91   KRAQM  77
            KRAQM
Sbjct  601  KRAQM  605
```

S1348A + 1448A Reverse primer

SCRIB protein, partial [Homo sapiens]
Sequence ID: gb|AAH09490.2|Length: 450Number of Matches: 1
Related Information
Gene-associated gene details
Map Viewer-aligned genomic context
Range 1: 106 to 198GenPeptGraphicsNext MatchPrevious Match

Alignment statistics for match #1

Score	Expect	Method	Identities	Positives	Gaps	Frame
146 bits(368)	8e-39	Compositional matrix adjust.	92/93(99%)	93/93(100%)	0/93(0%)	-2

```
Query  403  DELPANVKQAYRAFAAVPTSHppedapaqpptpgpaaaPEQLSFRERQKYFELEVRVPQA  224
            DELPANVKQAYRAFAAVPTSHPPEDAPAQPPTPGPAA+PEQLSFRERQKYFELEVRVPQA
Sbjct  106  DELPANVKQAYRAFAAVPTSHPPEDAPAQPPTPGPAASPEQLSFRERQKYFELEVRVPQA  165

Query  223  EGPPKRVSLVGADDLRKMQEEEARKLQQKRAQM  125
            EGPPKRVSLVGADDLRKMQEEEARKLQQKRAQM
Sbjct  166  EGPPKRVSLVGADDLRKMQEEEARKLQQKRAQM  198
```

S1448A + 1306A Forward primer

SCRIB protein, partial [Homo sapiens]
Sequence ID: gb|AAH14632.2|Length: 832Number of Matches: 1
Related Information
Gene-associated gene details
Map Viewer-aligned genomic context
Range 1: 524 to 814GenPeptGraphics Next Match Previous Match

Alignment statistics for match #1

Score	Expect	Method	Identities	Positives	Gaps	Frame
348 bits(892)	3e-108	Compositional matrix adjust.	290/291(99%)	291/291(100%)	0/291(0%)	+1

```
Query  25   RAFAAVPTSHppedapaqpptpgpaaspEQLSFRERQKYFELEVRVPQAEGPPKRVSLVG 204
            RAFAAVPTSHPPEDAPAQPPTPGPAASPEQLSFRERQKYFELEVRVPQAEGPPKRVSLVG
Sbjct  524  RAFAAVPTSHPPEDAPAQPPTPGPAASPEQLSFRERQKYFELEVRVPQAEGPPKRVSLVG 583

Query  205  ADDLRKMQEEEARKLQQKRAQMlreaaeagaearlaldgetlgeeeqedeqppWASPSPT 384
            ADDLRKMQEEEARKLQQKRAQMLREAAEAGAEARLALDGETLGEEEQEDEQPPWASPSPT
Sbjct  584  ADDLRKMQEEEARKLQQKRAQMLREAAEAGAEARLALDGETLGEEEQEDEQPPWASPSPT 643

Query  385  SRQSpaappplgggapVRTAKAERRHQERLRVQSPEPPAPERALSPaelraleaekralw 564
            SRQSPA+PPPLGGGAPVRTAKAERRHQERLRVQSPEPPAPERALSPAELRALEAEKRALW
Sbjct  644  SRQSPASPPPLGGGAPVRTAKAERRHQERLRVQSPEPPAPERALSPAELRALEAEKRALW 703

Query  565  raarMKSLEQDALRAQMVLSRSQEGRGTRGPLERLAEapspaptpsptpVEDLGPQTSTS 744
            RAARMKSLEQDALRAQMVLSRSQEGRGTRGPLERLAEAPSPAPTPSPTPVEDLGPQTSTS
Sbjct  704  RAARMKSLEQDALRAQMVLSRSQEGRGTRGPLERLAEAPSPAPTPSPTPVEDLGPQTSTS 763

Query  745  PGRLSPDFAEELRSLEPSPSPGPQEEDGEVALVLLGRPSPGAVGPEDVALC  897
            PGRLSPDFAEELRSLEPSPSPGPQEEDGEVALVLLGRPSPGAVGPEDVALC
Sbjct  764  PGRLSPDFAEELRSLEPSPSPGPQEEDGEVALVLLGRPSPGAVGPEDVALC  814
```

Single Mutations (D-mutants)

S1306D + 1448D Reverse primer

SCRIB protein, partial [Homo sapiens]
Sequence ID: gb|AAH14632.2|Length: 832Number of Matches: 1
Related Information
Gene-associated gene details
Map Viewer-aligned genomic context
Range 1: 329 to 605GenPeptGraphics Next Match Previous Match First Match

Alignment statistics for match #1

Score	Expect	Method	Identities	Positives	Gaps	Frame
421 bits(1081)	1e-137()	Compositional matrix adjust.	273/277(99%)	273/277(98%)	0/277(0%)	-1

Features:

```
Query  924  RXPPDEGIFISKVSPTgaagrdgrlrvglrlLEVNQQSLLGLTHGEAVQLLRSVGDTLTV 745
            R P DEGIFISKVSPTGAAGRDGRLRVGLRLLEVNQQSLLGLTHGEAVQLLRSVGDTLTV
Sbjct  329  RDPTDEGIFISKVSPTGAAGRDGRLRVGLRLLEVNQQSLLGLTHGEAVQLLRSVGDTLTV 388

Query  744  LVCDGFEASTDAALEVSPGVIANPFAAGIGHRNSLESISSIDRELSPEGPGKEKELPGQT 565
            LVCDGFEASTDAALEVSPGVIANPFAAGIGHRNSLESISSIDRELSPEGPGKEKELPGQT
Sbjct  389  LVCDGFEASTDAALEVSPGVIANPFAAGIGHRNSLESISSIDRELSPEGPGKEKELPGQT 448

Query  564  LHWGPEATEAAGRGLQPLKLDYRALAAVPSAGSVQRVPSGAAGGKMAEspcspsgqqppd 385
            LHWGPEATEAAGRGLQPLKLDYRALAAVPSAGSVQRVPSGAAGGKMAESPCSPSGQQPP
Sbjct  449  LHWGPEATEAAGRGLQPLKLDYRALAAVPSAGSVQRVPSGAAGGKMAESPCSPSGQQPPS 508

Query  384  ppspDELPANVKQAYRAFAAVPTSHppedapaqpptpgpaasPEQLSFRERQKYFELEVR 205
            PPSPDELPANVKQAYRAFAAVPTSHPPEDAPAQPPTPGPAASPEQLSFRERQKYFELEVR
Sbjct  509  PPSPDELPANVKQAYRAFAAVPTSHPPEDAPAQPPTPGPAASPEQLSFRERQKYFELEVR 568

Query  204  VPQAEGPPKRVSLVGAXDLRKMQEEEARKLQQKRAQM  94
            VPQAEGPPKRVSLVGA DLRKMQEEEARKLQQKRAQM
Sbjct  569  VPQAEGPPKRVSLVGADDLRKMQEEEARKLQQKRAQM  605
```

S1309D + 1448D Reverse primer

SCRIB protein, partial [Homo sapiens]
Sequence ID: gb|AAH14632.2|Length: 832Number of Matches: 1
Related Information
Gene-associated gene details
Map Viewer-aligned genomic context
Range 1: 337 to 605GenPeptGraphics Next Match Previous Match First Match

Alignment statistics for match #1

Score	Expect	Method	Identities	Positives	Gaps	Frame
409 bits(1051)	2e-133()	Compositional matrix adjust.	266/269(99%)	266/269(98%)	0/269(0%)	-1

Features:

```
Query  898  FXXKVSPTgaagrdgrlrvglrlLEVNQQSLLGLTHGEAVQLLRSVGDTLTVLVCDGFEA 719
            F  KVSPTGAAGRDGRLRVGLRLLEVNQQSLLGLTHGEAVQLLRSVGDTLTVLVCDGFEA
Sbjct  337  FISKVSPTGAAGRDGRLRVGLRLLEVNQQSLLGLTHGEAVQLLRSVGDTLTVLVCDGFEA 396

Query  718  STDAALEVSPGVIANPFAAGIGHRNSLESISSIDRELSPEGPGKEKELPGQTLHWGPEAT 539
            STDAALEVSPGVIANPFAAGIGHRNSLESISSIDRELSPEGPGKEKELPGQTLHWGPEAT
Sbjct  397  STDAALEVSPGVIANPFAAGIGHRNSLESISSIDRELSPEGPGKEKELPGQTLHWGPEAT 456

Query  538  EAAGRGLQPLKLDYRALAAVPSAGSVQRVPSGAAGGKMAEspcspsgqqppspppdpDELP 359
            EAAGRGLQPLKLDYRALAAVPSAGSVQRVPSGAAGGKMAESPCSPSGQQPPSPP PDELP
Sbjct  457  EAAGRGLQPLKLDYRALAAVPSAGSVQRVPSGAAGGKMAESPCSPSGQQPPSPPSPDELP 516

Query  358  ANVKQAYRAFAAVPTSHppedapaqpptpgpaasPEQLSFRERQKYFELEVRVPQAEGPP 179
             ANVKQAYRAFAAVPTSHPPEDAPAQPPTPGPAASPEQLSFRERQKYFELEVRVPQAEGPP
Sbjct  517  ANVKQAYRAFAAVPTSHPPEDAPAQPPTPGPAASPEQLSFRERQKYFELEVRVPQAEGPP 576

Query  178  KRVSLVGADDLRKMQEEEARKLQQKRAQM  92
            KRVSLVGADDLRKMQEEEARKLQQKRAQM
Sbjct  577  KRVSLVGADDLRKMQEEEARKLQQKRAQM  605
```

S1348D + 1448D Reverse primer

SCRIB protein, partial [Homo sapiens]
Sequence ID: gb|AAH14632.2|Length: 832Number of Matches: 1
Related Information
Gene-associated gene details
Map Viewer-aligned genomic context
Range 1: 395 to 626GenPeptGraphics Next Match Previous Match

Alignment statistics for match #1

Score	Expect	Method	Identities	Positives	Gaps	Frame
329 bits(843)	2e-103	Compositional matrix adjust.	227/232(98%)	227/232(97%)	0/232(0%)	-1

```
Query  722  EASTDAALEVSPXVIANPFAAGIGHRNSLESIXSIDRELSPEGPGKEKELPGQTLHWGPE  543
            EASTDAALEVSP VIANPFAAGIGHRNSLESI SIDRELSPEGPGKEKELPGQTLHWGPE
Sbjct  395  EASTDAALEVSPGVIANPFAAGIGHRNSLESISSIDRELSPEGPGKEKELPGQTLHWGPE  454

Query  542  ATEAAGRGLQPLKLDYRALAAVPSAGSVQRVPSGAAGGKMAEspcspsgqqppspppsPDE  363
            ATEAAGRGLQPLKLDYRALAAVPSAGSVQRVPSGAAGGKMAESPCSPSGQQPPSPPSPDE
Sbjct  455  ATEAAGRGLQPLKLDYRALAAVPSAGSVQRVPSGAAGGKMAESPCSPSGQQPPSPPSPDE  514

Query  362  LPANVKQAYRAXXAVPTSHppedapaqpptpgpaadpeQLSFRERQKYFELEVRVPQAEG  183
            LPANVKQAYRA  AVPTSHPPEDAPAQPPTPGPAA PEQLSFRERQKYFELEVRVPQAEG
Sbjct  515  LPANVKQAYRAFAAVPTSHPPEDAPAQPPTPGPAASPEQLSFRERQKYFELEVRVPQAEG  574

Query  182  PPKRVSLVGADDLRKMQEEEARKLQQKRAQMlreaaeagaearlaLDGETLG  27
            PPKRVSLVGADDLRKMQEEEARKLQQKRAQMLREAAEAGAEARLALDGETLG
Sbjct  575  PPKRVSLVGADDLRKMQEEEARKLQQKRAQMLREAAEAGAEARLALDGETLG  626
```

S1448D + 1306D Forward primer

SCRIB protein, partial [Homo sapiens]
Sequence ID: gb|AAH14632.2|Length: 832Number of Matches: 1
Related Information
Gene-associated gene details
Map Viewer-aligned genomic context
Range 1: 524 to 815GenPeptGraphics Next Match Previous Match

Alignment statistics for match #1

Score	Expect	Method	Identities	Positives	Gaps	Frame
350 bits(898)	2e-109	Compositional matrix adjust.	291/292(99%)	291/292(99%)	0/292(0%)	+1

```
Query  22   RAFAAVPTSHppedapaqpptpgpaaspEQLSFRERQKYFELEVRVPQAEGPPKRVSLVG 201
            RAFAAVPTSHPPEDAPAQPPTPGPAASPEQLSFRERQKYFELEVRVPQAEGPPKRVSLVG
Sbjct  524  RAFAAVPTSHPPEDAPAQPPTPGPAASPEQLSFRERQKYFELEVRVPQAEGPPKRVSLVG 583

Query  202  ADDLRKMQEEEARKLQQKRAQMlreaaeagaearlaldgetlgeeeqedeqppWASPSPT 381
            ADDLRKMQEEEARKLQQKRAQMLREAAEAGAEARLALDGETLGEEEQEDEQPPWASPSPT
Sbjct  584  ADDLRKMQEEEARKLQQKRAQMLREAAEAGAEARLALDGETLGEEEQEDEQPPWASPSPT 643

Query  382  SRQSpadppplgggapVRTAKAERRHQERLRVQSPEPPAPERALSPaelraleaekralw 561
            SRQSPA PPPLGGGAPVRTAKAERRHQERLRVQSPEPPAPERALSPAELRALEAEKRALW
Sbjct  644  SRQSPASPPPLGGGAPVRTAKAERRHQERLRVQSPEPPAPERALSPAELRALEAEKRALW 703

Query  562  raarMKSLEQDALRAQMVLSRSQEGRGTRGPLERLAEapspaptpsptpVEDLGPQTSTS 741
            RAARMKSLEQDALRAQMVLSRSQEGRGTRGPLERLAEAPSPAPTPSPTPVEDLGPQTSTS
Sbjct  704  RAARMKSLEQDALRAQMVLSRSQEGRGTRGPLERLAEAPSPAPTPSPTPVEDLGPQTSTS 763

Query  742  PGRLSPDFAEELRSLEPSPSPGPQEEDGEVALVLLGRPSPGAVGPEDVALCS  897
            PGRLSPDFAEELRSLEPSPSPGPQEEDGEVALVLLGRPSPGAVGPEDVALCS
Sbjct  764  PGRLSPDFAEELRSLEPSPSPGPQEEDGEVALVLLGRPSPGAVGPEDVALCS  815
```

Double Mutations (A-mutants)

S[1306+1309]A + 1448A Reverse primer

SCRIB protein, partial [Homo sapiens]
Sequence ID: gb|AAH14632.2|Length: 832Number of Matches: 1
Related Information
Gene-associated gene details
Map Viewer-aligned genomic context
Range 1: 363 to 626GenPeptGraphics Next Match Previous Match

Alignment statistics for match #1

Score	Expect	Method	Identities	Positives	Gaps	Frame
400 bits(1029)	6e-130	Compositional matrix adjust.	257/264(97%)	259/264(98%)	0/264(0%)	-3

```
Query  830  NQQSLXXLTHGEAVQLLRSVGDTLTVLVCDGFEASTDAALEVSPGVIANPFAAGIGHRNS  651
            NQQSL  LTHGEAVQLLRSVGDTLTVLVCDGFEASTDAALEVSPGVIANPFAAGIGHRNS
Sbjct  363  NQQSLLGLTHGEAVQLLRSVGDTLTVLVCDGFEASTDAALEVSPGVIANPFAAGIGHRNS  422

Query  650  LESISSIDRELSPEGPGKEKELPGQTLHWGPEATEAAGRGXQPLKLXYRALAAVPSAGSV  471
            LESISSIDRELSPEGPGKEKELPGQTLHWGPEATEAAGRG QPLKL YRALAAVPSAGSV
Sbjct  423  LESISSIDRELSPEGPGKEKELPGQTLHWGPEATEAAGRGLQPLKLDYRALAAVPSAGSV  482

Query  470  QRVPSGAAGGKMAEspcspsgqqppappaPDELPANVKQAYRAFAAVPTSHppedapaqp  291
            QRVPSGAAGGKMAESPCSPSGQQPP+PP+PDELPANVKQAYRAFAAVPTSHPPEDAPAQP
Sbjct  483  QRVPSGAAGGKMAESPCSPSGQQPPSPPSPDELPANVKQAYRAFAAVPTSHPPEDAPAQP  542

Query  290  ptpgpaasPEQLSFRERQKYFELEVRVPQAEGPPKRVSLVGADDLRKMQEEEARKLQQKR  111
            PTPGPAASPEQLSFRERQKYFELEVRVPQAEGPPKRVSLVGADDLRKMQEEEARKLQQKR
Sbjct  543  PTPGPAASPEQLSFRERQKYFELEVRVPQAEGPPKRVSLVGADDLRKMQEEEARKLQQKR  602

Query  110  AQMlreaaeagaearlxLDGETLG  39
            AQMLREAAEAGAEARL LDGETLG
Sbjct  603  AQMLREAAEAGAEARLALDGETLG  626
```

S[1348A+1448]A + 1306-09A Forward primer

SCRIB protein, partial [Homo sapiens]
Sequence ID: gb|AAH14632.2|Length: 832Number of Matches: 1
Related Information
Gene-associated gene details
Map Viewer-aligned genomic context
Range 1: 525 to 815GenPeptGraphics Next Match Previous Match

Alignment statistics for match #1

Score	Expect	Method	Identities	Positives	Gaps	Frame
303 bits(777)	3e-90	Compositional matrix adjust.	278/291(96%)	280/291(96%)	0/291(0%)	+3

```
Query  21   AFAAVPTSHppedapaqpptpgpaaapEQLSFRERQKYFELEVRVPQAEGPPKRVSLVGA  200
            AFAAVPTSHPPEDAPAQPPTPGPAA+PEQLSFRERQKYFELEVRVPQAEGPPKRVSLVGA
Sbjct  525  AFAAVPTSHPPEDAPAQPPTPGPAASPEQLSFRERQKYFELEVRVPQAEGPPKRVSLVGA  584

Query  201  DDLRKMQEEEARKLQQKRAQMlreaaeagaearlaldgetlgeeeqedeqppWASPSPTS  380
            DDLRKMQEEEARKLQQKRAQMLREAAEAGAEARLALDGETLGEEEQEDEQPPWASPSPTS
Sbjct  585  DDLRKMQEEEARKLQQKRAQMLREAAEAGAEARLALDGETLGEEEQEDEQPPWASPSPTS  644

Query  381  RQSpaappplgggapVRTAKAERRHQERLRVQSPEPPAPERALSPaelraleaekralwr  560
            RQSPA+PPPLGGGAPVRTAKAERRHQERLRVQSPEPPAPERALSPAELRALEAEKRALWR
Sbjct  645  RQSPASPPPLGGGAPVRTAKAERRHQERLRVQSPEPPAPERALSPAELRALEAEKRALWR  704

Query  561  aarMKSLEQDALRAQMVLXRSQEGRGTRGPLERLAEapspaptxsptxVEDLGPXTXTSP  740
            AARMKSLEQDALRAQMVL RSQEGRGTRGPLERLAEAPSPAPT SPT VEDLGP T TSP
Sbjct  705  AARMKSLEQDALRAQMVLSRSQEGRGTRGPLERLAEAPSPAPTPSPTPVEDLGPQTSTSP  764

Query  741  GRLSPDFAEELRSLxpspspxpxEEDGExxlvllGRRSPGAVGPEDVALCS  893
            GRLSPDFAEELRSL PSPSP P EEDGE  LVLLGR SPGAVGPEDVALCS
Sbjct  765  GRLSPDFAEELRSLEPSPSPGPQEEDGEVALVLLGRPSPGAVGPEDVALCS  815
```

Double Mutations (D-mutants)

S[1306+1309]D + 1448D Reverse primer

SCRIB protein, partial [Homo sapiens]
Sequence ID: gb|AAH14632.2|Length: 832Number of Matches: 1
Related Information
Gene-associated gene details
Map Viewer-aligned genomic context
Range 1: 371 to 626GenPeptGraphics Next Match Previous Match

Alignment statistics for match #1

Score	Expect	Method	Identities	Positives	Gaps	Frame
378 bits(971)	2e-121	Compositional matrix adjust.	248/256(97%)	248/256(96%)	0/256(0%)	-1

```
Query  798  THGEAVQXLRSVGDTLTXLVCDGFEASTDAALEVSPGVIANPFAAGIGHRNSLESIXSID  619
            THGEAVQ LRSVGDTLT LVCDGFEASTDAALEVSPGVIANPFAAGIGHRNSLESI SID
Sbjct  371  THGEAVQLLRSVGDTLTVLVCDGFEASTDAALEVSPGVIANPFAAGIGHRNSLESISSID  430

Query  618  RELSPEGPGKEKELPGQTLHWGPEATEAAGRGLQPLKLDYRALAAVPSAGSVQRVPSGAA  439
            RELSPEGPGKEKELPGQTLHWGPEATEAAGRGLQPLKLDYRALAAVPSAGSVQRVPSGAA
Sbjct  431  RELSPEGPGKEKELPGQTLHWGPEATEAAGRGLQPLKLDYRALAAVPSAGSVQRVPSGAA  490

Query  438  GGKMXEspcspsgqqppdppdpDELPANVKQAYRAXAAVPTSHppedapaqpptpgpaas  259
            GGKM ESPCSPSGQQPP PP PDELPANVKQAYRA AAVPTSHPPEDAPAQPPTPGPAAS
Sbjct  491  GGKMAESPCSPSGQQPPSPPSPDELPANVKQAYRAFAAVPTSHPPEDAPAQPPTPGPAAS  550

Query  258  PEQLSFRERQKYFELEVRVPQAEGPPKRVSLVGADDLRKMQEEEARKLQQKRAQMlreaa  79
            PEQLSFRERQKYFELEVRVPQAEGPPKRVSLVGADDLRKMQEEEARKLQQKRAQMLREAA
Sbjct  551  PEQLSFRERQKYFELEVRVPQAEGPPKRVSLVGADDLRKMQEEEARKLQQKRAQMLREAA  610


Query  78   eagaearlxLDGETLG  31
            EAGAEARL LDGETLG
Sbjct  611  EAGAEARLALDGETLG  626
```

S[1348D+1448]D + 1306-09D Forward primer

SCRIB protein, partial [Homo sapiens]
Sequence ID: gb|AAH14632.2|Length: 832Number of Matches: 1
Related Information
Gene-associated gene details
Map Viewer-aligned genomic context
Range 1: 526 to 816GenPeptGraphics Next Match Previous Match

Alignment statistics for match #1

Score	Expect	Method	Identities	Positives	Gaps	Frame
271 bits(693)	3e-78	Compositional matrix adjust.	235/291(81%)	237/291(81%)	0/291(0%)	+2

```
Query  23   FXAVPTSHppedapaqpptpgpaadpxQLSFRDRQKYFELEVRVPXAEGPPNRVSLVGAD  202
            F AVPTSHPPEDAPAQPPTPGPAA P QLSFR+RQKYFELEVRVP AEGPP RVSLVGAD
Sbjct  526  FAAVPTSHPPEDAPAQPPTPGPAASPEQLSFRERQKYFELEVRVPQAEGPPKRVSLVGAD  585

Query  203  DLRKMXEEEARKLLQKRAQMlreaaeagaearlaldgetlgeeeqedeqppWASPSPTSR  382
            DLRKM EEEARKL QKRAQMLREAAEAGAEARLALDGETLGEEEQEDEQPPWASPSPTSR
Sbjct  586  DLRKMQEEEARKLQQKRAQMLREAAEAGAEARLALDGETLGEEEQEDEQPPWASPSPTSR  645

Query  383  QSpadppplgggapVRTAKAERRLXXRLXVQSPXXPAXXXXLSPAXXRVLXAXXRALWRX  562
            QSPA PPPLGGGAPVRTAKAERR   RL VQSP  PA    LSPA  R L A  RALWR
Sbjct  646  QSPASPPPLGGGAPVRTAKAERRHQERLRVQSPEPPAPERALSPAELRALEAEKRALWRA  705

Query  563  ASMKSLEQDALXAXMVLSKSQXGXDTRGPLERLXEapspaptpsptpVEDLGXXTXTSXG  742
            A MKSLEQDAL A MVLS+SQ G  TRGPLERL EAPSPAPTPSPTPVEDLG  T TS G
Sbjct  706  ARMKSLEQDALRAQMVLSRSQEGRGTRGPLERLAEAPSPAPTPSPTPVEDLGPQTSTSPG  765

Query  743  XLSPXFXXXLRSLXPSRSPAPYEEDGEVALXFLGXXSXIAVXPEXVXLCSS  895
             LSP F   LRSL PS SP P EEDGEVAL  LG  S  AV PE V LCSS
Sbjct  766  RLSPDFAEELRSLEPSPSPGPQEEDGEVALVLLGRPSPGAVGPEDVALCSS  816
```

Triple Mutations (A-mutants)

S-AA(1348A) + 1448A Reverse Primer

SCRIB protein, partial [Homo sapiens]
Sequence ID: gb|AAH09490.2|Length: 450Number of Matches: 2
Related Information
Gene-associated gene details
Range 1: 45 to 231GenPeptGraphics Next Match Previous Match

Alignment statistics for match #1

Score	Expect	Method	Identities	Positives	Gaps	Frame
228 bits(581)	4e-68	Compositional matrix adjust.	183/187(98%)	186/187(99%)	0/187(0%)	-3

```
Query  586  GPEATEAAGRGLQPLKLDYRALAAVPSAGSVQRVPSGAAGGKMAEspcspsgqqppappa 407
            GPEATEAAGRGLQPLKLDYRALAAVPSAGSVQRVPSGAAGGKMAESPCSPSGQQPP+PP+
Sbjct  45   GPEATEAAGRGLQPLKLDYRALAAVPSAGSVQRVPSGAAGGKMAESPCSPSGQQPPSPPS 104

Query  406  PDELPANVKQAYRAFAAVPTSHppedapaqpptpgpaaaPEQLSFRERQKYFELEVRVPQ 227
            PDELPANVKQAYRAFAAVPTSHPPEDAPAQPPTPGPAA+PEQLSFRERQKYFELEVRVPQ
Sbjct  105  PDELPANVKQAYRAFAAVPTSHPPEDAPAQPPTPGPAASPEQLSFRERQKYFELEVRVPQ 164

Query  226  AEGPPKRVSLVGADDLRKMQEEEARKLQQKRAQMlreaaeagaearlaLDGETLGeeeqe  47
            AEGPPKRVSLVGADDLRKMQEEEARKLQQKRAQMLREAAEAGAEARLALDGETLGEEEQE
Sbjct  165  AEGPPKRVSLVGADDLRKMQEEEARKLQQKRAQMLREAAEAGAEARLALDGETLGEEEQE 224

Query  46   xeQPPWA  26
             EQPPWA
Sbjct  225  DEQPPWA  231
```

S-AA(1448A) + 1306-09A Forward primer

SCRIB protein, partial [Homo sapiens]
Sequence ID: gb|AAH14632.2|Length: 832Number of Matches: 1
Related Information
Gene-associated gene details
Map Viewer-aligned genomic context
Range 1: 525 to 815GenPeptGraphics Next Match Previous Match

Alignment statistics for match #1

Score	Expect	Method	Identities	Positives	Gaps	Frame
309 bits(791)	2e-92	Compositional matrix adjust.	281/291(97%)	283/291(97%)	0/291(0%)	+2

```
Query  23   AFAAVPTSHppedapaqpptpgpaaspEQLSFRERQKYFELEVRVPQAEGPPKRVSLVGA 202
            AFAAVPTSHPPEDAPAQPPTPGPAASPEQLSFRERQKYFELEVRVPQAEGPPKRVSLVGA
Sbjct  525  AFAAVPTSHPPEDAPAQPPTPGPAASPEQLSFRERQKYFELEVRVPQAEGPPKRVSLVGA 584

Query  203  DDLRKMQEEEARKLQQKRAQMlreaaeagaearlaldgetlgeeeqedeqppWASPSPTS 382
            DDLRKMQEEEARKLQQKRAQMLREAAEAGAEARLALDGETLGEEEQEDEQPPWASPSPTS
Sbjct  585  DDLRKMQEEEARKLQQKRAQMLREAAEAGAEARLALDGETLGEEEQEDEQPPWASPSPTS 644

Query  383  RQSpaappplgggapVRTAKAERRHQERLRVQSPEPPAPERALSPaelraleaekralwr 562
            RQSPA+PPPLGGGAPVRTAKAERRHQERLRVQSPEPPAPERALSPAELRALEAEKRALWR
Sbjct  645  RQSPASPPPLGGGAPVRTAKAERRHQERLRVQSPEPPAPERALSPAELRALEAEKRALWR 704

Query  563  aarMKSLEQDALRAQMVLXRSQEGRGTRGPLERLAEapspaptpsptpVEDLGPXTXTSP 742
            AARMKSLEQDALRAQMVL RSQEGRGTRGPLERLAEAPSPAPTPSPTPVEDLGP T TSP
Sbjct  705  AARMKSLEQDALRAQMVLSRSQEGRGTRGPLERLAEAPSPAPTPSPTPVEDLGPQTSTSP 764

Query  743  GRLSPDFAEELRslxpspspgpxxEDGELALVLLGRPSPXAVXPEDVALCS  895
            GRLSPDFAEELRSL PSPSPGP  EDGE+ALVLLGRPSP AV PEDVALCS
Sbjct  765  GRLSPDFAEELRSLEPSPSPGPQEEDGEVALVLLGRPSPGAVGPEDVALCS  815
```

Triple Mutations (D-mutants)

S-DD(1348D) + 1448A Reverse Primer

SCRIB protein, partial [Homo sapiens]
Sequence ID: gb|AAH14632.2|Length: 832Number of Matches: 2
Related Information
Gene-associated gene details
Range 1: 430 to 605GenPeptGraphics Next Match Previous Match

Alignment statistics for match #1

Score	Expect	Method	Identities	Positives	Gaps	Frame
216 bits(550)	4e-73	Compositional matrix adjust.	159/176(90%)	161/176(91%)	0/176(0%)	-2

```
Query  651  DREVSPEGXGKEKEXXGQXXHXGPEATEAAGRGXQPLXLDYRALAAVPSAGSVQRVPSGA 472
            DRE+SPEG GKEKE  GQ  H GPEATEAAGRG QPL LDYRALAAVPSAGSVQRVPSGA
Sbjct  430  DRELSPEGPGKEKELPGQTLHWGPEATEAAGRGLQPLKLDYRALAAVPSAGSVQRVPSGA 489

Query  471  AGGKMgespcspsgqqppdppdpdemPANVKQAYRAFAAVPTSHppedapaqpptpgpaa 292
            AGGKM ESPCSPSGQQPP PP PDE+PANVKQAYRAFAAVPTSHPPEDAPAQPPTPGPAA
Sbjct  490  AGGKMAESPCSPSGQQPPSPPSPDELPANVKQAYRAFAAVPTSHPPEDAPAQPPTPGPAA 549

Query  291  dpeQLSFRERQKYXXXEVRVPQAEGPPKRVSLVGADDLRKMQEEEARKLQQKRAQM  124
             PEQLSFRERQKY   EVRVPQAEGPPKRVSLVGADDLRKMQEEEARKLQQKRAQM
Sbjct  550  SPEQLSFRERQKYFELEVRVPQAEGPPKRVSLVGADDLRKMQEEEARKLQQKRAQM  605
```

S-DD(1448D) + 1348A Forward Primer

SCRIB protein, partial [Homo sapiens]
Sequence ID: gb|AAH09490.2|Length: 450Number of Matches: 1
Related Information
Gene-associated gene details
Range 1: 155 to 249GenPeptGraphics Next Match Previous Match

Alignment statistics for match #1

Score	Expect	Method	Identities	Positives	Gaps	Frame
113 bits(283)	2e-27	Compositional matrix adjust.	94/95(99%)	94/95(98%)	0/95(0%)	+2

```
Query  29   YFELEVRVPQAEGPPKRVSLVGADDLRKMQEEEARKLQQKRAQMlreaaeagaearlald 208
            YFELEVRVPQAEGPPKRVSLVGADDLRKMQEEEARKLQQKRAQMLREAAEAGAEARLALD
Sbjct  155  YFELEVRVPQAEGPPKRVSLVGADDLRKMQEEEARKLQQKRAQMLREAAEAGAEARLALD 214

Query  209  getlgeeeqedeqppWASPSPTSRQSPADPPPLGG  313
            GETLGEEEQEDEQPPWASPSPTSRQSPA PPPLGG
Sbjct  215  GETLGEEEQEDEQPPWASPSPTSRQSPASPPPLGG  249
```

Mutations in addition to specified c-terminal serine sites

E1293Stop + 1348A Reverse Primer

SCRIB protein, partial [Homo sapiens]
Sequence ID: gb|AAH44627.1|Length: 682Number of Matches: 1
Related Information
Gene-associated gene details
Range 1: 422 to 634GenPeptGraphics Next Match Previous Match First Match

Alignment statistics for match #1

Score	Expect	Method	Identities	Positives	Gaps	Frame
345 bits(885)	4e-111()	Compositional matrix adjust.	212/213(99%)	212/213(99%)	0/213(0%)	-1

Features:

```
Query  670  PRDPTDEGIFISKVSPTgaagrdgrlrvglrlLEVNQQSLLGLTHGEAVQLLRSVGDTLT 491
            PRDPTDEGIFISKVSPTGAAGRDGRLRVGLRLLEVNQQSLLGLTHGEAVQLLRSVGDTLT
Sbjct  422  PRDPTDEGIFISKVSPTGAAGRDGRLRVGLRLLEVNQQSLLGLTHGEAVQLLRSVGDTLT 481

Query  490  VLVCDGFEASTDAALEVSPGVIANPFAAGIGHRNSLESISSIDRELSPEGPGKEKELPGQ 311
            VLVCDGFEASTDAALEVSPGVIANPFAAGIGHRNSLESISSIDRELSPEGPGKEKELPGQ
Sbjct  482  VLVCDGFEASTDAALEVSPGVIANPFAAGIGHRNSLESISSIDRELSPEGPGKEKELPGQ 541

Query  310  TLHWGPEATEAAGRGLQPLKLDYRALAAVPSAGSVQRVPSGAAGGKMA*spcspsgqqpp 131
            TLHWGPEATEAAGRGLQPLKLDYRALAAVPSAGSVQRVPSGAAGGKMA SPCSPSGQQPP
Sbjct  542  TLHWGPEATEAAGRGLQPLKLDYRALAAVPSAGSVQRVPSGAAGGKMAESPCSPSGQQPP 601

Query  130  sppsPDELPANVKQAYRAFAAVPTSHPPEDAPA  32
            SPPSPDELPANVKQAYRAFAAVPTSHPPEDAPA
Sbjct  602  SPPSPDELPANVKQAYRAFAAVPTSHPPEDAPA  634
```

C1297S + 1348A Reverse Primer

SCRIB protein, partial [Homo sapiens]
Sequence ID: gb|AAH44627.1|Length: 682Number of Matches: 1
Related Information
Gene-associated gene details
Range 1: 489 to 629GenPeptGraphicsNext MatchPrevious MatchFirst Match

Alignment statistics for match #1

Score	Expect	Method	Identities	Positives	Gaps	Frame
226 bits(577)	1e-66()	Compositional matrix adjust.	134/141(95%)	134/141(95%)	0/141(0%)	-2

Features:

```
Query  460  EXSXDAALEVSPGVIANPFAAGIGHRNSLESISSIDRELSPEGPGKEKELPGQTLHWGPE 281
            E S DAALEVSPGVIANPFAAGIGHRNSLESISSIDRELSPEGPGKEKELPGQTLHWGPE
Sbjct  489  EASTDAALEVSPGVIANPFAAGIGHRNSLESISSIDRELSPEGPGKEKELPGQTLHWGPE 548

Query  280  ATEAAGRGLQPLKLXXXALAAVPSAGSVQRVPSGAAGGKMAEspsspsgqqppspps PDE 101
            ATEAAGRGLQPLKL   ALAAVPSAGSVQRVPSGAAGGKMAESP SPSGQQPPSPPSPDE
Sbjct  549  ATEAAGRGLQPLKLDYRALAAVPSAGSVQRVPSGAAGGKMAESPCSPSGQQPPSPPSPDE 608

Query  100  LPANVKQAYRAFAAVPTXHPP  38
            LPANVKQAYRAFAAVPT HPP
Sbjct  609  LPANVKQAYRAFAAVPTSHPP  629
```

S1445A + 1306A Forward Primer

SCRIB protein, partial [Homo sapiens]
Sequence ID: gb|AAH09490.2|Length: 450Number of Matches: 1
Related Information
Gene-associated gene details
Range 1: 116 to 261GenPeptGraphicsNext MatchPrevious Match

Alignment statistics for match #1

Score	Expect	Method	Identities	Positives	Gaps	Frame
130 bits(328)	3e-32	Compositional matrix adjust.	138/146(95%)	139/146(95%)	0/146(0%)	+3

```
Query  30   YXAFAAVPTSHppexapaqpptpgpaaspEQLSFRERQKYFELEVRVPQAEGPPKRVSLV  209
            Y AFAAVPTSHPPE APAQPPTPGPAASPEQLSFRERQKYFELEVRVPQAEGPPKRVSLV
Sbjct  116  YRAFAAVPTSHPPEDAPAQPPTPGPAASPEQLSFRERQKYFELEVRVPQAEGPPKRVSLV  175

Query  210  GADDLRKMQEEEARKLQQKRAQMlreaaeagaearlaldgetlgeeeqedeqppWASPSP  389
            GADDLRKMQEEEARKLQQKRAQMLREAAEAGAEARLALDGETLGEEEQEDEQPPWASPSP
Sbjct  176  GADDLRKMQEEEARKLQQKRAQMLREAAEAGAEARLALDGETLGEEEQEDEQPPWASPSP  235

Query  390  TSRQapaspppplgggapVRXXXXXRR  467
            TSRQ+PASPPPLGGGAPVR     RR
Sbjct  236  TSRQSPASPPPLGGGAPVRTAKAERR  261
```

S1445D + 1306A Forward Primer

SCRIB protein, partial [Homo sapiens]
Sequence ID: gb|AAH09490.2|Length: 450Number of Matches: 1
Related Information
Gene-associated gene details
Range 1: 116 to 331GenPeptGraphicsNext MatchPrevious Match

Alignment statistics for match #1

Score	Expect	Method	Identities	Positives	Gaps	Frame
204 bits(519)	4e-59	Compositional matrix adjust.	202/216(94%)	202/216(93%)	0/216(0%)	+1

```
Query  31   YXAFAAVPTSHppedapaqpptpgpaaspEQLSFRERQKYFELEVRVPQAEGPPKRVSLV  210
            Y AFAAVPTSHPPEDAPAQPPTPGPAASPEQLSFRERQKYFELEVRVPQAEGPPKRVSLV
Sbjct  116  YRAFAAVPTSHPPEDAPAQPPTPGPAASPEQLSFRERQKYFELEVRVPQAEGPPKRVSLV  175

Query  211  GADDLRKMQEEEARKLQQKRAQMlreaaeagaearlaldgetlgeeeqedeqppWASPSP  390
            GADDLRKMQEEEARKLQQKRAQMLREAAEAGAEARLALDGETLGEEEQEDEQPPWASPSP
Sbjct  176  GADDLRKMQEEEARKLQQKRAQMLREAAEAGAEARLALDGETLGEEEQEDEQPPWASPSP  235

Query  391  TSRQDpaspppplgggapVRTAKAERRHQERLRVQSPEPPAPERALSPaelraleaekral  570
            TSRQ PASPPPLGGGAPVRTAKAERRHQERLRVQSPEPPAPERALSPAELRALEAEKRAL
Sbjct  236  TSRQSPASPPPLGGGAPVRTAKAERRHQERLRVQSPEPPAPERALSPAELRALEAEKRAL  295

Query  571  wraarMXSLEQDALXXXMVLXRSXXXRGXRGXLXXL  678
            WRAARM SLEQDAL   MVL RS   RG RG L  L
Sbjct  296  WRAARMKSLEQDALRAQMVLSRSQEGRGTRGPLERL  331
```

S1449A + 1348A Forward Primer

SCRIB protein, partial [Homo sapiens]
Sequence ID: gb|AAH09490.2|Length: 450Number of Matches: 1
Related Information
Gene-associated gene details
Range 1: 155 to 295GenPeptGraphics Next Match Previous Match First Match

Alignment statistics for match #1

Score	Expect	Method	Identities	Positives	Gaps	Frame
145 bits(365)	1e-37()	Compositional matrix adjust.	128/141(91%)	129/141(91%)	0/141(0%)	+1

Features:

```
Query  25   YFELEVRVPXAEGPPKRVSLVGADDLRKMQEEEARKLQQKRAQMlreaaeagaearlald 204
            YFELEVRVP AEGPPKRVSLVGADDLRKMQEEEARKLQQKRAQMLREAAEAGAEARLALD
Sbjct  155  YFELEVRVPQAEGPPKRVSLVGADDLRKMQEEEARKLQQKRAQMLREAAEAGAEARLALD 214

Query  205  getlgeeeqedeqppWASPSPTSRQspasapplgggapVRTVKAERRXQERLXVQSPEXP 384
            GETLGEEEQEDEQPPWASPSPTSRQSPAS PPLGGGAPVRT KAERR QERL VQSPE P
Sbjct  215  GETLGEEEQEDEQPPWASPSPTSRQSPASPPPLGGGAPVRTAKAERRHQERLRVQSPEPP 274

Query  385  APXRALSPADFXALEXXKRAC  447
            AP RALSPA+  ALE  KRA
Sbjct  275  APERALSPAELRALEAEKRAL  295
```

S[1445+1448]A + 1348A Forward Primer

SCRIB protein, partial [Homo sapiens]
Sequence ID: gb|AAH09490.2|Length: 450Number of Matches: 2
Related Information
Gene-associated gene details
Range 1: 190 to 331GenPeptGraphics Next Match Previous Match

Alignment statistics for match #1

Score	Expect	Method	Identities	Positives	Gaps	Frame
121 bits(303)	1e-32	Compositional matrix adjust.	138/142(97%)	140/142(98%)	0/142(0%)	+2

```
Query  125  KLQHKRAQMlreaaeagaearlaldgetlgeeeqedeqppxASPSPTSRQapaappplgg 304
            KLQ KRAQMLREAAEAGAEARLALDGETLGEEEQEDEQPP ASPSPTSRQ+PA+PPPLGG
Sbjct  190  KLQQKRAQMLREAAEAGAEARLALDGETLGEEEQEDEQPPWASPSPTSRQSPASPPPLGG 249

Query  305  gapVRTAKAERRHQERLRVQSPEPPAPERALSPaelraleaekralwraarMKSLEQDAL 484
            GAPVRTAKAERRHQERLRVQSPEPPAPERALSPAELRALEAEKRALWRAARMKSLEQDAL
Sbjct  250  GAPVRTAKAERRHQERLRVQSPEPPAPERALSPAELRALEAEKRALWRAARMKSLEQDAL 309

Query  485  RAQMVLSRSQEGRGTRGPLERL  550
            RAQMVLSRSQEGRGTRGPLERL
Sbjct  310  RAQMVLSRSQEGRGTRGPLERL  331
```

S[1445+1448]D + 1348A Forward Primer

SCRIB protein, partial [Homo sapiens]
Sequence ID: gb|AAH09490.2|Length: 450Number of Matches: 1
Related Information
Gene-associated gene details
Range 1: 155 to 249GenPeptGraphics Next Match Previous Match

Alignment statistics for match #1

Score	Expect	Method	Identities	Positives	Gaps	Frame
112 bits(279)	6e-27	Compositional matrix adjust.	93/95(98%)	93/95(97%)	0/95(0%)	+1

```
Query  25   YFELEVRVPQAEGPPKRVSLVGADDLRKMQEEEARKLQQKRAQMlreaaeagaearlald 204
            YFELEVRVPQAEGPPKRVSLVGADDLRKMQEEEARKLQQKRAQMLREAAEAGAEARLALD
Sbjct  155  YFELEVRVPQAEGPPKRVSLVGADDLRKMQEEEARKLQQKRAQMLREAAEAGAEARLALD 214

Query  205  getlgeeeqedeqppWASPSPTSRQDPADPPPLGG  309
            GETLGEEEQEDEQPPWASPSPTSRQ PA PPPLGG
Sbjct  215  GETLGEEEQEDEQPPWASPSPTSRQSPASPPPLGG  249
```

Appendix B

Appendix B includes the following:

A6.3 Table of spectral count of proteins (shown in Table 6.3) significantly abundant between the S[1306+1309]A and S[1306+1309]D pull-down.

A6.4 Linear graph of proteins represented in Figure 6.4 (in Chapter 6) and Table A6.3.

A6.3. Table of spectral count of proteins significantly abundant between the S[1306+1309]A and S[1306+1309]D pull-down

	S[1306+1309]A						S[1306+1309]D						
Gene symbol	MS/MS Count aa-p1	MS/MS Count aa-p2	Mean MS/MS Count aa	Stdev aa	Uncertainty aa	Log transfrom error aa	MS/MS Count dd-p1	MS/MS Count dd-p2	MS/MS Count dd-p3	Mean MS/MS Count dd	Stdev dd	Uncertainty dd	Log transfrom error dd
MYH9	61	67	63.67	3.06	3.00	0.05	8	8	4	6.67	2.31	2.00	0.30
MYH10	36	30	32.67	3.06	3.00	0.09	2	4	2	2.67	1.15	1.00	0.38
SCRIB	795	825	818.33	20.82	20.00	0.02	910	921	917	916.00	5.57	5.50	0.01
MYL12B	7	10	8.67	1.53	1.50	0.17	0	0	1	0.33	0.58	0.50	1.50
MYL6	17	19	18.33	1.15	1.00	0.05	3	9	5	5.67	3.06	3.00	0.53
NEFM	29	28	26.67	3.21	3.00	0.11	44	44	47	45.00	1.73	1.50	0.03

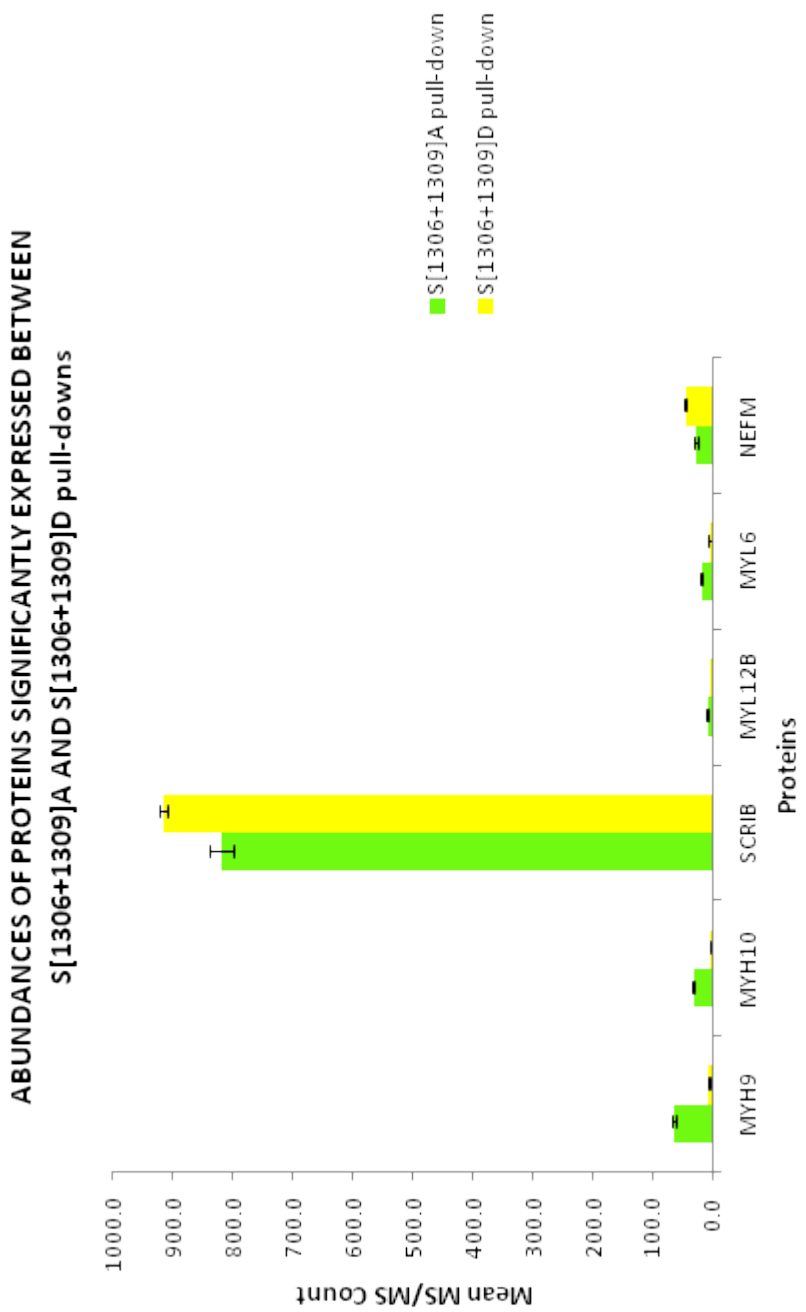

Figure A6.4 Linear bar graph of proteins that were identified in both the S[1306+1309]A and S[1306+1309]D pull-downs but showed significant differences in their abundance between the pull-downs. Bar graph y-axis represents spectral count. Log graph in figure 6.4 was used to clearly display variations in abundances, that the linear graph could not, between pull-downs, of each of the protein identified to be a significant binding partner of both S[1306+1309]A and S[1306+1309]D.